AFRL-VA-WP-TR-2005-3065

FATIGUE LIFE OF COMPOSITE STRUCTURES IN EXTREME ENVIRONMENTS

P.C. Chen

ZONA Technology, Inc.
7430 E. Stetson Drive, Ste. 205
Scottsdale, AZ 85251-3540

Dr. Marc P. Mignolet

Arizona State University

JUNE 2005

Final Report for 26 May 2001 – 30 September 2004

THIS IS A SMALL BUSINESS INNOVATION RESEARCH (SBIR) PHASE II REPORT.

Approved for public release; distribution is unlimited.

STINFO FINAL REPORT

AIR VEHICLES DIRECTORATE
AIR FORCE MATERIEL COMMAND
AIR FORCE RESEARCH LABORATORY
WRIGHT-PATTERSON AIR FORCE BASE, OH 45433-7542

NOTICE

Using Government drawings, specifications, or other data included in this document for any purpose other than Government procurement does not in any way obligate the U.S. Government. The fact that the Government formulated or supplied the drawings, specifications, or other data does not license the holder or any other person or corporation; or convey any rights or permission to manufacture, use, or sell any patented invention that may relate to them.

This report was cleared for public release by the Air Force Research Laboratory Wright Site Public Affairs Office (AFRL/WS) and is releasable to the National Technical Information Service (NTIS). It will be available to the general public, including foreign nationals.

THIS TECHNICAL REPORT IS APPROVED FOR PUBLICATION.

/s/

Timothy J. Beberniss
Aerospace Engineer
Structural Mechanics Branch

/s/

Kristina Langer, Ph.D.
Chief, Structural Mechanics Branch
Structures Division

/s/

David M. Pratt, Ph.D.
Technical Advisor
Structures Division
Air Vehicles Directorate

This report is published in the interest of scientific and technical information exchange and its publication does not constitute the Government's approval or disapproval of its ideas or findings.

REPORT DOCUMENTATION PAGE

Form Approved
OMB No. 0704-0188

1. REPORT DATE *(DD-MM-YY)*	2. REPORT TYPE	3. DATES COVERED *(From - To)*
June 2005	Final	05/26/2001 – 09/30/2004

4. TITLE AND SUBTITLE
FATIGUE LIFE OF COMPOSITE STRUCTURES IN EXTREME ENVIRONMENTS

5a. CONTRACT NUMBER
F33615-01-C-3111

5b. GRANT NUMBER

5c. PROGRAM ELEMENT NUMBER
0605502

6. AUTHOR(S)
P.C. Chen (ZONA Technology, Inc.)
Dr. Marc P. Mignolet (Arizona State University)

5d. PROJECT NUMBER
A076

5e. TASK NUMBER

5f. WORK UNIT NUMBER
0A

7. PERFORMING ORGANIZATION NAME(S) AND ADDRESS(ES)

ZONA Technology, Inc.
7430 E. Stetson Drive, Ste. 205
Scottsdale, AZ 85251-3540

Arizona State University

8. PERFORMING ORGANIZATION REPORT NUMBER
ZONA 04-27

9. SPONSORING/MONITORING AGENCY NAME(S) AND ADDRESS(ES)

Air Vehicles Directorate
Air Force Research Laboratory
Air Force Materiel Command
Wright-Patterson Air Force Base, OH 45433-7542

10. SPONSORING/MONITORING AGENCY ACRONYM(S)
AFRL/VASM

11. SPONSORING/MONITORING AGENCY REPORT NUMBER(S)
AFRL-VA-WP-TR-2005-3065

12. DISTRIBUTION/AVAILABILITY STATEMENT
Approved for public release; distribution is unlimited.

13. SUPPLEMENTARY NOTES
This is a Small Business Innovation Research (SBIR) Phase II report. Report contains color.

The appendices contain a number of preprints, resulting from Department of Air Force contract number F33615-01-C-3111. If published, the various publishers may assert copyright. If so, the United States has for itself and others acting on its behalf an unlimited, nonexclusive irrevocable, paid-up royalty-free worldwide license to use, modify, reproduce, release, perform, display or disclose the work by or on behalf of the Government. Any other form of use is subject to copyright restrictions.

14. ABSTRACT

Report developed under a SBIR contract.

Prediction of the dynamic response and the fatigue life of structures, i.e., panels, subjected to both high temperatures/ thermal gradients and high level acoustic excitations. The determination of reliable approximations of the statistics of the panel response to the random acoustic excitation will be accomplished by relying on two separate equivalent linearization strategies. The first method uses a Gaussian process. The second method relies on a mean equal to the buckled states and the panel response is obtained as the sum of zero mean fluctuations around these positions.

15. SUBJECT TERMS
SBIR report, Sonic Fatigue, Fatigue Life, Nonlinear Plate, Reduced Order Model

16. SECURITY CLASSIFICATION OF:			17. LIMITATION OF ABSTRACT:	18. NUMBER OF PAGES	19a. NAME OF RESPONSIBLE PERSON (Monitor)
a. REPORT	b. ABSTRACT	c. THIS PAGE			Timothy J. Beberniss
Unclassified	Unclassified	Unclassified	SAR	188	19b. TELEPHONE NUMBER *(Include Area Code)* (937) 904-6772

Standard Form 298 (Rev. 8-98)
Prescribed by ANSI Std. Z39-18

TABLE OF CONTENTS

List of Figures

List of Figures (cont.)

List of Tables

Foreword

The design of future reusable launch vehicles and supersonic aircraft such as the X-43 and Hyper-X creates new challenges/exacerbates old ones in various disciplines. Noteworthy in structural dynamics is the design of panels which may be subjected to the combination of a severe acoustic excitation (emanating for example from the engine) and a substantial heating from aerodynamic origin. Even in the absence of thermal effects (i.e. with an operational thermal protection system - TPS), the acoustic excitation may induce a response large enough to mandate the consideration of nonlinear structural models. Furthermore, in the event of a malfunctioning TPS, such panels may be expected to buckle and the severe acoustic excitation will then induce strongly nonlinear response features such as snap-through from one buckled configuration to another.

In fact, there are two nonlinearities to contend with: the nonlinearity of the panel response and the nonlinearity of the stress-displacement relationships arising from the von Karman strain definition, as well as the randomness of the acoustic excitation. The fast and reliable prediction of the panel response, i.e. displacement field, stress field, and fatigue life, in this extreme environment is thus a particularly challenging task which represents the focus of the present contract.

1. INTRODUCTION

The focus of the present investigation was on the determination of the fatigue life of structures subjected to an extreme environment including in particular thermal effects, i.e. temperature gradients on and across the panels, and an acoustic loading. The research effort can broadly be decomposed into four topics:

1. The development of simulation-free strategies (e.g. equivalent linearization) for the prediction of the probabilistic aspects of the response (displacement, stress, and strain fields) of the structure to the random (acoustic) and deterministic (thermal) excitations.
2. The prediction of the fatigue life of the structure considered from the estimated probabilistic aspects of the response.
3. The development of reduced order modeling schemes that render the above two tasks computationally efficient.
4. The development of a code, or set thereof, that permits the fast and accurate estimation of the response and fatigue life of panels.

The results achieved in all of these four areas during the contract period are described below.

2. SIMULATION-FREE PREDICTION OF THE RESPONSE

The work in this area has focused on several aspects of the equivalent linearization technique and on the prediction of the power spectral density of the response of the Duffing oscillator, the prototypical equation for the panel response. In regards to the former topic, the effort included

(a) the formulation and assessment of an alternative equivalent linearization approach based on the modeling of the potential energy of the system as opposed to the approximation of the force (see Zhang et al., 1991, Elishakoff and Zhang, 1992),

(b) the extension of the force-based equivalent linearization technique to the consideration of asymmetric thermal loading, i.e. situations where a thermal moment exists,

and

(c) the general formulation of the force-based equivalent linearization technique as applicable to a full finite element representation or a reduced order model of the structure.

These different efforts are described in the three following sub-sections.

2.1 Formulation and Assessment of the Potential Energy-Based Equivalent Linearization Technique

2.1.1 Equivalent Linearization Strategies

The equivalent linearization technique is, as its name suggests, a strategy for the approximation of a nonlinear system by a linear one. While the name generally refers to a specific strategy, there exists a large number of variations on the given theme, i.e. the equivalent linearization methods of Bruckner and Lin (1987), Iyengar (1988), Socha and Pawleta (1994) and Elishakoff and Colajanni (1997), Zhang et al. (1991) and Elishakoff and Zhang (1992), as well as the fixed mean techniques developed in the Phase I of this contract. Some of these approaches have been formulated to expand the applicability of the standard (also referred to as force-based) equivalent linearization approach. For example, the goal of Iyengar (1988) was to extract a higher order model (i.e. multiple natural frequencies) to include in the linear approximation the harmonics of the nonlinear response, Bruckner and Lin (1987) focused on parametrically excited systems, etc.

Some of the proposed variations have also attempted to improve the accuracy of the estimated mean and variance of the response by modifying the standard approach. While

the formulation by Socha and Pawleta (1994) and Elishakoff and Colajanni (1997) did not seem to be an improvement, it generated a controversy in the community which was finally clarified by Caughey (2001). Another approach, i.e. the potential energy-based approach of Zhang et al. (1991) and Elishakoff and Zhang (1992), has received less attention, although the preliminary results it yielded are quite promising (see Muravyov et al., 1999). In light of the need, for fatigue life prediction, of an efficient and accurate estimation technique of the probabilistic features of the response, the applicability and reliability of this potential energy-based equivalent linearization was investigated and compared to its force-based counterpart.

To exemplify the derivation of these two equivalent linearization techniques, consider the nonlinear equation of motion

$$\ddot{q} + 2\,\zeta\,\omega_0\,\dot{q} + f(q) = \bar{p}(t) \tag{1}$$

where $f(q)$ is a nonlinear restoring force and $\bar{p}(t)$ is a random (white or colored) excitation. In the present context, the restoring force is composed of three parts, the bending stiffness (unstable), the membrane effects (stable), and the constant thermal moments term, i.e.

$$f(q) = \omega_0^2\,(1-s)\,q + \gamma\,q^3 - \bar{p}_0 \tag{2}$$

The results of the Phase I efforts have shown that two specific situations must be considered. When the excitation level is small, the motions occur around the two buckled states and the equivalent linearization with an unknown, nonzero mean is adequate. As the sound pressure level is increased, this type of solution disappears but an accurate prediction of the statistics of the response can still be achieved through a combination of the zero mean equivalent linearization and a similar technique with a mean fixed, equal to each buckled state. On this basis, the following discussion will be divided into the unknown mean and fixed mean equivalent linearization approaches with force-based and potential energy-based formulations.

2.1.2 Unknown Mean Equivalent Linearization Strategies

The force-based equivalent linearization technique seeks the best approximation of $f(q)$ by a linear expression of the form $k_{eq}\, q - p_{eq}$ through the minimization of the error

$$E_{\text{mod}} = E\left\{\left[f(q) - k_{eq}\, q + p_{eq}\right]^2\right\} \tag{3}$$

where $E[\bullet]$ denotes the operation of mathematical expectation. The differentiation of E_{mod} with respect to the unknown parameters k_{eq} and p_{eq} yields the two conditions

$$E\left[q^2\right]k_{eq} - E[q]\, p_{eq} = E[\, f(q)\, q] \tag{4}$$

and

$$E[q]\, k_{eq} - \; p_{eq} = E[\, f(q)\,] \tag{5}$$

from which one obtains

$$k_{eq} = \frac{E\left[\, f(q)\left(q - \mu_q\right)\right]}{\sigma_q^2} \tag{6}$$

and

$$p_{eq} = \frac{\mu_q\, E\left[\, f(q)\left(q - \mu_q\right)\right] - \sigma_q^2\, E[\, f(q)\,]}{\sigma_q^2}. \tag{7}$$

In the above equations, μ_q and σ_q^2 denote the mean and variance of q defined as

$$\mu_q = E[q] \tag{8}$$

and

$$\sigma_q^2 = E\left[\left(q - \mu_q\right)^2\right] \; . \tag{9}$$

It should be noted that Eq. (6) and (7) could have been obtained more directly by using, instead of $k_{eq}\, q - p_{eq}$, the approximation $k_{eq}\left(q - \mu_q\right) + a_1$ which naturally involves the

central moments of q, i.e. $E\left[q-\mu_q\right]=0$ and the variance, Eq. (9). These two approximations are of course equivalent with $p_{eq}=k_{eq}\,\mu_q-a_1$ where

$$a_1=E\left[\,f(q)\,\right]\quad . \tag{10}$$

As often recognized, the equivalent linearization technique is really composed of two separate approximation steps: the first one, described above, is the modeling of the nonlinear restoring force by a linear expression. The second stage is the actual evaluation of the coefficients k_{eq} and p_{eq}. This effort requires the moments μ_q, σ_q^2, $E\left[\,f(q)\,\right]$, and $E\left[\,f(q)\left(q-\mu_q\right)\right]$, see Eq. (6), (7), and (10), but these quantities are in general unknown since the probabilistic description of the process $q(t)$ is not available. The standard resolution of this difficulty is the adoption of a specific distribution for the response $q(t)$; a Gaussian approximation being most often adopted as it is the correct description of the response of the approximate (linear) system

$$\ddot{q}+2\,\zeta\,\omega_0\,\dot{q}+k_{eq}\,q=p_{eq}+\overline{p}(t). \tag{11}$$

The Gaussian modeling of the response process $q(t)$ permits the evaluation of all required moments (e.g, $E\left[\,f(q)\,\right]$ and $E\left[\,f(q)\left(q-\mu_q\right)\right]$) in terms of the mean μ_q and variance σ_q^2. Additional properties of Gaussian random variables can also be used to further simplify the determination of the coefficients k_{eq} and p_{eq} of the equivalent linear model. For example, it can be shown (see Lutes and Sarkani, 1997) for such random variables that

$$E\left[\,g(q)\left(q-\mu_q\right)\right]=\sigma_q^2\;E\left[\,\frac{dg(q)}{dq}\,\right] \tag{12}$$

for any functions $g(q)$, so that Eq. (6) can be rewritten as

$$k_{eq} = E\left[\frac{df(q)}{dq} \right] \quad . \tag{13}$$

Once the coefficients k_{eq} and p_{eq} have been expressed in terms of μ_q and σ_q^2, a set of nonlinear equations for these moments can be derived by noting that the stationary response of the equivalent linear system, Eq. (11), is

$$\mu_q = \frac{p_{eq}}{k_{eq}} \tag{14}$$

and, for a white noise excitation process $\bar{p}(t)$,

$$\sigma_q^2 = \frac{\pi S_{\bar{p}\bar{p}}}{2\,\zeta\,\omega_0\,k_{eq}} \tag{15}$$

so that

$$k_{eq} = \frac{\pi S_{\bar{p}\bar{p}}}{2\,\zeta\,\omega_0\,\sigma_q^2} \tag{16}$$

and

$$p_{eq} = \frac{\pi S_{\bar{p}\bar{p}}\,\mu_q}{2\,\zeta\,\omega_0\,\sigma_q^2}\,. \tag{17}$$

The above process was demonstrated in detail in connection with the restoring force of Eq. (2) in the final report of the Phase I effort and thus will not be repeated here.

Zhang et al. (1991) and Elishakoff and Zhang (1992) suggested an alternative linear equivalent linearization technique that does not approximate the restoring force but rather the corresponding potential energy. Why the focus on the potential energy? Interestingly, it has been shown (Caughey, 1965, see Lutes and Sarkani, 1997) that the exact stationary probability density function of the response $q(t)$ can be written as

$$p_{q(t)}(q) = B \exp\left[-\frac{2\,\zeta\,\omega_0}{\pi S_{\bar{p}\bar{p}}} V(q) \right] \tag{18}$$

where B is a normalization constant, i.e. such that the total probability is 1, and $V(q)$ is the potential energy associated with $f(q)$, that is

$$V(q) = \int f(q)\, dq\,. \tag{19}$$

In this light, an approximation of the potential energy can then be viewed as a direct approximation of the probability density function of the response.

Following the standard (force-based) equivalent linearization strategy, it was proposed to model the potential $V(q)$ by the quadratic potential of a linear restoring force. A surprisingly important question that arises is the presence of a constant in the definition of the potential, i.e. assuming that $V(0) = 0$, should one try to approximate $V(q)$ by an expression of the form

$$V(q) \approx \frac{1}{2} k_{eq}\, q^2 - p_{eq}\, q + V_{eq} \tag{20}$$

or as

$$V(q) \approx \frac{1}{2} k_{eq}\, q^2 - p_{eq}\, q\,. \tag{21}$$

Practically speaking, there is no difference in the final equation of motion which are independent of a shift of the potential function. Nevertheless, as will be seen below, the approximation strategies based on Eq. (20) and (21) are different.

The modeling by Eq. (20) will be considered first. Following the discussion of the previous section, the alternate form

$$V(q) \approx a_2 \left(q - \mu_q\right)^2 + a_1 \left(q - \mu_q\right) + a_0 \tag{22}$$

will be used instead. A direct comparison Eq. (20) and (22) yields the correspondence

$$k_{eq} = 2\, a_2 \tag{23}$$

$$p_{eq} = k_{eq}\, \mu_q - a_1 \tag{24}$$

and

$$V_{eq} = a_0 + p_{eq}\, \mu_q - \frac{1}{2} \mu_q^2\,. \tag{25}$$

The coefficients a_0, a_1, and a_2 will be selected to minimize the modeling error

$$E_{\text{mod}}^{pot} = E\left\{\left[V(q) - a_2\left(q-\mu_q\right)^2 - a_1\left(q-\mu_q\right) - a_0\right]^2\right\}. \tag{26}$$

Differentiating E_{mod}^{pot} with respect to a_0, a_1, and a_2 yields the equations

$$a_2\ E\left[\left(q-\mu_q\right)^4\right] + a_1\ E\left[\left(q-\mu_q\right)^3\right] + a_0\ E\left[\left(q-\mu_q\right)^2\right] = E\left[V(q)\left(q-\mu_q\right)^2\right] \tag{27}$$

$$a_2\ E\left[\left(q-\mu_q\right)^3\right] + a_1\ E\left[\left(q-\mu_q\right)^2\right] + a_0\ E\left[\left(q-\mu_q\right)\right] = E\left[V(q)\left(q-\mu_q\right)\right] \tag{28}$$

$$a_2\ E\left[\left(q-\mu_q\right)^2\right] + a_1\ E\left[\left(q-\mu_q\right)\right] + a_0 = E\left[V(q)\right] \quad . \tag{29}$$

Simplifications of the above equations result by noting that $E\left[q-\mu_q\right]=0$ and by assuming that $E\left[\left(q-\mu_q\right)^3\right]=0$, i.e. that the distribution of the response selected for the evaluation of the moments exhibits no skewness (this is in particular the case for the Gaussian distribution corresponding to the response of the linearized equation of motion). Specifically, it is found that

$$a_1 = \frac{E\left[V(q)\left(q-\mu_q\right)\right]}{\sigma_q^2} \tag{30}$$

and the coupled equations

$$a_2\ E\left[\left(q-\mu_q\right)^4\right] + a_0\ E\left[\left(q-\mu_q\right)^2\right] = E\left[V(q)\left(q-\mu_q\right)^2\right] \tag{31}$$

$$a_2\ E\left[\left(q-\mu_q\right)^2\right] + a_0 = E\left[V(q)\right] \quad . \tag{32}$$

Combining Eq. (31) and (32) yields

$$a_2 = \frac{E\left[V(q)\left(q-\mu_q\right)^2\right] - \sigma_q^2\ E\left[V(q)\right]}{E\left[\left(q-\mu_q\right)^4\right] - \sigma_q^4}. \tag{33}$$

This equation will be further specialized to a Gaussian distribution of the response q, e.g. the one associated with the linearized equation of motion. In this case, $E\left[\left(q-\mu_q\right)^4\right]=3\,\sigma_q^4$ and Eq. (33) becomes

$$a_2=\frac{E\left[V(q)\left(q-\mu_q\right)^2\right]-\sigma_q^2\;E[V(q)]}{2\,\sigma_q^4}. \tag{34}$$

A first application of Eq. (12) to the above relation with $g(q)=V(q)\left(q-\mu_q\right)$ yields

$$a_2=\frac{1}{2\,\sigma_q^2}\left\{E\left[\frac{d\left[V(q)\left(q-\mu_q\right)\right]}{dq}\right]-E[V(q)]\right\}=\frac{1}{2\,\sigma_q^2}\left\{E\left[\frac{d[V(q)]}{dq}\left(q-\mu_q\right)\right]\right\}. \tag{35}$$

A second application of Eq. (12) with $g(q)=dV(q)/dq$ yields

$$a_2=\frac{1}{2}\left\{E\left[\frac{d^2[V(q)]}{dq^2}\right]\right\}. \tag{36}$$

Proceedings similarly with Eq. (30) and $g(q) = V(q)$ leads to

$$a_1=E\left[\frac{dV(q)}{dq}\right]. \tag{37}$$

Noting that $\frac{dV(q)}{dq}=f(q)$, it is seen that Eq. (36) and (37) in fact reduce to Eq. (10) and (13) so that this version of the potential energy-based equivalent linearization is in fact identical to the standard, force-based approach.

What about the modeling of Eq. (21), i.e. if we require both potentials to vanish at the undeformed position? Since a direct rewriting of Eq. (21) in the form of Eq. (22) is possible only with the imposition of constraints on the coefficients a_0, a_1, and a_2, it is actually easier to proceed with the original form of Eq. (21). Then, the coefficients k_{eq} and p_{eq} are the selected to minimize the modeling error

$$E_{\text{mod}=}^{pot} E\left\{\left[V(q)-\frac{1}{2}k_{eq}\ q^2-p_{eq}\ q\ \right]^2\right\}. \tag{38}$$

That is, such that

$$k_{eq}\ E\left[q^4\right]+\ p_{eq}\ E\left[q^3\right]=E\left[V(q)\,q^2\right] \tag{39}$$

$$k_{eq}\ E\left[q^3\right]+\ p_{eq}\ E\left[q^2\right]=E\left[V(q)\,q\right]\ \ . \tag{40}$$

Combining these relations with Eq. (16) and (17) and expressing all moments in terms of the mean μ_q and variance σ_q^2 using for example the Gaussian model of the response of the linearized equation of motion yields a system of 2 nonlinear equations in the two unknowns μ_q and σ_q^2. In the present case, i.e. with $f(q)$ defined by Eq. (2) and

$$V(q)=\frac{1}{2}\omega_0^2\ (1-s)\,q^2+\frac{\gamma}{4}q^4-\overline{p}_0\ q\,, \tag{41}$$

it is found after a series of algebraic manipulations that Eq. (39) and (40) take the form

$$\begin{aligned}\frac{\gamma}{4}\left(15\,\sigma_q^4\ \mu_q+10\,\sigma_q^2\ \mu_q^3+\mu_q^5\right)+\frac{1}{2}\left(\omega_0^2\ (1-s)-\frac{\pi\,S_{\overline{p}\overline{p}}}{2\,\zeta\,\omega_0\ \sigma_q^2}\right)\left(3\,\sigma_q^2\ \mu_q+\mu_q^3\right)\\ +\left(\frac{\pi\,S_{\overline{p}\overline{p}}\ \mu_q}{2\,\zeta\,\omega_0\ \sigma_q^2}-\overline{p}_0\right)\left(\sigma_q^2+\mu_q^2\right)=0\end{aligned} \tag{42}$$

and

$$\begin{aligned}\frac{\gamma}{4}\left(15\,\sigma_q^6+45\,\sigma_q^4\ \mu_q^2+15\,\sigma_q^2\ \mu_q^4+\mu_q^6\right)+\frac{1}{2}\left(\omega_0^2\ (1-s)-\frac{\pi\,S_{\overline{p}\overline{p}}}{2\,\zeta\,\omega_0\ \sigma_q^2}\right)\left(3\,\sigma_q^4+6\,\sigma_q^2\ \mu_q^2+\mu_q^4\right)\\ +\left(\frac{\pi\,S_{\overline{p}\overline{p}}\ \mu_q}{2\,\zeta\,\omega_0\ \sigma_q^2}-\overline{p}_0\right)\left(3\,\sigma_q^2\ \mu_q+\mu_q^3\right)=0\end{aligned} \tag{43}$$

The following linear combination of Eq. (42) and (43)

$$\frac{5\,\gamma}{4}\left(3\,\sigma_q^4+6\,\sigma_q^2\,\mu_q^2+\mu_q^4\right)+\frac{3}{2}\left(\omega_0^2\,(1-s)-\frac{\pi\,S_{\overline{pp}}}{2\,\zeta\,\omega_0\,\sigma_q^2}\right)\left(\sigma_q^2+\mu_q^2\right)+2\left(\frac{\pi\,S_{\overline{pp}}\,\mu_q}{2\,\zeta\,\omega_0\,\sigma_q^2}-\overline{p}_0\right)\mu_q=0 \tag{44}$$

can also be used as a somewhat simpler alternative to Eq. (43).

The assessment of this potential-based equivalent linearization was achieved in the absence of thermal moment terms, i.e. with $\overline{p}_0=0$. Accordingly, as discussed in the Phase I report, there exist typically two linear equivalent systems to be considered: the one corresponding to motions around the buckled states (low *SPL*), i.e. with $\mu_q\neq 0$, and the one modeling the frequent snap-through motions (high *SPL*), i.e. with $\mu_q=0$.

The determination of the nonzero mean μ_q and the variance σ_q^2 can be accomplished directly from Eq. (41) and (44) but a small additional simplification of these equations can be achieved. Indeed, proceeding with a linear combination of these relations leads to

$$\gamma\left(5\,\sigma_q^2\,\mu_q^2+\mu_q^4\right)+\omega_0^2\,(1-s)\,\mu_q^2=\frac{\pi\,S_{\overline{pp}}}{2\,\zeta\,\omega_0} \tag{45}$$

which represents a quadratic equation for μ_q^2 in terms of σ_q^2 and so does Eq.(44). Then, eliminating the terms in μ_q^4 from Eq. (44) and (45) yields

$$\mu_q^2=\frac{\sigma_q^2\left[\dfrac{\pi\,S_{\overline{pp}}}{2\,\zeta\,\omega_0}-6\,\omega_0^2\,(1-s)\,\sigma_q^2-15\,\gamma\,\sigma_q^4\right]}{\left[\dfrac{\pi\,S_{\overline{pp}}}{\zeta\,\omega_0}+\omega_0^2\,(1-s)\,\sigma_q^2+5\,\gamma\,\sigma_q^4\right]}. \tag{46}$$

Finally, inserting this expression for μ_q^2 in Eq. (44) leads to a sixth order equation for σ_q^2. The evaluation of the nonzero mean μ_q and the variance σ_q^2 proceeds from the solution of Eq. (44) and (45).

To characterize the response at high sound pressure levels when snap-throughs are frequent, the zero mean value solution is more appropriate. The corresponding variance can be determined from Eq. (44), i.e.

$$\frac{15}{4}\,\gamma\,\sigma_q^4 + \frac{3}{2}\,\omega_0^2\,(1-s)\,\sigma_q^2 - \frac{3\,\pi\,S_{\overline{pp}}^{--}}{4\,\zeta\,\omega_0} = 0 \tag{47}$$

that is

$$\sigma_q^2 = \frac{1}{5\,\gamma}\left[\sqrt{\omega_0^4\,(1-s)^2 + 5\,\gamma\,\frac{\pi\,S_{\overline{pp}}^{--}}{\zeta\,\omega_0}} - \omega_0^2\,(1-s)\right]. \tag{48}$$

It is interesting to compare this result with its counterpart obtained in connection with the force-based equivalent linearization technique. In the Phase I report, it was found that the variance of the zero mean response was expressed as

$$\sigma_q^2 = \frac{1}{6\,\gamma}\left[\sqrt{\omega_0^4\,(1-s)^2 + 6\,\gamma\,\frac{\pi\,S_{\overline{pp}}^{--}}{\zeta\,\omega_0}} - \omega_0^2\,(1-s)\right] \tag{49}$$

so that the only difference between the two predictive expressions for the variance is the factor $6\,\gamma$ in Eq. (49) (force-based approach) vs. $5\,\gamma$ in Eq. (48) (potential-based approach). This difference is consistent with the results of Muravyov et al. (1999) where it was noted that the expressions obtained for the equivalent stiffness in the two methods where identical except for a transformation $3\,\gamma \rightarrow 2.5\,\gamma$.

To assess how well the potential energy-based equivalent linearization performs in relation to its force-based counterpart, the titanium panel of Phase I was reconsidered here with s = 1.8 and values of the sound pressure level ranging in the domain 94-134 dB. A large discrepancy between the two approaches was observed in the low *SPL* range: while the force-based method yielded a variance similar to the Monte Carlo simulations, the above potential energy-based technique overestimated this moment by a factor of 4. This difference of behavior can be predicted from Eq. (44). Indeed, in the limit of $S_{\overline{pp}}^{--} \rightarrow 0$, Eq. (44) yields

$$\sigma_q^2 \approx -\frac{2}{\omega_0^2\,(1-s)}\;\frac{\pi\,S_{pp}^{--}}{2\,\zeta\,\omega_0} \tag{50}$$

while a similar analysis of the force-based equivalent linearization leads to the perturbation solution

$$\sigma_q^2 \approx -\frac{1}{2\,\omega_0^2\,(1-s)}\;\frac{\pi\,S_{pp}^{--}}{2\,\zeta\,\omega_0}. \tag{51}$$

The poor accuracy of the above potential energy-based equivalent linearization approach at low sound pressure level is somewhat mitigated by a slight improvement in accuracy of the variance estimate (Eq. (48)) at high excitation levels, see Table 1. Note however that the improvement is small in the infrequent-to-frequent snap-through transition zone, i.e. around *SPL* = 124 dB, where the error of the force-based equivalent linearization approach is by far the largest. The failure of both force- and potential energy-based approaches in this range of sound pressure levels should not be too surprising: it is symptomatic of the strongly nonlinear features of the corresponding response which cannot accurately be modeled by any linearized model.

	SPL = 124 dB	*SPL* = 134 dB
Monte Carlo Simulations	0.4137	0.5618
Variable Mean Formulations		
Force-Based E.L.; Eq. (49)	0.3308	0.5012
Potential Energy-Based E.L.; Eq. (48)	0.3534	0.5283
Fixed Mean Formulations		
Force-Based E.L.; see Phase I report	0.4794	0.5996
Potential Energy-Based E.L.; Eq. (59)	0.5269	0.6068

Table 1. Displacement variance estimates obtained by Monte Carlo simulations and the force- and potential energy-based equivalent linearization approaches, *s* = 1.8, *SPL* = 124 dB and 134 dB, one mode model, Eq. (1)-(2), isotropic panel of Phase I.

2.1.3 Fixed Mean Equivalent Linearization Strategies

Equivalent linearization strategies with fixed mean values, $\mu_q = Q_i$, can also be developed as above but Eq. (14) is imposed as an a-priori constraint on the minimization of E_{mod} and E_{mod}^{pot}. Accordingly, the three following equivalent linearization strategies can be formulated:

force-based equivalent linearization: minimize, with respect to k_{eq}, the modeling error

$$E_{\text{mod}} = E\left\{\left[f(q) - k_{eq}\,(q - Q_i)\right]^2\right\} \tag{52}$$

potential energy-based equivalent linearization with unspecified zero level: minimize, with respect to $a_2 = \frac{1}{2}k_{eq}$ and a_0, the modeling error

$$E_{\text{mod}}^{pot} = E\left\{\left[V(q) - a_2\,(q - Q_i)^2 - a_0\right]^2\right\} \tag{53}$$

potential energy-based equivalent linearization with specified zero level: minimize, with respect to k_{eq}, the modeling error

$$E_{\text{mod}}^{pot} = E\left\{\left[V(q) - \frac{1}{2}k_{eq}\,q^2 - k_{eq}\,Q_i\,q\right]^2\right\}. \tag{54}$$

Consider first the force-based equivalent linearization method. Differentiating Eq. (52) with respect to k_{eq} leads to

$$k_{eq} = \frac{E\left[f(q)(q - Q_i)\right]}{\sigma_q^2} = E\left[\frac{df(q)}{dq}\right] \tag{55}$$

where the last equality results from the application of Eq. (12) with $g(q) = f(q)$. By comparison with the results from the previous section, it is seen that the specification of the mean has not changed the definition of the equivalent stiffness, compare Eq. (13) and (55).

Proceeding next with the potential energy-based equivalent linearization of Eq. (53), it should be noted that this minimization problem is identical to the one of Eq. (26) except for the constraint $a_1 = 0$. The minimization of E_{mod}^{pot} with respect to $a_2 = \frac{1}{2} k_{eq}$ and a_0, thus yields Eq. (27) and (29) in which the coefficients a_1 should be set to zero. However, the terms involving this parameter do disappear from these two equations, see Eq. (31) and (32), so that the definition of a_2 (see Eq. (36)) and a_0 for the fixed mean case are the same as those presented for the variable mean.

From the above findings and the results of the previous section it can then be argued that the force-based and potential energy-based (unspecified level) equivalent linearization strategies are identical to each other in both variable and fixed mean cases.

In this light, it remains then to assess the last approach, i.e. the minimization of Eq. (54). Differentiating E_{mod}^{pot}, Eq. (54), with respect to k_{eq} yields

$$k_{eq} = \frac{E\left[V(q)\left(\frac{1}{2} q^2 - Q_i\, q\right)\right]}{E\left[\left(\frac{1}{2} q^2 - Q_i\, q\right)^2\right]}. \tag{56}$$

For the potential energy of Eq. (41), one finds

$$k_{eq} = \frac{\omega_0^2\,(1-s)\,E\left[q^2\left(q^2 - 2\,Q_i\,q\right)\right] + \frac{\gamma}{2} E\left[q^4\left(q^2 - 2\,Q_i\,q\right)\right] - 2\,\overline{p}_0\,E\left[q\left(q^2 - 2\,Q_i\,q\right)\right]}{3\,\sigma_q^4 - 2\,Q_i^2\,\sigma_q^2 + Q_i^4} \tag{57}$$

Evaluating the various expected values in terms of the mean Q_i and variance σ_q^2 and using Eq. (15), it is found that

$$\begin{aligned} &\omega_0^2\,(1-s)\left(3\,\sigma_q^4 - Q_i^4\right) + \frac{\gamma}{2}\left(5\,\sigma_q^6 + 15\,\sigma_q^4\,Q_i^2 - 5\,\sigma_q^2\,Q_i^4 - Q_i^6\right) \\ &- 2\,\overline{p}_0\left(\sigma_q^2\,Q_i - Q_i^3\right) = \frac{\pi\,S_{\overline{pp}}}{2\,\zeta\,\omega_0\,\sigma_q^2}\left(3\,\sigma_q^4 - 2\,Q_i^2\,\sigma_q^2 + Q_i^4\right) \end{aligned}. \tag{58}$$

Finally, regrouping terms of similar power in σ_q^2 yields the fourth order equation

$$\frac{5\,\gamma}{2}\,\sigma_q^8 + \left[\frac{15\,\gamma}{2}\,Q_i^2 + 3\,\omega_0^2\,(1-s)\right]\sigma_q^6 - \left[\frac{5\,\gamma}{2}\,Q_i^4 + 2\,\overline{p}_0\,Q_i + \frac{3\,\pi\,S_{\dot{p}\dot{p}}^{--}}{2\,\zeta\,\omega_0}\right]\sigma_q^4$$
$$-\left[\frac{\gamma}{2}\,Q_i^6 + \omega_0^2\,(1-s)\,Q_i^4 - 2\,\overline{p}_0\,Q_i^3 - \frac{\pi\,S_{\dot{p}\dot{p}}^{--}}{\zeta\,\omega_0}\,Q_i^2\right]\sigma_q^2 - \frac{\pi\,S_{\dot{p}\dot{p}}^{--}}{2\,\zeta\,\omega_0}\,Q_i^4 = 0 \quad . \tag{59}$$

The assessment of the accuracy of this procedure has first revealed the same deficiency as its variable mean counterpart, i.e. an overestimation of the variance in the low *SPL* range by a factor of 4 with respect to Monte Carlo simulations results. This behavior is predictable from Eq. (59) which, in the limit $S_{\dot{p}\dot{p}}^{--} \to 0$, yields

$$\sigma_q^2 \approx -\frac{2}{\omega_0^2\,(1-s)}\,\frac{\pi\,S_{\dot{p}\dot{p}}^{--}}{2\,\zeta\,\omega_0} \tag{60}$$

as already obtained in Eq. (50).

In the high *SPL* range, it is seen from Table 1 that the fixed mean potential energy-based equivalent linearization method with specified zero level yields an even larger overprediction of the variance as compared to the corresponding force-based approach.

Combining the observations obtained at both low and high sound pressure levels, it is then concluded that the fixed mean potential energy-based equivalent linearization method with specified zero level does not appear to have any accuracy advantage, at the contrary, over the similar force-based technique.

2.1.4 Potential Energy-Based Equivalent Linearization Strategies - Summary

The results of the previous sections have demonstrated that there is not a single potential energy-based equivalent linearization technique but rather a class of such methods which differ from each other by the treatment of the constant in the potentials. Quite surprisingly, different choices imply quite different linearized systems although that constant does not per say enter the linearized equation of motion.

It was demonstrated that the potential energy-based approach in which the constant in the potential is part of the minimization problem and is selected to achieve the minimum of the modeling error is identical to the standard force-based technique.

A different approach was also formulated in which the constant is selected as to yield a zero potential for the undeformed panel. The results of this technique, with both unknown (section 1.1.1) and fixed mean (section 1.1.2), were not satisfactory in the low sound pressure level range as the variance of the motions around the buckled state predicted by this equivalent linearization formulation was 4 times too large.

At high sound pressure levels, however, the corresponding approximation of the variance was found to match slightly better the simulation results than the estimate obtained by the force-based equivalent linearization when considering the variable mean formulation. At the contrary, the fixed mean potential energy-based approach performed significantly worse than its force-based counterpart.

It is concluded from this entire set of observations that the potential energy-based formulation does not appear to provide any significant improvement over the force-based strategy and can, in fact, yield substantially worse results. On this basis, the force-based equivalent linearization technique will be retained, until further notice, as the estimation technique of the mean and variance of the system displacements.

2.2 Assessment of Force-Based Equivalent Linearization Strategies in the Presence of Thermal Moments

The application of the force-based equivalent linearization strategy to the acoustic response of thermally buckled panel has been presented in detail in the Phase I report. However, the assessment of this approach had been limited to cases in which no thermal moment was present, i.e. with $\overline{p}_0 = 0$ in Eq. (2). To demonstrate the general

applicability of the equivalent linearization technique, it was necessary to also investigate cases with thermal moments, i.e. with $\overline{p}_0 \neq 0$ in Eq. (2). In this connection, note that the term $\overline{p}_0$ creates an asymmetry in the problem so that the motions around the two buckled states cannot be considered as identical to each other. In fact, the presence of two buckled states is no longer guaranteed! The corresponding positions Q_i satisfy the condition $f(Q_i) = 0$ or

$$\omega_0^2 (1-s) Q_i + \gamma Q_i^3 = \overline{p}_0 \tag{61}$$

which yields either one or three real roots. A single real root is obtained for $\overline{p}_0$ outside of the domain $[-p_L , p_L]$ where

$$p_L = \sqrt{\frac{-4 \omega_0^6 (1-s)^3}{27 \gamma}} . \tag{62}$$

In such cases, the bimodal character of the response probability density function can be expected to be lost.

The lack of symmetry of the response implies the need to revisit the combination of estimates taking place at low *SPL* in the equivalent linearization technique #1 (variable mean) and for all excitation levels in the equivalent linearization technique #2 (mean fixed to the buckled states). Specifically, the conditional arguments developed in the Phase I report still hold, i.e.

$$\mu_q = E[q] = q_1 \mu_{q_2} + q_2 \mu_{q_2} \tag{63}$$

and

$$E\left[q^2\right] = q_1\left(\sigma_{q_1}^2 + \mu_{q_1}^2\right) + q_2\left(\sigma_{q_2}^2 + \mu_{q_2}^2\right) \tag{64}$$

$$\sigma_q^2 = q_1\left(\sigma_{q_1}^2 + \mu_{q_1}^2\right) + q_2\left(\sigma_{q_2}^2 + \mu_{q_2}^2\right) - \left(q_1 \mu_{q_1} + q_2 \mu_{q_2}\right)^2 \tag{65}$$

where μ_{q_1} and σ_{q_1} (resp. μ_{q_2} and σ_{q_2}) are the mean and variance of q given that the panel responds around the top (resp. bottom) buckling position. Further, q_1 and q_2 denote the probabilities that the response exhibits motions around the top and bottom

bucked states, respectively, and $q_1 \neq q_2$ for $\bar{p}_0 \neq 0$. The evaluation of these probabilities requires a phenomenological approximation of the response. Specifically, a one-step Markov chain model will be assumed here in which the probability of the response exiting the domains $q \approx Q_i$ is given by the transition (snap-throughs) probabilities

$$p_{12} = \text{Prob}\left[q \approx Q_1 \rightarrow q \approx Q_2\right] \tag{66}$$

and

$$p_{21} = \text{Prob}\left[q \approx Q_2 \rightarrow q \approx Q_1\right] \tag{67}$$

Once a transition (snap-through) has had an opportunity to happen, the probability for the response to be in the neighborhood of the buckling state Q_1 (resp. Q_2) has become

For Q_1: $$q_1(1-p_{12}) + q_2 p_{21} \tag{68}$$

For Q_2: $$q_2(1-p_{21}) + q_1 p_{12} \tag{69}$$

Since the response process is stationary, these two probabilities must still equal q_1 and q_2 respectively so that

$$q_1(1-p_{12}) + q_2 p_{21} = q_1 \tag{70}$$

$$q_1 + q_2 = 1 \tag{71}$$

or

$$q_1 = \frac{p_{21}}{p_{12} + p_{21}} \qquad \text{and} \qquad q_2 = \frac{p_{12}}{p_{12} + p_{21}} \tag{72}$$

The evaluation of p_{12} and p_{21} in terms of μ_{q_1}, σ_{q_1}, μ_{q_2}, and σ_{q_2} is now required to complete the process. It can be argued (see Phase I report for a related discussion) that these probabilities are associated with the exit from the potential wells of the buckled states so that

$$p_{12} = \exp\left[-\frac{(R_1 - \mu_{q_1})^2}{2\sigma_{q_1}^2}\right] \tag{73}$$

$$p_{21} = \exp\left[-\frac{(R_2 - \mu_{q_2})^2}{2\sigma_{q_2}^2} \right] \tag{74}$$

where $R_1 > Q_1$ and $R_2 < Q_2$ are the values of q at which the potential energy equals that of the unstable third equilibrium position Q_3, i.e.

$$V(R_i) = V(Q_3) \qquad i = 1,2 \tag{75}$$

Equations (63), (65), (72)-(75) are applicable to both equivalent linearization techniques as long as two mean values μ_{q_1}, μ_{q_2} are obtained.

In the absence of experimental data, the assessment of the equivalent linearization technique with $\bar{p}_0 \neq 0$ was limited to the analysis of the composite panel of Phase I with $\bar{p}_0 = 0.85 p_L$. Many of the computational issues discussed in connection with $\bar{p}_0 = 0$ were again encountered, but their resolution was generally less obvious. In particular, the discrimination of the bona fide mean values μ_q for the equivalent linearization #1 from the spurious (non-physical) ones was more challenging. These values are the solutions of (see Phase I report for derivation)

$$2\gamma^2 \mu_q^6 + 2\gamma\omega_0^2 (1-s)\mu_q^4 - \bar{p}_0 \gamma \mu_q^3 + 3\gamma \left(\frac{\pi S_{\bar{p}\bar{p}}}{2\zeta\omega_0} \right) \mu_q^2 + \bar{p}_0 \omega_0^2 (1-s)\mu_q - \bar{p}_0^2 = 0 . \tag{76}$$

It was found that the number of real roots for $\bar{p}_0 \neq 0$ did not decrease from 5 to 1 as seen for $\bar{p}_0 = 0$ but rather from 4 down to 2 at the sound pressure level of 112dB. Further, one of these two mean values yielded a fictitious negative variance and thus had to be eliminated. The remaining value of μ_q did not seem to capture the physics very well as the time histories of the displacement for *SPL* ≥ 112dB still appeared to exhibit a bimodal character. This observation was reflected by a rather poor matching between estimated and true values of the mean and standard deviation of the response. According, it was concluded that a second solution still had to be used for *SPL* ≥ 112dB. This finding did

seem to conflict with the case $\bar{p}_0 = 0$ for which only $\mu_q = 0$ is used at large *SPL* for the equivalent linearization approach #1. However, it should be restated that this mean value is in effect a *double* root of Eq. (76) so that two (identical for $\bar{p}_0 = 0$) mean values were in fact used. Which other mean value estimate should then be considered?

To address this issue, the equivalent linarization technique #2 was revisited and it was noted that the mean values it relies upon (i.e. Q_1 and Q_2) do in fact correspond to the mean values estimated by the equivalent linearization technique #1 in the limit $SPL \to -\infty$. On this basis, it was decided to use for the equivalent linearization method #1 with $\bar{p}_0 \neq 0$ and large *SPL*, a second mean value μ_{q_2} that equals its value for the critical *SPL* (112dB here) at which the number of roots decreases from 4 to 2. Thus, μ_{q_2} stays constant for *SPL* $\geq$ 112dB and its associated variance can be evaluated as in equivalent linearization #2 with Q_i replaced by μ_{q_2}.

To estimate the critical value of the sound pressure level, note that the disappearance of real, nonzero mean values of Eq. (76) has been observed, for both $\bar{p}_0 = 0$ and $\bar{p}_0 \neq 0$, to be as follows: as the *SPL* increases, two real roots approach each other and split into a complex conjugate pair right after becoming a double root. Accordingly, the critical value of the sound pressure level is such that a double root exists for the equivalent linearization mean. This solution then satisfies not only Eq. (76) but also its partial derivative with respect to μ_{q_1}, i.e.

$$12\,\gamma^2\mu_q^5 + 8\,\gamma\,\omega_0^2(1-s)\mu_q^3 - 3\bar{p}_0\,\gamma\,\mu_q^2 + 6\,\gamma\left(\frac{\pi\,S_{\bar{p}\bar{p}}}{2\,\zeta\,\omega_0}\right)\mu_q + \bar{p}_0\,\omega_0^2(1-s) = 0\,. \quad (77)$$

Eliminating $S_{\bar{p}\bar{p}}$ from Eq. (76) and (77) yields

$$8\,\gamma^2\mu_q^6 + 4\,\gamma\,\omega_0^2(1-s)\mu_q^4 - \bar{p}_0\,\gamma\,\mu_q^3 - \bar{p}_0\,\omega_0^2(1-s)\mu_q + 2\bar{p}_0^2 = 0\,. \quad (78)$$

Then, the appropriate μ_{q_2} for large *SPL* is the real solution of Eq. (78) that gives identical values of $S_{\overline{p}\,\overline{p}}$ as computed from Eq. (76) and Eq. (77).

For clarity, the above procedure was named equivalent linearization technique #3 and can be summarized as follows: for given values of $\overline{p}_0$ and the sound pressure level *SPL*, the roots of Eq. (76) are obtained and their corresponding variance estimated as in the Phase I report. The values of μ_{q_1} and μ_{q_2} are then obtained as the roots closest to Q_1 and Q_2 respectively, that yield positive values of $\sigma^2_{q_1}$ and $\sigma^2_{q_2}$. If only one such solution is found, an alternate μ_{q_2} (or μ_{q_1}) is obtained from Eq. (78). As a check, the selected value of the sound pressure level should exceed the value obtained from either Eq. (76) or (77) for that value of μ_q. Finally, the values of μ_{q_1}, μ_{q_2}, σ_{q_1}, and σ_{q_2} are used to compute μ_q and σ^2_q according to Eq. (63), (65), (72)-(75).

The results of this complicated, but physical, effort are shown in Fig. 1 and 2. In a fairly close parallel to the case $\overline{p}_0 = 0$, it is found that equivalent linearization #3 is very accurate for low *SPL* but that its accuracy decreases (especially for the mean value) past the critical value (*SPL* = 112dB) even with the addition of the second root μ_{q_2}.

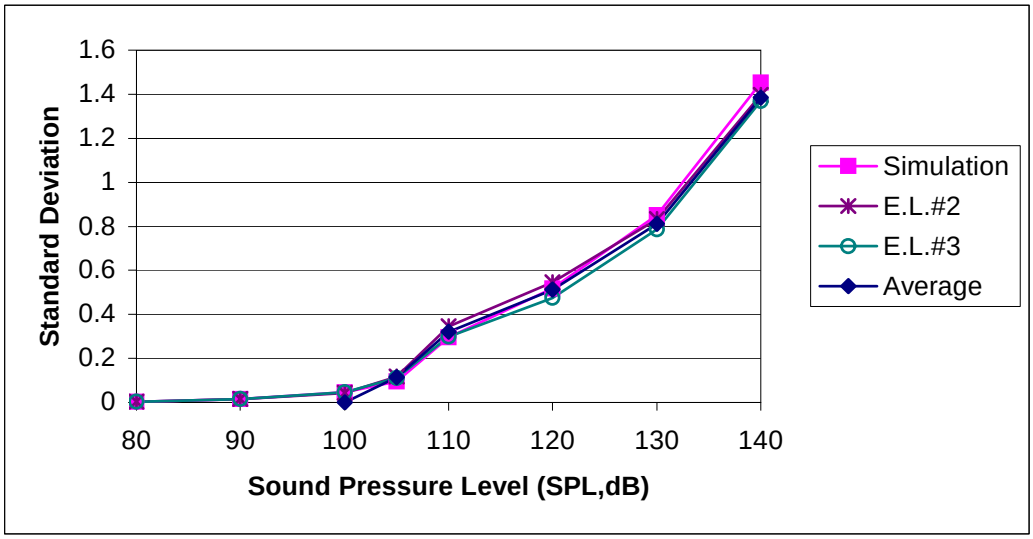

Figure 1. Standard Deviation of the Response as Function of the Sound Pressure Level Obtained by Simulation and by the Equivalent Linearization Strategies #2 and #3 and their Average for s=1.8 and $\overline{p}_0 = 0.85 p_L$, Simply-Supported Composite Plate.

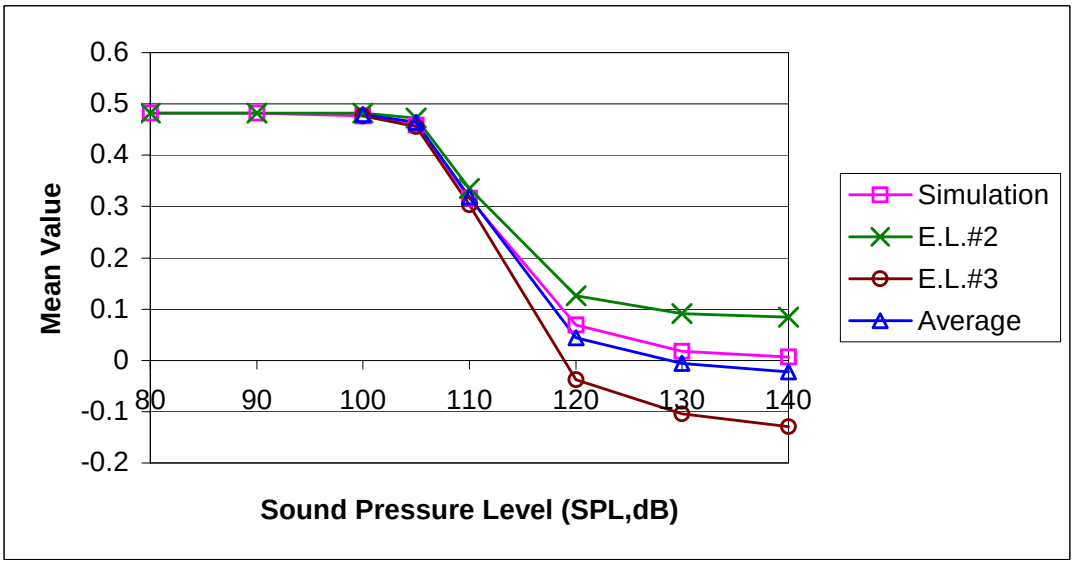

Figure 2. Mean Value of the Response as Function of the Sound Pressure Level Obtained by Simulation and by the Equivalent Linearization Strategies #2 and #3 and their Average for s=1.8 and $\overline{p}_0 = 0.85 p_L$, Simply-Supported Composite Plate.

Equivalent linearization #2 exhibits similar characteristics but the average of the estimates of the equivalent linearization techniques #2 and #3 yields very good approximations of both mean value and standard deviation for sound pressure levels exceeding the critical value (*SPL*=112dB here).

2.3 Force-Based Equivalent Linearization - General Formulation

Given the successes of the force-based equivalent linearization technique, see Phase I report and the current results (i.e. Fig. 1 and 2), and the unclear benefits of its potential-energy based alternative, it is currently planned to proceed with the force-based approach in the present Phase II efforts. Accordingly, it is necessary to formulate the corresponding variable and fixed mean equivalent linearization techniques. To this end, let the N nonlinear equations of motion of the system be expressed as

$$M\ \underline{\ddot{w}} + C\ \underline{\dot{w}} + \underline{K}_{NL} = \underline{F}_0 + \underline{F}(t) \tag{79}$$

where $\underline{w}$ is the displacement vector (in-plane and out-of-plane components) and M and C denote the constant $N \times N$ mass and damping matrices. Further, $\underline{K}_{NL}$ is the vector of nonlinear restoring forces the elements of which can be expressed as

$$\left(\underline{K}_{NL}\right)_i = \sum_{j=1}^{N} K_{ij}^{(1)}\ w_j + \sum_{j,l=1}^{N} K_{ilj}^{(2)}\ w_l\ w_j + \sum_{j,l,p=1}^{N} K_{iljp}^{(3)}\ w_l\ w_j\ w_p\,. \tag{80}$$

Finally, $\underline{F}_0$ and $\underline{F}(t)$ denote the constant (e.g. thermal moment effects) and zero mean random (e.g. acoustic excitation) forces acting on the system.

It is desired to replace the set of nonlinear differential equations of Eq. (79)-(80) by linearized ones of the form

$$M\ \underline{\ddot{w}} + C\ \underline{\dot{w}} + K_{eq}\ \underline{w} = \underline{F}_{eq} + \underline{F}(t) \tag{81}$$

where K_{eq} and $\underline{F}_{eq}$ are the $N \times N$ equivalent stiffness matrix and N-component equivalent constant force vector, respectively. In the present force-based equivalent linearization strategy, this matrix and vector will be determined by requiring the minimization of the modeling error

$$E_{\text{mod}} = E\left[\left|\underline{K}_{NL} - \underline{F}_0 - K_{eq}\ \underline{w} + \underline{F}_{eq}\right|^2\right] \tag{82}$$

where $\left|\underline{x}\right|^2 = \underline{x}^T\ \underline{x}$ is the squared norm of an arbitrary vector $\underline{x}$ with the superscript ^{T} denoting the operation of matrix transposition.

In the equivalent linearization technique #1, the matrix K_{eq} and the vector $\underline{F}_{eq}$ are independently selected to minimize E_{mod}, Eq. (82). The result of this minimization is (see Eq. (10) and (13) and Lutes and Sarkani, 1997)

$$\left(K_{eq}\right)_{ij} = E\left[\frac{\partial K_{NL,i}}{\partial w_j}\right] \tag{83}$$

and

$$\underline{F}_{eq} = \underline{F}_0 - E\left[\underline{K}_{NL}\right] + K_{eq}\ E\left[\underline{w}\right] \quad . \tag{84}$$

Consistently with the single mode effort, the expected values of the displacement vector will be determined by using the response of the linearized system, i.e. under the assumption of a Gaussian stationary process. Then, combining Eq. (80), (83), and (84), it is found that

$$\left(K_{eq}\right)_{ij} = K_{ij}^{(1)} + \sum_{l=1}^{N}\left[K_{ilj}^{(2)} + K_{ijl}^{(2)}\right]\mu_l + \sum_{l,p=1}^{N}\left[K_{iljp}^{(3)} + K_{ijlp}^{(3)} + K_{ilpj}^{(3)}\right]\left(\sigma_{lp} + \mu_l\ \mu_p\right) \tag{85}$$

and

$$\begin{aligned}\left(F_{eq}\right)_i = \left(F_0\right)_i + \sum_{j=1}^{N}\left[\left(K_{eq}\right)_{ij} - K_{ij}^{(1)}\right]\mu_j - \sum_{j,l=1}^{N} K_{ilj}^{(2)}\left(\sigma_{lj} + \mu_l\ \mu_j\right) \\ - \sum_{j,l,p=1}^{N} K_{iljp}^{(3)}\left(\mu_p\ \sigma_{lj} + \mu_l\ \sigma_{jp} + \mu_j\ \sigma_{lp} + \mu_p\ \mu_l\ \mu_j\right)\end{aligned} \quad . \tag{86}$$

where $\mu_l = E\left[w_l\right]$ and $\sigma_{lj} = E\left[\left(w_l - \mu_l\right)\left(w_j - \mu_j\right)\right]$ are the elements of the mean vector and covariance matrix of the response of the linearized system, Eq. (81).

The equivalent linearization technique #2 rests on the assumption that the mean vector $\underline{\mu}$ is fixed, e.g. equal to the buckled states $\underline{w}_{buck}$ for which $\underline{K}_{NL} = \underline{F}_0$. Then, the vector $\underline{F}_{eq}$ can no longer be treated as an independent variable in the minimization of Eq. (82). Rather, it is needed to enforce the constraint

$$\underline{F}_{eq} = K_{eq}\ \underline{\mu} \tag{87}$$

which is most conveniently accomplished by rewriting Eq. (82) as

$$E_{\text{mod}} = E\left[\left| \underline{K}_{NL} - \underline{F}_0 - K_{eq} \left(\underline{w} - \underline{\mu} \right) \right|^2 \right]. \tag{88}$$

The minimization of E_{mod} with respect to the elements of the matrix K_{eq} yields again Eq. (83) so that Eq. (85) also applies in equivalent linearization #2 but with $\underline{\mu}$ specified.

To complete the formulation of the equivalent linearization techniques, it remains to evaluate the statistics of the response of the linear system, Eq. (81). Clearly, the mean value is obtained by solving Eq. (87) for both equivalent linearization schemes. To estimate the covariance matrix

$$\sigma = E\left[\left(\underline{w} - \underline{\mu} \right) \left(\underline{w} - \underline{\mu} \right)^T \right] , \tag{89}$$

it will be assumed that the random force vector can be represented as the output to white noise input ($\underline{S}$) of the auxiliary system

$$\dot{\underline{G}} + H \, \underline{G} = \underline{S} \tag{90}$$

where the vector $\underline{G}$ can be partitioned as $\underline{G}^T = \left[\underline{F}^T \;\; \underline{E}^T \right]$ with $\underline{E}$ a vector of internal states. This representation covers a very broad class of Gaussian vector processes (see Wiener and Masani 1957, 1958, in the discrete case) as the dimension of $\underline{G}$, n_G, tends to infinity. For a finite value of n_G, the matrix H can be selected so that the corresponding spectral matrix of the forces $S_{\underline{F}\,\underline{F}}(\omega)$ obtained as

$$S_{\underline{F}\,\underline{F}}(\omega) = \hat{I} \left[H + i \, \omega \, I_{n_G} \right] S_0 \left[H - i \, \omega \, I_{n_G} \right]^T \hat{I}^T \tag{91}$$

matches "at best" a specified target expression $\hat{S}_{\underline{F}\,\underline{F}}(\omega)$. In the above expression, I_p is the $p \times p$ identity matrix, S_0 is the constant spectral matrix of the white noise process $\underline{S}(t)$, and $\hat{I}$ is the constant $N \times n_G$ matrix that extracts the forces $\underline{F}(t)$ from the vector $\underline{G}(t)$, i.e.

$$\underline{F}(t) = \hat{I} \, \underline{G}(t) \quad \text{and} \quad \hat{I} = \left[I_N \;\; 0 \right]. \tag{92}$$

The equations of motion of the linearized system, Eq. (81), and Eq. (90) can be combined in the first order form

$$\dot{\underline{U}} + P\,\underline{U} = \underline{Q} \tag{93}$$

where

$$\underline{U}^T = \left[\underline{w}^T \quad \dot{\underline{w}}^T \quad \underline{G}^T\right] \tag{94}$$

$$P = \begin{bmatrix} 0_N & -I_N & 0_N \\ M^{-1}K_{eq} & M^{-1}C & -M^{-1}\hat{I} \\ 0_N & 0_N & H \end{bmatrix} \tag{95}$$

$$\underline{Q}^T = \left[\underline{0}^T \quad \underline{0}^T \quad \underline{S}^T\right] . \tag{96}$$

Given the state space representation of Eq. (93), the covariance matrix $K_{\underline{U}\underline{U}}$ of the vector process $\underline{U}$ is readily determined as the solution of the Lyapunov equation (see Lutes and Sarkani, 1997)

$$P\,K_{\underline{U}\underline{U}} + K_{\underline{U}\underline{U}}\,P^T = 2\,\pi\,\hat{S}_0 \tag{97}$$

where $\hat{S}_0$ is the spectral matrix of the white noise process $\underline{Q}(t)$, that is

$$\hat{S}_0 = \begin{bmatrix} 0 & 0 & 0 \\ 0 & 0 & 0 \\ 0 & 0 & S_0 \end{bmatrix}. \tag{98}$$

Finally, the covariance matrix of the displacements, σ of Eq. (89), represents the top left $N \times N$ block of $K_{\underline{U}\underline{U}}$.

A comparison of the above multi-degree-of-freedom formulation with its single mode counterpart provides a better overall perspective: Eq. (83) and (84) provide the definition of the equivalent linear system given the response statistics as Eq. (13) and (10) did in the single mode case. Further, Eq. (90)-(98) yield the response statistics given the equivalent linear system properties and thus parallel Eq. (15). While closed form solutions for the equivalent linear system properties and response could often be derived in the single

mode case, the solution of Eq. (85)-(87) and (94)-(98) must be sought numerically by an iteration procedure.

2.4 SPECTRAL ESTIMATION

2.4.1 State-of-the-Art and Proposed Effort

Analytic estimates of the fatigue life are often constructed from the spectrum of the stress process, in particular from the spectral moments (see Lutes and Larsen, 1990, Lutes and Sarkani, 1997, for general approaches and Kim et al., 2003, for a panel specific analysis). Accordingly, it is important to dispose of a general approach to obtain an estimate of the power spectral density of the response/stresses from the reduced order model of the panel.

The reliable estimation of the power spectral density of the response of a nonlinear system is a classically difficult problem. The noteworthy general approaches which have been proposed to achieve this task include the equivalent linearization technique (see for example Roberts and Spanos, 1990), the recurrence strategy of Roy and Spanos (1993), the random system modeling of Soize (1995) and Soize and Le Fur (1997), and finally the Bouc (1994) and Bellizzi and Bouc (1999a, 1999b) amplitude-based approximation.

Some comments on these different approaches is in order. The recursion technique of Roy and Spanos (1993) is based on a continued fraction expansion of the Kolmogorov equation (i.e. the backward or adjoint Fokker-Planck equation). Reliable approximations of the power spectral densities of the response of a series of nonlinear oscillators were indeed obtained but by taking fairly large number of terms (15-20 say). Further, no extension of this approach to the multi-degree-of-freedom situation has yet been proposed.

System nonlinearities typically have several effects on the response spectral densities. Three or more effects are usually detected. First, there is shift in the peak frequency, increase for a hardening system and decrease for a softening one. Second, there is a broadening of the peak taking place and which result in fact from the frequency shift.

Indeed, the response of a linear/nonlinear system can be decomposed into cycles that have different/random magnitudes, even in the narrowband case. Since the frequency shift induced by nonlinearities increases in magnitude with increasing amplitude of motion, it is concluded that the largest cycles will be associated with a different frequency that the small ones. Thus, in nonlinear systems, the energy is diffused over a frequency band. Associated with the spread of energy is a decrease of the peak spectral values, which is the third typical effect of nonlinearities.

Capturing the peak broadening effect is one of the challenges of the power spectral estimation problem. Soize (1995) proposed the consideration of a linear system with random coefficients to incorporate the variability of the frequency and obtained excellent results for Duffing oscillators with varying degrees of nonlinearity. Bouc (1994) followed a different approach in which the parameters of a linear system approximation are functions of the amplitude process (solved separately). Very good results were also obtained with this technique for Duffing-type systems. Note finally that both of these methods have been extended to the multi-degree-of-freedom situation (see Soize et Le Fur (1997) and Bellizzi and Bouc (1999a, 1999b)).

These approaches certainly appear quite promising but the postbuckling analysis of panels is particularly challenging because of the strength of the nonlinearity, of the presence of multiple equilibrium positions, and finally, because of the recognized existence of multiple peaks of the power spectrum of the response in certain frequency ranges even with a single-degree-of-freedom system model. A critical inspection of the conditions under which the random (i.e. of Soize, 1995, and Soize and Le Fur, 1997) and amplitude-dependent (i.e. of Bouc (1994) and Bellizzi and Bouc (1999a, 1999b)) system models were developed sheds some doubt on the reliability of these two approaches given the above peculiarities of postbuckling problems.

It should be noted that all of these approaches, even the recursion technique, are based on/involved linear or linear type systems. In this light, one could wonder if indeed these methods *can* yield reliable approximations of the power spectral density of the response

of strongly nonlinear systems. Surprisingly, the answer is yes; it is possible to select the coefficients of a constant coefficients linear system subjected to white noise so that its power spectral density matches to within any accuracy a given spectral shape (see Wiener and Masani, 1957, 1958). This property, in the discrete time case, has been used extensively by one of the investigators (see Mignolet, 1993) to produce fast algorithms for the simulation of random processes and, later on, for the structural identification of systems (Mignolet and Red-Horse, 1994). How do such techniques account for/model broad peaks such as those obtained in the strongly nonlinear systems considered here? This task is achieved by a combination of three different factors:

(i) by "fictitious" increases in the damping

(ii) by appropriate changes of the excitation strength to adjust the peak levels and

(iii) by placing several natural frequencies close enough to each other so that their peaks merge into a single broadened one.

It is thus concluded from the above discussion that the response of a nonlinear single-degree-of-freedom system excited by white noise can be very accurately modeled (in terms of power spectral density, not probability density function) by one of the response components of a multi-degree-of-freedom system in which not only the frequencies (as might be expected from peak shifting) but also the damping and excitation terms are appropriately selected. These thoughts are akin to those leading to the equivalent linearization technique but in fact are broad generalization of them. Indeed, for a nonlinearity in restoring force (i.e. stiffness) only, the equivalent linearization technique leads simply to a stiffness correction leaving unchanged the order of the system (i.e. the single-degree-of-freedom nature) as well as the damping and excitation terms. This sole focus on the stiffness leads, as is well recognized, to a poor power spectral estimate as seen in Fig.3 for the single-degree-of-freedom problem associated with Eq. (2) with s = 1.8. As could be expected the lack of change of the excitation strength and of the damping ratio leads to a peak that is very much sharper than the true peak and is also substantially higher. The value of varying the excitation strength and damping coefficient is clearly seen by comparing the matching of the nonlinear spectrum curve of Fig. 3 by its

equivalent linear and "optimum" single-degree-of-freedom approximations, where the latter corresponds to a linear single-degree-of-freedom with adjusted stiffness, damping coefficient, and excitation strength.

The proposed approach is thus to model the response $q(t)$ of the nonlinear equation (1), (2) by $x(t)$ satisfying the linear equation

$$\ddot{x} + c_{eq}\ \dot{x} + k_{eq}\ x = \alpha\ p(t) \tag{99}$$

in a first approximation, or

$$\ddot{x} + c_{eq,11}\ \dot{x} + c_{eq,12}\ \dot{z} + k_{eq,11}\ x + k_{eq,12}\ z = \alpha_1\ p(t) \tag{100}$$

and

$$\ddot{z} + c_{eq,21}\ \dot{x} + c_{eq,22}\ \dot{z} + k_{eq,21}\ x + k_{eq,22}\ z = \alpha_2\ p(t) \tag{101}$$

in a second approximation, etc. Note in Eq. (100) and (101) that $z(t)$ is essentially an auxiliary, or unobservable, variable.

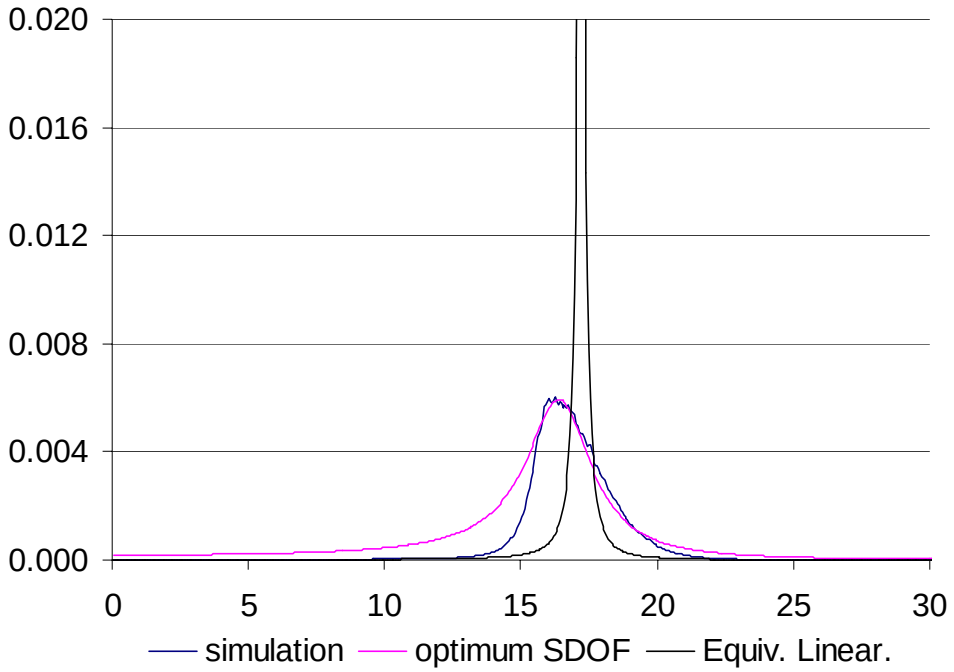

Figure 3. Exact spectrum (simulation) and its approximations by the equivalent linearization approach, and by the "optimum" SDOF curve

Having established the model to be used, it is necessary next to devise a procedure for the selection of the structural coefficients of Eq. (99) and (100) that does not involve the

knowledge of the properties of the exact solution $q(t)$. A first reaction is to proceed along the lines of the equivalent linearization approach. For clarity, assume first that the coefficient α is restricted to be equal to 1. Then, the standard (or force based) equivalent linearization strategy is to seek the values of c_{eq} and k_{eq} that minimize the error E_{eq} defined as

$$E_{eq} = E\left\{\left[2\,\zeta\omega_0\,\dot{x} + \omega_0^2\,(1-s)\,x + \gamma\,x^3 - c_{eq}\,\dot{x} - k_{eq}\,x\right]^2\right\} \tag{102}$$

for a fixed process x(t). Since a stationary process and its derivative are uncorrelated, it is readily found that the minimum of E_{eq} is achieved when

$$c_{eq} = 2\zeta\,\omega_0 \tag{103}$$

and

$$k_{eq} = \omega_0^2\,(1-s) + 3\,\gamma\,E\left[x^2\right] \tag{104}$$

Thus, an adjustment of the damping (and consequently a broadening of the spectral peak) cannot occur in the context of the standard formulation. The shortcoming of this strategy is in fact deeper, the present work has shown that a nontrivial two-degree-of-freedom type approximation of the form of Eq. (100) and (101) does not exist; the minimization of $E_{eq}^{(2)}$ defined as

$$E_{eq}^{(2)} = E\left\{\left[2\,\zeta\omega_0\,\dot{x} + \omega_0^2\,(1-s)\,x + \gamma\,x^3 - c_{eq,11}\,\dot{x} - c_{eq,12}\,\dot{z} - k_{eq,11}\,x - k_{eq,12}\,z\right]^2\right\} \tag{105}$$

renders the single-degree-of-freedom model of Eq. (99) with Eq. (103) and (104). To clarify the source of this weakness, assume that the term $\gamma\,q^3$ is approximated by a linear functional of q and $\dot{q}$, $F(q,\dot{q})$. The error to be minimized is thus

$$E_{eq}^{(3)} = E\left\{\left[\gamma\,q^3 - F(q,\dot{q})\right]^2\right\} = \gamma^2\,E\left[q^6\right] - 2\,\gamma\,E\left[q^3 F(q,\dot{q})\right] + E\left[F^2(q,\dot{q})\right]. \tag{106}$$

Since the response process $q(t)$ is assumed to be known, the first term in the second right-hand-side of Eq. (106) is a constant and does not intervene in the minimization. Further,

the linear equivalent strategy technique relies on moments that are evaluated under an assumed distribution, usually Gaussian. Under such an assumption, it is found that the second term in the second right-hand-side of Eq. (106) can be expressed as

$$\gamma\, E\left[q^3 F(q,\dot{q})\right] = 3\,\gamma\, E\left[q^2\right] E\left[q\, F(q,\dot{q})\right] \tag{107}$$

so that the linear functional $F(q,\dot{q})$ need to minimize the expression

$$E_{eq}^{(3)} = \gamma^2\, E\left[q^6\right] - 6\,\gamma\, E\left[q^2\right] E\left[q\, F(q,\dot{q})\right] + E\left[F^2(q,\dot{q})\right] \tag{108}$$

or

$$E_{eq}^{(3)} = \gamma^2 \left\{ E\left[q^6\right] - 9\left\{E\left[q^2\right]\right\}^3 \right\} + E\left\{ \left[3\,\gamma\, E\left[q^2\right] q - F(q,\dot{q})\right]^2 \right\}. \tag{109}$$

In this latter form, Eq. (109), it is concluded that $F(q,\dot{q}) = 3\,\gamma\, E\left[q^2\right] q$ will indeed provide the best approximation. The above discussion demonstrates that higher order approximations (i.e. with more than one-degree-of-freedom) of the type of Eq. (100) and (101) are not possible in the context of the standard formulation of the equivalent linearization technique.

Further, the above derivations associate this weakness with the lack of importance of the term $\gamma^2\, E\left[q^6\right]$ in the minimization process. Equivalently stated, the weakness of the equivalent linearization is the assumption that the response process $q(t)$ is fixed. In fact, this assumption is particularly curious as the moments of the response are to be evaluated later on by relying on the response of the equivalent linear system itself. It would thus seem appropriate to immediately consider all moments as functions of the unknown parameters of the equivalent linear system and to proceed with the minimization of Eq. (106). In fact, such an idea has been proposed in the past by Socha and Pawleta (1994) and Elishakoff and Colajanni (1997) and has recently been referred to as the SPEC (for the initial of the 4 co-authors) equivalent linearization by Crandall (2001).

While the SPEC co-authors have argued that the initial consideration of the response process as fixed was a flaw of the standard equivalent linearization procedure, Crandall

has demonstrated that in fact the standard and SPEC formulations are based on two different minimization criteria, thereby establishing both techniques on a firm foundation. The very surprising conclusions obtained by Socha and Pawleta (1994), Elishakoff and Colajanni (1997), and Crandall (2001) is that the SPEC formulation leads in fact to generally worse estimates of the variance of the response than does the standard approach.

Note however that these various investigators have all held the damping constant, focusing only on the selection of an equivalent stiffness. The question to be addressed in regards to the present focus are thus as follows:

(1) can the SPEC equivalent linearization lead to an increase in the damping/peak broadening? To this point, no increase in damping has ever been reported in connection with a nonlinearity on the restoring force only.

(2) can the SPEC equivalent linearization include or be re-formulated to include a varying excitation strength? To this point, no equivalent linearization formuation has ever been proposed that provides the tuning of the excitation.

(3) can the SPEC equivalent linearization include or be re-formulated to include an increase dynamics, i.e. auxiliary variables of the type shown in Eq. (100) and (101)? To this point again, no such procedure has been proposed.

Given the highly innovative work proposed, it was decided to proceed in careful steps and to address each of these questions in crescendo.

2.4.2 Damping Estimation in SPEC Equivalent Linearization

The capability to capture the peak broadening in part by an increase in the system damping was considered to be the first and most important requisite of the proposed formulation. To this end, the Duffing system described by Eq. (1) and (2) was considered and the minimization of Eq. (106) was reconsidered but under the assumption that the response process $q(t)$ does depend on the equivalent stiffness and damping coefficients. Note that no variation of the excitation strength was considered in this first problem, i.e. $\alpha = 1$. Thus, a substantial increase in the system damping would also lead to a dramatic

reduction of the peak value of the power spectrum which may then be below its nonlinear (exact) counterpart.

Since the response process is stationary, it is uncorrelated (independent given the Gaussian assumption) of its velocity and the error of Eq. (7) can be rewritten as

$$E_{eq} = E\left[\left(\bar{k}\, x + \gamma\, x^3\right)^2\right] + \bar{c}^{\,2}\; E\left[\dot{x}^2\right] \tag{110}$$

where, for simplicity of notation,

$$\bar{k} = \omega_0^2\,(1-s) - k_{eq} \quad \text{and} \quad \bar{c} = 2\,\zeta\,\omega_0 - c_{eq}\,. \tag{111), (112}$$

Note that the last term on the right-hand-side of Eq. (110) is minimized when $\bar{c} = 0$ but since the first term does also depend on the equivalent damping coefficient implicitly through the response process *q*, the condition $\bar{c} = 0$ does not necessarily minimize the entire error of Eq. (110) as it did in the standard formulation, see Eq. (103). Using the expression of the variances of the response of the equivalent linear system, i.e.

$$E\left[x^2\right] = \frac{\pi\, S_{pp}}{k_{eq}\; c_{eq}} \quad \text{and} \quad E\left[\dot{x}^2\right] = \frac{\pi\, S_{pp}}{c_{eq}}\,, \tag{103), (104}$$

and assuming a Gaussian distribution of *x* yields the equivalent form of E_{eq}

$$E_{eq} = \bar{k}^2\,\frac{\pi\, S_{pp}}{k_{eq}\; c_{eq}} + 6\,\bar{k}\,\gamma\left(\frac{\pi\, S_{pp}}{k_{eq}\; c_{eq}}\right)^2 + 15\,\gamma^2\left(\frac{\pi\, S_{pp}}{k_{eq}\; c_{eq}}\right)^3 + \bar{c}^{\,2}\,\frac{\pi\, S_{pp}}{c_{eq}}\,. \tag{105}$$

The minimization of the above equation with respect to k_{eq} and c_{eq} (with Eq. (101) and (102)) leads to the values of these coefficients and to the approximate power spectral density

$$S_{xx}(\omega) = \frac{\alpha^2\; S_{pp}}{\left(\omega^2 - k_{eq}\right)^2 + c_{eq}^2\;\omega^2} \tag{106}$$

where $\alpha = 1$ here.

The application of the above approach to the nonlinear equation (1), and (2) for the 104dB excitation considered led to the SPEC-k curve of Fig. 4 when, as proposed by the

SPEC authors and Crandall (2001), only the stiffness of the equivalent linear system is optimized and $c_{eq} = 2\zeta\,\omega_0$. It also led to the SPEC-kc curve when both equivalent stiffness and damping coefficients are selected to minimize Eq. (105).

Certainly, neither the SPEC-k nor the SPEC-kc approximations of the exact power spectral density are very good. Nevertheless, it is clearly seen that the SPEC-kc curve has a much higher damping ratio than do the SPEC-k and/or standard equivalent linear systems (see Fig. 3). To obtain a better perspective on its peak width, the SPEC-kc approximation was scaled by a factor of 6.5 that renders its peak value equal to its simulation counterpart. Surprisingly, a comparison of the corresponding curve (noted SPEC-kc*6.5 on Fig. 4) and the simulation results indicate that the SPEC-kc approach yields a very reliable estimate of the relative peak width (i.e. damping ratio) of the spectrum. These results also demonstrate the need to consider a non unit force magnification factor α. The occurrence of the peak of the SPEC-kc spectrum at a frequency substantially lower than that of the simulation spectrum may appear surprising but it is a consequence of the lack of a force magnification factor. Indeed, the SPEC-kc approximation with $\alpha = 1$ implies a response level that is much less than its exact counterpart. Thus, the SPEC-kc approximation should exhibit a much smaller frequency shift than the exact spectrum, as observed on Fig. 4.

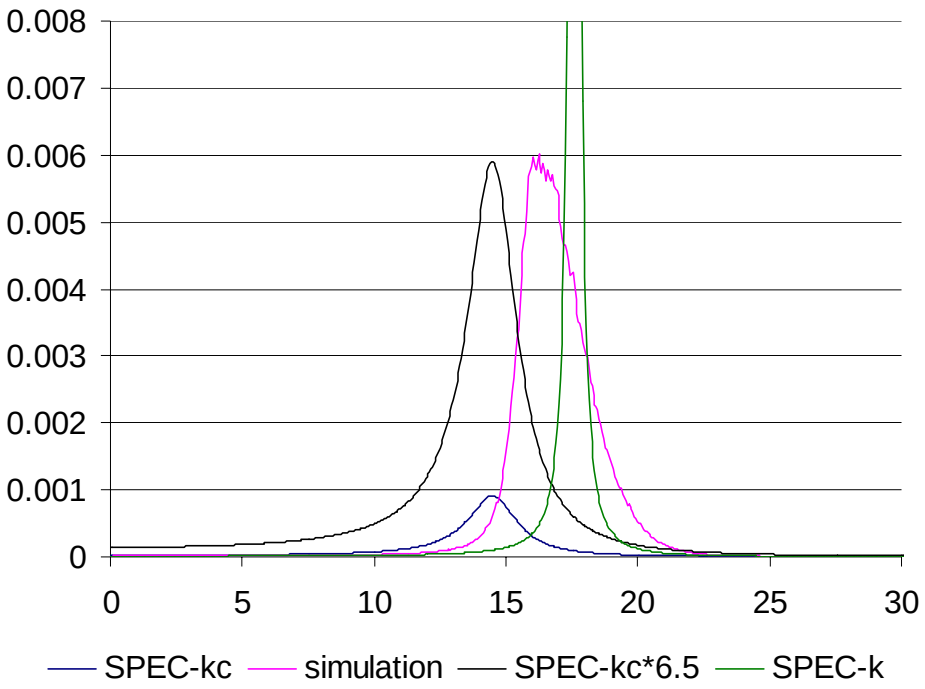

Figure 4. Exact spectrum (simulation) and its approximations by the SPEC-k and SPEC-kc techniques. Also included is the SPEC-kc scaled by a factor of 6.5.

It is thus concluded that the minimization of Eq. (92) considering that the response process is indeed dependent on the equivalent linear system parameters provides the first known mean to broaden the peak within the context of the equivalent linearization technique. This important finding validates the SPEC formulation and motivates continued efforts in this direction, more specifically, the consideration of a non unit force magnification.

2.4.3 Force Magnification Estimation in SPEC Equivalent Linearization

Since the answer to the first question is yes, i.e. peak broadening can be partially captured by the SPEC strategy, it is now desired to include a force magnification coefficient $\alpha \neq 1$ in the formulation. It would seem at first that the inclusion of this term is straightforward and can be achieved by the consideration of an additional equivalent mass in the system, i.e. $m_{eq} = 1/\alpha$. Then, the parameters k_{eq}, c_{eq}, and α would be evaluated by minimizing the error

$$E_{eq} = E\left\{\left[\ddot{x} + 2\,\zeta\omega_0\,\dot{x} + \omega_0^2\,(1-s)\,x + \gamma\,x^3 - \beta\,\ddot{x} - \beta\,c_{eq}\,\dot{x} - \beta\,k_{eq}\,x\right]^2\right\} \quad (107)$$

where $\beta = 1/\alpha$. The minimization of Eq. (107) is however not properly defined as the acceleration process $\ddot{x}$ has infinite power (variance) as it involves a white noise component, see Eq. (1) and (2).

The above approach is thus not appropriate and an alternate formulation must be sought. While the variance of $\ddot{x}$ is infinite, this process has a well defined power spectrum. Accordingly, it is proposed here to reformulate the selection of the optimum values of k_{eq}, c_{eq}, and α as a minimization problem in the *frequency* (spectral) domain. To this end, introduce the error process $E(t)$ as

$$E(t) = (1-\beta)\,\ddot{x} + (2\,\zeta\omega_0 - \beta\,c_{eq})\,\dot{x} + \left[\omega_0^2\,(1-s) - \beta\,k_{eq}\right]x + \gamma\,x^3 \quad . \qquad (108)$$

As stated above, note that $E_{eq} = \mathrm{var}(E(t)) = E\left[E^2(t)\right]$. Instead of minimizing this quantity, it is desired to minimize the *power spectrum* $S_{EE}(\omega)$ of the error process. This function can be derived from Eq. (108) by first evaluating the autocorrelation function $R_{EE}(\tau) = E\left[E(t)\,E(t+\tau)\right]$. Specifically, it is found that

$$\begin{aligned}
R_{EE}(\tau) &= (1-\beta)^2\,E\left[\ddot{x}(t)\,\ddot{x}(t+\tau)\right] + (2\,\zeta\omega_0 - \beta\,c_{eq})^2\,E\left[\dot{x}(t)\,\dot{x}(t+\tau)\right] \\
&+ \left[\omega_0^2\,(1-s) - \beta\,k_{eq}\right]^2\,E\left[x(t)\,x(t+\tau)\right] + \gamma^2\,E\left[x^3(t)\,x^3(t+\tau)\right] \\
&+ (1-\beta)(2\,\zeta\omega_0 - \beta\,c_{eq})\left\{E\left[\ddot{x}(t)\,\dot{x}(t+\tau)\right] + E\left[\dot{x}(t)\,\ddot{x}(t+\tau)\right]\right\} \\
&+ (1-\beta)\left[\omega_0^2\,(1-s) - \beta\,k_{eq}\right]\left\{E\left[\ddot{x}(t)\,x(t+\tau)\right] + E\left[x(t)\,\ddot{x}(t+\tau)\right]\right\} \\
&+ (2\,\zeta\omega_0 - \beta\,c_{eq})\left[\omega_0^2\,(1-s) - \beta\,k_{eq}\right]\left\{E\left[\dot{x}(t)\,x(t+\tau)\right] + E\left[x(t)\,\dot{x}(t+\tau)\right]\right\} \\
&+ \gamma\,(1-\beta)\left\{E\left[\ddot{x}(t)\,x^3(t+\tau)\right] + E\left[x^3(t)\,\ddot{x}(t+\tau)\right]\right\} \\
&+ \gamma\left[\omega_0^2\,(1-s) - \beta\,k_{eq}\right]\left\{E\left[x^3(t)\,x(t+\tau)\right] + E\left[x(t)\,x^3(t+\tau)\right]\right\} \\
&+ \gamma\,(2\,\zeta\omega_0 - \beta\,c_{eq})\left\{E\left[\dot{x}(t)\,x^3(t+\tau)\right] + E\left[x^3(t)\,\dot{x}(t+\tau)\right]\right\}
\end{aligned} \qquad (109)$$

Substantial simplifications do occur in this equation. Note first that

$$E\left[\ddot{x}(t)\,\dot{x}(t+\tau)\right] + E\left[\dot{x}(t)\,\ddot{x}(t+\tau)\right] = \frac{d}{dt}E\left[\dot{x}(t)\,\dot{x}(t+\tau)\right]$$

which vanishes in the stationary limit as all moments become independent of the time shift *t*. The same result is obtained in connection with $E\left[x(t)\,\dot{x}(t+\tau)\right]+E\left[\dot{x}(t)\,x(t+\tau)\right]$. Next, the term $E\left[\ddot{x}(t)\,x(t+\tau)\right]+E\left[x(t)\,\ddot{x}(t+\tau)\right]$ can be expressed as

$$E\left[\ddot{x}(t)\,x(t+\tau)\right]+E\left[x(t)\,\ddot{x}(t+\tau)\right]=\frac{d}{dt}\left\{E\left[\dot{x}(t)\,x(t+\tau)\right]+E\left[x(t)\,\dot{x}(t+\tau)\right]\right\}-2\,E\left[\dot{x}(t)\,\dot{x}(t+\tau)\right]$$
$$=-2\,E\left[\dot{x}(t)\,\dot{x}(t+\tau)\right]$$

where the last equality results again from the stationary assumption.

The next group of terms involves the third power of *x* and can generically be written as $E\left[x^3(t)\,y(t+\tau)\right]+E\left[y(t)\,x^3(t+\tau)\right]$ where *y* is either *x*, $\dot{x}$, or $\ddot{x}$. Relying on an assumed joint Gaussian distribution of the response processes *x*, $\dot{x}$, and $\ddot{x}$, it is found that

$$E\left[x^3(t)\,y(t+\tau)\right]+E\left[y(t)\,x^3(t+\tau)\right]=3\,E\left[x^2\right]\left\{E\left[x(t)\,y(t+\tau)\right]+E\left[y(t)\,x(t+\tau)\right]\right\}\quad .$$

With these simplifications, Eq. (109) becomes

$$R_{EE}(\tau)=(1-\beta)^2\,R_{\ddot{x}\ddot{x}}(\tau)+\left\{\left(2\,\zeta\omega_0-\beta\,c_{eq}\right)^2-2\,(1-\beta)\left[\omega_0^2\,(1-s)-\beta\,k_{eq}+3\,\gamma\,\sigma_x^2\right]\right\}R_{\dot{x}\dot{x}}(\tau)$$
$$+\left\{\left[\omega_0^2\,(1-s)-\beta\,k_{eq}\right]^2+6\,\gamma\left[\omega_0^2\,(1-s)-\beta\,k_{eq}\right]\sigma_x^2\right\}R_{xx}(\tau)+\gamma^2\,E\left[x^3(t)\,x^3(t+\tau)\right] \tag{110}$$

It remains to evaluate the last expectation in the above relation, i.e. $E\left[x^3(t)\,x^3(t+\tau)\right]$.

Specifically, relying again on a Gaussian distribution of the response process, it is found that

$$E\left[x^3(t)\,x^3(t+\tau)\right]=9\,\sigma_x^4\,R_{xx}(\tau)+6\,R_{xx}^3(\tau). \tag{111}$$

Finally, the power spectral density of the error process, $S_{EE}(\omega)$, can be found by taking the Fourier transform of Eq. (110) which yields

$$S_{EE}(\omega)=A(\omega)\,S_{xx}(\omega)+B(\omega) \tag{112}$$

where $S_{xx}(\omega)$ is specified by Eq. (106) and

$$A(\omega) = (1-\beta)^2\ \omega^4 + \left\{\left(2\,\zeta\omega_0 - \beta\, c_{eq}\right)^2 - 2\,(1-\beta)\left[\omega_0^2\,(1-s) - \beta\, k_{eq} + 3\,\gamma\,\sigma_x^2\right]\right\}\omega^2$$
$$+ \left\{\left[\omega_0^2\,(1-s) - \beta\, k_{eq}\right]^2 + 6\,\gamma\left[\omega_0^2\,(1-s) - \beta\, k_{eq}\right]\sigma_x^2 + 9\,\gamma^2\,\sigma_x^4\right\} \tag{113}$$

and

$$B(\omega) = \frac{3}{\pi}\int_{-\infty}^{+\infty} R_{xx}^3(\tau)\, d\tau\,. \tag{114}$$

This very last term remains to be computed to complete the evaluation of the power spectral density of the error process. In the case of a single-degree-of-freedom system excited by white noise, it is known (see Lutes and Sarkani, 1997) that

$$R_{xx}(\tau) = \frac{\alpha^2\ \pi\ S_{pp}}{k_{eq}\ c_{eq}}\, e^{-c_{eq}\,\tau/2}\left(\cos\omega_d\,\tau + \frac{c_{eq}}{2\,\omega_d}\sin\omega_d\,\tau\right) \tag{115}$$

where $\omega_d^2 = k_{eq} - c_{eq}^2/4$. Raising this expression to the third power and integrating over the entire domain of lag values yields a closed form expression of $B(\omega)$ as a sum of rational terms in ω which is omitted here for brevity.

Regrouping all of these results provides an expression for the power spectrum of the error process $S_{EE}(\omega)$, see Eq. (112). Since $E(t)$ is a genuine random process, its power spectral density is a non-negative function of the frequency ω. Accordingly, $S_{EE}(\omega)$ itself can be used as an error to be minimized for the selection of the optimal values of the equivalent linear system parameters k_{eq}, c_{eq}, and α. Several variants of this process have been investigated, i.e.

(a) a purely local approach where the minimization is accomplished at each frequency separately yielding frequency dependent parameters k_{eq}, c_{eq}, and α

(b) a more averaged approach where the error over certain frequency domains is performed and the parameters k_{eq}, c_{eq}, and α are constant within each of these domains

and, finally,

(c) a purely global approach where the error over the entire *finite* frequency domain of interest is minimized yielding unique coefficients k_{eq}, c_{eq}, and α.

Unfortunately, these efforts were not fruitful and another approach, based on the methodology of Bouc (1994) and Soize (1995), was undertaken. This formulation is described in the next section.

2.4.4 Random Parameter Linear System Modeling

This approach is described in details in Appendix A:

Yang, B., and Mignolet, M.P., "Implicit Modeling of the Power Spectral Density of the Response of a Class of Nonlinear Oscillators," *Proceedings of the 9th Joint Specialty Conference on Probabilistic Mechanics and Structural Reliability,* Albuquerque, New Mexico, Jul. 26-28, 2004.

In addition, it was shown that this method could produce reliable estimates of the power spectral density of the stresses as follows. For a single mode solution, any stress is related to the displacement $q(t)$ through the memoryless quadratic transformation

$$S = C_0 + C_1\, q + C_2\, q^2 . \tag{116}$$

Then, the determination of the power spectral density of the stress process can be achieved by first estimating its autocorrelation function

$$R_{SS}(\tau) = E\left[S(t)\, S(t+\tau)\right] - \{E\left[S\right]\}^2 \tag{117}$$

which is independent of the stress shift C_0. The determination of $R_{SS}(\tau)$ in terms of its displacement counterpart $R_{qq}(\tau)$ requires the evaluation of third and fourth order moments of the form $E\left[q(t)\, q^2(t+\tau)\right]$ and $E\left[q^2(t)\, q^2(t+\tau)\right]$ which in turn necessitate the joint probability density function of $q(t)$ and $q(t+\tau)$, that is unfortunately not available in closed form, even for the one mode model. It is proposed here to remedy this situation by first assuming a joint Gaussian probability density function of $q(t)$ and

$q(t + \tau)$ and then rescaling the achieved power spectral density according to the total energy of the stress process.

Under the assumptions that the random variables $q(t)$ and $q(t + \tau)$ are zero mean and jointly Gaussian, it is found that

$$E\left[q(t)\, q^2(t+\tau)\right] = 0 \tag{118}$$

and

$$E\left[q^2(t)\, q^2(t+\tau)\right] = 2\left\{R_{qq}(\tau)\right\}^2 + \sigma_q^4 . \tag{119}$$

Combining Eq. (116)-(119), it is found that

$$R_{SS}(\tau) = C_1^2\ R_{qq}(\tau) + 2\ C_2^2\ \left\{R_{qq}(\tau)\right\}^2 , \tag{120}$$

or in terms of spectrum

$$S_{SS}(\omega) = C_1^2\ S_{qq}(\omega) + 2\ C_2^2\ \overline{S}(\omega) \tag{121}$$

where

$$\overline{S}(\omega) = \frac{1}{2\pi} \int_{-\infty}^{+\infty} \left\{R_{qq}(\tau)\right\}^2 d\tau . \tag{122}$$

The above result is strongly dependent on the assumed Gaussian character of the process $q(t)$ and leads in fact to an overestimation of the energy in the second lobe (second harmonics) of the stress spectrum although its overall shape appears correct. Thus, the second step in the estimation process is to rectify that energy and it is accomplished under the assumption that $q(t)$ is narrowband. Accordingly Eq. (121) is modified as

$$S_{SS}(\omega) = C_1^2\ S_{qq}(\omega) + 2\ \eta\ C_2^2\ \overline{S}(\omega) \tag{123}$$

for a value of $\eta \neq 1$ to be selected. To this end, consider first the autocovariance of $S_2(t) = q^2(t)$

$$K_{S_2 S_2}(\tau) = E\left[q^2(t)\, q^2(t+\tau)\right] . \tag{124}$$

Then, assume that $q(t)$ is narrowband and thus that it can be written as

$$q(t) = A(t)\cos(\Omega t + \Phi) \tag{125}$$

where Ω is the center frequency of the process, Φ is a uniform random variable in [0, 2π], and $A(t)$ is a slowly varying process independent of Φ. Then,

$$K_{S_2S_2}(\tau) = E\left[A^2(t)\,A^2(t+\tau)\right]\left[\frac{1}{4} + \frac{1}{8}\cos 2\Omega\tau\right]. \tag{126}$$

As expected, it is seen from the above equation that the energy of the process $S_2(t)$ is distributed in two domains: around the zero frequency, i.e. the term 1/4 $E\left[A^2(t)\,A^2(t+\tau)\right]$, and around the second harmonic (2Ω), i.e. 1/8 $E\left[A^2(t)\,A^2(t+\tau)\right]$.

The ratio of these two terms being 2, it is then concluded that the energy around the second harmonics is approximately 1/3 of the total energy, i.e. 1/3 of $K_{S_2S_2}(0)$ where

$$K_{S_2S_2}(0) = E\left[q^4(t)\right] = \kappa_4\,\sigma_q^4. \tag{127}$$

in which κ_4 denotes the kurtosis of the displacement process $q(t)$.

On the basis of these findings, it is proposed to evaluate η in Eq. (121) so that the energy in the second lobe of the stress spectrum (second harmonics of the displacement process) be equal to 1/3 of the total power arising from the quadratic term in Eq. (116). That is,

$$2\eta \int_{\omega\in\Omega_2} \overline{S}(\omega)\,d\omega = \frac{1}{3}(\kappa_4 - 1)\,\sigma_q^4 \tag{128}$$

where Ω_2 denotes the domain of frequencies double those of the displacement process.

This approach was applied to the response process $q(t)$ of the dimensionless one mode model of Appendix A with γ = 769.532 and with C_1 = 18.962 and C_2 = 11.792, which are representative of a 154dB excitation on the titanium panel considered in Phase I. Shown in Fig. 5 are the stress spectra obtained by Monte Carlo (MC) simulation of Eq. (1), (2), and (116), from Eq. (121), and from Eq. (123) and (128) (the latter two models were based on the autocorrelation function $R_{qq}(\tau)$ from Bouc (1994)). While the original, Gaussian approximation, Eq. (121), substantially overestimates the energy in the second lobe, the proposed approximation of Eq. (123) and (128) leads to an excellent

match of this second lobe and thus can reliably be used e.g. for ensuing fatigue-life computations.

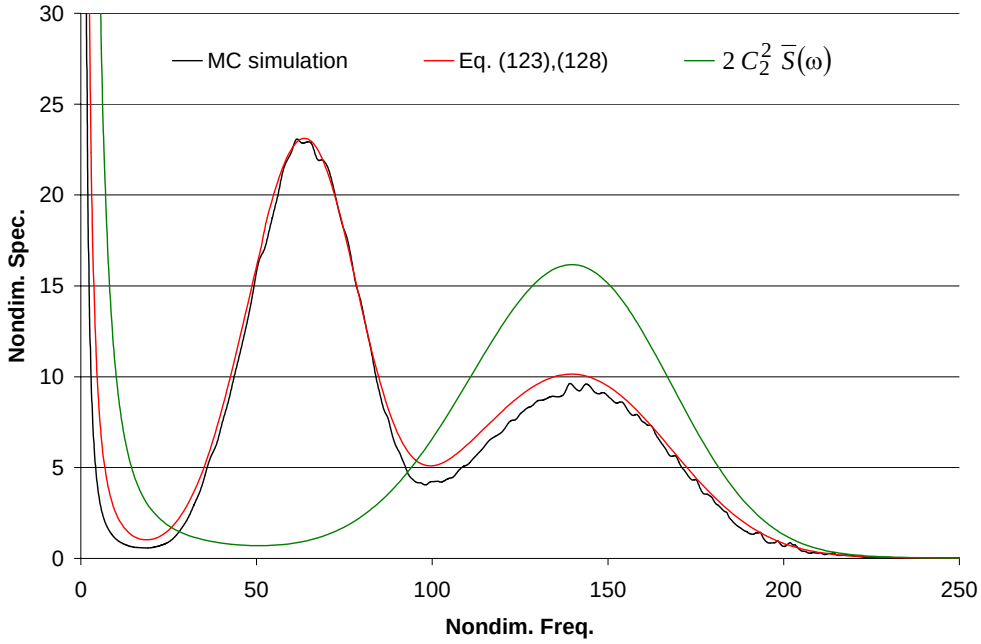

Figure 5. Comparison of stress spectra computed by Monte Carlo simulations of Eq. (1), (2), and (116) ("MC simulation"), and by using the method of Appendix A with either Eq. (121) or Eq. (123) and (128).

3. FATIGUE LIFE AND ACCUMULATED DAMAGE PREDICTION

An original and accurate model for the accumulated damage induced on a panel undergoing large deformations was derived as a part of this contract and is given in details in Appendix B:

Yang, B., Mignolet, M.P., and S.M. Spottswood, "Modeling of Damage Accumulation for Duffing Oscillator-Type Systems Under Severe Random Excitations," *Probabilistic Engineering Mechanics*, Vol. 19, pp. 185-194, 2004.

Additional results not included in the paper are presented here for completeness.

3.1 Additional Comments on Narrowbandedness

A better check of narrowbandedness than the spectrum is the assessment of the frequencies at which the stress ranges occur. To this end, the simulation data of the paper was revisited and the stress ranges were recorded together with the time (or half-period) needed to achieve these stress ranges. This information was then gathered into the two-dimensional histograms of the population of stress ranges and half-periods which are shown in Fig. 6-10 for the 94 dB, 124 dB, 134 dB, 144 dB, and 154 dB sound pressure levels, respectively. The plot corresponding to the 94 dB *SPL* is presented here as a good narrowband example. In these figures, the red and blue colors indicate the largest and lowest number of occurrences, respectively. A number of important observations can be drawn from these figures.

First and foremost, the domains of high occurrences, as marked in red, correspond to narrow half-period intervals thereby providing a strong support to the narrowband assumption. The presence in these figures of 2 main "ridges" and some secondary ones should also be noted. The "ridge" corresponding to small values of the range corresponds to motions around the buckled states while the other one is associated with the snap-throughs. At low *SPL*, see Fig. 6 and 7 for 94 dB and 124 dB sound pressure levels, the small ridge is dominant but a switch occurs between 124 dB and 134 dB and the

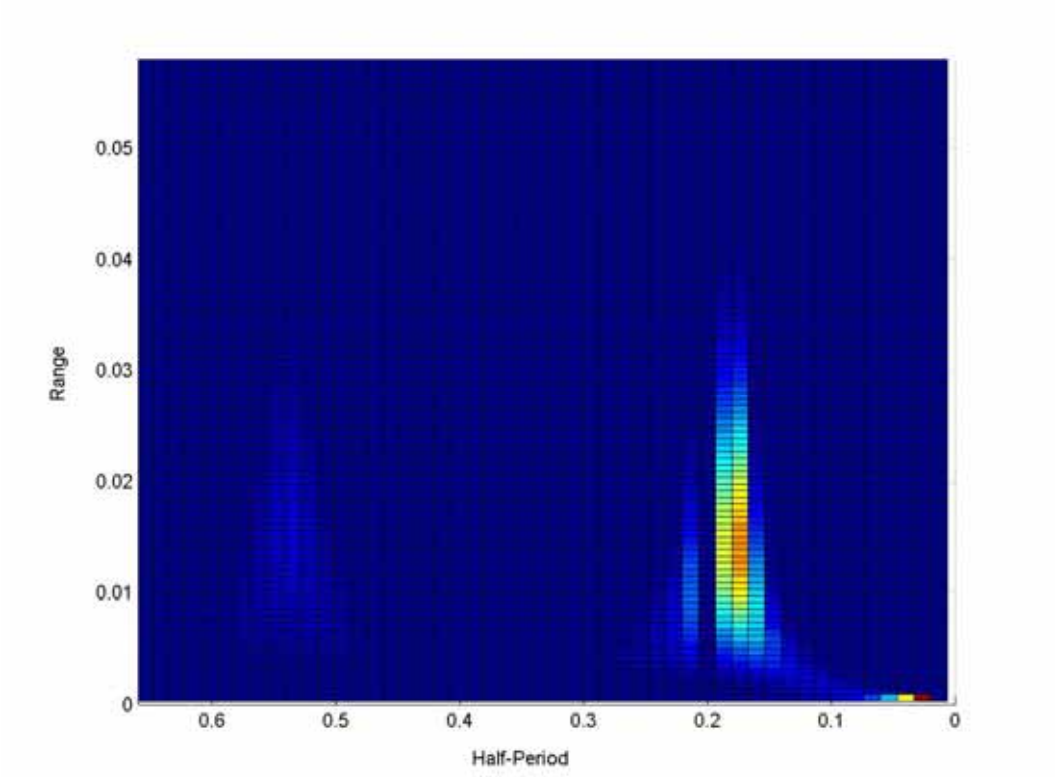

Figure 6. Two-dimensional histogram of ranges and half-periods, *SPL* = 94 dB

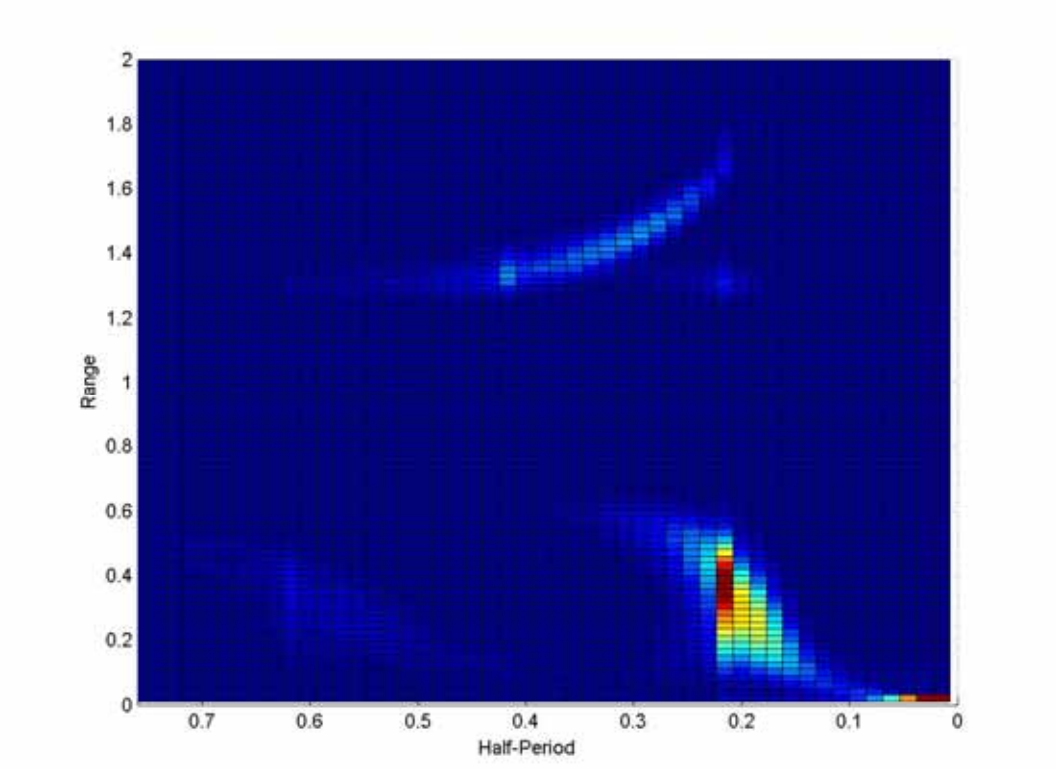

Figure 7. Two-dimensional histogram of ranges and half-periods, *SPL* = 124 dB

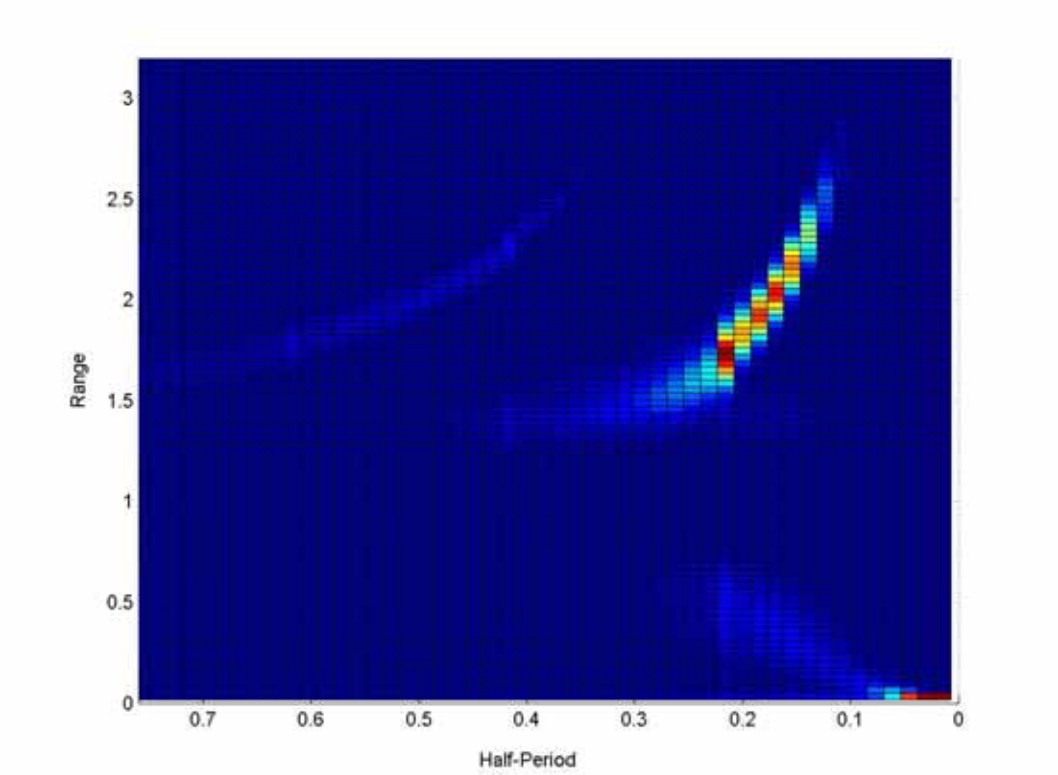

Figure 8. Two-dimensional histogram of ranges and half-periods, *SPL* = 134 dB

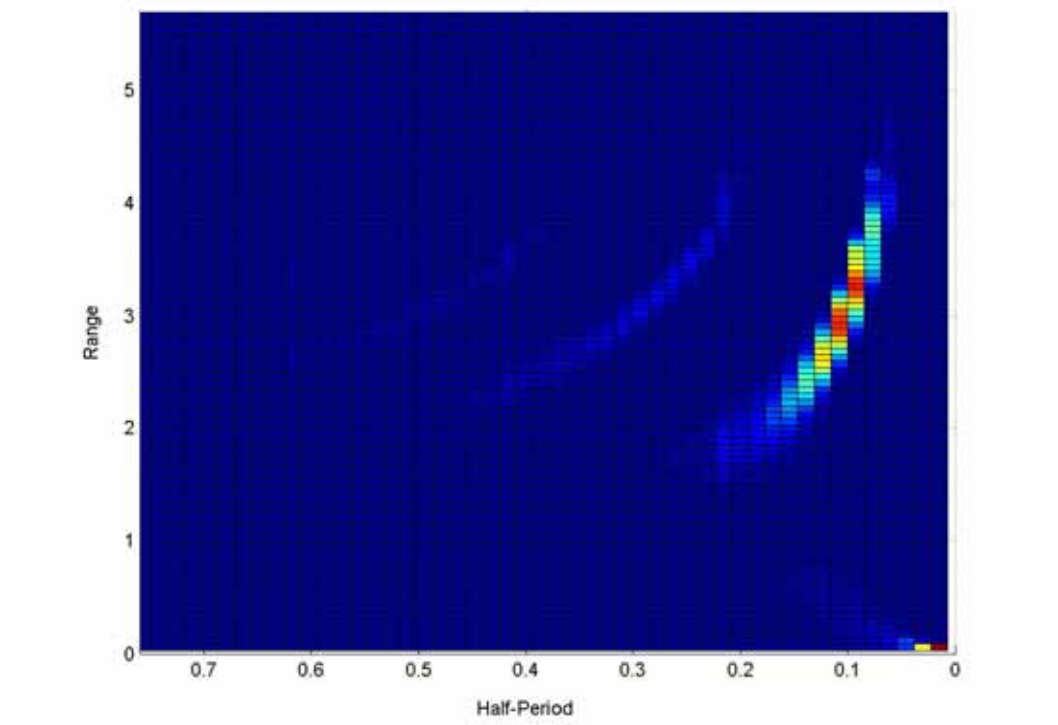

Figure 9. Two-dimensional histogram of ranges and half-periods, *SPL* = 144 dB

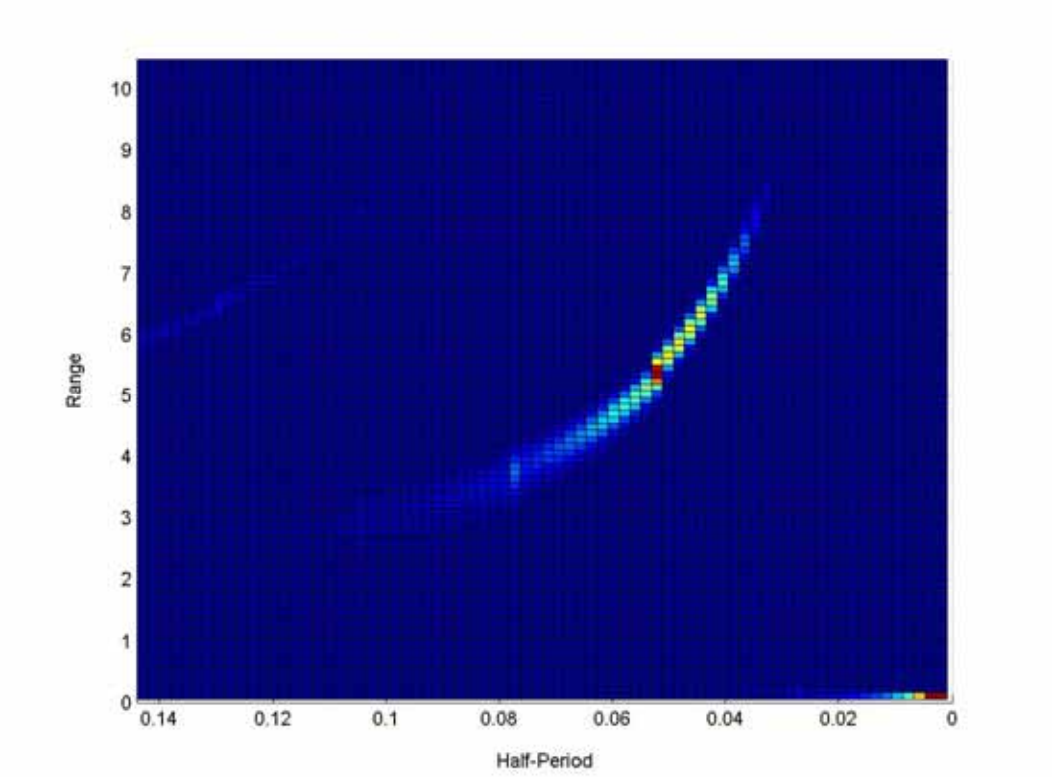

Figure 10. Two-dimensional histogram of ranges and half-periods, *SPL* = 154 dB

dominant behavior (as characterized by the red zone) moves to the snap-through (high range) ridge. Note further that the peaks of the two ridges occur in the same domain of half-periods so that snap-throughs and motions around the buckled states appear to be characterized by the same frequency, i.e. they are part of the same process.

Next, attention should be paid to the secondary ridges that occur in all pictures and that correspond to harmonics of the half-periods. In classical non-linear terminology, these ridges would be associated with subharmonics of the fundamental frequency while similar ridges for the superharmonics (integer fractions of the dominant half-period) do not seem to be present. The presence of subharmonics is often found to be associated with a chaotic, or potentially chaotic, behavior and thus is not surprising here in view of the established chaotic nature of the snap-through process in some conditions (see Moon, 1992, for a discussion).

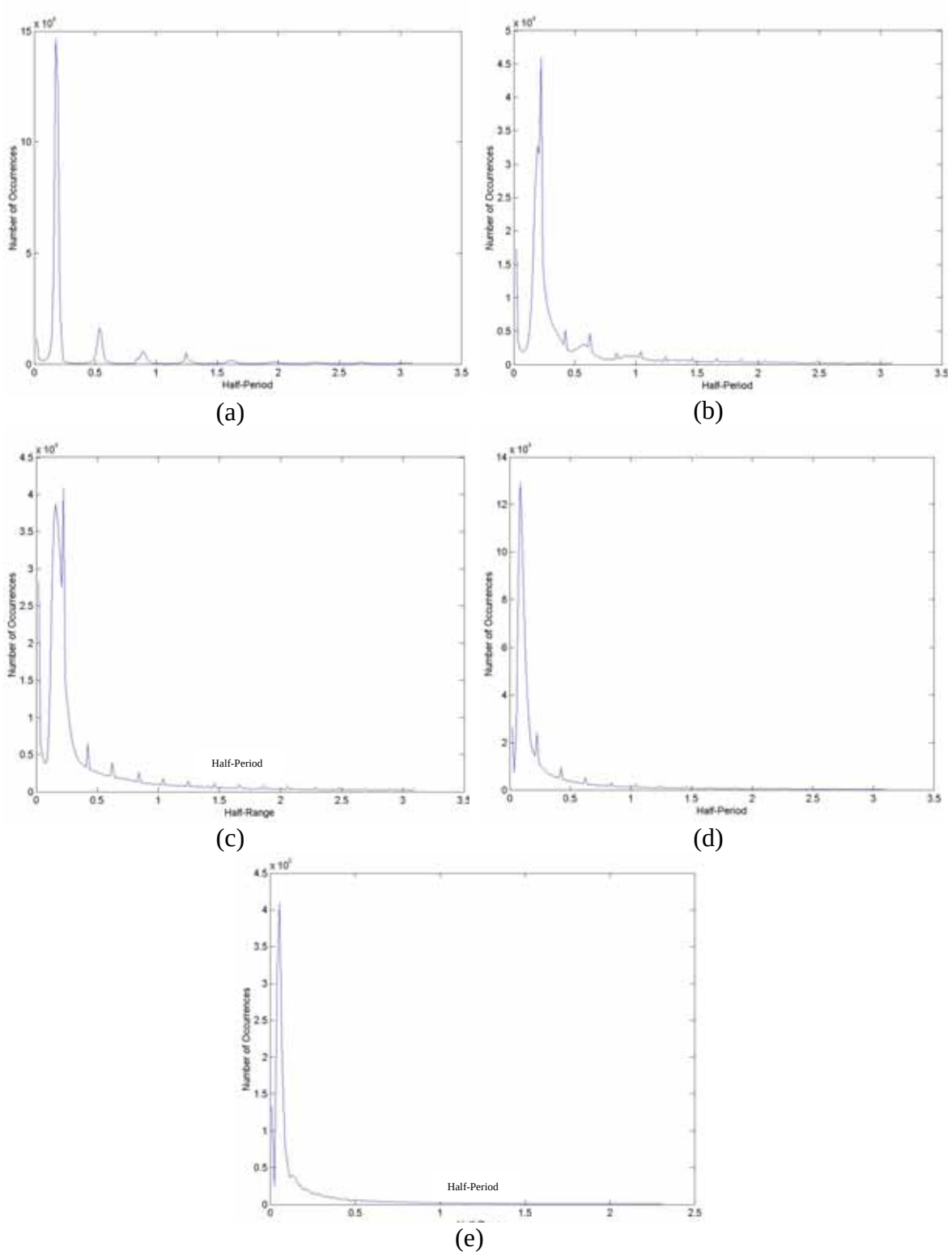

Figure 11. Histograms of the half-period for
(a) *SPL* = 94 dB, (b) 124 dB, (c) 134 dB, (d) 144 dB, and (e) 154 dB

Finally, note the sharp peak occurring at very small values of both the range and the half-period. In fact, these half-period values are equal to one or two of the time steps used for the numerical integration of the equations of motion fairly independently of the time step used. It is thus concluded that this peak is associated with the cut-off frequency of the simulation and, consequently, is a numerical effect not a physical phenomenon.

From the joint distribution of the ranges and half-periods of Fig. 6-10 one can also obtain the marginal distributions of the half-periods and the ranges. The histograms of the half-periods are shown first in Fig. 11 (a)-(e). It is seen from these figures that the peak of the half-period distribution is only slightly broader at the high sound pressure levels (*SPL* of 124 dB - 154 dB) than it is for the low ones, thus further validating the narrowband assumption.

Interestingly, the subharmonics are particularly visible in these figures, especially at the lowest sound pressure levels. As the excitation strengthens, the tail of the distribution of the half-periods appears to absorb the small peaks associated with the subharmonics which are finally completely invisible in Fig. 11 (e) for a *SPL* of 154 dB. These subharmonics are nevertheless present as can be seen from the secondary ridge in Fig. 10.

While the changes in the distribution of half-periods appear minimal, see Fig. 11, the probability density function of the stress ranges experiences dramatic modifications as the sound pressure level increases, see Fig. 12-16. At low sound pressure levels, see Fig. 12 for 94 dB, the small motions around the buckled states are approximately Gaussian and a Rayleigh probability density function of the stress ranges is obtained as confirmed by the match of the simulation and Rayleigh curves. Near the upper end of the transition zone, i.e. for sound pressure levels of 124 and 134 dB, the probability density function exhibits two peaks, one corresponding to the motions around the buckled states and the other to the snap-throughs. Note, see Fig. 13, that the peak associated with the motions around the buckled states does no longer follow a Rayleigh distribution as seen by the fairly poor matching of the simulation and Rayleigh curves (the Rayleigh probability density function was obtained by matching the peak location and peak value of the

simulation results). This observation further confirms the complexity of the transition zone in which the two peaks are present and equally important.

While the peak corresponding to the snap-throughs (the right peak) may appear somewhat reminiscent of a Rayleigh distribution as well at the 124 dB excitation level (see Fig. 13), it is certainly not the case at the higher sound pressure levels. This departure from the Rayleigh distribution is clearly associated with a strong non-Gaussian character of the stress process.

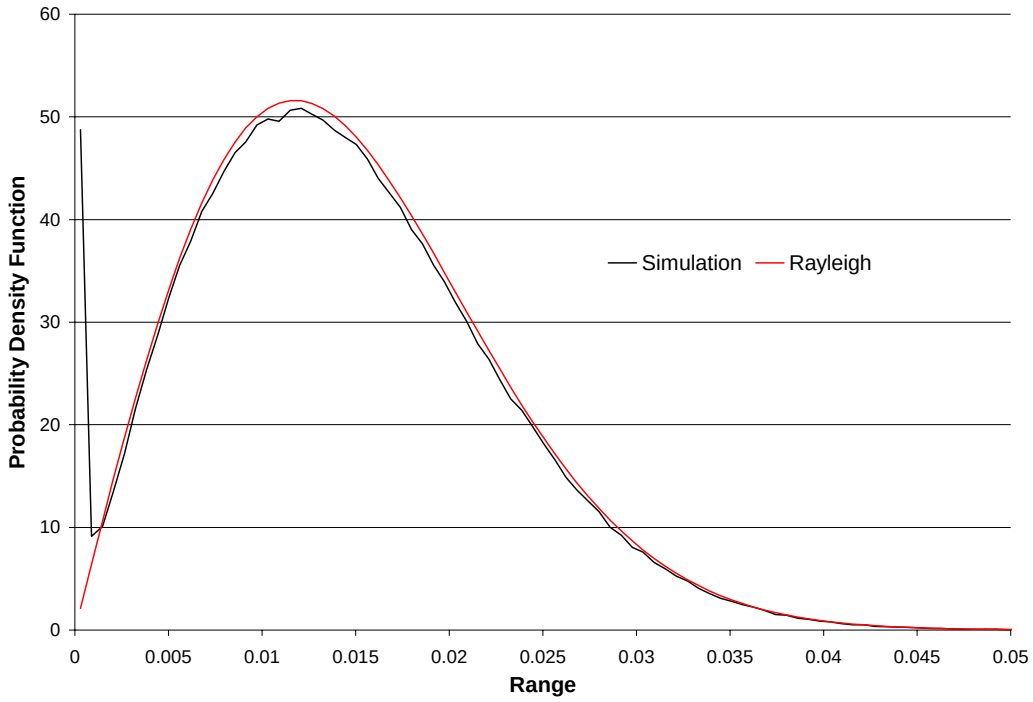

Figure 12. Probability density function of the stress ranges and its Rayleigh approximation, *SPL* = 94 dB.

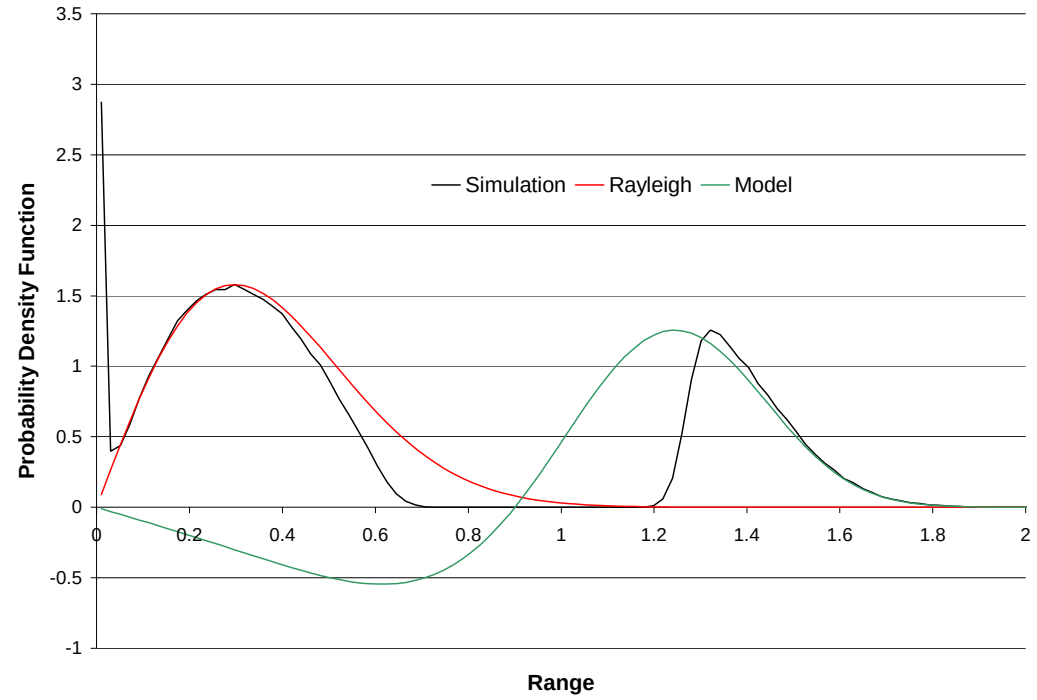

Figure 13. Probability density function of the stress ranges and its approximations by the Rayleigh distribution and the model of Eq. (B.25), *SPL* = 124 dB.

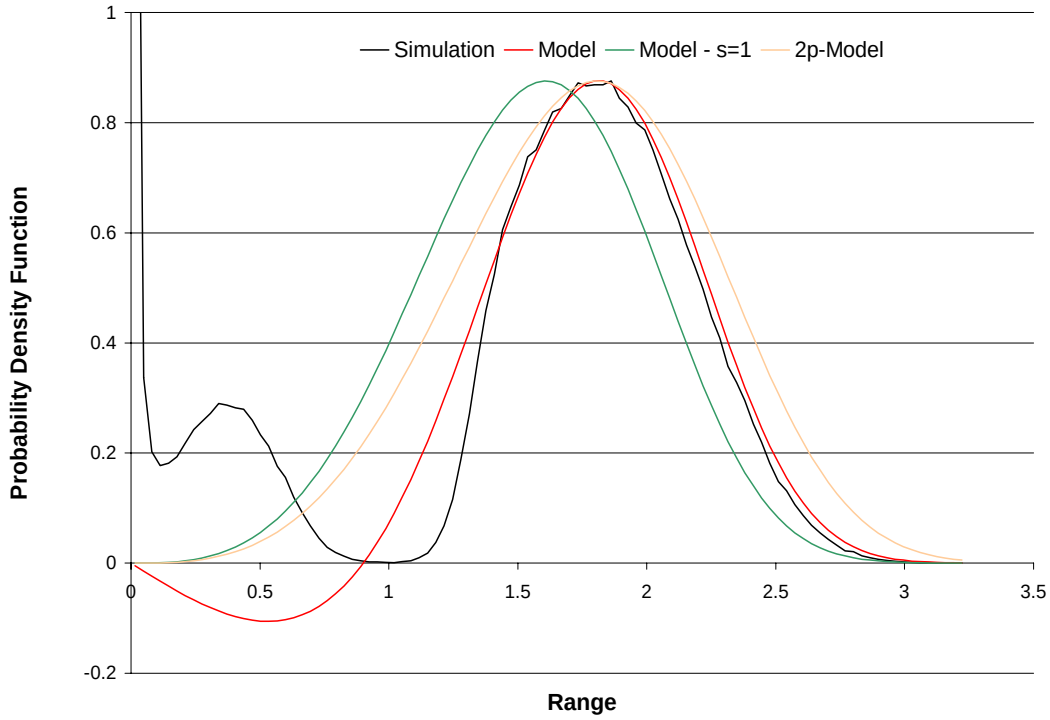

Figure 14. Probability density function of the stress ranges and its approximations by Eq. (B.25) ("Model"), Eq. (B.26) ("Model - *s* = 1"), and Eq. (B.28) ("2p- Model"), *SPL* = 134 dB.

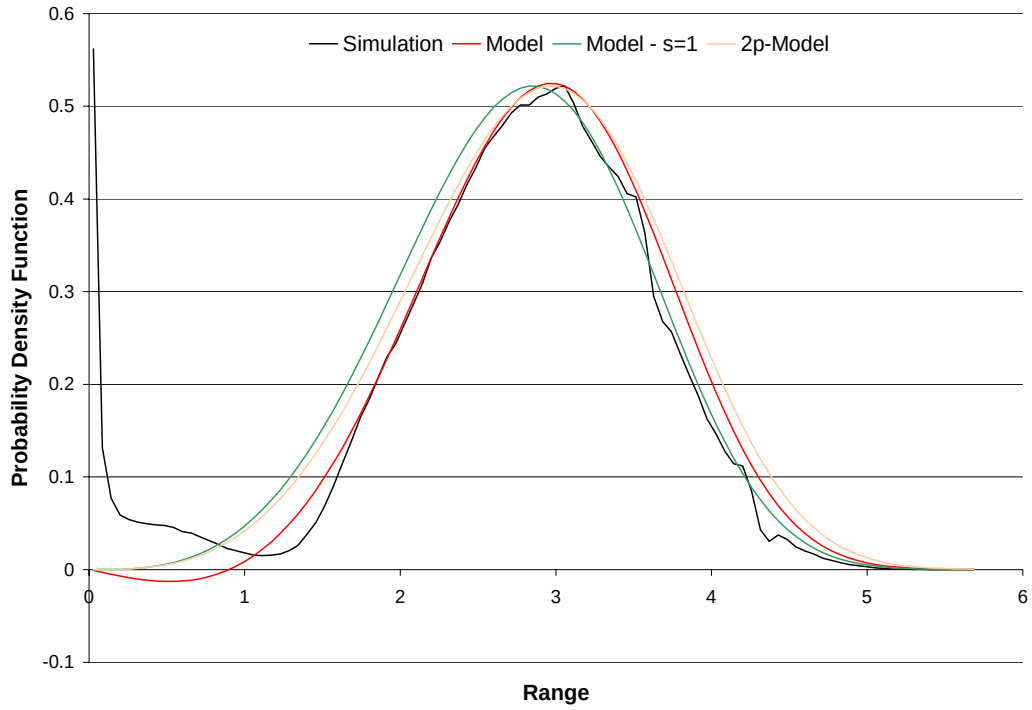

Figure 15. Probability density function of the stress ranges and its approximations by Eq. (B.25) ("Model"), Eq. (B.26) ("Model - *s* = 1"), and Eq. (B.28) ("2p- Model"), *SPL* = 144 dB.

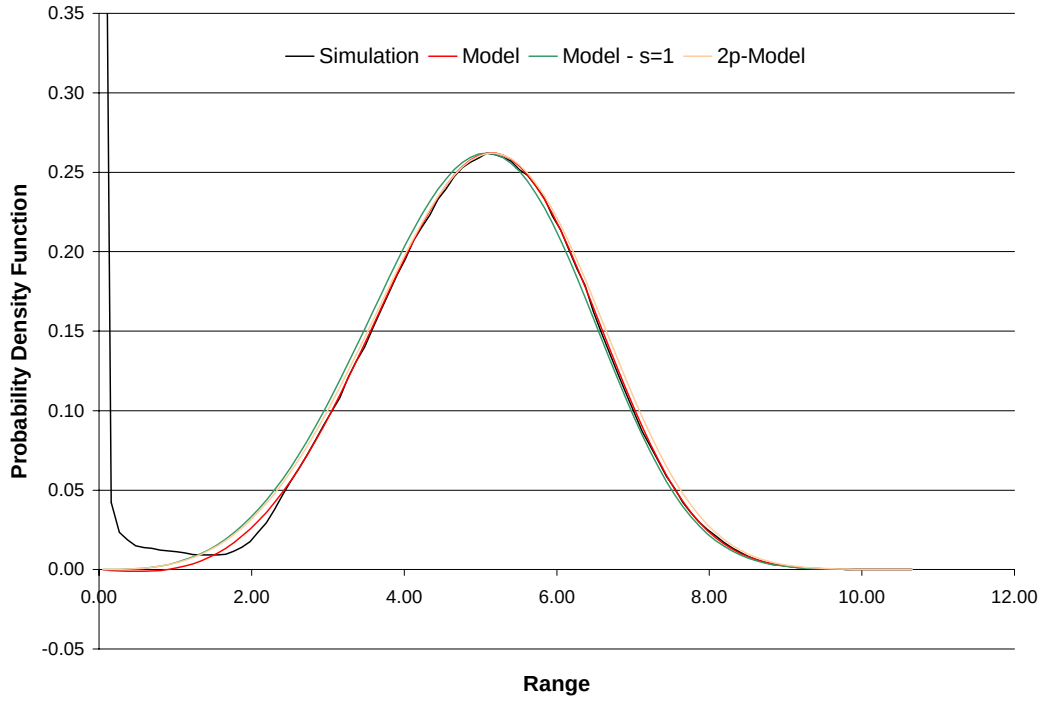

Figure 16. Probability density function of the stress ranges and its approximations by Eq. (B.25) ("Model"), Eq. (B.26) ("Model - *s* = 1"), and Eq. (B.28) ("2p- Model"), *SPL* = 154 dB.

Figures 6-10 have provided a strong argument in favor of narrowbandedness but one final check can be made to fully confirm this property of the stress process. Specifically, since Eq. (B.11)-(B.13) (i.e. Eq. (11)-(13) of Appendix B) are exact in the case of a narrowband process, it was decided to compute the expected damage from these equations using an estimate of the frequency and the probability density of the stress ranges obtained by simulation, i.e. the data of Fig. 13-16. For simplicity and consistency, the frequency of the process was selected as $\omega = \sigma_{\dot{q}} / \sigma_q$. The results of these computations are shown in Fig. 17 for the excitation levels of 124 dB, 134 dB, 144 dB, and 154 dB, and for the values of *m* in the domain [1, 8]. Surprisingly, it is found that the errors are independent of *m*! This situation can only occur if the

(a) the process is narrowband, and

(b) the distribution of stress ranges is exact, and

(c) the estimate of the frequency is in error.

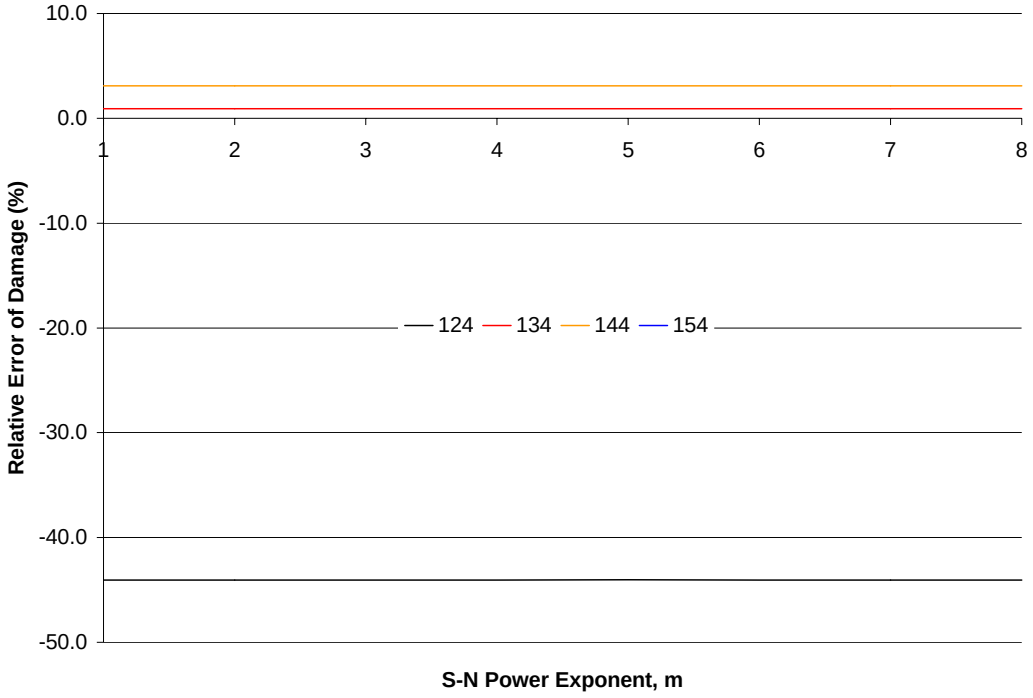

Figure 17. Relative error on the prediction of the expected damage as a function of the S-N exponent *m* for different *SPL* (124 dB, 134 dB, 144 dB, and 154 dB), Eq. (11)-(14) and the exact (simulation) distribution of stress ranges.

In fact, a simple correction could be made to eliminate all errors: if the frequency of the process is selected so that the damage corresponding to $m = 1$ equals the Rayleigh value (which is exact if the velocity process is Gaussian as is the case here) then all errors become negligible.

It is then concluded from the above discussions that the stress process is indeed narrowband in the high sound pressure level regime.

3.2 Additional Comments on the Experimental Data

While the general behavior of the prediction errors was similar for the experimental data and for the one-mode model simulations, there were some noticeable differences, e.g. the reliability of the 2-parameter model, Eq. (B.28). Two potential origins of these differences were investigated: (i) the narrowbandedness of the strain processs and (ii) the C_2 effect on the strains. To investigate the narrowband character of the experimentally measured strains, the two-dimensional histogram of the ranges and half-periods was produced for each sound pressure level. The plots corresponding to *SPL* of 152 dB, 158 dB, 167 dB, and 172 dB are shown in Fig. 18-21. Besides the high occurrence of very short ranges at a high frequency, the dominant contribution to the damage originates from a small band of half-periods suggesting that the strain process can be considered to be narrowband. The presence of subharmonics of the fundamental frequency, as already seen in Fig. 6-10, can also be noted in Fig. 18-21 but are especially clear on Fig. 21. From these figures, the probability density function of the strain ranges is readily extracted and is seen in Fig. 22 for all sound pressure levels. A comparison of these different curves clearly indicates that there no sharp transition in this data, as opposed to the simulation results of the buckled panel.

The assessment of the membrane effects, i.e. the coefficient C_2, on the displacement-strain relation brought up some important issues not present in the single mode model and which are under continued investigation. Specifically, the one-mode model yields the

quadratic displacement-strain/stress relation of Eq. (1) and (2). In a complex multi-mode situation however it could be expected that the membrane ($C_2\ q^2$) and bending ($C_1\ q$) effects would not originate in the same combination q of modal contributions. Thus, it could be expected that Eq. (2) might take the form

$$S = C_0 + C_1\ q + C_2\ y^2 \tag{129}$$

where q and y would be different random variables. This issue will be re-addressed in details in connection with the reduced order simulations in which both displacements and stresses will be recorded (see Appendix C).

It was then desired here to assess the level of the membrane effects on the reliability or lack thereof of the results shown in Appendix B. To this end, both Eq. (1), (2) and (129) were considered and the coefficients C_0, C_1, C_2, and/or the variances of the underlying processes q and y ($E\left[q^2\right]$ and $E\left[y^2\right]$) were estimated from the characteristics of the measured strains.

Equations (1) and (2) were considered first. It was assumed that the underlying process q was symmetric and zero mean. A nonzero mean effect would be transferred to the coefficient C_0. Although it was argued in the Phase I final report that Eq. (1),(2) are

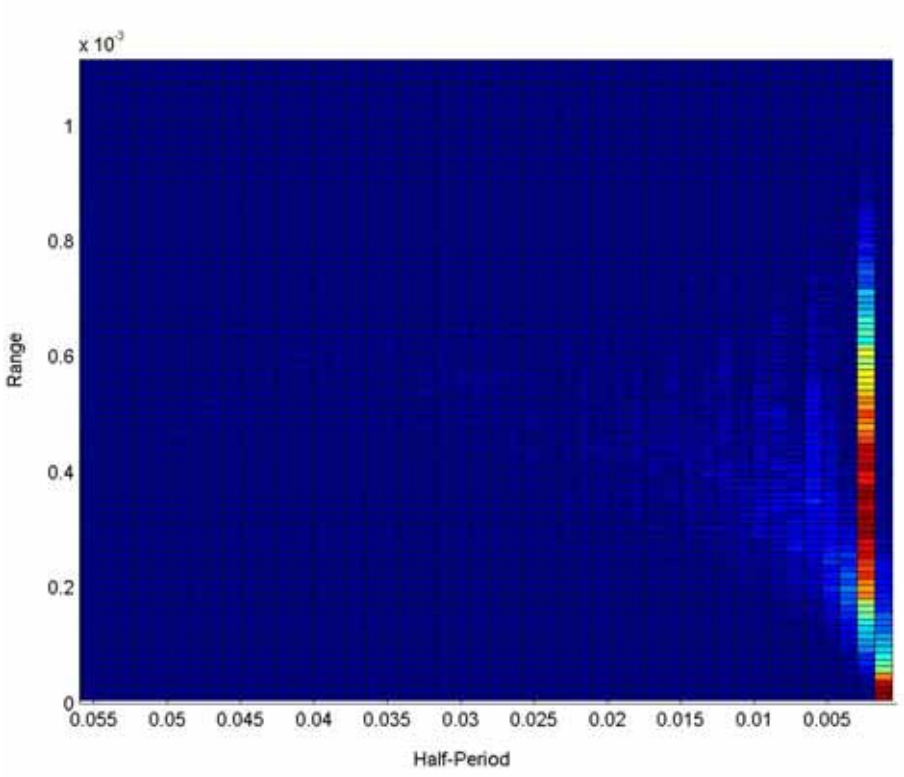

Figure 18. Histogram of ranges and half-periods, experimental data, *SPL* = 152 dB.

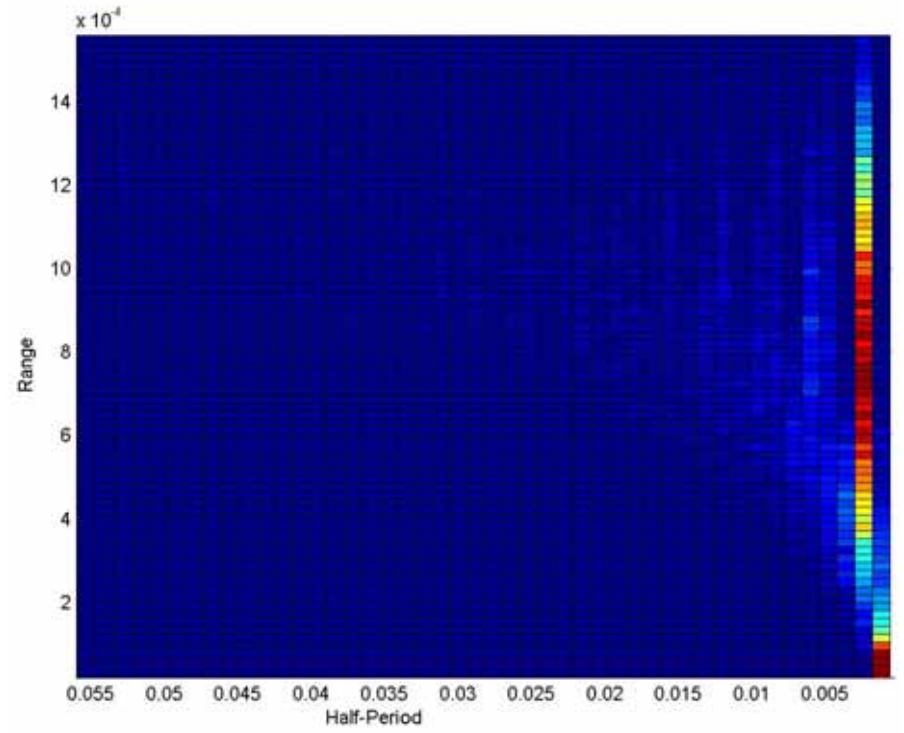

Figure 19. Histogram of ranges and half-periods, experimental data, *SPL* = 158 dB.

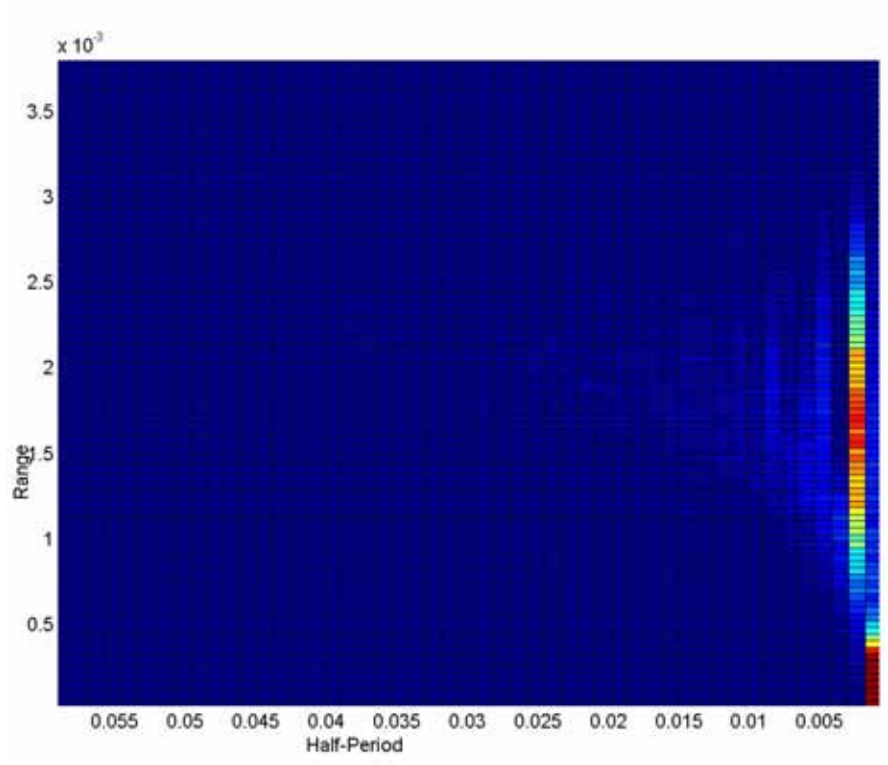

Figure 20. Histogram of ranges and half-periods, experimental data, *SPL* = 167 dB.

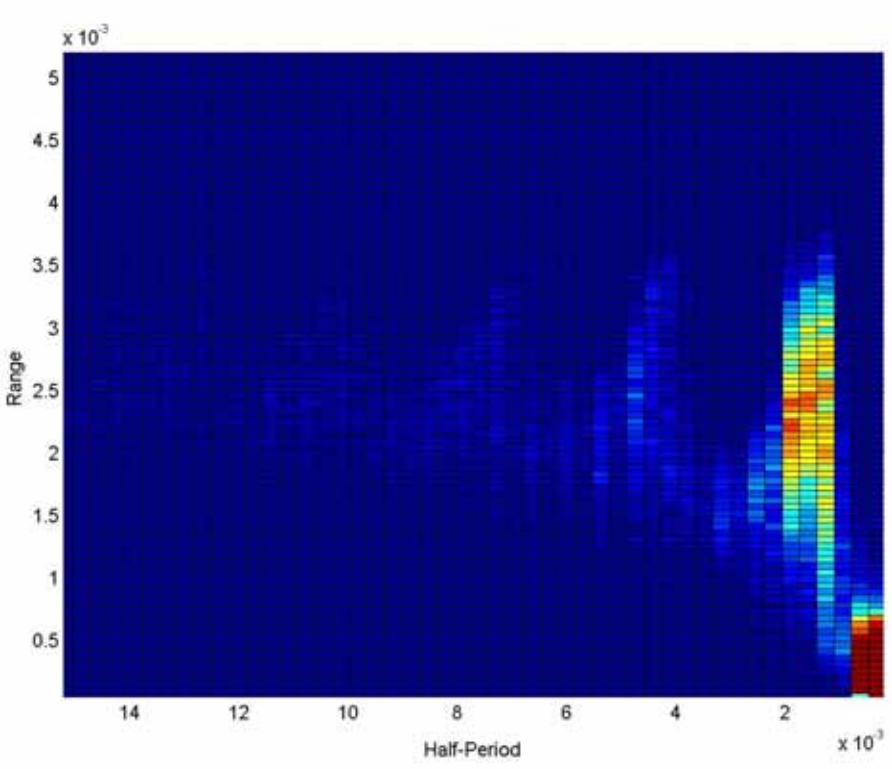

Figure 21. Histogram of ranges and half-periods, experimental data, *SPL* = 172 dB.

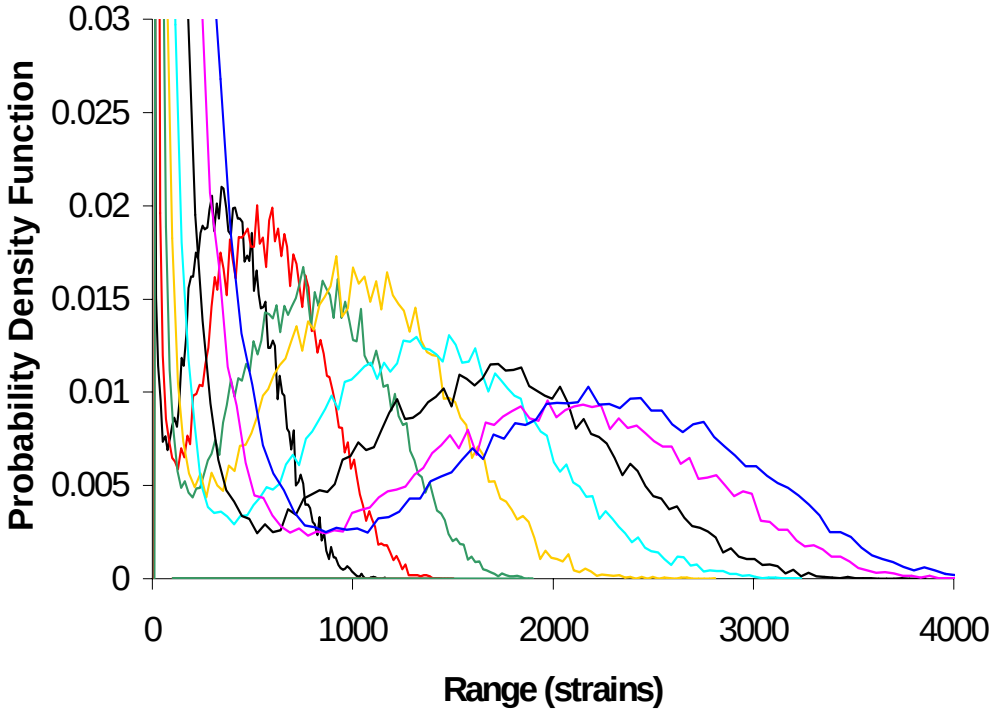

Figure 22. Probability density function of strain ranges, experimental data, all *SPL*.

not one-to-one, it was noted that the time histories of the strains did not include any bottoming out occurrences so that the range of values of q did not appear to come near the minimum of the quadratic expression and thus the transformation could be thought of as one-to-one and monotonic, increasing say. Then, $\text{Prob}\left[S > C_0\right] = \text{Prob}\left[q > 0\right] = 0.5$ in view of the symmetry of the process q and it is concluded that the coefficient C_0 equals the median of the strain distribution.

Since q is unknown, it is not possible to evaluate separately C_1, C_2, and $E\left[q^2\right]$. Accordingly, it will be assumed that C_1 = 1. Then, C_2 and $E\left[q^2\right]$ can be estimated from the mean and variance of the strains. Specifically, it is found that

$$\mu_S = E[S] = C_0 + C_2\, E\left[q^2\right] \tag{130}$$

and

$$E\left[(S-\mu_S)^2\right] = C_1^2\ E\left[q^2\right] + C_2^2\left(\kappa_{4q}-1\right)\left\{E\left[q^2\right]\right\}^2 \tag{131}$$

where κ_{4q} is the unknown coefficient of kurtosis of the underlying response process *q*. Solving these two nonlinear equations yields

$$E\left[q^2\right] = E\left[(S-\mu_S)^2\right] - \left(\kappa_{4q}-1\right)\left[\mu_S - C_0\right]^2 \tag{132}$$

and

$$C_2 = \frac{\mu_S - C_0}{E\left[q^2\right]}\ . \tag{133}$$

It would seem that the estimation of C_2 and $E\left[q^2\right]$ is circular: the coefficient κ_{4q} is necessary to obtain these parameters but it is also a part of the solution as the process *q* is unknown. In fact, it was found in all cases that the second term on the right-hand-side of Eq. (41) was in the range of 0.1% to 1% of the first term so that $\sigma_q \approx \sigma_S$. It was thus concluded that the membrane effects were negligible according to the model of Eq. (1) and (2). Interestingly, the coefficients C_2 were found to be approximately constant: equal to 154 at 152 dB and 114 at 172 dB. As a final check, the third moment of the strains were recomputed from Eq. (1) and (2) under the assumption of a Gaussian distribution for the process *q* and they were found to be at least of the same order of magnitude as the third moment of the data.

The estimation of the parameters of the model of Eq. (129) requires the joint probability density function of the random variables *q* and *y*, or at least some information about their correlation. If they are fully correlated, *q* and *y* are proportional to each other and the model of Eq. (1) and (2) is recovered. Thus, the opposite limiting case where *q* and *y* are independent was assumed to get a range of perspectives on the magnitude of the membrane effects. The arguments that led to the estimation of C_0 as the median of the strains do not apply any longer and this parameter and the variances $E\left[q^2\right]$ and $E\left[y^2\right]$

(the values of both parameters C_1 and C_2 must be assumed) were estimated from the first three moments of the strains. Proceeding as in Eq. (130) and (131), it was found that

$$\mu_S = E[S] = C_0 + C_2 \, E\left[y^2\right] \tag{134}$$

and

$$E\left[(S - \mu_S)^2\right] = C_1^2 \, E\left[q^2\right] + C_2^2 \left(\kappa_{4y} - 1\right) \left\{E\left[y^2\right]\right\}^2 \tag{135}$$

The evaluation of the third moment was for simplicity accomplished under the assumption of a Gaussian random variable *y* and led to

$$E\left[(S - \mu_S)^3\right] = 8 \, C_2^3 \left\{E\left[y^2\right]\right\}^3 . \tag{136}$$

Solving Eq. (135) and (136) for $E\left[q^2\right]$ and $E\left[y^2\right]$ led to the conclusion that the membrane term accounted for about 10%-20% of the variance of the strains, see Eq. (135), throughout the entire range of sound pressure levels.

3.3 Validation of the Damage Accumulation Model to Reduced Order Modeling Data

The damage accumulation model introduced in Appendix B was successfully validated to data generated by the reduced order modeling strategy (ELSTEP/FAT). This validation is presented in Appendix C:

Radu, A., Yang, B., Kim, K., and Mignolet, M.P., "Prediction of the Dynamic Response and Fatigue Life of Panels Subjected to Thermo-Acoustic Loading," *Proceedings of the 45th Structures, Structural Dynamics, and Materials Conference,* Palm Springs, California, Apr. 19-22, 2004. Paper AIAA-2004-1557.

4. REDUCED ORDER MODELING

The work in this area has focused on the formulation of a reliable reduced order modeling strategy of panels subjected to thermo-acoustic effects and the development of an associated general purpose software. This work is described in details in Appendices C, D, and E.

Appendix D:

Mignolet, M.P., Radu, A.G., and Gao, X., "Validation of Reduced Order Modeling for the Prediction of the Response and Fatigue Life of Panels Subjected to Thermo-Acoustic Effects," *Proceedings of the 8th International Conference on Recent Advances in Structural Dynamics*, Southampton, United Kingdom, Jul. 14-16, 2003.

Appendix E:

ELSTEP/FAT v.β2.0 User's Manual.

5. REFERENCES

Bellizzi, S., and Bouc, R., 1999a, "Analysis of Multi-Degree of Freedom Strongly Non-Linear Mechanical Systems with Random Input. Part I: Non-Linear Modes and Stochastic Averaging," *Probabilistic Engineering Mechanics*, Vol. 14, pp. 229-244.

Bellizzi, S., and Bouc, R., 1999b, "Analysis of Multi-Degree of Freedom Strongly Non-Linear Mechanical Systems with Random Input. Part II: Equivalent Linear System with Random Matrices and Power Spectral Density Matrix," *Probabilistic Engineering Mechanics*, Vol. 14, pp. 245-256.

Bouc, R., 1994, "The Power Spectral Density of Response for a Strongly Non-Linear Random Oscillator," *Journal of Sound and Vibration*, Vol. 175, No. 3, pp. 317-331.

Bruckner, A., and Lin, Y.K., 1987, "Generalizations of the Equivalent Linearization Method for Non-Linear Random Vibration Problems," *International Journal of Non-Linear Mechanics*, Vol. 22, No. 8, pp. 227-235.

Caughey, T.K., 1965, "On the Response of a Class of Nonlinear Oscillators to Stochastic Excitation," *Les Vibrations Forcées dans les Systèmes Non-Linéaires*, Editions du Centre National de la Recherche Scientifique, Paris, France, pp. 393-405.

Crandall, S.H., 2001, "Is Stochastic Equivalent Linearization a Subtly Flawed Procedure?," *Probabilistic Engineering Mechanics*, Vol. 16, No. 2, April, pp. 169-176.

Elishakoff, I., and Colajanni, P., 1997, "Stochastic Linearization Critically Re-Examined," *Chaos, Solitons, Fractals*, Vol. 8, pp. 1957-1972.

Elishakoff, I, and Zhang, R., 1992, "Comparison of New Energy-Based Versions of the Stochastic Linearization Technique," *Proceedings of the IUTAM Symposium, Nonlinear Stochastic Mechanics*, Bellomoto, N., and Casciati, F., (Eds), Springer-Verlag, pp. 201-211.

Iyengar, R.N., 1988, "Higher Order Linearization in Non-Linear Random Vibration," *International Journal of Non-Linear Mechanics*, Vol. 23, No. 5/6, pp. 385-391.

Kim, K., Yang, B., Mignolet, M.P., and Spottswood, S.M., "Fatigue Life Prediction of Panels Subjected to Thermo-Acoustic Loading," *Proceedings of the 44th Structures, Structural Dynamics, and Materials Conference*, Norfolk, Virginia, Apr. 7-10, 2003. Paper AIAA-2003-1776.

Lutes, L.D., and Larsen, C.E., 1990, "Improved Spectral Method for Variable Amplitude Fatigue," *Journal of Structural Engineering*, Vol. 116, No. 4, pp. 1149-1164.

Lutes, L.D., and Sarkani, S., 1997, *Stochastic Analysis of Structural and Mechanical Vibrations*, Prentice-Hall.

Mignolet, M.P., 1993, "Simulation of Random Processes and Fields by ARMA Models: A Review," Chapter 7, Cheng, A.H-D., and Yang, C.Y., (Eds), *Computational Stochastic Mechanics*, pp. 149-173, Elsevier.

Mignolet, M.P., and Red-Horse, J.R., 1994, "ARMAX Identification of Vibrating Structures: Model and Model Order Estimation," *Proceedings of the 35th Structures, Structural Dynamics, and Materials Conference*, Hilton Head, South Carolina, Apr. 18-20, pp. 1628-1637.

Moon, F., 1992, *Chaotic and Fractal Dynamics, an Introduction for Applied Scientists and Engineers*, Wiley-Interscience.

Muravyov, A.A., Turner, T.L., Robinson, J.H., and Rizzi, S.A., "A New Stochastic Equivalent Linearization Implementation for Prediction of Geometrically Nonlinear Vibrations," *Proceedings of the 40th Structures, Structural Dynamics, and Materials Conference*, 1999. Paper AIAA-1999-1376.

Roberts, J.B., and Spanos, P.D., 1990, *Random Vibration and Statistical Linearization*, Wiley.

Roy, R.V., and Spanos, P.D., 1993, "Power Spectral Density of Nonlinear System Response: The Recursion Method," *Journal of Applied Mechanics*, Vol. 60, pp. 358-365.

Socha, L, and Pawleta, M., 1994, "Corrected Equivalent Linearization of Stochastic Dynamic Systems," Machine Dynamics Problems, Vol. 7, pp. 149-161.

Soize, C., 1995, "Stochastic Linearization Method with Random Parameters for SDOF Nonlinear Dynamical Systems: Prediction and Identification Procedures," *Probabilistic Engineering Mechanics*, Vol. 10, pp. 143-152.

Soize, C., and Le Fur, O., 1997, "Modal Identification of Weakly Non-Linear Multidimensional Dynamical Systems Using a Stochastic Linearisation Method with Random Coefficients," *Mechanical Systems and Signal Processing*, Vol. 11, No. 1, pp. 37-49.

Wiener, N., and Masani, P., 1957, “The Prediction Theory of Multivariate Stochastic Processes, I. The Regularity Condition,” *Acta Mathematica*, Vol. 98, November, pp. 111-150.

Wiener, N., and Masani, P., 1958, “The Prediction Theory of Multivariate Stochastic Processes, II. The Linear Predictor,” *Acta Mathematica*, Vol. 99, April, pp. 93-137.

Zhang, X., Elishakoff, I, and Zhang, R., 1991, “A Stochastic Linearization Technique Baed on Minimum Mean Square Deviation of Potential Energy,” *Stochastic Structural Dynamics*, Lin, Y.K, and Elishakoff, I, (Eds), Springer-Verlag, pp. 328-338.

Appendix A

"Implicit Modeling of the Power Spectral Density of the Response of a Class of Nonlinear Oscillators"

Proceedings of the 9th Joint Specialty Conference on Probabilistic Mechanics and Structural Reliability,
Albuquerque, New Mexico, Jul. 26-28, 2004.

Implicit Modeling of the Power Spectral Density of the Response of a Class of Nonlinear Oscillators

B. Yang, and M.P. Mignolet, M. ASCE
Arizona State University, Tempe, AZ 85287-6106
bo.yang@asu.edu,marc.mignolet@asu.edu

Abstract

This paper addresses the representation of the power spectral density of the Duffing Oscillator through the random stiffness linear single-degree-of-freedom model. Some similar existing representations are reviewed and a new parametric distribution of the stiffnesses is proposed. The estimation of the two parameters of this model is then addressed. Examples of application demonstrate that the proposed representation is simple and accurate from systems behaving almost linearly to those exhibit a very strong nonlinearity.

Introduction

The power spectral density represents one of the most basic description of the time varying aspects of a stochastic process and thus is an essential information to estimate. Yet, accurately determining this power spectrum without recourse to comprehensive Monte Carlo simulations is in general a particularly difficult task even for the simplest systems, e.g. single-degree-of-freedom nonlinear oscillators subjected to white noise excitation. Although the stationary probability density function of the response is known in closed form for a class of such systems, no similar expression is available for its power spectrum. In fact, this scarcity of solution arises because the spectrum relates to the full nonstationary Fokker-Planck equation of which only a handful of solutions exist (e.g. Caughey and Dienes, 1961, and the extension of Mignolet and Fan, 1993).

In light of these difficulties, it has sometime been suggested to rely on the equivalent linearization approach which is known to provide good estimates of the variance of the response in many situations. While this approach achieves some success, i.e. it does predict quite well the shifting of the spectrum as the excitation level is increased for the Duffing system considered here, it also fails to account for other aspects such as the peak broadening (see Soize, 1995, for a discussion). Capturing this feature of nonlinearity requires a more sophisticated model than the equivalent linear system. In fact, an improved shaping of the power spectrum can be obtained by representing the response of the nonlinear oscillator as that of a linear multi-degree-of-freedom system. The application of either the recursion method (Roy and Spanos, 1993) or the cumulant closure strategy (Cai and Lin, 1996) does lead to such a model.

Another group of efforts have relied on the representation of the solution of the nonlinear stochastic differential equation as the response of a linear system with random coefficients (e.g. see Miles, 1989, Bouc, 1994, Soize, 1995, Krenk and Roberts, 1999). Such a model can be justified by decomposing any realization of the response process into a series of half cycles of different amplitudes and, generally, different frequencies given the nonlinearity of the system. In fact, a more formal and complete derivation of

this model has been accomplished on the basis of the statistical averaging by Bouc (1994) and Krenk and Roberts (1999). A different approach was adopted by Soize (1995) who postulated such a model with random stiffness and/or damping ratio following a specific distribution and identified its parameters using the variance of the response and/or its velocity. Interestingly, these concepts have been generalized to multi-degree-of-freedom systems (see Soize and Le Fur, 1997, and Bellizzi and Bouc, 1999).

In light of these successes, the goal of this paper is to revisit the connections between the power spectrum and the distribution of random frequencies and to propose and validate a new parametric probability density function of these random variables for the Duffing oscillator.

Representation of the Power Spectrum of the Duffing Oscillator Response

Proceeding with appropriate normalizations (e.g. see Bouc, 1994), the general governing equation of a Duffing oscillator can be rewritten in the compact form

$$\ddot{X} + 2\zeta\,\dot{X} + X + \lambda\,X^3 = \sqrt{4\zeta}\,W(t) \tag{1}$$

where ζ is the damping ratio in the linearized system, λ is a measure of the nonlinearity, and $W(t)$ is a white noise process of power spectral density $1/2\pi$. Situations in which the white noise power is different from $1/2\pi$ can be recast in the form of Eq. (1) by scaling the process $X(t)$ by the standard deviation of the response of the linearized system. This transformation modifies the value of λ and thus demonstrates that this parameter is a function of the actual nonlinearity strength but also the excitation level.
Following previous investigators, the power spectrum of the response $X(t)$ will be represented as

$$S_{XX}(\omega) = \frac{1}{2\pi}\int_0^\infty \frac{4\zeta}{\left(\omega^2 - k\right)^2 + 4\zeta^2\,\omega^2}\,p_K(k)\,dk \tag{2}$$

where $p_K(k)$ denotes the probability density function of the random stiffnesses. In fact, the right-hand-side of Eq. (2) can be viewed as the expectation of the conditional spectrum, given $K = k$, of the random stiffness linear single-degree-of-freedom system

$$\ddot{Y} + 2\zeta\,\dot{Y} + K\,Y = \sqrt{4\zeta}\,W(t). \tag{3}$$

In the limit of a zero damping ratio, it is found from Eq. (2) that

$$p_\Omega(\omega) = 2\,\omega^2\,S_{XX}(\omega) \qquad \omega \geq 0 \tag{4a}$$

where $K = \Omega^2$ and, in parallel, from Eq. (3)

$$\dot{X}(t) \approx \dot{Y}(t) = a\cos(\Omega t + \Phi) \tag{4b}$$

with appropriate amplitude a and random phase Φ. Equations (4) provide a simple representation of the response process consistent with the random frequency simulation algorithm (see Goto and Toki, 1969, and Shinozuka, 1971).

For nonzero damping ratios, Bouc (1994) proceeded with a stochastic averaging strategy and obtained a representation of the power spectrum similar to Eq. (2) but expressed in

terms of the distribution of the amplitude of the process $X(t)$. His solution can be recast in the form of Eq. (2) with

$$p_K^B(k) = B\,\sqrt{k}\,(3\,k-1)\,(k-1)\exp\left[-\frac{(3\,k-1)^2}{10\,\lambda}\right] \quad k \geq 1 \tag{5}$$

where B is the appropriate normalization constant. The power spectral density obtained from Eq. (5) and from a thorough Monte Carlo simulation of Eq. (1) are shown in Fig. 1(a) for $\lambda = 10$ and $\zeta = 0.01$. Note the excellent matching of these two curves. For completeness, the corresponding probability density function of the stiffnesses is also shown in Fig. 1(b)

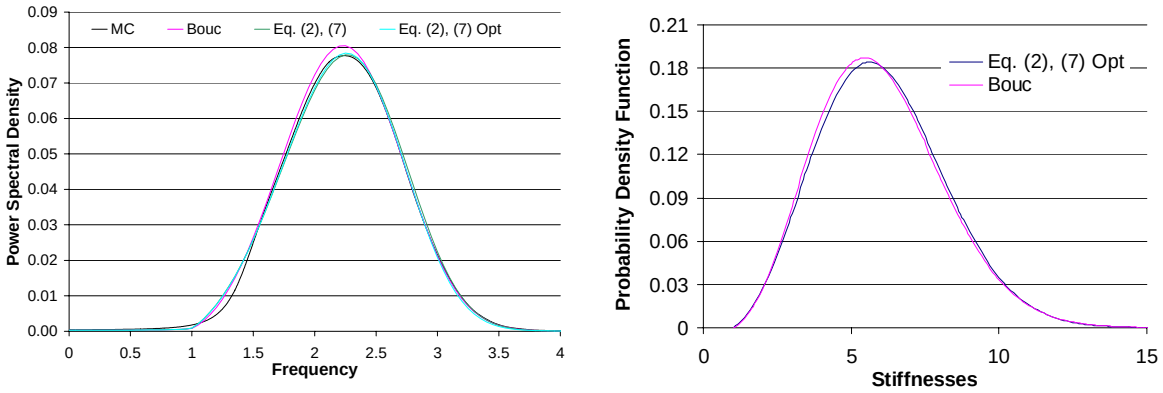

(a) (b)

Figure 1. (a) Power spectral density and (b) probability density function of stiffnesses for the Duffing oscillator for $\lambda = 10$ and $\zeta = 0.01$. "MC": Monte Carlo simulations, "Bouc": from Bouc (1994), "Eq. (2), (7)": Using Eq. (2) and (7) with the parameters a and b evaluated from the variance, mean stiffness, and moment equation conditions. "Eq. (2), (7) Opt": Using Eq. (2) and (7) with the parameters a and b evaluated from an optimum match of the MC spectrum

Soize (1995) proceeded differently and postulated a parametric distribution of the stiffnesses as

$$p_K^S(k) = C\,k\,(k-1)\exp\left[-\frac{(k-1)^2}{b^2}\right] \quad k \geq 1 \tag{6}$$

where C is a normalization constant and the coefficient b is selected so that the variance of the process $X(t)$ predicted from Eq. (2) matches its exact value. Note that a good qualitative agreement with the Monte Carlo simulation results was achieved but the accuracy of the matching/prediction is nevertheless limited by the presence of only 1 adjustable parameter.

To palliate this situation, the following 2 parameter model

$$p_K(k) = D\,(1+\lambda\,k)\,(k-1)\exp\left[-\frac{(k-a)^2}{b^2}\right] \quad k \geq 1 \tag{7}$$

is introduced here where D is the appropriate normalization constant. As a first verification of the adequacy of the model, an optimization effort was undertaken in which

the parameters *a* and *b* were selected to obtain the closest matching of the power spectral densities obtained from Eq. (2) and (7) and from Monte Carlo simulations. The corresponding optimum distribution of stiffnesses and the corresponding approximation of the power spectrum are also shown in Fig. 1. Note in particular the excellent matching of the simulated power spectrum by its approximation from Eq. (2) which supports the validity of the parametric distribution of Eq. (7).

Estimation of the Distribution Parameters

Having validated the adequacy of the distribution of Eq. (7), it remains to devise a strategy for the evaluation of its two parameters *a* and *b* from basic information about the process. To this end, three different conditions will now be described.

Variance Conditions

Proceeding as Soize (1995), it is first required that the approximate power spectral density of Eq. (2) yields variances of the displacement process and of its velocity that are equal to their exact values which can be predicted from the stationary probability density function. Equivalently, it is required that

$$\int_{-\infty}^{\infty} S_{XX}(\omega)\, d\omega = \sigma_X^2 \quad \text{and} \quad \int_{-\infty}^{\infty} \omega^2 S_{XX}(\omega)\, d\omega = \sigma_{\dot{X}}^2 = 1 \tag{8}$$

Using the properties of the spectrum of linear single-degree-of-freedom systems, it is readily shown that the second condition is automatically satisfied while the second one can be rewritten simply as

$$E\left[\frac{1}{K}\right] = \sigma_X^2 \,. \tag{9}$$

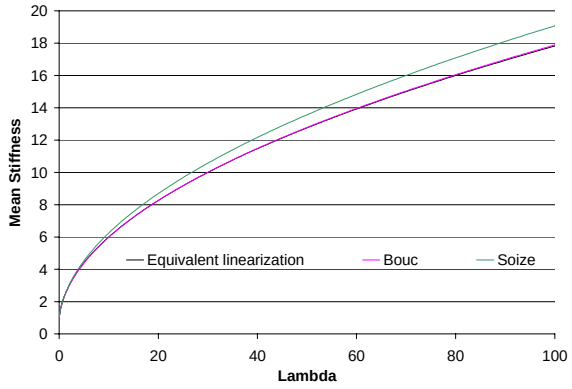

Figure 2. Mean stiffness predicted from the Bouc (1994) and Soize (1995) models and equivalent linear stiffness

Mean Stiffness Condition

Since only one variance condition can be used to estimate the two model parameters, additional constraints must be sought. To this end, the distribution of the random stiffness corresponding to the Bouc model, i.e. Eq. (5), was investigated and its moments were evaluated. The mean stiffness, $E[K]$, was of particular interest as it provides an overall,

deterministic measure of the stiffness of the random coefficient system of Eq. (3). In that light, it was more specifically desired to compare the values of this mean stiffness and of the deterministic stiffness obtained from the equivalent linearization technique (Roberts and Spanos, 1991). These two quantities were evaluated over a broad range of values of the nonlinearity parameter λ and a remarkable agreement between them was obtained throughout, see Fig. 2. This finding thus suggests that the equivalent linearization technique can be viewed as a simplified case of the random parameter model of Eq. (2) in which the distribution of the stiffnesses is simply a Dirac delta function.

Moment Equation Condition

The use of the variance and mean stiffness conditions alone for the determination of the two parameters *a* and *b* of the distribution of stiffness did not provide a matching of the approximate (Eq. (2)) and simulated power spectra as good as could be expected from Fig. 1. Accordingly, a third condition that involves more directly the dynamics of the Duffing oscillator was sought. One such condition is the moment equation

$$-E\left[\dot{X}^2\right]+E\left[X^2\right]+\lambda\,E\left[X^4\right]=0 \tag{10}$$

which however involves the fourth order moment $E\left[X^4\right]$ and thus requires a more detailed model than Eq. (2).

A conditional approach similar in spirit to the one of Bouc (1994) will be followed by assuming that the value of the stiffness K is fixed, i.e. $K=k$. Then, two possible approximation strategies can be devised. First, it can be argued that the motion corresponding to a fixed frequency/stiffness must be close to harmonic with a slowly varying amplitude A and frequency Ω. Then, it is found that

$$E\left[\dot{X}^2\right]=\frac{1}{2}E\left[A^2\,\Omega^2\right],\qquad E\left[X^2\right]=\frac{1}{2}E\left[A^2\right],\quad \text{and } E\left[X^4\right]=\frac{3}{8}E\left[A^4\right] \tag{11}$$

Combining Eq. (10) and (11) yields

$$E\left[A^2\left(\Omega^2-1-\frac{3}{4}\lambda\,A^2\right)\right]=0 \tag{12}$$

This equation is in particular satisfied if the amplitude A is defined according to

$$\Omega^2=1+\frac{3}{4}\lambda\,A^2 \text{ or } A^2=\frac{4}{3\lambda}\left(\Omega^2-1\right) \tag{13}$$

Reintroducing this expression for the amplitude in Eq. (11) yields for the variances of the displacement and velocity

$$E\left[X^2\right]=\frac{1}{2}E\left[A^2\right]=\frac{2}{3\lambda}E\left[\left(\Omega^2-1\right)\right]=E\left[\frac{1}{K}\right] \tag{14a}$$

$$E\left[\dot{X}^2\right]=\frac{1}{2}E\left[A^2\,\Omega^2\right]=\frac{2}{3\lambda}E\left[\Omega^2\left(\Omega^2-1\right)\right]=1. \tag{14b}$$

where the last equalities of Eq. (14a) and (14b) originate from Eq. (8) and (9). Considering Ω^2 to be a function of K (one would expect $\Omega^2=K$), Eq. (14a) and (14b) imply the following equalities

$$\frac{2}{3\lambda}\left(\omega^2-1\right)p_{\Omega^2}\left(\omega^2\right)d\omega^2=\frac{1}{k}\,p_K(k)\,dk \tag{15a}$$

$$\frac{2}{3\lambda}\,\omega^2\left(\omega^2-1\right)p_{\Omega^2}\left(\omega^2\right)d\omega^2=p_K(k)\,dk\,. \tag{15b}$$

The above equations yield directly

$$\omega^2=k \tag{16a}$$

as expected, and in turn the condition

$$p_{\Omega^2}\left(\omega^2\right)=\frac{3\lambda}{2}\,\frac{1}{k\,(k-1)}\,p_K(k) \tag{16b}$$

which is however not consistent with Eq. (16a). Since Eq. (14) were only the integrated versions of Eq. (15), it is suggested here that it is sufficient to satisfy Eq. (16b) overall, i.e.

$$\frac{3\lambda}{2}\,E\left[\frac{1}{K\,(K-1)}\right]=1\,. \tag{17}$$

A different condition can be obtained from Eq. (10) by relying on the conditionally Gaussian character of the solution of Eq. (3) given $K=\Omega^2=k$. With this assumption, Eq. (10) becomes

$$E\left[\frac{1}{K}+\frac{3\lambda}{K^2}\right]=1\,. \tag{18}$$

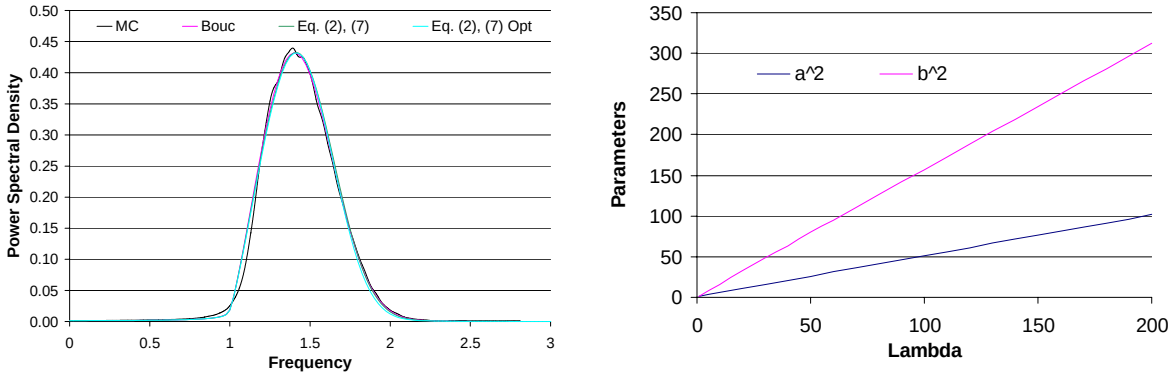

(a) (b)

Figure 3. (a) Power spectral density for the Duffing oscillator for λ = 1 and ζ = 0.01. "MC": Monte Carlo simulations, "Bouc": from Bouc (1994), "Eq. (2), (7)": Using Eq. (2) and (7) with the parameters a and b evaluated from the variance, mean stiffness, and moment equation conditions. "Eq. (2), (7) Opt": Using Eq. (2) and (7) with the parameters a and b evaluated from an optimum match of the MC spectrum. (b) Values of the parameters a^2 and b^2 vs. λ.

Numerical Results

To assess the reliability of the parameter estimation procedure, the Duffing oscillator with λ = 10 and ζ = 0.01 was reconsidered and the exact variance of the displacement

$X(t)$ was used in Eq. (9). Further, the mean stiffness and moment equation conditions (Eq. (17)) were also enforced and the parameters a and b of the model of Eq. (7) were selected as to best fit all three conditions. This process yielded the approximate power spectrum also shown in Fig. 1(a). Clearly, an excellent matching of the simulation results is achieved. In fact, an excellent matching was obtained throughout the range $\lambda > 0$, see also Fig. 3(a) for $\lambda = 1$. For values $\lambda \leq 1$, the optimization process was achieved under the additional physical constraint $a > 1$. For completeness, the dependence of the coefficients a and b on λ is displayed in Fig. 3(b). Note in particular that a^2 and b^2 display an almost linear behavior with respect to λ throughout the entire range of values of this parameter.

Summary

The focus of this paper has been on the simple and reliable prediction of the power spectral density of the response of the Duffing oscillator. The representation of its response in terms of the response of a linear single-degree-of-freedom with random stiffness provides an excellent format for the modeling of its power spectral density as an expectation, see Eq. (2). In this light, the contributions of the present effort can be summarized as follows.

(1) A revisit of existing models has led to the observation that the mean of the distribution of the random stiffnesses agrees very closely with the equivalent linear stiffness obtained by the equivalent linearization technique.

(2) A novel two-parameter probability density function of the random stiffnesses has been proposed which was shown to have the flexibility to yield an accurate representation of the power spectrum of the Duffing oscillator for a broad class of nonlinearity strength.

(3) An identification procedure of the two parameters of the model was developed that relies on three conditions: the matching of the exact variance of the response, the matching of the mean stiffness with the equivalent linear stiffness, and the satisfaction of a moment equation.

(4) Numerical examples have demonstrated that both the model and the identification strategy of the parameters lead to an excellent agreement between the predicted power spectrum and the one obtained from Monte Carlo simulations.

(5) It was observed that the coefficients of the model exhibit a very simple relationship with respect to the nonlinearity parameter λ, i.e. their squares are almost linear functions of λ.

Acknowledgements

The support of this investigation by the Air Force Research Laboratory under contract F33615-01-C-3111 is gratefully acknowledged.

References

Bellizzi, S., and R. Bouc, (1999), "Analysis of Multi-Degree of Freedom Strongly Non-Linear Mechanical Systems with Random Input. Part I: Non-Linear Modes and Stochastic Averaging," *Probabilistic Engineering Mechanics,* **14**, 229-244.

Bellizzi, S., and R. Bouc, (1999), "Analysis of Multi-Degree of Freedom Strongly Non-Linear Mechanical Systems with Random Input. Part II: Equivalent Linear System with Random Matrices and Power Spectral Density Matrix," *Probabilistic Engineering Mechanics,* **14**, 245-256.

Bouc, R., (1994), "The Power Spectral Density of Response for a Strongly Non-Linear Random Oscillator," *Journal of Sound and Vibration*, **175**(3), 317-331.

Caughey, T.K., and J.K. Dienes, (1961), "Analysis of a Nonlinear First-Order System with a White Noise Input," *Journal of Applied Physics,* **32**, 2476-2479.

Cai, G.Q., and Y.K. Lin, (1996), "Response Spectral Densities of Strongly Nonlinear Systems Under Random Excitation," *Probabilistic Engineering Mechanics*, **12**(1), 41-47.

Goto, H., and K. Toki, (1969), "Structural Response to Nonstationary Random Excitation," *Proceedings of the 4th World Conference on Earthquake Engineering,* Santiago, Chile, **1**, 130-144.

Krenk, S., and J.B. Roberts, (1999), "Local Similarity in Non-Linear Random Vibration," *Journal of Applied Mechanics,* **66**, 225-235.

Mignolet, M.P., and G.W. Fan, (1993), "Nonstationary Response of Some First Order Non-Linear Systems Associated with the Seismic Sliding of Rigid Structures," *International Journal of Non-Linear Mechanics,* **28**(4), 393-408.

Miles, R.N., (1989), "An Approximate Solution for the Spectral Response of Duffing's Oscillator with Random Input," *Journal of Sound and Vibration*, **132**, 43-49.

Roberts, J.B., and P.D. Spanos, (1990), *Random Vibration and Statistical Linearization,* Wiley.

Roy, R.V., and P.D. Spanos, (1993), "Power Spectral Density of Nonlinear System Response: The Recursion Method," *Journal of Applied Mechanics,* **60**, 358-365.

Shinozuka, M., (1971), "Simulation of Multivariate and Multi-Dimensional Random Processes," *Journal of the Acoustical Society of America,* **49**, 357-367.

Soize, C., (1995), "Stochastic Linearization Method with Random Parameters for SDOF Nonlinear Dynamical Systems: Prediction and Identification Procedures," *Probabilistic Engineering Mechanics,* **10**, 143-152.

Soize, C., and O. Le Fur, (1997), "Modal Identification of Weakly Non-Linear Multidimensional Dynamical Systems Using a Stochastic Linearisation Method with Random Coefficients," *Mechanical Systems and Signal Processing,* **11**(1), 37-49.

Appendix B

"Modeling of Damage Accumulation for Duffing Oscillator-Type Systems Under Severe Random Excitations"

Probabilistic Engineering Mechanics, Vol. 19, pp. 185-194, 2004.

MODELING OF DAMAGE ACCUMULATION FOR DUFFING-TYPE SYSTEMS UNDER SEVERE RANDOM EXCITATIONS

B. Yang & M P. Mignolet
Department of Mechanical and Aerospace Engineering, Arizona State University, AZ, USA

S.M. Spottswood
Air Force Research Laboratory, Air Vehicles Directorate, Wright-Patterson, OH, USA

Keywords: fatigue life, aircraft panels, Duffing equations, buckled panels, peaks distribution

ABSTRACT: The focus of this investigation is on the prediction of the fatigue life of aircraft panels subjected to thermal effects and a severe random acoustic excitation. The prototypical equations for this problem, i.e. the single and double well Duffing oscillators subjected to a bandlimited white noise, are first considered. A review of some currently available approaches, i.e. the Rayleigh approximation and the single spectral moment method both with and without Gaussianity correction, strongly suggests that an accurate prediction of the fatigue life for this nonlinear system requires a dedicated model. To this end, an approximation of the probability density function of the peaks of the stationary response of the Duffing oscillators is derived. This model is then used in conjunction with either a narrowband assumption or the single spectral moment methodology to yield a prediction of the fatigue life. The application of this approach to simulation data from both single and double well Duffing oscillators, as well as on the experimental response of an unbuckled panel, demonstrates the reliability of this novel approximation.

1 INTRODUCTION

The accurate prediction of the fatigue life of aircraft panels can represent a particularly challenging task, especially for the proposed supersonic and hypersonic vehicles such as the X-43 and Hyper-X. Indeed, the panels of these aircraft will be subjected to especially harsh operating conditions, e.g. surface temperatures possibly exceeding 3000^{o}F [1] and severe random acoustic loading from the engine exhaust. In normal operating conditions, thermal protection systems are expected to dramatically mitigate the thermal effects, i.e. reducing the temperature to a few hundred degrees, and thus should prevent the buckling of the panels that would otherwise take place.

While the acoustic loading may be sufficient to induce large motions of the panel in normal conditions, a strong nonlinearity of the response would result in the event of a malfunction of the thermal protection system. Indeed, the panels would then be expected to buckle and the acoustic excitation would induce "snap-throughs", i.e. large amplitude motions from one buckled position to another. To these snap-thoughs are associated high amplitude stress cycles producing a dramatic reduction in the fatigue life of the panels.

The previous investigations of this problem have primarily focused on the important physical description and prediction of the panel response (see [2]-[6] and references therein) with some efforts extending to the assessment of the fatigue life, e.g. [3], [7]. Given the importance of the problem, however, it would be very desirable to dispose of a general framework for the prediction of the fatigue life of buckled and unbuckled panels subjected to a random acoustic loading from a specified finite element model of the panels. The

present effort focuses on a specific component of the above framework, i.e. the modeling of the damage accumulation process and, more specifically, on relating the fatigue life to certain characteristics (e.g. moments, spectral moments) of the response process. This goal will be achieved through first the analysis of a prototypical single-degree-of-freedom system and next the validation of the obtained model on test data.

2 THE PROTOTYPICAL MODEL

It has been shown (e.g., [2]), that the response of heated panels subjected to a transverse loading can be modeled by the dimensionless Duffing equation

$$\ddot{q} + 2\,\zeta\,\omega_0\,\dot{q} + \omega_0^2\,(1-s)\,q + \gamma\,q^3 = \bar{p}_0 + \bar{p}(t) \quad (1)$$

where ω_0 is the natural frequency of the panel in small motions around its unheated undeformed state and s is the ratio of the average panel temperature to its buckling temperature. Further, ζ denotes the damping ratio of the panel and γ the nonlinear stiffening coefficient arising from the large deformations (including membrane effects). Finally, the loading is characterized by the constant term $\bar{p}_0$ modeling the effects of the thermal moments (if the panel and/or the temperature distribution are not symmetric) and the random process $\bar{p}(t)$ representing the acoustic excitation.

Once the panel displacement $q(t)$ has been determined, the stresses can be evaluated by the quadratic, memoryless transformation

$$S = C_0 + C_1\,q + C_2\,q^2 \quad (2)$$

where C_0, C_1, and C_2 are constant coefficients that depend on the stress and the location on the panel considered.

To distinguish the specific issues associated with the nonlinearity of the dynamics of the system, i.e. γ, from those relevant to the nonlinearity of the stress-displacement relation, i.e. C_2, the special case $C_2 = 0$ was considered in the simulation studies. The fatigue life estimated from the stress and displacement time histories only differ by a scaling factor. Thus, it is sufficient to only consider the displacement ranges for the comparison investigated here.

The response of the system of Eq. (1) exhibits two different asymptotic behaviors for buckled panels with two buckled states, e.g. $s > 1$ and $\bar{p}_0 = 0$. Specifically, at low excitation (sound pressure) levels, the system primarily vibrates around each of the buckled states with an occasional transition from one state to the other. However, at severe excitation levels, the situation of interest here, the panel experiences very frequent snap-throughs and the response is fully nonlinear. Finally, a small transition region exists between these two limiting cases. For unbuckled panels, the response evolves slowly from that of a linear system to a fully nonlinear response similar to the one obtained for buckled panels.

3 ASSESSMENT OF THE RAYLEIGH METHOD AND THE SINGLE MOMENT APPROACH

The Rayleigh formula provides an estimate of the damage accumulated over a time T by assuming:

(i) that the random process is Gaussian, and

(ii) that the random process is narrowband.

These two assumptions imply that the peak-to-peak ranges are distributed according to a Rayleigh distribution exhibiting a standard deviation equal to twice the standard deviation of the stress process. Further, the narrowbandedness leads to a simple estimate of the time interval over which the stress ranges take place, and thus ultimately of the number of cycles present in the time interval T. Accordingly, it is found that the expected accumulated damage can be expressed as

$$E[D] = 2^{3m/2}\,\Gamma(1+m/2)\,\sigma_{\dot{S}}\,\sigma_S^{m-1}\,T/(2\,\pi\,K) \quad (3)$$

where σ_S and $\sigma_{\dot{S}}$ are the standard deviations of the stress process and its time derivative and m

and K are the exponent and coefficient of the S-N curve, respectively.

To account for the expected deviations from the Gaussian assumption, (i) above, the correction factor proposed by Winterstein [8] has been considered. Specifically, the expected damage of Eq. (3) is divided by Gaussianity Ratio (GR) defined as

$$GR = 1 - m\,(m-1)\,(\kappa_4 - 3)/24 \quad \text{for} \quad \kappa_4 < 3 \tag{4a}$$

and

$$GR = \left[1 + m\,(m-1)\,(\kappa_4 - 3)/24\right]^{-1} \text{for} \, \kappa_4 > 3 \tag{4b}$$

where κ_4 denotes the coefficient of kurtosis of the stress process.

The single moment approach [9] was proposed for situations in which the process would be somewhat broadband and/or exhibits several narrow bands. The expected damage accumulated over a time T was postulated in the form of

$$E[D] = (\lambda_a)^{-b}\, T / c \tag{5}$$

where λ_a denotes the spectral moment of order a of the stress process, i.e.

$$\lambda_a = \int_{-\infty}^{+\infty} S_{SS}(\omega)\, \omega^a \, d\omega \tag{6}$$

where $S_{SS}(\omega)$ is the power spectral density of the stress process. Using dimensional analysis, it is concluded that the coefficients a and b must be given as

$$a = 2/m \qquad b = -m/2 \ . \tag{7}$$

Finally, the scaling coefficient c is determined so that the estimate of Eq. (5) reduces to a "standard" reference. For example, in connection with Gaussian processes, the reference is the narrowband limit and thus the moment estimate should reduce to the Rayleigh formula of Eq. (3). Then,

$$c = c_{Narr} = 2\,\pi\,K / \left[2^{3m/2}\,\Gamma(1 + m/2)\right] \ . \tag{8a}$$

When taking the nonlinearity into account, the standard reference should be the non-Gaussian narrowband limit and thus, Eq. (5) should converge to the Rayleigh estimate divided by the GR factor. Thus, one would obtain a different value of the coefficient c, namely

$$c = c_{GR} = 2\,\pi\,K\,GR / \left[2^{3m/2}\,\Gamma(1 + m/2)\right] \ . \tag{8b}$$

To assess the reliability of these different estimates, a titanium panel was selected with dimensions a = 0.508 m, b = 0.208 m, h = 0.001524 m, and material constants $E = 1.1 \times 10^{11}$ Pa, $\nu = 0.34$, and $\rho = 4520$ kg/m^3 for which $\omega_0 = 14.67$ and $\gamma = 769.532$. The temperature field considered was such that s = 1.8 and $\bar{p}_0 = 0$. Further, the acoustic loading was modeled as a $[-f_b, f_b]$ bandlimited white noise of power spectral density $S_0 = \left(p_0^2/2\pi\right) 10^{SPL/10}$ where $p_0 = 2\ 10^{-5}$ Pa is the reference pressure and SPL denotes the sound pressure level in dB based on the reference cut-off frequency of 2π. A dimensionless time step of 1.7×10^{-3} was adopted to solve Eq. (1). This choice implied a physical cut-off frequency $f_b = 2.5937\times10^4$ Hz. Accordingly, the overall sound pressure level ($OASPL$) can be obtained as $OASPL = SPL + 10 \log f_b$ where $10 \log f_b$ = 44 dB. Note finally that the power spectral density of the dimensionless pressure $\bar{p}$ is

$$S_{\bar{P}\bar{P}} = 64\left(\frac{b}{\pi h}\right)^8 \frac{\left(1-\nu^2\right)^2}{E^2} \frac{S_0}{\theta};$$

$$\theta = \sqrt{\frac{12\left(1-\nu^2\right)}{\pi^4} \frac{\rho b^4}{E h^2}} \tag{9}$$

It was found that the corresponding low to high SPL transition zone extends upwards of 114 dB (or 158 dB overall SPL) to approximately 134 dB. Thus, the reliability of the Rayleigh and single moment estimates was carried out in the domain $SPL \in [124, 154]$ dB and for $m \in [1,8]$ by comparison with rainfall analyses [10]. Shown in Fig. 1 are the relative errors on the accumulated damage corresponding to the Rayleigh, Rayleigh with GR correction, single moment (Eq. (8a)), and single moment with GR correction (Eq. (8b)).

Several observations can be drawn from the above figures. First, all errors are very small for m = 1 as is expected since every damage prediction formula considered recovers the exact solution

$$E[D] = \sigma_{\dot{s}}\, T / \left(\sqrt{2\pi}\, K\right) . \tag{10}$$

Next, a comparison of Fig. 1 readily indicates that the Rayleigh formula largely overestimates the damage for large S-N power exponent. The single moment method provides a definite improvement over the Rayleigh formula, but its error still rapidly grows with the exponent of the S-N curve. The *GR* correction factor for the Rayleigh formula and single moment approach provides a substantial improvement in damage estimate, but the errors are still too large to be considered satisfactory.

It should finally be noted that the behavior of all four errors appears to converge, for any fixed value of *m,* as the sound pressure level increases from 124 dB to 154dB thereby suggesting that there exists a common behavior in the high *SPL* domain.

The unbuckled situation, $s<1$, is also of great interest as it usually represents the design condition of the panel. To assess the differences in reliability of the four methods for the unbuckled case, the comparisons of Fig. 1 were repeated for $s = 0$, see Fig. 2. For the lowest *SPL* (124 dB), there is a marked improvement over the $s = 1.8$ case of the damage estimates obtained by the Rayleigh and single moment methods with or without the Gaussianity ratio, probably due to the mild nonlinearity present. At the two highest *SPL* (144 dB and 154 dB) however, the curves corresponding to $s = 0$ and $s = 1.8$ are almost identical thereby suggesting that the damage becomes only weakly dependent on the temperature or state (buckled or unbuckled) of the panel.

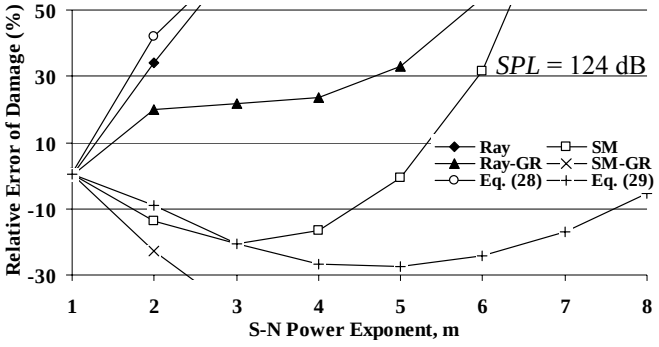

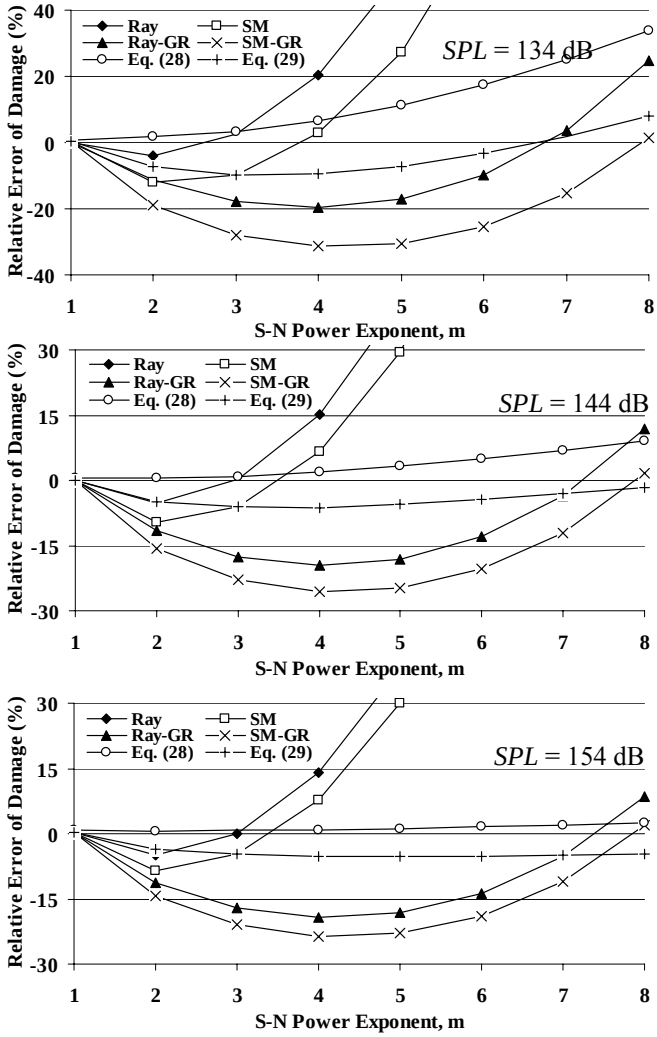

Figure 1. Relative error on the prediction of the expected damage as a function of the S-N exponent *m* for different *SPL* and different methods ("Ray" = Rayleigh, "SM" = Single Moment, "GR" = with Gaussianity Ratio), $s = 1.8$.

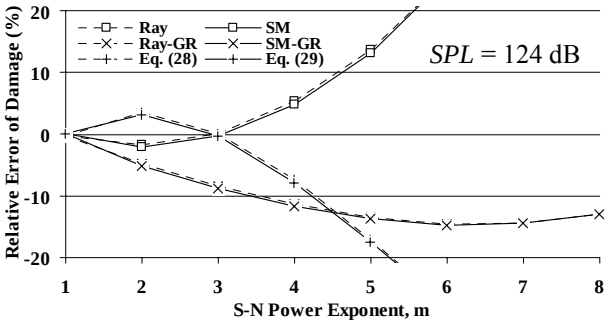

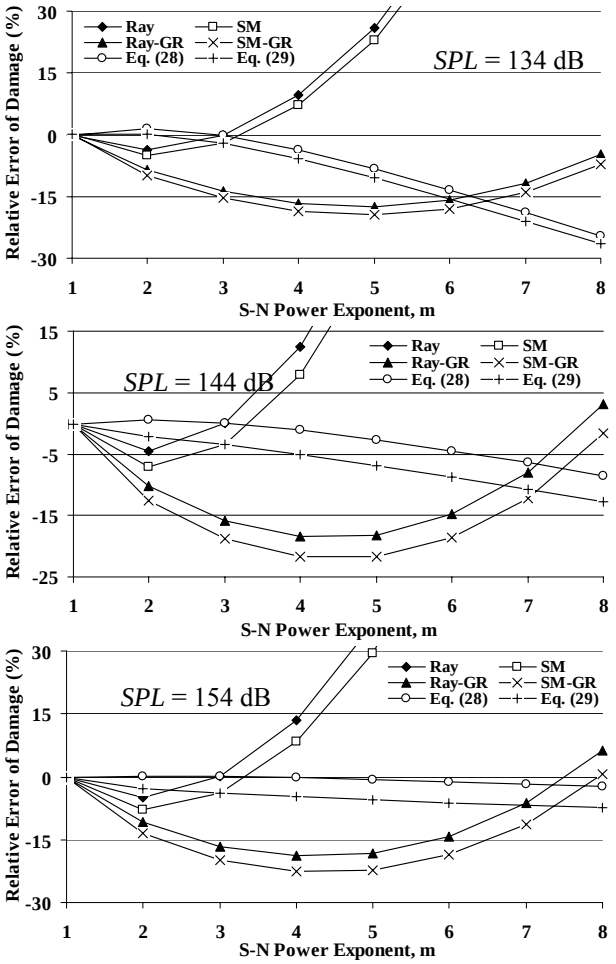

Figure 2. Relative error on the prediction of the expected damage as a function of the S-N exponent *m* for different *SPL* and different methods ("Ray" = Rayleigh, "SM" = Single Moment, "GR" = with Gaussianity Ratio), *s* = 0.

4 DAMAGE ACCUMULATION PROCESS IN THE HIGH SPL REGIME

The *GR* correction factor for the Rayleigh formula was derived for a particular class of narrowband non-Gaussian processes and thus the sharp reduction of error seen in Fig. 1 is somewhat indicative that the response process in the high *SPL* range may be narrowband. If this possibility was confirmed, substantial simplifications in the estimation of the accumulated damage would follow, even without the Gaussian distribution property. For a narrowband process, a cycle will have an approximately constant period of $2\pi/\omega$ and the expected value of the damage can be expressed as

$$E[D] = (\omega T / 2\pi)\, E[\Delta D] \quad (11)$$

where $E[\Delta D]$ is the expected damage corresponding to one cycle. This term can be further written as

$$E[\Delta D] = E\left[S_r^m\right] / K \quad (12)$$

where S_r denotes the stress range process. If the probability density function of the response is symmetric, as here in the absence of the thermal moment term $\bar{p}_0$, the narrowbandedness assumption further implies that the stress range is twice the peak stress S_P so that

$$K\, E[\Delta D] = 2^m\, E\left[S_P^m\right] = 2^m \int_0^\infty s^m p_{S_P}(s)\, ds \quad (13)$$

It remains to assess if the response process is indeed narrowband. A first perspective of the potential narrowbandedness can be obtained from the power spectral densities of the process which are shown in Fig. 3 for the 124-154 dB sound pressure levels and *s* = 1.8. It appears from this figure that the response exhibits a single dominant peak which is not particularly narrow: if these spectra corresponded to a single-degree-of-freedom system, the corresponding damping ratios would be between 21% and 26% as estimated by the half-power bandwidth technique. Further, note the presence of a peak of the spectrum near the zero frequency for the 124 dB and, to a lesser extent, the 134 dB excitations.

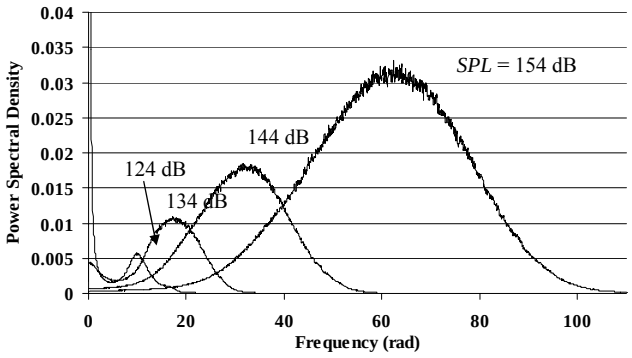

Figure 3. Response power spectral density for different *SPL* and *s* = 1.8

It is unclear if these results validate or invalidate the narrowbandedness assumption of the stress

ranges. Certainly, it could be argued that the Rayleigh formula requires a correction factor for single-degree-of-freedom systems with damping ratios similar to the 21%-26% observed here (see [11]). Ultimately, however, it is not the spectrum which is relevant to the damage accumulation process. In fact, from Eq. (11) and (12), it is seen that a better check of the narrowbandedness requires the assessment of the frequencies at which the stress ranges occur. To this end, the simulation data was revisited and the stress ranges were recorded together with the time (or half-period) needed to achieve these stress ranges. This information led to the probability density functions of half-periods shown in Fig. 4 which do support the narrowbandedness of the stress process, especially at high *SPL*.

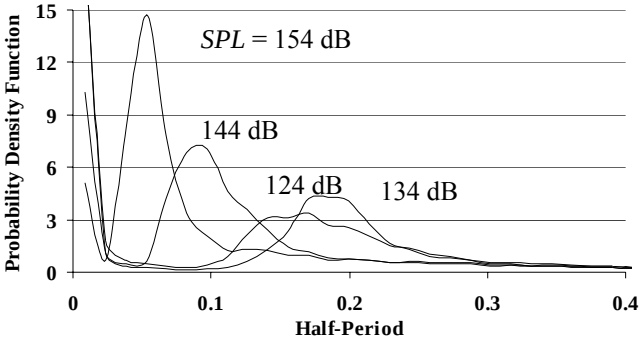

Figure 4. Probability density function of the half-period for different *SPL* and *s* = 1.8.

To fulfill the fatigue estimate, a reliable prediction of the frequency is required. In fact, the frequency of the process can be selected so that the damage corresponding to m =1 equals the Rayleigh value. That is,

$$\omega = \sqrt{2\pi}\sigma_{\dot{S}} \Big/ \left[2\int_0^\infty s\ p_{S_p(s)}\ ds \right]. \qquad (14)$$

5 DISTRIBUTION OF PEAKS AND RANGES

The above figures have shown the validity of narrowbandedness assumption but it remains to establish a model for the distribution of the stress ranges. To this end, the derivation of the Rayleigh distribution in the Gaussian case was revisited. In fact, this probability density function stems, in the narrowband limit, from the S.O. Rice distribution which characterizes the peaks of a stationary Gaussian process. In this light, it appears that the prediction of the accumulated damage in the high *SPL* regime necessitates the derivation of the equivalent of the Rice distribution for the one-mode model of Eq. (1). This derivation is accomplished below under some weak assumptions.

The probability density function for the peaks of an arbitrary stationary process $q(t)$ is given by

$$p_P(u) = \int_{-\infty}^{0} |z|\ p_{\dot{q}q\ddot{q}}(u,0,z)\,dz \Big/ \int_{-\infty}^{0} |z|\, p_{\dot{q}\ddot{q}}(0,z)\,dz \qquad (15)$$

where $p_{q\dot{q}\ddot{q}}(u,v,z)$ is the joint probability density function of $q(t)$, $\dot{q}(t)$, and $\ddot{q}(t)$ and $p_{\dot{q}\ddot{q}}(v,z)$ is similarly defined (see [11]).

When $\overline{p}(t)$ is a white noise process of spectral value $S_{\overline{p}\overline{p}}$, $\dot{q}(t)$ is a Gaussian random variable with zero mean and variance equal to $\pi S_{\overline{p}\overline{p}} / (2\zeta\omega_0)$. Further, the distribution of $q(t)$ is

$$p_q(u) = A \exp\left[-\frac{2\,\zeta\,\omega_0}{\pi\, S_{\overline{p}\overline{p}}}\, G(u) \right] \qquad (16)$$

where $G(u) = -\,\overline{p}_0\, u + \frac{1}{2}\omega_0^2\,(1-s)\,u^2 + \frac{1}{4}\gamma\, u^4 \qquad (17)$

Considering next the distribution of $\ddot{q}(t)$, it is noted that this random variable is uncorrelated with the velocity $\dot{q}(t)$ as $E[\dot{q}(t)\,\ddot{q}(t)] = 0$ under stationary assumptions. If one assumes the stronger independence of these random variables, Eq. (15) becomes

$$p_P(u) = \frac{\int_{-\infty}^{0} |z|\ p_{q\ddot{q}}(u,z)\,dz}{\int_{-\infty}^{0} |z|\ p_{\ddot{q}}(z)\,dz} = \frac{1}{B'} \int_{-\infty}^{0} |z|\, p_{q\ddot{q}}(u,z)\,dz \qquad (18)$$

where $B' = \int_{-\infty}^{0} |z|\ p_{\ddot{q}}(z)\,dz$ is simply a normalization constant for the distribution of peaks. To obtain a closed form relation similar to the Rice distribution, it is necessary to further simplify Eq. (18). This can be accomplished by expressing the joint probability density function of $q(t)$ and $\ddot{q}(t)$ in terms of the marginal distribution

of $q(t)$ ($p_q(u)$, see Eq. (16)) and the conditional distribution of $\ddot{q}(t)$ given $q(t)$, $p_{\ddot{q}}(z\,|\,q(t)=u)$. That is,

$$p_{q\ddot{q}}(u,z) = p_q(u)\, p_{\ddot{q}}(z\,|\,q(t)=u) \tag{19}$$

Note further that the knowledge of the value of $q(t) = u$ does not affect the distribution of either the velocity $\dot{q}(t)$ or the white noise excitation $\bar{p}(t)$ since these two random variables are both independent of $q(t)$. The independence of $q(t)$ and $\bar{p}(t)$ arises from the second order dynamics of the panel, $\bar{p}(t)$ instantaneously affects only $\ddot{q}(t)$ and $\dot{q}(t)$, the response $q(t)$ involves only the values of $\bar{p}(t)$ in the past, i.e. $\tau < t$. With these independence properties and the equation of motion (1), $\ddot{q}(t)$ given $q(t) = u$ can be written as

$$\ddot{q} = \bar{p}(t) - 2\,\zeta\,\omega_0\,\dot{q} + g(u) \tag{20}$$

where

$$g(u) = \bar{p}_0 - \omega_0^2\,(1-s)\,u - \gamma\,u^3. \tag{21}$$

Since $\bar{p}(t)$ and $\dot{q}(t)$ are both Gaussian, one could assume them to be jointly Gaussian. Then, the distribution of $\ddot{q}(t)$ given $q(t) = u$ is seen from Eq. (20) to be Gaussian with mean

$$\mu_* = g(u) \tag{22}$$

and variance

$$\sigma_*^2 = E\left[(\bar{p} - 2\,\zeta\,\omega_0\,\dot{q})^2\right] = \sigma_{\bar{p}}^2 - 4\,\zeta^2\omega_0^2\,\sigma_{\dot{q}}^2 \tag{23}$$

where $\sigma_{\bar{p}}^2$ is the variance of the white noise process $\bar{p}(t)$. If this process is truly white, i.e. includes all frequency up to infinity equally, then $\sigma_{\bar{p}}^2 = \infty$. However, this situation is only a convenient model, physical process does not exhibit a zero length correlation and thus have a cut-off frequency ω_b about which little energy exists. In such bandlimited (or clipped) white noise cases, $\sigma_{\bar{p}}^2 = 2\,S_{\bar{p}\bar{p}}\,\omega_b$. In computational efforts, ω_b is likely to be dictated by the time step with which the equations of motion are integrated while, in experimental efforts, this quantity will be related to the sampling time of the response process. With the above assumptions, it is finally found that

$$p_P(u) = B\,p_q(u)\left\{\sigma_*\exp\left[-\frac{g^2(u)}{2\,\sigma_*^2}\right] - \sqrt{2\pi}\,g(u)\,\Phi\left(-\frac{g(u)}{\sigma_*}\right)\right\} \tag{24}$$

where $\Phi(z)$ denotes the cumulative distribution function of a standard Gaussian random variable.

Note the very strong parallel between Eq. (24) and the Rice distribution, which is recovered for $g(u) = u$. Indeed, the probability density function of Eq. (24) involves primarily two components, i.e. those corresponding to the two terms in brackets. While the parameter σ_* may still be related to a measure of bandwidth in the process, as done in connection with the Rice distribution, a different interpretation of the two terms will be sought here.

Specifically, note first that the terms $\sigma_*\exp\left[-g^2(u)/2\,\sigma_*^2\right]$ and $g(u)\,\Phi\left(-g(u)/\sigma_*\right)$ exhibit very different behaviors. The first expression is maximum at the buckled states of the panel, i.e. at the values Q_i such that $g(Q_i) = 0$ and rapidly decreases away from these locations. On the contrary, the second term vanishes there and increases monotonically for $|u| > |Q_i|$. In fact, a plot of these expressions reveals that they may only have a very small intersection. Physically, the first term of Eq. (24) is associated with the motions around and in between the bottom and top buckled states, respectively, while the single peak of the second term corresponds to the snap-throughs with excursion exceeding, sometimes significantly, the buckled states.

The use of Eq. (24) or a similar distribution of the peaks for the prediction of the probability density function of the *ranges* must accomplished carefully: the peaks near the buckled states tend to be associated with valleys situated in the same neighborhood and thus create small ranges. On the contrary, the peaks corresponding to snap-throughs lead to ranges equal to twice the peak excursion. When the peaks of the distribution are clearly separated as is the case in the high *SPL* regime, the peak distribution can be used to produce an approximate probability density function of the

ranges. In the low *SPL* regime, the snap-throughs occur very rarely and the rightmost peak is of negligible magnitude, the Rayleigh approximation is then fully appropriate. In the transition zone, however, both terms interact and a careful analysis must be undertaken.

Since the focus of the present effort is on the high *SPL* regime only, it can be assumed that the peaks of the distribution of peak values are well separated and that the ranges occurring in the neighborhood of the buckled states have a negligible effect on the accumulated damage. Then, the first term in the bracket of Eq. (24) can be neglected and the values of $|g(u)|$ will be assumed large enough so that $\Phi\left(-g(u)/\sigma_*\right)\approx 1$. Then, one obtains the following approximate probability density function of the ranges

$$p_{S_r}(z) = B\, g(z/2)\exp\left[-\frac{2\,\zeta\,\omega_0}{\pi\, S_{\overline{pp}}}\, G(z/2)\right] \qquad (25)$$

which is defined in $z\in\left[2\,Q_1,\infty\right)$ and the coefficient *B* should be selected so that the integral of $p_{S_r}(z)$ over that interval equals 1. The range of values of *z* does not extend below $2\,Q_1$ since $p_{S_r}(z)$ is negative there.

The assessment of the reliability of this approximation of the exact ranges was done in two ways. First, the distribution of the ranges obtained by simulation was fitted to the approximation of Eq. (25). In this fitting, the coefficient *B* was selected so that the simulated and approximate distributions share the same peak value. As expected, the matching between these two curves is excellent at very high sound pressure levels, see Fig. 5 for *SPL* = 154 dB and slowly degrades as the excitation strength approaches the transition zone.

The second assessment was performed directly on the estimated accumulated damage by introducing Eq. (25) in Eq. (11)-(13). The frequency ω was selected from Eq. (14) so that the accumulated damage predicted for *m* = 1 from Eq. (11)-(13) with Eq. (25) matched exactly the value of Eq. (10). Shown in Fig. 6 are the errors of the accumulated damage predicted in this manner. Clearly, the results are excellent in the high *SPL* range.

Note that Eq. (25) can be viewed as a 3-parameter model for the fatigue life prediction as it is necessary to evaluate $\sigma_q^2 = \pi\, S_{\overline{pp}}/2\,\zeta\,\omega_0$, $\omega_0^2\,(1-s)$, and γ. For the one mode approximation of Eq. (1), expressions for these parameters are be derived easily (see [1]) but their evaluation in connection with a full finite element representation and/or a reduced model thereof may not be as straightforward.

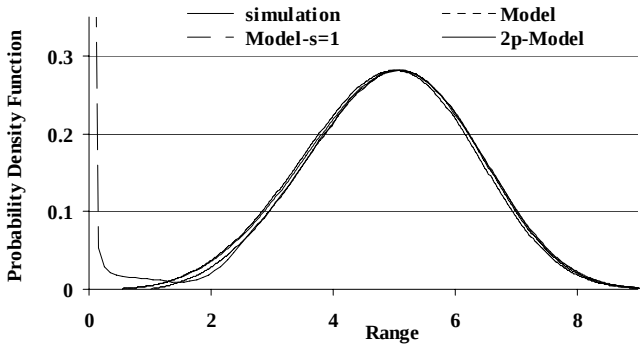

Figure 5. Probability density function of the stress ranges and its approximation by Eq. (25) ("Model"), Eq. (26) ("Model-s=1"), and Eq. (27) ("2p-Model"), for *s* = 1.8, *SPL* = 154dB.

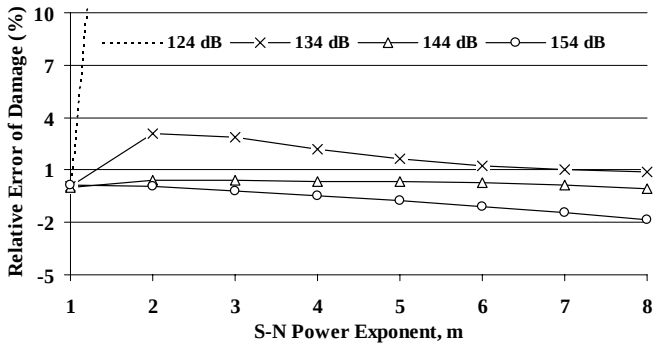

Figure 6. Relative error on the prediction of the expected damage as a function of the S-N exponent *m* for different *SPL*, 3-parameter model, Eq. (25), *s* = 1.8.

A 2-parameter model of the damage would be preferable as its coefficients could be evaluated from the standard deviations of the displacement and the velocity.

Having established and validated the model of Eq. (25), additional simplifications of it were then pursued. To this end, it was first argued that the effects of a nonzero value of $\bar{p}_0$ would be negligible in the very high *SPL* regime, although this parameter should play an important role at lower excitation levels through the asymmetry of the buckling states it creates. Next, it was found that the $\omega_0^2\,(1-s)$ terms in Eq. (25) were typically much smaller than their γ related counterparts for the ranges z observed in the high *SPL* regime. Equivalently, it appeared that the distribution of ranges and the accumulated damages corresponding to s = 1 and s = 1.8 should converge to each other as the sound pressure level is increased. This expectation is confirmed by the "Model - s = 1" curves of Fig. 5 but the reliability of this approximation at *SPL* values 134 dB was not found encouraging.

In fact, a direct comparison of the s = 1 and s = 1.8 results is not fully appropriate as the corresponding response processes have different standard deviations σ_q. A more relevant check of the 2-parameter corresponding to Eq. (25) with its s = 1 and $\bar{p}_0 = 0$ counterpart, i.e.

$$p_q(u) = B' \exp\left[-\gamma u^4/\left(4\sigma_{\dot{q}}^2\right)\right] \tag{26}$$

would thus be achieved by selecting γ so that the standard deviation of the response with s = 1 be equal to that of s = 1.8 with the original γ. After some algebraic manipulations, it was found that

$$\gamma \approx \sigma_{\dot{q}}^2/\left(2.188\,\sigma_q^4\right). \tag{27}$$

It is clearly seen from Fig. 5 that the approximate probability density function of the ranges is very well matched by using the value of γ given by Eq. (27) as opposed to the original one (compare the matching of the simulation data by the "Model - s = 1" and "2p-Model" curves).

How about the predicted damage? After obtaining expressions for the mth moment $E\left[S_r^m\right]$ appearing in Eq. (12) and forcing again the frequency of the process to be such that the Rayleigh formula is recovered for m = 1, it was finally found that

$$E[D] = \frac{\sigma_{\dot{q}}\,T_{fin}}{\sqrt{2\pi}\,K}\,\frac{\Gamma(1+m/4)}{\Gamma(1.25)}\left[3.4402\,\sigma_q\right]^{(m-1)} \tag{28}$$

The relative difference between the accumulated damage produced by this formula and obtained by the rainflow analysis is shown in Fig. 1 and 2 for the *SPL* of 124 dB - 154 dB for s = 1.8, respectively. By comparison with Fig. 6, it is seen that the 2-p model (Eq. (28)) is not as accurate as the model of Eq. (25) but it reaches somewhat similar levels of accuracy as the Rayleigh formula and the single moment method corrected by the *GR* factor. In fact, the error of the 2-parameter model is significantly less than for these two methods for the 144 dB and 154 dB excitations but higher for the 124 dB and 134 dB cases. Note however that Eq. (28) does not require the difficult evaluation of the coefficient of kurtosis.

Could the model be further improved without needing a third parameter? A re-inspection of the power spectral densities of Fig. 3 has demonstrated that the peak bandwidth narrows slightly but steadily as the sound pressure level is increased above the transition zone. For example, at 134 dB, the width of the peak is equivalent to that of a single-degree-of-freedom system with 25.9% damping but the equivalent damping ratio at 144 dB and 154 dB is 23.6% and 22.0%, respectively. In this light, the lack of accuracy of the 2-p model, Eq. (28), could either be attributed to the role of the $\omega_0^2\,(1-s)$ terms or to an increase bandwidth of the peak. With the latter interpretation, Eq. (28) only requires a bandwidth correction such as that provided by the single moment method.

Accordingly, a version of this method was formulated that reduces not to the Rayleigh formula but rather to Eq. (28) when the process becomes perfectly narrowband. Proceeding as above yields the accumulated damage predictor of Eq. (5) with the coefficients a and b still given by Eq. (7) but the parameter c must then be selected as

$$c_{NL} = \sqrt{2\pi}\, K\, \frac{\Gamma(1.25)}{\Gamma(1+m/4)}\, [0.29068]^{(m-1)} \qquad (29)$$

To assess the validity and reliability of this last approach, the error in the prediction of the accumulated damage was evaluated as a function of *m* for the four levels of sound pressure levels of 124 dB, 134 dB, 144 dB, and 154 dB. The results of this study are also shown in Fig. 1 and 2 for *s* = 1.8 and 0, respectively. Comparing the various results presented in these figures, it is seen that this estimate is almost everywhere more accurate than either the Rayleigh with the *GR* factor and the single moment with the *GR* factor. Further, Eq. (29) is generally at least as accurate as its 2-parameter counterpart Eq. (28). On this basis, it is suggested that the modified, non-linear single moment estimate of the accumulated damage be used when the 3-parameter model is not applicable.

6 VALIDATION ON EXPERIMENTAL DATA

Having established reliable prediction approaches of the accumulated damage in high *SPL* regimes, it was desired to check their validity on experimental measurements. The acoustic testing of a clamped composite panel at ambient temperature was conducted at the A.F.R.L. The sound pressure level was varied in 8 tests from 152 dB to 172 dB (overall *SPL*) and the time varying strain at the center of the panel was recorded at a sampling rate of 8,000 samples per second for 60 seconds.

The consideration of this data brought one major novel issues with respect to the theoretical work carried out before, i.e. only strain measurements were obtained so the nonlinearity of the dynamics (displacements) could not be separated from the nonlinearity of the displacement-strain relation.

The first task was to analyze the response of the panel and to assess if it could be analyzed in terms of low and/or high *SPL* regimes. To evaluate the potential linearity of the panel, the standard deviations of the strain and strain velocity were computed and plotted vs. the sound pressure level, see Fig. 7. In this log-linear plot, a straight line would be representative of linearity. A preliminary analysis of the standard deviation of the strain, see Fig. 7, suggested that the panel might be in a linear range for the excitation levels of 152 dB - 161 dB but nonlinearity at the highest *SPL* values was clear. Further, the standard deviation of the strain velocity was found to exhibit an approximately linear behavior. In the one-mode model, the velocity is perfectly linear but the strain velocity is not owing to the effect of the coefficient C_2, in Eq. (2), i.e.

$$\dot{S} = \dot{q}\,(C_1 + 2\,C_2\; q). \qquad (30)$$

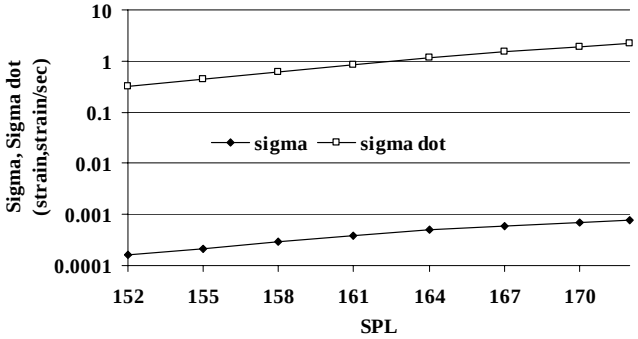

Figure 7. Evolution of the standard deviations of the panel strain and strain velocity as functions of sound pressure level (*SPL*), experimental data.

It was thus tentatively concluded from the close linearity of the standard deviation of the strain velocity that:

(i) the effect of the coefficient C_2 is probably small

(ii) the velocity is probably quite linear and thus its marginal distribution may be considered Gaussian. With this assumption, the Rayleigh formula should be exact or close to for *m* = 1. This expectation will be confirmed later.

Notwithstanding this analysis, it was found necessary to devise a test of the validity of both linearity and full nonlinearity (high *SPL* behavior). Considering first the linearity, it was noted that a Gaussian response would occur in the small displacements range and thus that the C_2 effect

would also be small. Thus, linearity of the displacements should also correlate well with linearity of the strains and thus a Gaussian strain distribution would also be expected. Shown in Fig. 8 is the evolution of the coefficient of kurtosis of the strains as a function of sound pressure level. Clearly, these values are away from 3 even at the lowest excitation levels: the coefficient of kurtosis equals 2.70 at 152 dB. On this basis, it was concluded that the low *SPL* regime in which the response remains close to linear is not seen in this experimental data.

A simple test was then sought to validate the applicability of the high *SPL* limit analysis of Eq. (26)-(29). To this end, it was noted from Eq. (27) that the ratio $\sigma_q^2 / \sigma_{\dot{q}}$ is constant when the 2-parameter model is applicable. The evolution of this ratio as a function of the sound pressure level was then plotted for the present experimental data, see Fig. 8. This figure strongly suggests that $\sigma_q^2 / \sigma_{\dot{q}}$ converges to a constant value at the high *SPL* values in agreement with Eq. (27). From these two sets of observations, it is concluded that the panel is in the transition zone at the lowest excitation levels but reaches the high *SPL* regime in the last 2 or 3 experiments.

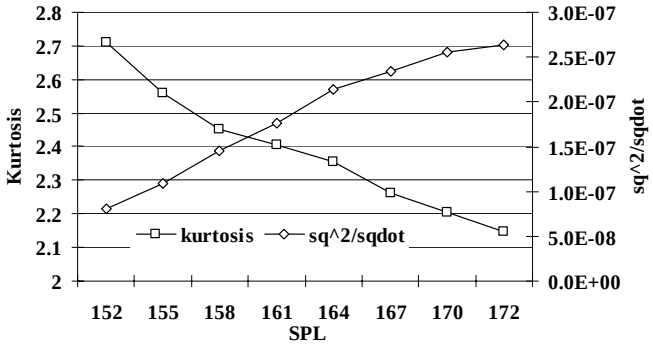

Figure 8. Evolution of the coefficient of kurtosis and $\sigma_q^2 / \sigma_{\dot{q}}$ of the panel strain as functions of sound pressure level (*SPL*), experimental data.

With this perspective, the accumulated damage predicted by the Rayleigh formula, the single moment method, the Rayleigh formula with *GR* correction, the single moment method with *GR* correction, the 2-parameter model of Eq. (28), and the modified single moment method of Eq. (29) were compared to the results of a rainflow analysis, see Fig. 9. The observations drawn from these figures are in close agreement with those obtained in connection with the one-mode model. First, the Rayleigh formula and single moment method typically yield unacceptably large errors that increase with *SPL* and with the exponent *m* approximately monotonically. In fact, it is only for $m = 1$ that the Rayleigh formula may be accurate, as justified above, it leads to errors that slowly increase with the sound pressure level from 0.2% at 152 dB to 6.9% at 172 dB. Note again in this context that the nonlinearity associated with C_2 was not accounted for in the modeling effort leading to Eq. (28) and (29).

Further, the use of the *GR* correction factor in connection with both the Rayleigh formula and the single moment method led to a dramatic decrease in the damage prediction error. In particular, the single moment method with the correction leads to errors less than 15% at high *SPL* and almost all values of *m*. Note however the clear monotonic (decreasing) trend of the errors as a function of sound pressure level. A similar statement can be made for the Rayleigh formula with the *GR* correction factor with the exception that the trend is an increase of the errors with *SPL*. Accordingly, it can be expected that these two methods will not fair as well at higher excitation levels.

The 2-parameter model of Eq. (28) performs particularly well in the intermediate values of sound pressure levels, i.e. between 156 dB and 166 dB, but the error starts increasing again above 166 dB. This surprising behavior might be a consequence of either the increasing role of the membrane strain, not included in the model of Eq. (28), and/or the bandwidth of the peak. Last but not least, the modified single moment method based on Eq. (29) performs extremely well and fully according to expectations: the errors are largest for the lowest sound pressure levels while the panel is in the transition zone but errors less than 10% are

obtained for almost all cases with *SPL* > 156 dB! Note finally the trend of these errors toward convergence to a constant level which does suggest that the physics of the problem is being captured.

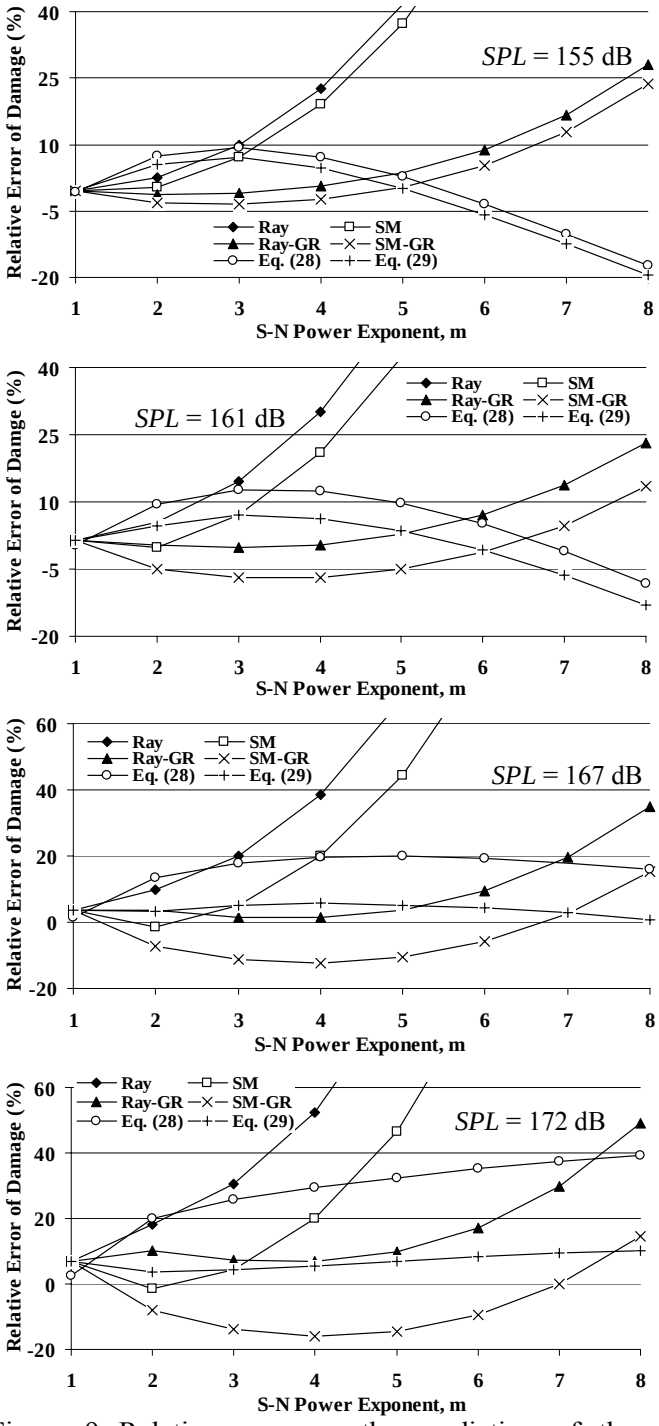

Figure 9 Relative error on the prediction of the expected damage as a function of the S-N exponent *m* for different *SPL* and different methods, experimental data.

7 SUMMARY

The focus of this study has been on the prediction of the fatigue life of aircraft panels subjected to thermoacoustic effects. The reliability of some existing prediction strategies, i.e. the Rayleigh formula and the single spectral moment method both with and without Gaussianity correction, was assessed by comparison with rainflow results on both simulated data from the one-mode model of Eq. (1) and experimentally measured strain time histories. It was found that the error in the predicted accumulated damage over a fixed time was extremely large for both the Rayleigh formula and the single moment method without the Gaussianity correction. The inclusion of the GR factor led however to a dramatic improvement although the resulting errors could still be large, see Fig. 1, 2, and 9.

A different approach was then undertaken and an approximation of the probability density function of the peaks of the response of the Duffing system of Eq. (1) was obtained, see Eq. (24) and (25) and Fig. 5. It was then argued that the response process to a severe acoustic excitation could be considered narrowband, notwithstanding its broad peak (see Fig. 3), with a frequency given by Eq. (14). The combination of these results provided a very reliable damage prediction approach for the model of Eq. (1) as seen in Fig. 6. The applicability of this approach is however conditional on the availability of the parameters $\sigma_{\dot{q}}^2 = \pi S_{\overline{pp}} / 2\zeta\omega_0$, $\omega_0^2 (1-s)$, and γ some of which may be difficult to estimate from a complex finite element model.

To palliate this situation, a simplification of the model was then accomplished by neglecting the linear stiffening terms in regards to the cubic ones. This assumption, which is valid at high response levels, led to the simplified probability density function of peaks of Eq. (26) and to the damage estimate of Eq. (28). Since only two parameters are present in this model, the knowledge of the standard deviations of the response and the velocity are sufficient to predict the fatigue life.

Good agreement with rainflow results was obtained with this method for both the simulated and test data, see Fig. 1, 2, and 9.

The trend of the errors shown in Fig. 1, 2, and 9 suggested that the 2-parameter model was slightly affected by a bandwidth effect which could be corrected by the single moment method. Accordingly, a final model was introduced in the form of a single spectral moment estimate, Eq. (5), but with the coefficient *c* selected to match the 2-parameter estimate in the narrowband limit, see Eq. (29). This final damage estimation approach matched very well the rainflow results at high response levels for both simulated and test data, see Fig. 1, 2, and 9.

8 ACKNOWLEDGEMENTS

The support of this investigation by the Air Force Research Laboratory under contract F33615-01-C-3111 is gratefully acknowledged.

REFERENCES

[1] Blevins, R.D., Holehouse, I., and Wentz, K.R., 1993, "Thermoacoustic Loads and Fatigue of Hypersonic Vehicle Skin Panels," *Journal of Aircraft*, Vol. 30, No. 6, pp. 971-978.

[2] Lee, J., 1993, "Large-Amplitude Plate Vibration in an Elevated Thermal Environment," *Applied Mechanics Reviews,* Vol. 46, No. 11, Part 2, pp. S242-S254.

[3] Vaicaitis, R., 1994, "Nonlinear Response and Sonic Fatigue of National Aerospace Space Plane Surface Panels," *Journal of Aircraft,* Vol. 31, No. 1, pp. 10-18.

[4] Moorthy, J., Mei, C., and Shirahatti, U., 1995, "Numerical Simulation of Acoustically Induced Nonlinear Vibrations of a Plate with Temperature Gradient," *Proceedings of the 36th Structures, Structural Dynamics, and Materials Conference,*AIAA-95-1378-CP, New Orleans, LA, Apr. 10-13, 1844-1854.

[5] Rizzi S.A., and Muravyov, A.A., 2001, "Improved Equivalent Linearization Implementations Using Nonlinear Stiffness Evaluation", NASA Technical Memorandum TM-2001-210838, Langley Research Center, Hampton, Virginia.

[6] McEwan, M.I., Wright, J.R., Cooper, J.E., and Leung, A.Y.T., 2001, "A Combined Modal/Finite Element Analysis Technique for the Dynamic Response of a Non-Linear Beam to Harmonic Excitation," *Journal of Sound and Vibration*, Vol. 243, No. 4, pp. 601-624.

[7] Chilakamarri, KB., and Lee, J., 2000, "Thermal-Acoustic Fatigue Damage Accumulation Model of Random Snap-Throughs," *Proceedings of the 8th ASCE Specialty Conference on Probabilistic Mechanics and Structural Reliability.*

[8] Winterstein, S.R., 1985, "Non-Normal Responses and Fatigue Damage," Journal of Engineering Mechanics, Vol. 111, No.10, pp. 1291-1295.

[9] Lutes, L.D., and Larsen, C.E., 1990, "Improved Spectral Methods for Variable Amplitude Fatigue," *Journal of Structural Engineering*, Vol. 116, No. 4, pp. 1149-1164.

[10] Downing, S.D., and Socie, D.F.,1982 Simple Rainflow counting Algorithms, International Journal of Fatigue, pp. 31-40.

[11] Lutes, L.D., and Sarkani, S., 1997 "Stochastic Analysis of Structural and Mechanical Vibrations, Prentice-Hall.

Appendix C

"Prediction of the Dynamic Response and Fatigue Life of Panels Subjected to Thermo-Acoustic Loading"

Proceedings of the 45th Structures, Structural Dynamics, and Materials Conference, Palm Springs, California, Apr. 19-22, 2004. Paper AIAA-2004-1557.

PREDICTION OF THE DYNAMIC RESPONSE AND FATIGUE LIFE OF PANELS SUBJECTED TO THERMO-ACOUSTIC LOADING

A.G. Radu[†], B. Yang[‡], K. Kim[‡], and M.P. Mignolet[*]
Arizona State University, Tempe, Arizona 85287-6106

ABSTRACT

This paper focuses on the formulation and validation of a reduced order model for the prediction of the response - displacements, stresses, fatigue life - of aircraft panels subjected to a severe thermo-acoustic loading. The reduced order modeling starts with a finite element model from a standard package (MSC.NASTRAN) and produces a set of cubic nonlinear differential equations which are efficiently marched in time. The basis for the representation of the displacement field includes transverse deflection modes of the linear panel and some associated in-plane modes (the dual modes). A partial static condensation approach is proposed for the numerically efficient integration of the reduced order model governing equations. Validation cases demonstrate the accuracy of the proposed static condensation and of the good to excellent reliability of the reduced order model for the prediction of the displacements and stresses of panels in the nonlinear range in static and dynamic cases. The computational efficiency of the reduced order model permits the generation of time histories of stresses long enough for the accurate assessment of the fatigue life of panels.

INTRODUCTION

Sonic fatigue has been recognized as an important problem for the design of aircraft panels for at least three decades (see the review by Clarkson, 1994) and will be of significant concern for the next generation launch technology (NGLT) vehicles. Indeed, their panels are expected to be subjected to severe acoustic excitations, sound pressure levels (*SPL*) larger than 150dB emanating for example from the engine exhaust, while heated to significant temperatures, 3000°F has been estimated (see Blevins et al., 1993) for similar vehicles without thermal protection system (*TPS*), see Fig. 1. Even with an operational TPS, the temperature of the panels may still be high enough to notably reduce the effective stiffness of the panels, and possibly induce their buckling. Given the critical nature of the panels and the dynamic loading they are subjected to, the accurate estimation of their fatigue life is of paramount importance. Unfortunately, the extreme conditions (acoustic and thermal) the panel is subjected to render the fatigue life estimation a very difficult task. Most notably, the severe acoustic excitation typically induces panel responses that exceed the linear range. While the nonlinearity is highly beneficial, i.e. it leads to significant decreases of the stresses in the panels, it unfortunately dramatically increases the complexity of the problem, especially in connection with a random process modeling of the acoustic excitation.

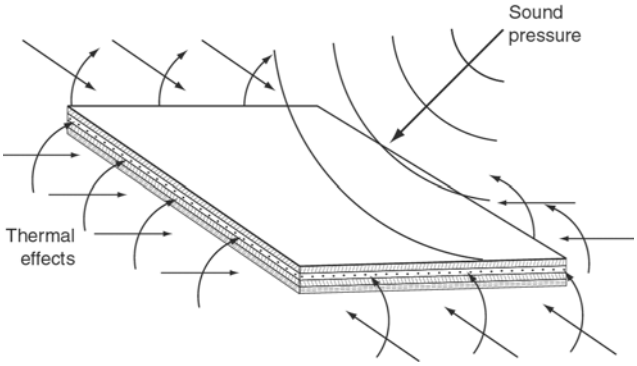

Figure 1. Surface Panel Thermal/Acoustic Loading.

Linear random vibration problems, even of very complex structures, are generally fairly straightforward as the solution procedure closely follows the one corresponding to deterministic (non-random) excitations, i.e. proceeds using modal analysis techniques. No such correlation exists in the nonlinear case and the solution of even the most simple problems, e.g. of the response of single-degree-of-freedom systems to white noise excitation, may require a formidable mathematical arsenal. These general observations suggest directly that the structural dynamic analysis of aircraft panels subjected to a severe acoustic excitation and thermal effects has typically been accomplished in one of the following two ways:

(1) by using a very simplified structural model and relying on available exact/approximate solutions of the corresponding random vibration problem, or
(2) proceeding with a Monte Carlo simulation of a finite element model of the panel.

[†] Postdoctoral Fellow, Department of Mechanical and Aerospace Engineering.
[‡] Research Assistant, Department of Mechanical and Aerospace Engineering.
[*] Professor, Department of Mechanical and Aerospace Engineering, Associate Fellow, AIAA.

The work carried out under option (1) has usually relied on the approximate representation of the panel displacement field through a "single mode model", i.e. as $\underline{s}(x,y,z,t) = q(t)\,\underline{\Psi}(x,y,z)$ where $\underline{\Psi}(x,y,z)$ is a pre-determined vector, typically an approximate/exact linear mode shape of the panel, providing the spatial characterization of the response and $q(t)$ is a scalar random process representing the temporal changes of the magnitude of the response. Proceeding in this manner leads to Duffing type equations for $q(t)$; i.e. the single (resp. double) well equation for unbuckled (resp. buckled) panel. Fortunately, an exact solution for the probability density function of the response exists, in the stationary limit, for the Duffing oscillator subjected to a white noise excitation and thus a fairly complete analysis of the response can be achieved (see for example Ng (1988, 1989), Lee, (1993, 1995, 1997, 2001), Lee and Wentz (1997), Lee et al. (1998), Vaicaitis (1994), Choi and Vaicaitis (1989), Vaicaitis and Arnold (1990), Ghazarian and Locke (1995), Murphy et al. (1996), Kavallieratos (1992), Sun et al. (1998), Chilakamarri and Lee (2000), Chen et al. (2000)). These analyses have provided an excellent phenomenological understanding of the response properties through the range of sound pressure levels and temperatures comparing very favorably with experimental results (e.g. Ng (1988, 1989), Lee and Wentz (1997), Istenes et al. (1995), Spottswood et al. (2000), Spottswood and Wolfe (2001), and Spottswood and Mignolet (2002)).

The weakness of single-mode analyses is, as expected, the lack of an equally good *quantitative* prediction of the panel response and one would naturally expect that the time marching of a full finite element model, i.e. option (2), would represent the answer to quantitative analyses and design. Unfortunately, the computational effort associated with such Monte Carlo studies is surprisingly large with using standard packages, e.g. MSC.NASTRAN. Such computational times may be acceptable for specification applications, e.g. post-mortem analyses, but are prohibitively large at the design stage. Adopting specially written finite element approaches might provide a reduction of this time (see the comprehensive efforts of Mei and coworkers in Mei, 2003).

An exciting, middle-of-the-road approach has recently surfaced that provides the flexibility of the finite element modeling and a computational efficiency comparable to that of the single-mode model, but without the benefit of simple exact/approximate solutions. This approach centers around the derivation of a reduced order model (ROM) corresponding to an "approximate modal" expansion of the form

$$\underline{s}(x,y,z,t) = \sum_{i=1}^{m} q_i(t)\,\underline{\Psi}_i(x,y,z) \qquad (1)$$

where, as in the single-mode model, the vectors $\underline{\Psi}_i(x,y,z)$ denote a set of prescribed displacement patterns and $q_i(t)$ the generalized coordinates of the ROM.

In this light, the goal of this paper is to present a ROM formulation recently devised and to demonstrate its reliability, in comparison to full finite element models, for the prediction of the displacement and stress fields on panels and the corresponding fatigue life.

NONLINEAR EQUATIONS OF MOTION

Central to the derivation of the equations of motion for the finite element model is the von Karman strains definition

$$\varepsilon_x = \frac{\partial u}{\partial x} + \frac{1}{2}\left(\frac{\partial w}{\partial x}\right)^2 \quad \varepsilon_y = \frac{\partial v}{\partial y} + \frac{1}{2}\left(\frac{\partial w}{\partial y}\right)^2 \quad \varepsilon_z = \frac{\partial w}{\partial z} = 0$$

$$\gamma_{xy} = \frac{1}{2}\left[\frac{\partial u}{\partial y} + \frac{\partial v}{\partial x} + \left(\frac{\partial w}{\partial x}\right)\left(\frac{\partial w}{\partial y}\right)\right] \qquad (2)$$

$$\gamma_{xz} = \frac{1}{2}\left[\frac{\partial u}{\partial z} + \frac{\partial w}{\partial x}\right] \qquad \gamma_{yz} = \frac{1}{2}\left[\frac{\partial v}{\partial z} + \frac{\partial w}{\partial y}\right]$$

which is relevant to panels exhibiting moderately large rotations $\frac{\partial w}{\partial x}$ and $\frac{\partial w}{\partial y}$. Given the quadratic nature of these displacement-strain relations, it can be shown that the panel displacements satisfy the cubic nonlinear equations

$$M\,\ddot{\underline{s}} + C\,\dot{\underline{s}} + \underline{K}_{NL} = \underline{F}_0 + \underline{F}(t) \qquad (3)$$

where $\underline{K}_{NL}$ is the vector of nonlinear restoring forces the elements of which can be expressed as

$$\left(\underline{K}_{NL}\right)_i = \sum_{j=1}^{N} K_{ij}^{(1)} s_j + \sum_{j,l=1}^{N} K_{ilj}^{(2)} s_l\, s_j + \sum_{j,l,p=1}^{N} K_{iljp}^{(3)} s_l\, s_j s_p \qquad (4)$$

where N is the total number of degrees-of-freedom in the finite element model. Further, every stress component S at every point of the panel can be written in the form

$$S = S^{(0)} + \sum_{i=1}^{N} S_i^{(1)}\, s_l + \sum_{i,j=1}^{N} S_{ij}^{(2)}\, s_i\, s_j\,. \qquad (5)$$

In practical problems, the total number of degrees-of-freedom in the finite element is large leading to a highly time consuming effort. It is thus desirable to obtain a simplified approach. To this end, it has been suggested to proceed with an approximate, assumed mode representation of the displacement field as

$$\underline{s}(x,y,z,t) = \sum_{i=1}^{m} q_i(t)\,\underline{\Psi}_i(x,y,z). \qquad (6)$$

This *linear* change of variables does not change the character of Eq. (4) and (5) which simply become

$$\overline{M}\;\underline{\ddot{q}} + \overline{C}\;\underline{\dot{q}} + \underline{\overline{K}}_{NL} = \underline{\overline{F}}_0 + \underline{\overline{F}}(t) \qquad (7)$$

$$\left(\underline{\overline{K}}_{NL}\right)_i = \sum_{j=1}^{N} \overline{K}_{ij}^{(1)}\; q_j + \sum_{j,l=1}^{N} \overline{K}_{ilj}^{(2)}\; q_l\, q_j + \sum_{j,l,p=1}^{N} \overline{K}_{iljp}^{(3)}\, q_l\, q_j\, q_p \qquad (8)$$

where $\underline{q}$ denotes the vector of components q_j and

$$S = \overline{S}^{(0)} + \sum_{i=1}^{N} \overline{S}_i^{(1)}\; q_l + \sum_{i,j=1}^{N} \overline{S}_{ij}^{(2)}\; q_i\; q_j\;. \qquad (9)$$

It is then concluded that

(i) the nonlinearity is in stiffness only, and

(ii) the determination of the reduced order models of Eq. (8) and (9) only requires the estimation of the coefficients $\overline{K}_{ij}^{(1)}$, $\overline{K}_{ilj}^{(2)}$, $\overline{K}_{iljp}^{(3)}$, $S^{(0)}$, $\overline{S}_i^{(1)}$, $\overline{S}_{ij}^{(2)}$.

These observations were well recognized by Rizzi and Muravyov (2002) and Muravyov and Rizzi (2003) who devised an elegant strategy for the evaluation of the coefficients $\overline{K}_{ij}^{(1)}$, $\overline{K}_{ilj}^{(2)}$, and $\overline{K}_{iljp}^{(3)}$ from a series of static solutions in which the forces required to obtain a specified displacement field are determined. Specifically, assume first that a single mode is kept in the expansion of Eq. (3), i.e.

$$\underline{s}(x,y,z,t) = q_j(t)\,\underline{\Psi}_j(x,y,z). \qquad (10)$$

Then, the external force that must be exerted on the panel to obtain this static displacement is

$$F_{1i} = \overline{K}_{ij}^{(1)}\; q_j + \overline{K}_{ijj}^{(2)}\; q_j^2 + \overline{K}_{ijjj}^{(3)}\; q_j^3. \qquad (11)$$

Further, the displacement field

$$\underline{s}(x,y,z,t) = -\,q_j(t)\,\underline{\Psi}_j(x,y,z) \qquad (12)$$

can similarly be accomplished with the forces

$$F_{2i} = -\,\overline{K}_{ij}^{(1)}\; q_j + \overline{K}_{ijj}^{(2)}\; q_j^2 - \overline{K}_{ijjj}^{(3)}\; q_j^3. \qquad (13)$$

The knowledge of the forces of Eq. (11) and (13) provides a direct strategy for the evaluation of the coefficient $\overline{K}_{ijj}^{(2)}$. Specifically, it is found that

$$\overline{K}_{ijj}^{(2)} = \frac{F_{1j} + F_{2j}}{2\,q_j^2} \qquad (14)$$

To determine the remaining two coefficients, $\overline{K}_{ij}^{(1)}$ and $\overline{K}_{ijjj}^{(3)}$, an additional force equation must be obtained. For example, a *linear* static solution sequence can be performed that yields directly $\overline{K}_{ij}^{(1)}$ so that $\overline{K}_{ijjj}^{(3)}$ can then be computed from

$$\overline{K}_{ijjj}^{(3)} = \frac{F_{1i} - \overline{K}_{ij}^{(1)}\; q_j - \overline{K}_{ijj}^{(2)}\; q_j^2}{q_j^3}. \qquad (15)$$

This approach is not appropriate if the panel temperature effects are to be included in the reduced order model as the MSC.NASTRAN linear static solver (SOL 101) does not account for in-plane stresses, e.g. thermal stresses. In this case, one proceeds with the nonlinear force evaluation corresponding to the displacement field

$$\underline{s}(x,y,z,t) = \hat{q}_j(t)\,\underline{\Psi}_j(x,y,z) \qquad (16)$$

where $\hat{q}_j \neq q_j$. That is,

$$F_{3i} = \overline{K}_{ij}^{(1)}\; \hat{q}_j + \overline{K}_{ijj}^{(2)}\; \hat{q}_j^2 + \overline{K}_{ijjj}^{(3)}\; \hat{q}_j^3 \qquad (17)$$

Combining Eq. (11), (14), and (17) then permits the evaluation of the remaining two coefficients, $\overline{K}_{ij}^{(1)}$ and $\overline{K}_{ijjj}^{(3)}$.

During these static solution sequences, both the forces and the entire stress field are evaluated. While the forces lead to the coefficients $\overline{K}_{ij}^{(1)}$, $\overline{K}_{ijj}^{(2)}$, and $\overline{K}_{ijjj}^{(3)}$, the stress fields

$$S = \overline{S}^{(0)} + \overline{S}_j^{(1)}\; q_j + \overline{S}_{jj}^{(2)}\; q_j^2, \qquad (18)$$

$$S = \overline{S}^{(0)} - \overline{S}_j^{(1)}\; q_j + \overline{S}_{jj}^{(2)}\; q_j^2 \qquad (19)$$

and

$$S = \overline{S}^{(0)} + \overline{S}_j^{(1)}\; \hat{q}_j + \overline{S}_{jj}^{(2)}\; \hat{q}_j^2. \qquad (20)$$

can similarly be used for the determination of the coefficients $S^{(0)}$, $\overline{S}_j^{(1)}$, and $\overline{S}_{jj}^{(2)}$ for any stress S at any grid point of the finite element model.

The evaluation of the coefficients $\overline{K}_{ilj}^{(2)}$, $\overline{K}_{illj}^{(3)}$, and $\overline{S}_{lj}^{(2)}$ for $l \neq j$ proceeds as above but in connection with the displacement fields

$$\underline{s}(x,y,z,t) = q_j(t)\,\underline{\Psi}_j(x,y,z) + q_l(t)\,\underline{\Psi}_l(x,y,z) \qquad (21)$$

and

$$\underline{s}(x,y,z,t) = q_j(t)\,\underline{\Psi}_j(x,y,z) - q_l(t)\,\underline{\Psi}_l(x,y,z). \qquad (22)$$

Finally, the coefficients $\overline{K}_{iljp}^{(3)}$ can be evaluated from the single assumed displacements field

$$\underline{s}(x,y,z,t) = q_j\,\underline{\Psi}_j(x,y,z) + q_l\,\underline{\Psi}_l(x,y,z) + q_p\,\underline{\Psi}_p(x,y,z) \qquad (23)$$

It should be noted that the above procedure for the evaluation of the coefficients is exact, the only approximation in the reduced order modeling is the modal expansion of Eq. (6).

The above procedure has been described for an arbitrary basis $\underline{\Psi}_j(x,y,z)$, j = 1, ..., N, but these functions must be defined to obtain numerical results. Further, the closeness of the ROM results to their finite element counterparts can be expected to be dependent on the choice of the functions $\underline{\Psi}_j(x,y,z)$. Since the present problem focuses mainly on the transverse vibrations of the panel, it is appropriate to include in the set $\underline{\Psi}_j(x,y,z)$ functions such as the mode shapes of the panel under small deflections around one of its typical configuration, e.g. unbuckled or buckled. These functions represent a basis for the transverse deflections but unfortunately do not include any in-plane motions. In large deflections, a coupling of the transverse and in-plane deflections exists with the latter inducing the "membrane" stiffening effect. It is thus necessary to include both in-plane and transverse displacement bases in the set $\underline{\Psi}_j(x,y,z)$.

In this regard, it should be noted that

(i) the in-plane motions are typically induced by their transverse counterparts and exhibit an amplitude that is related in first approximation to the square of the out-of-plane displacements,

and

(ii) the natural frequencies of the in-plane modes (for a flat panel) are generally much higher than their transverse counterparts so that the in-plane problem is, to first order, a static one.

On this basis, it has been proposed (Mignolet et al., 2003) to rely on a dual basis $\underline{\Psi}_i = (\underline{\hat{\Psi}}_i, \underline{\overline{\Psi}}_i)$ in which $\underline{\hat{\Psi}}_i$ would be represent the selected transverse modes of the linear panel and $\underline{\overline{\Psi}}_i$ would be representative of the second order, in-plane displacements induced by $\underline{\hat{\Psi}}_i$. These functions would be obtained from the static nonlinear response of the panel to transverse loads $p\,\underline{\hat{\Psi}}_i$. Specifically, consider two different values of p, i.e. p and 2 p. Then, the corresponding two displacement fields (each including both in-plane and out-of-plane components) $\underline{s}_1$ and $\underline{s}_2$ can be combined to form $\underline{\overline{\Psi}}_i$ through an elimination of the linear (out-of-plane) terms, e.g. as

$$\underline{\overline{\Psi}}_i = \underline{s}_2 - 2\,\underline{s}_1 . \qquad (24)$$

Note that a similar discussion has been conducted by Gordon et al. (2003) to justify the use of in-plane modes (referred to as the dual basis above and as the companion by Gordon et al. (2003)).

The above discussion focused on the representation of the nonlinear terms in the ROM. The coefficients of the linear terms, i.e. $\overline{M}$, $\overline{C}$, $\overline{F}_0$, and $\overline{F}(t)$ must also be determined. In fact, from the formulation of the ROM as a Galerkin approximation, it is found that the components of these matrices and vectors are

$$\overline{M}_{ij} = \underline{\Psi}_i^T\, M\, \underline{\Psi}_j ; \qquad \overline{C}_{ij} = \underline{\Psi}_i^T\, C\, \underline{\Psi}_j ;$$

$$\overline{F}_{0,i} = \underline{\Psi}_i^T\, \underline{F}_0 ; \quad \text{and} \quad \overline{F}_i(t) = \underline{\Psi}_i^T\, \underline{F}(t). \qquad (25)$$

One case of particular interest is the impingement of an acoustic wave on the panel. When the wave is at normal incidence to the panel, one has

$$\underline{F}(t) = \underline{v}\, p(t) \qquad (26)$$

where $\underline{v}$ is a constant (with respect to time) vector. In the case of an acoustic excitation at non-normal incidence, the loading on the panel involves the pressure time history over a range of time, i.e.

$$\underline{F}(t) = \sum_j \underline{v}_j\, p(t - \tau_j) \qquad (27)$$

where the time shifts $\tau_j = j\,\Delta t$ are associated with the propagation of the wave along the panel.

It was found that the natural frequencies associated with the dual modes are much higher than those corresponding to the transverse mode. Given the in-plane nature of the dual modes, this observation is not unexpected but it implies a substantial increase of the computational effort associated with the numerical integration of the ROM equations of motion by requiring an appropriately small time step to track the dual mode dynamics. In many cases, it may be expected that the loading on the panel will not exhibit any energy at such high frequencies and thus it is acceptable to proceed with a static condensation of the dual modes. That is, their mass and damping coefficients are ignored and the values of the dual mode coordinates are evaluated at each time step from their transverse counterparts to satisfy $\underline{\overline{K}}_{NL} = \underline{\overline{F}}_0$. In all examples considered below, it was found that the magnitude of the in-plane displacements is small enough to remain in the linear range. Thus, the nonlinear algebraic equations $\underline{\overline{K}}_{NL} = \underline{\overline{F}}_0$ can be linearized with respect to the dual modes only to provide an efficient computation of their generalized coordinates.

REDUCED ORDER MODEL VALIDATION

The validation of the above ROM is being achieved on the basis of two flat rectangular clamped aluminum panels of dimensions 0.3556m x 0.254m x 0.00102m (Panel 1) and 0.3048m x 0.254mx 0.00102m (Panel 2) both of which were discretized with 14x10 CQUAD4 elements. The validation encompasses the following aspects:

(1) validation of the ROM on static loads

(2) validation of the static condensation of the dual modes

(3) dynamic validation

(4) assessment of fatigue life/accumulated damage.

The ROM provides a modeling of the response that should be valid under a broad range of excitations. In particular, the ROM should be applicable to static loads and the consideration of such problems provides a first and fast perspective of its reliability. In this investigation, the panel 2 was assumed to be loaded with a uniform static pressure varying in the range of 1 to 3600 Pa. For each load condition, a full NASTRAN static analysis was carried out to establish the baseline for the assessment of the ROM results. Shown in Fig. 2 and 3 are the displacement and stress at the middle of the panel as obtained from the NASTRAN analysis and with the reduced order model with 1, 3, and 6 transverse modes and their associated duals. There is clearly an excellent agreement between the NASTRAN prediction and the 12-mode (6 transverse and 6 duals) ROM. To test the reduced order modeling in a strongly nonlinear situation, the panel was next assumed to be subjected to a temperature equal to 1.8 times its buckling temperature in addition to the pressure described above. As can be seen from Fig. 4, an excellent prediction of the displacements of the middle of the panel are again obtained.

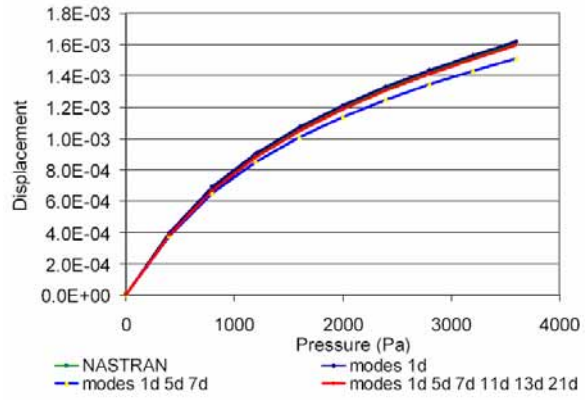

Figure 2. Static response of an unbuckled panel to a uniform pressure. Center displacement as a function of pressure.

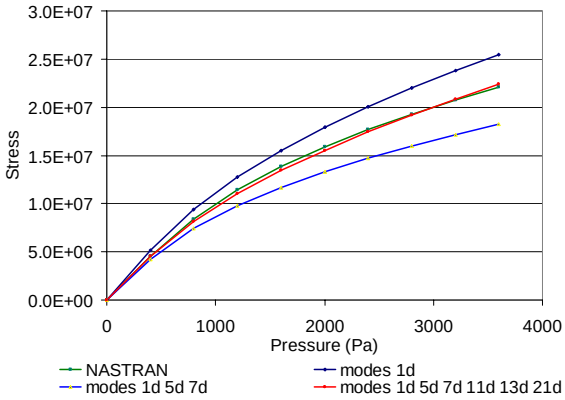

Figure 3. Static response of an unbuckled panel to a uniform pressure. Stress σ_{xx} as a function of pressure.

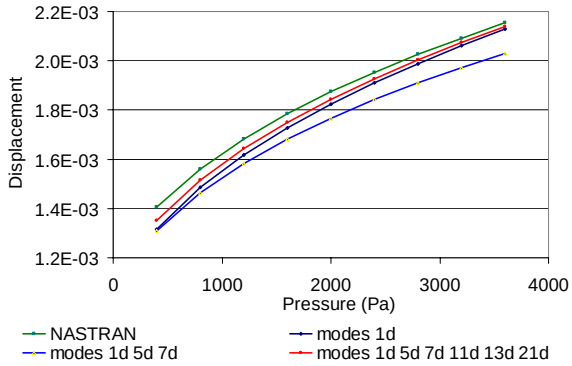

Figure 4. Static response of a buckled panel to a uniform pressure. Center displacement as a function of pressure.

Having established the reliability of the reduced order modeling in static cases, it was desired next to validate its usefulness in dynamic problems. This process was achieved in two steps. First, the static condensation procedure described above was evaluated and then, in the second phase, a comparison on the response of the panel to a random loading was performed. For the static condensation validation, the panel 2 was subjected to a white noise excitation of overall sound pressure level (OA*SPL*) equal to 153 dB in the range of 0-2083 Hz and a 6 transverse mode models (with associated duals) was considered. The full solution of the reduced order model equations is compared to its statically condensed counterpart in Fig. 5 (for the displacement at the middle of the panel) and Fig. 6 (for the corresponding stress). Clearly, the spectra of the full and condensed solutions are very close to each other through the entire frequency range of the exictation/response.

On the basis of the excellent matching of Fig. 5 and 6, the static condensation was relied upon for the full dynamic validation conducted on Panel 1. The linear response of the panel was first explored to establish a

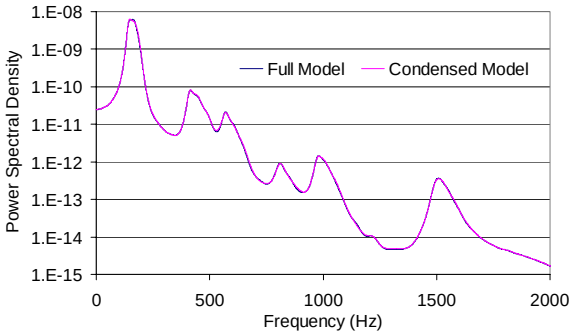

Figure 5. Comparison of power spectra of the displacement at the center of the panel for the full and statically condensed models.

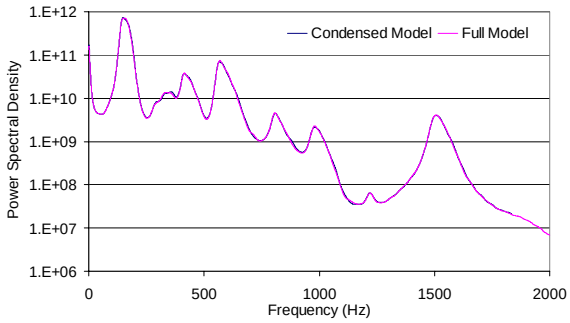

Figure 6. Comparison of power spectra of the stress σ_{xx} at the center of the panel for the full and statically condensed models.

firm ground for the comparison of the nonlinear responses. Shown in Fig. 7 are the power spectral densities of the displacement of the center of the panel estimated from time histories of its linear response when subjected to a 100dB white noise excitation in the range of 0-2083 Hz. Clearly, the agreement between the MSC.NASTRAN and reduced order model results is excellent, as expected.

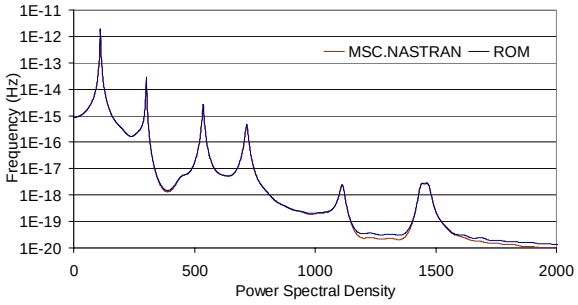

Figure 7. Comparison of power spectra of the displacement at the center of the panel for MSC.NASTRAN and the reduced order model Linear system

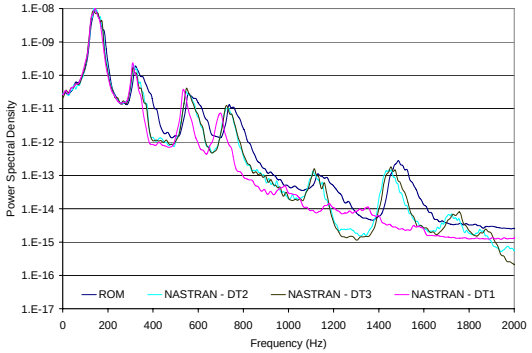

Figure 8. Comparison of power spectra of the displacement at the center of the panel for MSC.NASTRAN and the reduced order model Nonlinear system - 147dB

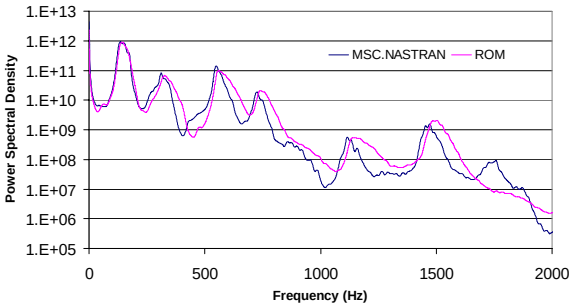

Figure 9. Comparison of power spectra of the stress σ_{xx} at the center of the panel for MSC.NASTRAN and the reduced order model Nonlinear system - 147dB

A white noise excitation of sound pressure level 147dB in the same frequency range was generated to assess the dynamic nonlinear prediction capabilities of the proposed reduced order. A series of NASTRAN nonlinear solutions were performed with the standard tolerance and maximum time steps DT1 = 2.4 10^{-4} s., DT2 = 4 10^{-5} s., and DT3 = 2 10^{-5} s. The corresponding power spectral densities of the displacement at the center of the panel are shown in Fig. 8 together with the 16-mode (8 transverse and 8 duals) ROM prediction. An excellent matching of the dominant component of the response, i.e. the first peak, is achieved. Further, the predicted levels of the next three peaks is also very good although the frequency and width of the peaks do not coincide as well. Overall, a good matching at least is achieved. A similar perspective can be obtained from the power spectral densities of the stress σ_{xx}, see Fig. 9.

The computational efficiency of the reduced order modeling technique allows for the generation of the very long time histories of the displacements and stresses which are required for an accurate estimation of the fatigue life of the panels. To exemplify this

computation, a time history of 1.5 million time steps (Δt = 2.4 10^{-4} s.) was generated with the reduced order model for the 147dB excitation. This large data set was then processed by the rainflow algorithm (Downing and Socie, 1982) to obtain the probability density function of the rainflow ranges shown in Fig. 10. Note the very smooth features of this distribution, even far in the right tail. From the ensemble of rainflow ranges and their associated half-periods, an estimate of the damage accumulated in the panel over the total time (= 360 s.) can be determined. This data can finally be used to predict the fatigue life of the panel under the 147 dB white noise excitation but it can also be used to validate estimators of this fatigue life. A recent investigation (Yang et al., 2004) has reviewed and compared several

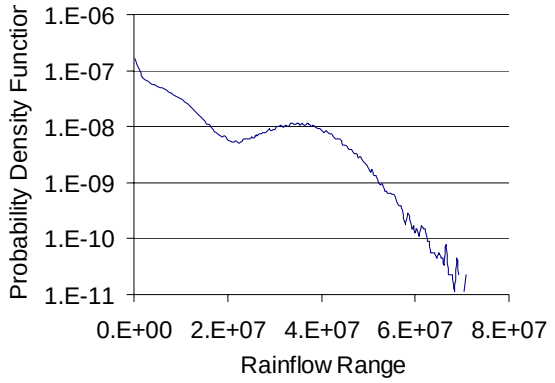

Figure 10. Probability density function of the rainflow ranges - ROM at 147dB

estimators of the accumulated damage. Specifically,

Rayleigh approximation:

$$E[D]_R = 2^{3m/2}\,\Gamma(1+m/2)\,\sigma_{\dot S}\,\sigma_S^{m-1}\,T/(2\pi K) \quad (28)$$

where σ_S and $\sigma_{\dot S}$ are the standard deviations of the stress process and its time derivative and *m* and *K* are the exponent and coefficient of the S-N curve, respectively. Finally, *T* is the total time.

Rayleigh approximation with Gaussianity correction:

$$E[D]_R\,/GR \quad (29)$$

where the Gaussianity Ratio is defined as

$$GR = 1 - m\,(m-1)(\kappa_4 - 3)/24 \quad \text{for} \quad \kappa_4 < 3 \quad (30)$$

and

$$GR = \left[1 + m\,(m-1)(\kappa_4 - 3)/24\right]^{-1} \text{ for } \kappa_4 > 3 \quad (31)$$

where κ_4 denotes the coefficient of kurtosis of the stress process.

Single moment estimate (Lutes and Larsen, 1990):

$$E[D]_{SM} = (\lambda_a)^{-b}\,T/c \quad (32)$$

where λ_a denotes the spectral moment of order *a* of the stress process, i.e.

$$\lambda_a = \int_{-\infty}^{+\infty} S_{SS}(\omega)\,\omega^a\,d\omega \quad (33)$$

where $S_{SS}(\omega)$ is the power spectral density of the stress process. Further, the coefficients *a* and *b* are

$$a = 2/m \qquad b = -m/2\ . \quad (34)$$

Finally, the scaling coefficient *c* usually selected as

$$c = c_{Narr} = 2\,\pi\,K/\left[2^{3m/2}\,\Gamma(1+m/2)\right]\ . \quad (35)$$

Single moment estimate with Gaussianity correction:

$$E[D]_{SM}\,/GR \quad (36)$$

Modified Rayleigh formula (Yang et al., 2004):

$$E[D] = \frac{\sigma_{\dot q}\,T_{fin}}{\sqrt{2\pi}\,K}\,\frac{\Gamma(1+m/4)}{\Gamma(1.25)}\left[3.4402\,\sigma_q\right]^{(m-1)} \quad (37)$$

Modified single moment method (Yang et al., 2004):
Use Eq.(32) with

$$c_{NL} = \sqrt{2\pi}\,K\,\frac{\Gamma(1.25)}{\Gamma(1+m/4)}\,\left[0.29068\right]^{(m-1)} \quad (38)$$

Equations (28), (29), and (32) are standard damage estimators while Eq. (37) and (38) have been specifically derived for the nonlinear response of structures (see Yang et al., 2004). These two expressions were shown to outperform the other 4 estimators on the basis of single mode time histories and some limited experimental data. Multi-mode/finite element data could however not be produced to provide a better assessment of Eq. (37) and (38). With the 1.5 million time step time histories, this validation can be accomplished. In fact, Fig. 11 confirms that Eq. (37) and (38) outperform all other approaches leading to errors on the accumulated damage that are below 30% over the range $m \in [1,8]$.

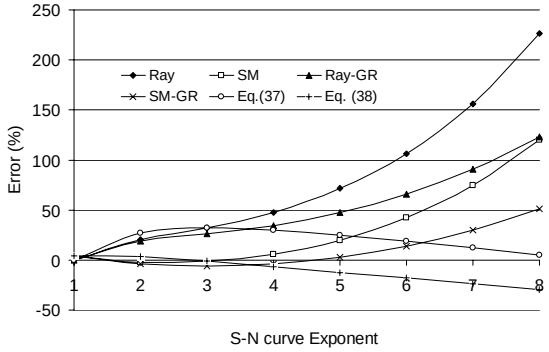

Figure 11. Relative error on the prediction of the expected damage as a function of the S-N exponent *m* for different methods ("Ray" = Rayleigh, "SM" = Single Moment, "GR" = with Gaussianity Ratio)

SUMMARY

In this paper, a complete reduced order modeling scheme has been presented to reduce a full finite element model into a set of *n* discrete coordinates representing the contributions of *n* arbitrarily specified "modes" to the overall panel response. Included in these modes are in-plane motions of the panel that are statically associated with the transverse deflections and are referred to as dual modes. The nonlinear terms in the *n* corresponding differential equations are then obtained by evaluating the forces required to produce a given set of panel displacements. These terms may be evaluated in the presence of a nonzero panel temperature as to include the softening thermal effects. Further, the strategy was extended to include the determination of the coefficients in the generalized quadratic relation between the displacement and stress fields. In this fashion, a displacement and stress reduced order model is obtained. Further, computational issues have been shown to motivate a static condensation of the dual modes.

Several aspects of this approach were validated here. First, the deflection and stresses corresponding to a static loading on either an unbuckled or a buckled panel were considered and the reduced order model results were shown to provide a very good match of full finite element computations (NASTRAN). Next, the static condensation of the dual mode was critically assessed and it was shown that this approach does not produce any noticeable difference, beside computational time, on the predicted displacements and stresses. A nonlinear dynamic load case was then considered to further assess the reliability of the reduced order modeling. The power spectral densities of the displacement and stress considered and estimated from NASTRAN and the reduced order model were found to match quite satisfactorily. Finally, the computational efficiency of the reduced order modeling technique was utilized to produce a long time history of stress from which an accurate estimate of the accumulated damage could be derived. This data allowed the comparison of several fatigue life predictors and demonstrated the superiority of two such estimators recently proposed.

ACKNOWLEDGEMENTS

The support of this investigation by the Air Force Research Laboratory and NASA under contracts F33615-01-C-3111 and NNL04AA07C is gratefully acknowledged.

REFERENCES

Blevins, R.D., Holehouse, I., and Wentz, K.R., 1993, "Thermoacoustic Loads and Fatigue of Hypersonic Vehicle Skin Panels," *Journal of Aircraft*, Vol. 30, No. 6, pp. 971-978.

Chen, P.C., Liu, D.D., and Mignolet, M.P., 2000, "Formulation and Application of a Stochastic Fatigue Damage Accumulation Model for the Response of Buckled Composite Panels," *Air Force Research Laboratory*, Report No. AFRL-VA-WP-TR-2000-3013.

Choi, S-T., and Vaicaitis, R., 1989, "Nonlinear Response and Fatigue of Stiffened Panels," *Probabilistic Engineering Mechanics*, Vol. 4, No. 3, pp. 150-160

Chilakamarri, K.B., and Lee, J., 2000, "Thermal-Acoustic Fatigue Damage Accumulation Model of Random Snap-Throughs," *Proceedings of the 8th ASCE Specialty Conference on Probabilistic Mechanics and Structural Reliability.*

Clarkson, B.L., 1994, *Review of Sonic Fatigue Technology,* NASA Contractor Report 4587.

Downing, S.D., and Socie, D.F., 1982, "Simple Rainflow Counting Algorithms," *International Journal of Fatigue*, pp. 31-40.

Ghazarian, N., and Locke, J., 1995, "Non-Linear Random Response of Antisymmetric Angle-Ply Laminates Under Thermal-Acoustic Loading," *Journal of Sound and Vibration*, Vol. 186, No. 2, pp. 291-309.

Gordon, R., Spottswood, S.M., and Hollkamp, J., "Nonlinear Sonic Fatigue Response Prediction from Finite Element Modal Models: A Comparison with Experiments," *Presented at the 44th Structures, Structural Dynamics, and Materials Conference*, Norfolk, Virginia, Apr. 7-10, 2003. Paper AIAA-2003-1709.

Istenes, R.R., Rizzi, S.A., and Wolfe, H.F., 1995, "Experimental Nonlinear Random Vibration Results of Thermally Buckled Composite Panels," *Proceedings of the 36th Structures, Structural Dynamics, and Materials Conference,*AIAA-95-1345-CP, New Orleans, LA, Apr. 10-13, 1559-1568.

Kavallieratos, P.A., 1992, *Nonlinear Response of Composite Panels to Random Excitation*, Ph. D. Dissertation, Columbia University.

Lee, J., 1993, "Large-Amplitude Plate Vibration in an Elevated Thermal Environment," *Applied Mechanics Reviews,* Vol. 46, No. 11, Part 2, pp. S242-S254.

Lee, J., 1995, "Applicability of the Equivalent Linearization Technique for Thermally Buckled Plate Random Vibration," *Proceedings of the 36th Structures, Structural Dynamics, and Materials Conference*, New Orleans, Louisiana, pp. 1272-1279, AIAA Paper 95-1304.

Lee, J., 1997, "Random Vibration of Thermally Buckled Plates: II Nonzero Temperature Gradient Across the Plate Thickness," *Applied Mechanics Reviews,* Vol. 50, No. 11, Part 2, pp. S105-S116.

Lee, J., and Wentz, K.R., 1997, "Strain Power Spectra of a Thermally Buckled Plate in Random Vibration, " *Proceeding by the Sixth International Conference on Recent Advances in Structural Dynamics*, Southampton, United Kingdom, Jul. 14-17, Vol. 2, pp. 903-917.

Lee, J., 2001, "Displacement and Strain Statistics of Thermally Buckled Plates," *Journal of Aircraft*, Vol.37.

Lee, J., Vaicaitis, R., Wentz, K., Clay, C., Anselmo, E., and Crumbacher, R., "Prediction of Statistical Dynamics of Thermally Buckled Composite Panels," *Proceedings of the 39th Structures, Structural Dynamics, and Materials Conference*, Long Beach, California, Apr. 20-23, 1998, Vol. 3, pp. 2539-2549, AIAA Paper 98-1975.

Lutes, L.D., and Larsen, C.E., 1990, "Improved Spectral Methods for Variable Amplitude Fatigue," *Journal of Structural Engineering*, Vol. 116, No. 4, pp. 1149-1164.

Mei, C., "Three Decades' Interesting Experience in Nonlinear Finite Element Formulation Development and Aerospace Applications," 7th International Conference on Recent Advances in Structural Dynamics, Southampton, United Kingdom, July 14-16, 2003.

Mignolet, M.P., Radu, A.G., and Gao, X., 2003, "Validation of Reduced Order Modeling for the Prediction of the Response and Fatigue Life of Panels Subjected to Thermo-Acoustic Effects," 7th International Conference on Recent Advances in Structural Dynamics, Southampton, United Kingdom, July 14-16, 2003.

Muravyov, A.A., and Rizzi, S.A., 2003, "Determination of nonlinear stiffness with Application to Random Vibration of Geometrically Nonlinear Structures," *Computers and Structures*, Vol. 81, pp. 1513-1523.

Murphy, K.D., Virgin, L.N., and Rizzi, S.A., 1996, "Characterizing the Dynamic Response of a Thermally Loaded, Acoustically Excited Plate," *Journal of Sound and Vibration*, Vol. 196, No. 5, pp. 635-658.

Rizzi, S.A., and Muravyov, A.A., 2002, "Equivalent Linearization Analysis of Geometrically Nonlinear Random Vibrations Using Commercial Finite Element Codes," NASA Technical Paper NASA/TP-2002-211761, Langley Research Center, Hampton, Virginia.

Spottswood, S.M., and Mignolet, M.P., 2002, "Experimental Nonlinear Response of Tapered Ceramic Matrix Composite Plates to Base Excitation," *AIAA Journal*, Vol. 40, No. 8, pp. 1682-1687, 2002.

Spottswood, S.M., Wolfe, H.F. and Brown, D.L., 2000, "A Fatigue Life Estimation Comparison Utilizing Experimental and Spectral Density Based Probability Distributions", *ICNPAA Conference*, Embry-Riddle Aeronautical University, Daytona Beach, FL, May 10-12.

Spottswood, S.M., and Wolfe, H.F., 2001, "Comparing Fatigue Life Estimates using Experimental and Spectral Density Based Probability Distributions", 4*2nd Structures, Structural Dynamics and Materials Conference*, Seattle, WA.

Sun, J.Q., Bao, W., and Miles, R.N., 1998, "Fatigue Life Prediction of Nonlinear Plates Under Random Excitations," *Journal of Vibration and Acoustics*, Vol. 120, pp. 353-360.

Vaicaitis, R., 1994, "Nonlinear Response and Sonic Fatigue of National Aerospace Space Plane Surface Panels," *Journal of Aircraft,* Vol. 31, No. 1, pp. 10-18.

Vaicaitis, R., and Arnold, R., 1990, "Time Domain Monte Carlo Approach for Nonlinear Response and Sonic Fatigue," *Proceedings of the 13th AIAA Aeroacoustics Conference*, Tallahassee, FL, Oct.22-24, AIAA Paper AIAA-90-3938.

Yang, B., Mignolet, M.P., and S.M. Spottswood, "Modeling of Damage Accumulation for Duffing Oscillator-Type Systems Under Severe Random Excitations," *Probabilistic Engineering Mechanics*, Vol. 19, pp. 185-194, 2004.

Appendix D

"Validation of Reduced Order Modeling for the Prediction of the Response and Fatigue Life of Panels Subjected to Thermo-Acoustic Effects"

Proceedings of the 8th International Conference on Recent Advances in Structural Dynamics, Southampton, United Kingdom, Jul. 14-16, 2003.

VALIDATION OF REDUCED ORDER MODELING FOR THE PREDICTION OF THE RESPONSE AND FATIGUE LIFE OF PANELS SUBJECTED TO THERMO-ACOUSTIC EFFECTS

Marc P. Mignolet
Adrian G. Radu
Department of Mechanical and Aerospace Engineering, Arizona State University
Tempe, Arizona, 85287-6106, USA. Emails: marc.mignolet@asu.edu and raduag@asu.edu

Xiaowei Gao
ZONA Technology, 7430 E. Stetson Drive, Suite 205
Scottsdale, AZ 85251-3540, USA. Email: gao@zonatech.com

ABSTRACT

This paper focuses on the validation of a reduced order modeling strategy for aircraft panels subjected to combined thermal effects and an incident acoustic wave strong enough to induce a severe geometrically nonlinear behavior. The response of flat panels to two different excitations scenarios serves as a basis to assess the appropriateness of several modal bases for the reduced order modeling. This comparison emphasizes the importance of the in-plane displacement field and of a reliable modeling of the curvature of the deformed panels. Consistently with these observations, a novel basis is introduced that involves separate representations of the transverse displacements and their induced in-plane counterparts.

INTRODUCTION

The reliable and efficient design of the panels of reusable launch vehicles and other future hypersonic vehicles represents a difficult technological challenge. Indeed, these panels will be subjected to thermal effects originating from the aerodynamics and potentially severe acoustic loads emanating for example from the engine exhaust. To avoid a degradation of the structural properties, thermal protection systems (TPS) are expected to be used to "shield" the structural components from the high temperatures. While the normal operating temperature of a thermally protected panel should be much less than the 3000°F that might be obtained without TPS [1], it still might be large enough to induce a decrease of the panel stiffness, either from constrained thermal expansion or from a reduction of the mechanical properties. In all cases, a severe acoustic loading of these panels will induce large deflections and a substantially reduced fatigue life which must be carefully estimated to avoid an unforeseen failure.
The prediction of the fatigue life of the panels is however a rather challenging task as

(i) the acoustic excitation is best represented as a random process,

(ii) the presence of large deflections implies the nonlinearity of the governing equations for the panel response and the non-Gaussian character of its probability density function,

and

(iii) the presence of large deflections also implies a nonlinearity of the displacement-stress relationship (due to the von Karman strain definition) and thus a further deviation of the

distribution of the peak and ranges from the classical models (e.g. Rayleigh, Dirlik, etc., see [2]).

A good qualitative understanding of the dynamic behavior of the panel response through the entire range of sound pressure level (*SPL*) and temperature can be obtained from the published literature in this area (see [1], [3]-[17] and references therein). While a *qualitative* perspective on the dynamic response of the panels is important, it is its accurate *quantitative* prediction which is ultimately required for design considerations. Quite naturally, it would seem that this prediction could be accomplished using standard finite element packages. This is indeed possible but the computational time needed to obtain a time history of the response long enough to derive accurate estimates of the statistics of the response and the expected fatigue life is surprisingly large. For example, achieving this latter task with an accuracy of the order of a few percents for a panel with 1,000 degrees-of-freedom and a material with a S-N curve of exponent 8 appears to require one to several hundred CPU hours on a top of the line single processor PC (2.4 GHz, 2 GB RAM) running the nonlinear NASTRAN dynamic solution with the standard accuracy.

While a decrease of this CPU time will naturally arise from the ever increasing processors speed, it is also expected that much more complex models would be studied in practical applications and would include in particular thermal protection systems. Even if such a computational time may be acceptable to analyze a specific panel, it is not appropriate in the design phase when changes may occur frequently and when fast analysis capabilities are needed. These difficulties of a straightforward finite element approach have been well recognized in [9], [10], and [13] who suggested to proceed with reduced order modeling techniques in which the panel displacement field is approximately represented as a linear combination of a series of assumed "modes". With this representation, the number of degrees-of-freedom is reduced to *m*, the number of modes considered, which is small enough to permit an efficient solution of the problem.

A distinguishing feature of the work of Rizzi and Muravyov [13] lies in the finite element code used, i.e. as opposed to developing separate finite element capabilities, they have efficiently linked their reduced order modeling strategy to NASTRAN thereby allowing the use of all elements and resources inside NASTRAN. Then, the goal of this paper is to report on current validation efforts and extensions of the nonlinear stiffness evaluation approach of [13] to include the panel temperature effects and a stress reduced order modeling to lead to the efficient estimation of the fatigue life of panels subjected to a random acoustic excitation and temperature effects. For clarity, the formulation of the reduced order modeling strategy will first be briefly revisited.

REDUCED ORDER MODELING FORMULATION

In the absence of material nonlinearity, large deformations are assumed to only affect the panel dynamics through the von Karman strains, i.e.

$$\varepsilon_x = \frac{\partial u}{\partial x} + \frac{1}{2}\left(\frac{\partial w}{\partial x}\right)^2 \qquad \varepsilon_y = \frac{\partial v}{\partial y} + \frac{1}{2}\left(\frac{\partial w}{\partial y}\right)^2 \qquad \varepsilon_z = \frac{\partial w}{\partial z} = 0 \tag{1}$$

$$\gamma_{xy} = \frac{1}{2}\left[\frac{\partial u}{\partial y} + \frac{\partial v}{\partial x} + \left(\frac{\partial w}{\partial x}\right)\left(\frac{\partial w}{\partial y}\right)\right] \qquad \gamma_{xz} = \frac{1}{2}\left[\frac{\partial u}{\partial z} + \frac{\partial w}{\partial x}\right] \qquad \gamma_{yz} = \frac{1}{2}\left[\frac{\partial v}{\partial z} + \frac{\partial w}{\partial y}\right]$$

where $u(x, y, t)$, $v(x, y, t)$, and $w(x, y, t)$ are the in-plane and out-of-plane displacement fields, respectively. In a finite element formulation, the determination of these functions is reduced to the computation of the nodal displacements, e.g. the in-plane, out-of-plane displacements and rotations at these points, which are stored in the vector $\underline{w}(t)$. Given the quadratic nature of the above displacement-strain relations, it is expected that this panel displacement vector satisfies the cubic nonlinear equations

$$M\ \ddot{\underline{w}} + C\ \dot{\underline{w}} + \underline{K}_{NL} = \underline{F}_0 + \underline{F}(t) \tag{2}$$

where M and C denote the mass and damping matrices of the panel. Further, $\underline{F}_0$ and $\underline{F}(t)$ are respectively a constant excitation vector arising for example from an asymmetry of the panel or of its temperature distribution and the time-varying force vector associated with the acoustic pressure. Finally, $\underline{K}_{NL}$ is the vector of nonlinear restoring forces the elements of which can be expressed as

$$\left(\underline{K}_{NL}\right)_i = \sum_{j=1}^{N} K_{ij}^{(1)}\ w_j + \sum_{j,l=1}^{N} K_{ilj}^{(2)}\ w_l\ w_j + \sum_{j,l,p=1}^{N} K_{iljp}^{(3)}\ w_l\ w_j\ w_p \tag{3}$$

where N is the number of physical degrees of freedom. Further, every physical stress component S (= σ_{xx}, or σ_{yy}, ...) at every point of the panel can be written in the form

$$S = S^{(0)} + \sum_{i=1}^{N} S_i^{(1)}\ w_i + \sum_{i,j=1}^{N} S_{ij}^{(2)}\ w_i\ w_j\ . \tag{4}$$

where the coefficients $S^{(0)}$, $S_i^{(1)}$, $S_{ij}^{(2)}$ depend in general on both the stress and point considered. Note that not all the coefficients $K_{ij}^{(1)}$, $K_{ilj}^{(2)}$, $K_{iljp}^{(3)}$, $S^{(0)}$, $S_i^{(1)}$, $S_{ij}^{(2)}$ are non-zero. For example, one can expect the coefficients $K_{iii}^{(2)}$ to vanish for flat symmetric panels and a constant stress level $S^{(0)}$ only occurs when the panel is heated.

The proposed reduced order modeling schemes are based on the representation of the displacement vector in a "modal expansion" of the type

$$\underline{w}(t) = \sum_{i=1}^{m} q_i(t)\,\underline{\Psi}_i \tag{5}$$

where the vectors $\underline{\Psi}_i$ form an appropriately selected basis. Governing equations for the coordinates q_j are then obtained by requiring that the error in Eq. (2) be orthogonal to the basis selected. This process does not change the character of Eq. (2)-(4) which simply become

$$\overline{M}\ \ddot{\underline{q}} + \overline{C}\ \dot{\underline{q}} + \overline{\underline{K}}_{NL} = \overline{\underline{F}}_0 + \overline{\underline{F}}(t) \tag{6}$$

$$\left(\overline{\underline{K}}_{NL}\right)_i = \sum_{j=1}^{m} \overline{K}_{ij}^{(1)}\ q_j + \sum_{j,l=1}^{m} \overline{K}_{ilj}^{(2)}\ q_l\ q_j + \sum_{j,l,p=1}^{m} \overline{K}_{iljp}^{(3)}\ q_l\ q_j\ q_p \tag{7}$$

where $\underline{q}$ denotes the vector of components q_j and

$$S = S^{(0)} + \sum_{i=1}^{m} \overline{S}_i^{(1)}\, q_i + \sum_{i,j=1}^{m} \overline{S}_{ij}^{(2)}\, q_i\, q_j\,. \tag{8}$$

The reduced order coefficients (masses, stiffnesses, etc.) appearing in Eq. (6)-(8) are related to their counterparts for the original system of Eq. (2)-(4) through the transformations

$$\overline{M} = \underline{\hat{\Psi}}^T\, M\, \underline{\hat{\Psi}}\,, \qquad \overline{C} = \underline{\hat{\Psi}}^T\, C\, \underline{\hat{\Psi}}\,, \qquad \overline{K}^{(1)} = \underline{\hat{\Psi}}^T\, K^{(1)}\, \underline{\hat{\Psi}} \tag{9}$$

$$\overline{K}_{irj}^{(2)} = \sum_{p,l=1}^{N} K_{ilp}^{(2)}\, \Psi_{r,l}\, \Psi_{j,p}\,; \quad K_{irsj}^{(3)} = \sum_{p,l=1}^{N} K_{ilpq}^{(3)}\, \Psi_{r,l}\, \Psi_{s,p}\, \Psi_{j,q}\,; \quad \underline{\overline{F}}_0 = \underline{\hat{\Psi}}^T\, \underline{F}_0 \tag{10}$$

$$\underline{\overline{F}}(t) = \underline{\hat{\Psi}}^T\, \underline{F}(t); \quad \overline{S}_j^{(1)} = \sum_{i=1}^{N} S_i^{(1)}\, \Psi_{j,i}\,; \quad \text{and} \quad \overline{S}_{rs}^{(2)} = \sum_{i,j=1}^{N} S_{ij}^{(2)}\, \Psi_{r,i}\, \Psi_{s,j} \tag{11}$$

where $\Psi_{r,l}$ designates the component l of $\underline{\Psi}_r$ and $\underline{\hat{\Psi}}$ is the "modal matrix"

$$\underline{\hat{\Psi}} = \left[\underline{\Psi}_1\ \underline{\Psi}_2 \cdots \underline{\Psi}_m\ \right]. \tag{12}$$

It is then concluded that

(i) the nonlinearity is in stiffness only,

(ii) the determination of the reduced order models of Eq. (6)-(8) only requires the estimation of the coefficients $\overline{K}_{ij}^{(1)}$, $\overline{K}_{ilj}^{(2)}$, $\overline{K}_{iljp}^{(3)}$, $S^{(0)}$, $\overline{S}_i^{(1)}$, $\overline{S}_{ij}^{(2)}$.

(iii) since the equations (6) are obtained through a Galerkin approach, these coefficients depend only on a small part of the basis, i.e. the parameter $\overline{K}_{ilj}^{(2)}$ depend only on the vectors $\underline{\Psi}_i$, $\underline{\Psi}_j$, and $\underline{\Psi}_l$, neither on the rest of the basis nor on the order *m*.

These observations were well recognized by Rizzi and Muravyov [13] who devised an elegant strategy for the evaluation of the coefficients $\overline{K}_{ij}^{(1)}$, $\overline{K}_{ilj}^{(2)}$, and $\overline{K}_{iljp}^{(3)}$ from a series of nonlinear static solutions in which the forces required to obtain a specified displacement field are determined (through a DMAP alter in NASTRAN [13]). Specifically, assume first that a single mode is kept in the expansion of Eq. (5), i.e.

$$\underline{w}(t) = q_j(t)\, \underline{\Psi}_j\,. \tag{13}$$

Then, the external force that must be exerted on the panel to obtain this static displacement is

$$F_{1i} = \overline{K}_{ij}^{(1)}\, q_j + \overline{K}_{ijj}^{(2)}\, q_j^2 + \overline{K}_{ijjj}^{(3)}\, q_j^3\,. \tag{14}$$

Further, the displacement field

$$\underline{w}(t) = -\, q_j(t)\, \underline{\Psi}_j \tag{15}$$

can similarly be accomplished with the forces

$$F_{2i} = -\,\overline{K}_{ij}^{(1)}\, q_j + \overline{K}_{ijj}^{(2)}\, q_j^2 - \overline{K}_{ijjj}^{(3)}\, q_j^3\,. \tag{16}$$

The knowledge of the forces of Eq. (14) and (16) provides a direct strategy for the evaluation of the coefficient $\overline{K}_{ijj}^{(2)}$. Specifically, it is found that

$$\overline{K}_{ijj}^{(2)} = \frac{F_{1i} + F_{2i}}{2\, q_j^2} \tag{17}$$

To determine the remaining two coefficients, $\overline{K}_{ij}^{(1)}$ and $\overline{K}_{ijjj}^{(3)}$, an additional force equation must be obtained. For example, a *linear* static solution sequence can be performed that yields directly $\overline{K}_{ij}^{(1)}$ so that $\overline{K}_{ijjj}^{(3)}$ can then be computed from

$$\overline{K}_{ijjj}^{(3)} = \frac{F_{1i} - \overline{K}_{ij}^{(1)}\, q_j - \overline{K}_{ijj}^{(2)}\, q_j^2}{q_j^3}. \tag{18}$$

This approach is not appropriate if the panel temperature effects are to be included in the reduced order model as the NASTRAN linear static solver does not account for in-plane stresses, such as those created by the panel heating/cooling. In this case, one proceeds with the nonlinear force evaluation corresponding to the displacement field

$$\underline{w}(t) = \hat{q}_j(t)\, \underline{\Psi}_j \tag{19}$$

where $\hat{q}_j \neq q_j$. That is,

$$F_{3i} = \overline{K}_{ij}^{(1)}\, \hat{q}_j + \overline{K}_{ijj}^{(2)}\, \hat{q}_j^2 + \overline{K}_{ijjj}^{(3)}\, \hat{q}_j^3. \tag{20}$$

Combining Eq. (14), (17), and (20) then permits the evaluation of the remaining two coefficients, $\overline{K}_{ij}^{(1)}$ and $\overline{K}_{ijjj}^{(3)}$.

During these static solution sequences, both the forces and the entire stress field are evaluated. While the forces lead to the coefficients $\overline{K}_{ij}^{(1)}$, $\overline{K}_{ijj}^{(2)}$, and $\overline{K}_{ijjj}^{(3)}$, the stress fields

$$S = \overline{S}^{(0)} + \overline{S}_j^{(1)}\, q_j + \overline{S}_{jj}^{(2)}\, q_j^2, \tag{21}$$

$$S = \overline{S}^{(0)} - \overline{S}_j^{(1)}\, q_j + \overline{S}_{jj}^{(2)}\, q_j^2 \tag{22}$$

and

$$S = \overline{S}^{(0)} + \overline{S}_j^{(1)}\, \hat{q}_j + \overline{S}_{jj}^{(2)}\, \hat{q}_j^2. \tag{23}$$

can similarly be used for the determination of the coefficients $S^{(0)}$, $\overline{S}_j^{(1)}$, and $\overline{S}_{jj}^{(2)}$ for any stress S at any grid point of the finite element model.

The evaluation of the coefficients $\overline{K}_{ilj}^{(2)}$, $\overline{K}_{illj}^{(3)}$, and $\overline{S}_{lj}^{(2)}$ for $l \neq j$ proceeds as above but in connection with the displacement fields

$$\underline{w}(t) = q_j(t)\, \underline{\Psi}_j + q_l(t)\, \underline{\Psi}_l \tag{24}$$

and

$$\underline{w}(t) = q_j(t)\,\underline{\Psi}_j - q_l(t)\,\underline{\Psi}_l\,. \tag{25}$$

Finally, the coefficients $\overline{K}^{(3)}_{iljp}$ can be evaluated from the single assumed displacements field

$$\underline{w}(t) = q_j(t)\,\underline{\Psi}_j + q_l(t)\,\underline{\Psi}_l + q_p(t)\,\underline{\Psi}_p\,. \tag{26}$$

REDUCED ORDER MODELING VALIDATION

On-going validation efforts are focused primarily on the selection of the "best" basis for the appropriate representation of both the displacement and stress fields.

Transverse Displacements Modeling

To investigate the modeling of the transverse displacements, a flat rectangular clamped aluminum panel of dimensions 0.3556m x 0.254m x 0.00102m was considered and was discretized with 14x10 CQUAD4 elements. It was further subjected to the combined effects of a uniform temperature equal to 1.8 times the buckling temperature and to a normally incident white noise acoustic wave with a sound pressure level (*SPL*) of 104dB. The excitation level and the temperature were selected to give a reasonably broad response of the panel, i.e. in the range of ± twice the buckling deformations. Next, a time history of this excitation was generated as a series of independent identically distributed normal deviates and was specified as input to a nonlinear transient NASTRAN analysis. The corresponding time histories of the displacement and stresses of the panel were then determined for 15,000 time steps (set at 0.000282 sec.) with the NASTRAN standard two-point Newmark integration scheme (no equivalent linearization technique was used). It should be noted that the small time step selected here to capture well the panel dynamics implies a very high Nyquist frequency, 1773 Hz, and consequently a very large number of excited modes. It was noted that 39 modes were present in the frequency band of the white noise excitation.

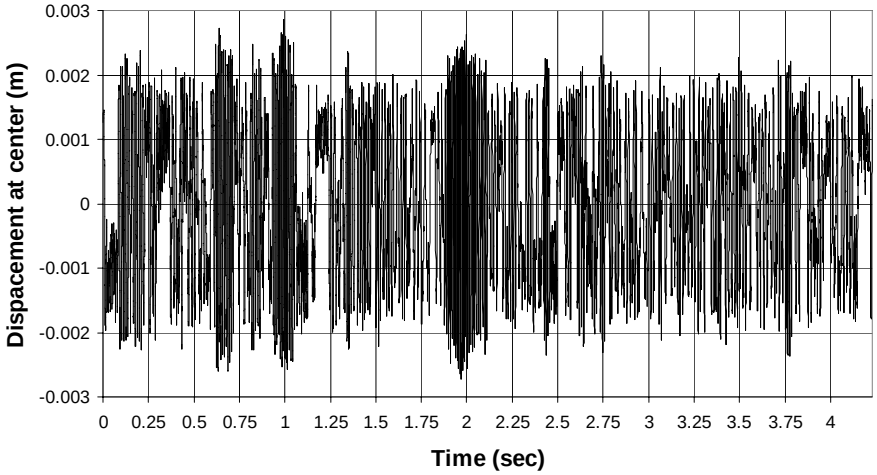

Figure 1. Time history of the displacement of the panel center

In the case of panels experiencing snap-throughs, as seen in Fig. 1, there are several bases that seem appropriate for a single-mode reduced order model. In fact, 5 such bases were identified:

(i) basis 1: the buckled shape of the panel, see Fig. 2(a).

(ii) basis 2: the "umbrella" (i.e. the zero nodal line) mode of vibration of the unbuckled, linear panel, i.e. without any temperature effect, see Fig. 2(b).

(iii) basis 3: the "umbrella" mode of linear vibrations of the buckled panel, i.e. with temperature but in small additional motions. Note that the "umbrella" mode was in fact found to be the second mode with a natural frequency of 133.94 Hz while the first mode of frequency of 132.68 Hz. did in fact exhibit one nodal line, see Fig. 2(c) and 2(d).

(iv) basis 4: the linear eigenvector of the panel buckling problem, see Fig. 2(e).

(v) basis 5: the approximate mode proposed by Lee [5], see Fig. 2(f).

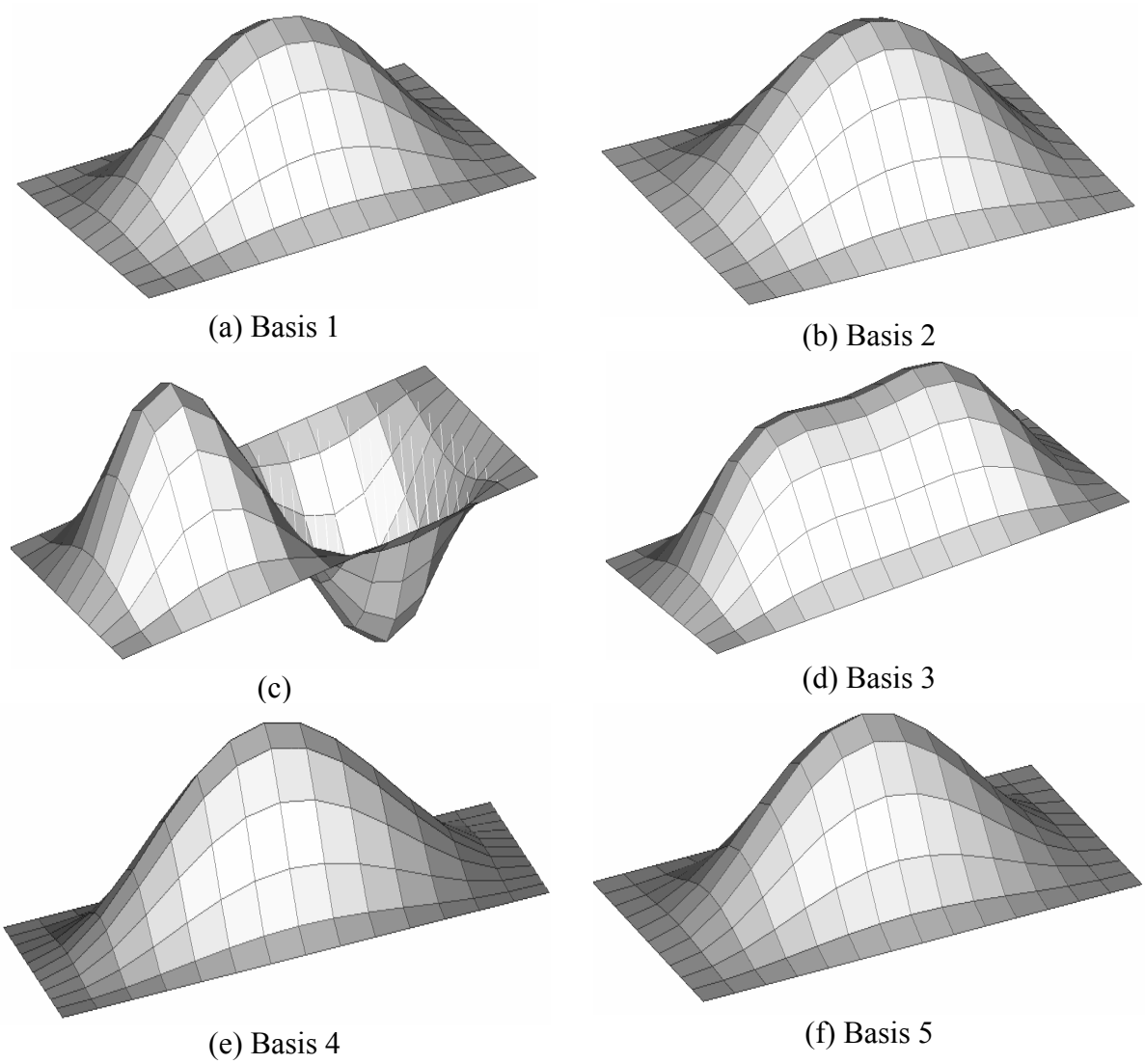

Figure 2. Various responses of the panel. (a) Buckled shape of the panel (basis 1). (b) First linear mode of vibration of the unbuckled panel (basis 2). (c) First linear mode of vibration of the buckled panel. (d) Second linear mode of vibration of the buckled panel (basis 3). (e) First linear buckling mode of the panel (basis 4). (f) Assumed mode of [5] (basis 5).

The first assessment focused on the representation of the panel response by the 5 single-mode models. To this end, a modal assurance criterion (MAC) type parameter was defined for each of the five single-mode model as

$$\alpha_i = \frac{\underline{w}^T \underline{\psi}_i}{\sqrt{\left(\underline{w}^T \underline{w}\right)\left(\underline{\psi}_i^T \underline{\psi}_i\right)}} \qquad i = 1, 2, 3, 4, 5. \tag{27}$$

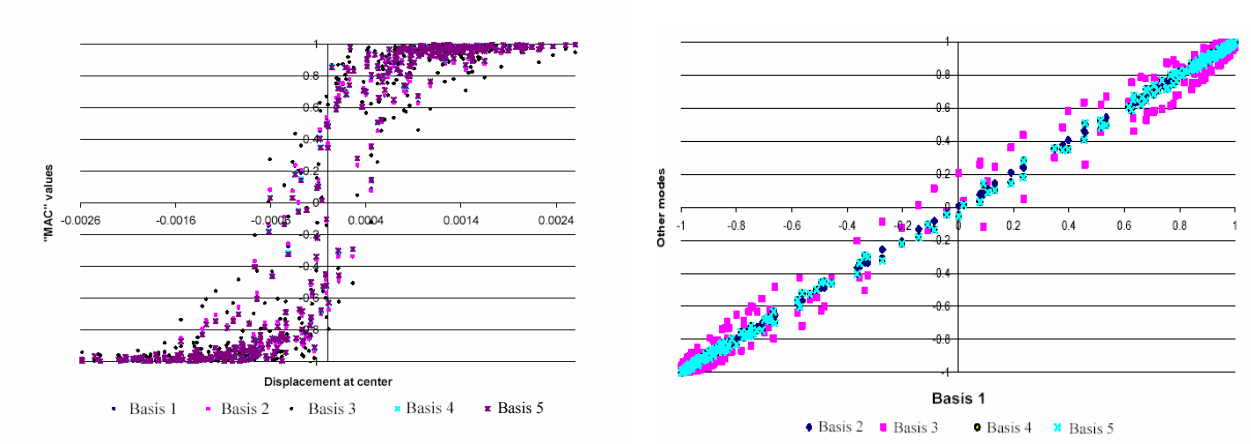

(a) (b)

Figure 3. MAC values α_i, Eq. (27), for the five bases (a) as functions of the displacement of the panel center, and (b) as functions of the MAC values α_i of basis 1.

From the Cauchy-Schartz inequality, a unit value of α_i implies that the panel displacement field $\underline{w}$ is exactly represented by the basis $\underline{\psi}_i$. The time histories of the coefficients α_i do not display any clear trend but a much more interesting correlation is obtained when plotting the values of α_i vs. the displacement of the panel center, see Fig. 3(a), and versus each other, see Fig. 3(b). It appears from these figures that

(i) the coefficients α_i achieve values close to 1 (in magnitude) when the panel deformation is "large", and

(ii) the differences between the values of α_i corresponding to the different bases, see Fig. 3(a) and (b), are typically only small. This observation is particularly appropriate for the bases 1, 2, 4, and 5; the third basis, i.e. the linear mode of vibration of the buckled panel, appears to exhibit a larger scatter/variability in MAC value.

To obtain a better understanding of this situation, the displacement field of the entire panel was plotted at a series of times, see Fig. 4(a)-(d) and Table 1 for some representative results. It is seen that the displacements near the buckled position, see Fig. 4(a), are very consistent with the basis 3, i.e. they tend to be associated with vibrations of the panel around the buckled position. For larger displacements however, the "double peak" of the response seen on Fig. 2(d) and 4(a) seems to disappear and the panel displacement is much closer to the buckled shape, see Fig. 4(b).

These observations are certainly consistent with the expectation that large displacements are associated with large values of the dominant mode(s). Given the uniform distribution of the pressure, the buckling mode (basis 1) and the second mode of the buckled panel (basis 3) should exhibit large modal forces and thus should dominate the response, as confirmed in Fig. 4(a) and (b). When small response levels are observed, other modes should also be present, as seen in Fig. 4(c), or may entirely dominate the displacement field, see Fig.4(d).

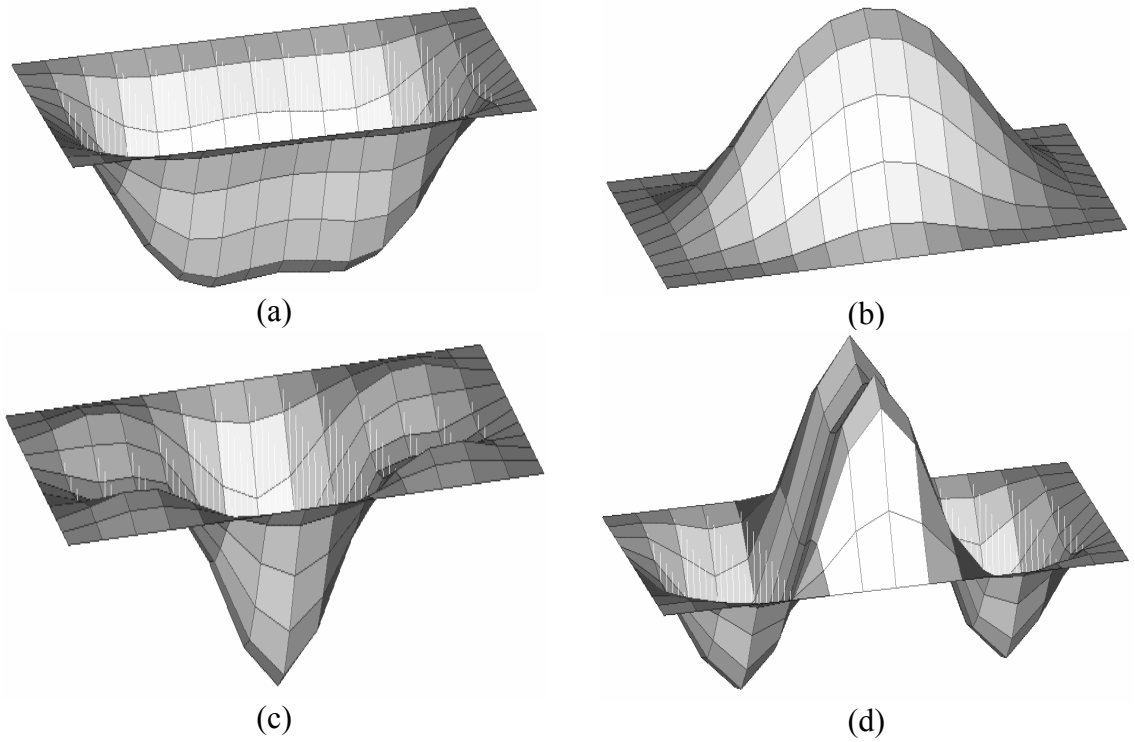

Figure 4. Deformed shape of the panel at four typical times. (a) t = 0.287605sec., (b) t = 0.644511sec., (c) t = 0.292011sec., and (d) t = 0.30523sec.

Table 1. Center deflection ratio (center deflection at given time divided by center deflection at buckling) and MAC values α_i at the four typical times of Fig. 4

Time (sec.)	Center Deflec. Ratio	α_1	α_2	α_3	α_4	α_5
0.287605	-0.979	-0.979	-0.996	-0.968	-0.967	-0.968
0.644511	2.057	0.995	0.993	0.950	0.998	0.998
0.292011	-0.546	-0.896	-0.894	-0.792	-0.915	-0.916
0.30523	0.244	0.237	0.239	0.049	0.281	0.281

From the standpoint of the prediction of the largest transverse deflections, it is seen from the above results that (i) a small order reduced order model is fully appropriate, and (ii) that the choice of one basis as opposed to another similar one should affect only very little the response prediction.

Validation Example and In-Plane Displacements Modeling

Since fatigue damage is primarily associated with large deflections/large cycles, it may be expected that the above observations would also hold in connection with the fatigue life. Note however that the accumulated damage is governed by the stresses, not the deflections, and thus an assessment of the appropriateness of reduced order models for fatigue life estimation should focus on their approximation of the stresses. To narrow the breadth of the analysis, a non-heated panel was considered for which bases 2 and 5 could be used. A sixth basis was also considered that is similar to basis 5 but involves the clamped-clamped beam modes, see [8] for details. Since the specific coefficients of the basis 6 were stated in [8] for an aspect ratio of 1.2, a second panel (flat clamped aluminum panel of dimensions 0.3048m x 0.254mx 0.00102m) was discretized with 14x10 CQUAD4 elements and was used instead of panel 1 for the remainder of the validation.

Prior to the assessment of the stresses modeling, it was deemed noteworthy to confirm the general applicability of the reduced order scheme. First, the effects of the scaling factors q and $\hat{q}$, see Eq. (13), (15), and (19), were investigated. To this end, a series of computations were performed with values of these coefficients ranging from 10^{-6} to 10^{-1}, i.e. from a thousand times smaller to a hundred times larger than the panel thickness. It was found that the resulting reduced order coefficients (stiffnesses and stresses) were very stable, keeping at least 5 significant digits say for the dominant terms, except for very small and very large values of the scaling factors. Accordingly, it seems recommended to select q and $\hat{q}$ to be of the order of the panel thickness. Further, it was noticed that the terms $K_{iii}^{(2)}$ and $S^{(0)}$, although not quite zero, were very small in comparison with the remaining stiffness and stress coefficients. Finally, a series of computations performed at different temperatures demonstrated that only the first terms, i.e. $\overline{K}_{ij}^{(1)}$ and $S^{(0)}$, were dependent on temperature. In fact, the linear stiffness coefficients $\overline{K}_{ij}^{(1)}$ appeared to vary almost exactly linearly with temperature. All of these results, which are perfectly in agreement with the von Karman strains and with approximate analyses (e.g. [5-8]), support the validity of the reduced order modeling scheme.

It was next questioned how the assessment of the reliability of the stress modeling should be conducted. The most straightforward approach is to compute the fatigue life (or fatigue damage accumulated after a "long" time) obtained with the full finite element and compare it with the corresponding estimates obtained with the three different reduced order models. Clearly, this comparison would have to be performed for different sound pressure levels and various S-N curves (e.g. various exponents of the S-N curve). While this parametric study would yield the expected perspective, it would not provide a good basis for the detailed assessment which is desired here. Since the nonlinearity only affects the stiffnesses and the stresses, it was felt that the analysis of the *static* response of the panel for various load levels would provide a simple, yet clear, basis for the desired validation. Note in this regard that the fatigue life of the panel depends on the level of variability of the stresses, e.g. on their variances, and that the contributions of different modes to the variances are approximately in the same ratio (ω_i^3 vs. ω_i^2) as they are for the static response in a linear multimodal situation.

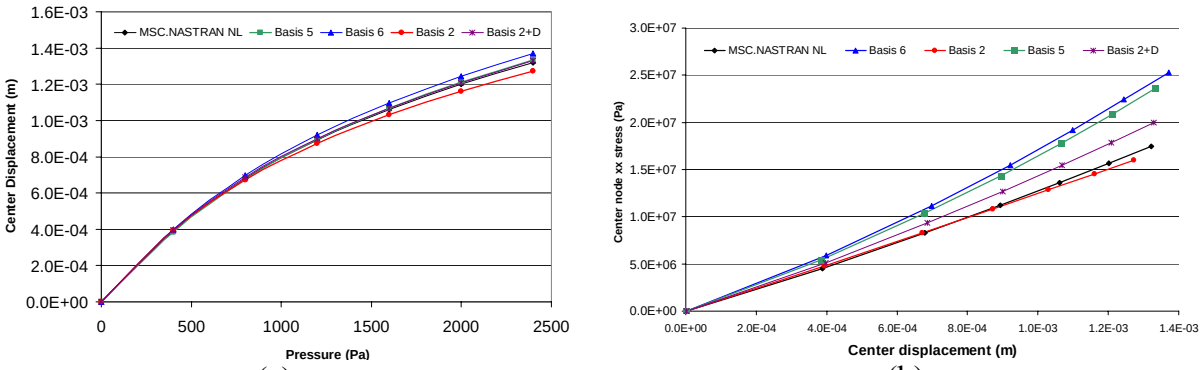

(a) (b)

Figure 5. Static response of the panel to a uniform pressure. (a) Center displacement as a function of pressure and (b) stress σ_{xx} at center as a function of its transverse displacement

Shown in Fig. 5(a) are the transverse displacements of the center of the panel predicted by the NASTRAN solution (SOL 106), the corresponding single-mode reduced order model (basis 2), and the approximations derived in [5] (basis 5) and [8] (basis 6). While the agreement is in general very good, it appears that the reduced order model corresponding to basis 2 exhibits a nonlinear stiffness coefficient $K_{iiii}^{(3)}$ that is slightly too large, at the contrary of the approximations of [5] and [8]. The similarity of the displacements predicted from these three bases is however consistent with the previous findings (see Fig. 3).

The stresses are not independent of the displacements: they are determined through the memoryless quadratic transformation of Eq. (4) or (8). The stresses predicted by the reduced order modeling thus result from two cascaded approximations: the modeling of the displacement field and the approximation of the quadratic transformation. Having established the reliability of the displacement field obtained from the reduced order models, see Fig. 5(a), it remains to assess the accuracy of the estimated quadratic transformation. To this end, the stress in the *x*-direction at the center of the bottom of the panel (largest normal stress at that point) was analyzed as a function of the displacement of that point. Shown in Fig. 5(b) are the corresponding plots for the NASTRAN data, the current reduced order model, and the two approximations of [5] and [8]. Surprisingly, it is found that these latter approximations substantially overpredict the stress while the reduced order model provides an close fit of the NASTRAN data over that range. It should be noted that both the reduced order modeling and the approximations of [5] and [8] are perfect parabolas but, interestingly, the NASTRAN data is also very closely by a quadratic polynomial (R^2=0.999977), see Table 2. Note that the constant stress coefficient $S^{(0)}$ was found to be very close to zero in all cases as can be expected from the lack of temperature. Further, the linear coefficients $S_i^{(1)}$ were all found to exceed their NASTRAN counterpart by 7% to 19% but a much larger scatter exists in connection with the quadratic terms: the reduced order model coefficient is smaller (by a factor of 3.4) than the NASTRAN value but the approximations of [5] and [8] are larger, by a factor of 2.5.

Table 2. Stress coefficients obtained from NASTRAN, the reduced order models with the basis 2 with or without its dual, and the approximations of [5] and [8].

Solution	$S^{(0)}$	$S_i^{(1)}$	$S_{ij}^{(2)}$
NASTRAN	$-2.241\ 10^{4}$	$1.123\ 10^{10}$	$1.513\ 10^{12}$
Reduced Order Modeling (Basis 2)	4.21810^{-2}	$1.202\ 10^{10}$	$4.363\ 10^{11}$
Harmonic approximate modes (Basis 5, [5])	$4.112\ 10^{-2}$	$1.275\ 10^{10}$	$3.705\ 10^{12}$
Clamped beam approximate modes (Basis 6, [8])	$-7.118\ 10^{-2}$	$1.339\ 10^{10}$	$3.704\ 10^{12}$
Reduced Order Modeling (Basis 2 + Dual)	$5.180\ 10^{1}$	$1.201\ 10^{10}$	$2.299\ 10^{12}$

In understanding the results of Fig. 5, it is important to note that the approximations of [5] and [8] rely on approximate modes but do include in-plane displacements proportional to the square of the magnitude of their transverse counterparts. On the contrary, the reduced order model is based on an exact linear mode that is devoid of in-plane motions. In fact, it is this lack of in-plane displacement which is believed to be the source of the observed stiffer behavior. Indeed, since there is no in-plane displacement allowed, the panel is constrained and therefore appears stiffer than it would be if in-plane displacements were taking place.

In regards to the results of Fig. 5(b), it should be noted that the stresses are directly related to the curvatures of the transverse displacement field, not the displacements themselves. Thus, a good matching of the deformed shapes, as seen in Fig. 3 and 5(a), does not guarantee an equally good approximation of the stresses. This observation, and the findings of Fig. 5(b), are in fact neither specific to plates nor to nonlinearity, a similar argument can be developed in connection with linear beams where an overprediction of the stress at the middle by 23.4% and 7% using the bases 5 and 6, respectively, is obtained.

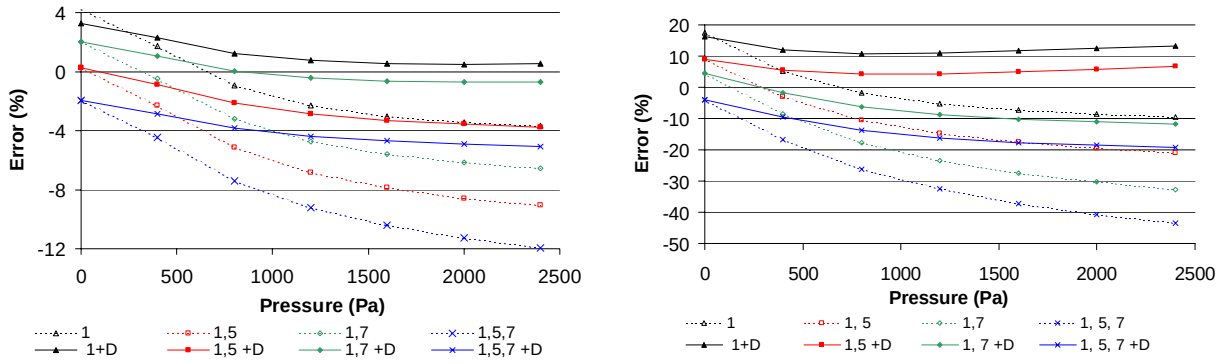

(a) (b)

Figure 6. Reduced order modeling errors in the static response of the panel to a uniform pressure for different combinations of modes. (a) Center displacement as a function of pressure and (b) stress σ_{xx} at center as a function of its transverse displacement

Could the reduced order modeling prediction be improved by selecting two or more modes of the linear panel? Clearly, the static transverse displacements are not exactly proportional to the first mode and thus contributions of higher order modes are expected, albeit small for the uniform loading considered here. Nonetheless, the inclusion of higher order modes does not produce any in-plane displacement and thus does not resolve the fundamental issue of Fig. 5(a). In fact, a series of two mode combinations were studied, i.e. modes 1 and 3 (the (1,1) mode), 1 and 5 (the (0,2) mode), and 1 and 7 (the (2,0) mode), and the results, see Fig. 6, confirmed this expectation: mode 3 contributed very little as it was not excited directly and the inclusion of modes 5 and 7 led to larger, not smaller, differences with the NASTRAN results of Fig. 5(a).

These observations appear to indicate that the improvement of the reduced order model prediction must be achieved through the inclusion of an in-plane displacement field. Since the relative magnitude of the transverse and in-plane displacements is expected to vary as a function of the excitation magnitude (see the approximations of [5] and [8]), it does not appear appropriate to consider a single basis including both types of displacements. Rather, it is proposed here to have a dual basis $(\underline{\Psi}_i, \underline{\overline{\Psi}}_i)$ in which $\underline{\Psi}_i$ would be as before the transverse modes of the linear panel and $\underline{\overline{\Psi}}_i$ would represent the in-plane displacements.

Several options are possible in regards to the selection of $\underline{\overline{\Psi}}_i$, e.g. as the in-plane vibration modes of the panel. While this choice appears straightforward, it does not correspond to the physics of the present problem; in-plane modes will generally be very high frequency modes at the contrary of the lower frequencies excited here. In this light, the in-plane motions present can then be viewed as quasi-static (an observation already used in the literature, e.g. [5] and [8]). Then, a natural choice for $\underline{\overline{\Psi}}_i$ would be the in-plane displacement field associated with one of the imposed displacements of Eq. (13), (15), or (19). Unfortunately, we were not able to extract this information from typical NASTRAN solutions and thus an alternative approach was undertaken.

If the panel has constant thickness and density, the transverse modes are orthogonal to each other with respect to the unit operator and a static displacement of the linear panel of the form of Eq. (13) is generated by a similar load, i.e. proportional to $\underline{\Psi}_i$. The in-plane motions resulting on the nonlinear panel from this pressure distribution can thus be viewed as directly related to the transverse displacement field $\underline{\Psi}_i$ and thus can be used to obtain $\underline{\overline{\Psi}}_i$. In this regard, note that the deflections generated by a static load proportional to $\underline{\Psi}_i$ will primarily be transverse and that this large component must be extracted to yield the in-plane vector $\underline{\overline{\Psi}}_i$. If the applied pressure is not too large, the transverse response will essentially be linear with respect to the applied load at the contrary of the in-plane motions which will exhibit a quadratic type behavior. On the basis of these observations, the selection of $\underline{\overline{\Psi}}_i$ was achieved as follows. First, the static nonlinear response of the panel to a load $p\,\underline{\Psi}_i$ was obtained for two different values of p, i.e. p and 2 p. Then, the corresponding two displacement fields (each including both in-plane and out-of-plane components) $\underline{w}_1$ and $\underline{w}_2$ were combined to eliminate their transverse components and to form $\underline{\overline{\Psi}}_i$ as

$$\underline{\overline{\Psi}}_i = \underline{w}_2 - 2\,\underline{w}_1 \,. \tag{28}$$

This strategy was used with p = 60 Pa to obtain the dual modes for the first, fifth, and seventh transverse modes of the linear panel. Reduced order models based on some or all of these 6 modes (3 transverse and 3 in-plane) were then determined through the procedure of Eq. (5)-(26) and the corresponding displacements and stress at the center of the panel were recomputed, see Fig. 5 and 6. Note first the excellent agreement of the displacements obtained by including only the first mode and its dual, see Fig. 5(a). As justified above, the inclusion of the mode $\underline{\overline{\Psi}}_i$ has freed the in-plane motions and has decreased the apparent stiffness of the panel thereby leading to larger transverse displacements. An improvement of the stress estimate is also obtained as the quadratic coefficient $S_{ij}^{(2)}$ obtained with the first mode and its dual is much closer to the NASTRAN value than the coefficient $S_{ij}^{(2)}$ corresponding to the first mode only, see Table 2. This result may not be clear from Fig. 5(b) because of the limited range of pressures considered there. The above results demonstrate the influence of the in-plane mode but the comparison of the mode 1 and mode 1+D (1 and its dual) may seem inappropriate as the number of assumed modes is not the same. To palliate this situation, compare the predicted displacements and stresses obtained with either modes 1 and 5 or 1 and 7 with those predicted from the mode 1 and its dual. It is clearly seen from Fig. 6 that both displacements and stresses are better matched with the latter combination of modes than any other pair. It is thus concluded that a two-mode reduced order model must include the dual mode.

The effect of a higher number of modes was finally considered. In the linear case, it can be demonstrated that the convergence of the displacements and stresses is achieved in an oscillatory fashion, i.e. by repeatedly overshooting the exact solution. Further, modes 5 and 7 will provide contributions that are opposite in sign to both the one of mode 1 and to those of the next three modes (the modes (4,0), (0,4), and (2,2)). Accordingly, it is expected that the modes 1 and 5, 1 and 7, and especially 1, 5, and 7 may/will lead to larger negative errors than obtained for mode 1 alone. This result is clearly seen in Fig. 6 for both displacements and stresses and reduced order models with or without duals. Note however:

(i) that the magnitude of the overshoot is substantially reduced by the inclusion of the duals,

(ii) the rapid convergence, as the pressure is increased, of the errors associated with the reduced order models with duals at the contrary of those without duals. This finding suggests that the nonlinear effects are intrinsically captured by using the duals modes.

SUMMARY

This paper focused on the validation of a reduced order modeling strategy for aircraft panels subjected to a combination of thermal effects and an incident acoustic wave strong enough to induce a severe geometrically nonlinear behavior. The approach involved both the derivation of the nonlinear governing equations of the reduced order model and the displacements-stress relationship. Of particular importance in this strategy is the selection of the “modal basis” that will be used to approximate the panel displacement field. While the shape of the transverse displacement field is well represented by a series of different functions, the stresses require an

accurate modeling of the curvatures of the panel. Accordingly, it is recommended that the modal basis be constructed from exact responses of the panel considered. A comparison of different approximations/reduced order models of the static nonlinear response of a panel further demonstrated the need for in-plane displacements in the modal basis. Accordingly, a novel dual basis was introduced that contains separately the transverse displacements and their induced in-plane counterparts and is formed by the combination of two similar nonlinear static responses, see Eq. (28). A series of comparisons, see Fig. 5 and 6, clearly demonstrate the value of considering the in-plane modes in addition to their transverse counterparts.

ACKNOWLEDGEMENTS

The support of this investigation by the Air Force Research Laboratory under contract F33615-01-C-3111 is gratefully acknowledged. The authors also wish to thank Capt. S.M. Spottswood and Dr. S. A. Rizzi for their support of and interest in this work.

REFERENCES

1. Blevins, R.D., Holehouse, I. and Wentz, K.R., Thermoacoustic Loads and Fatigue of Hypersonic Vehicle Skin Panels. *J. Aircraft*, 1993, **30**, 971-978.
2. Bouyssy, V., Naboishikov, S.M. and Rackwitz, R., Comparison of Analytical Counting Methods for Gaussian Processes. *Structural Safety*, 1993, **12**, 35-57.
3. Ghazarian, N. and Locke, J., Non-Linear Random Response of Antisymmetric Angle-Ply Laminates Under Thermal-Acoustic Loading. *J. Sound and Vibration*, 1995, **186**, 291-309.
4. Istenes, R.R., Rizzi, S.A. and Wolfe, H.F., Experimental Nonlinear Random Vibration Results of Thermally Buckled Composite Panels. *Proc. 36th Structures, Structural Dynamics, and Materials Conf.*, 1995, 1559-1568.
5. Lee, J., Large-Amplitude Plate Vibration in an Elevated Thermal Environment. *Applied Mechanics Rev.*, 1993, **46**, Part 2, S242-S254.
6. Lee, J., Random Vibration of Thermally Buckled Plates: II Nonzero Temperature Gradient Across the Plate Thickness. *Applied Mechanics Rev.*, 1997, **50**, Part 2, S105-S116.
7. Lee, J., Displacement and Strain Statistics of Thermally Buckled Plates. *J. Aircraft*, 2001, **37**.
8. Lee, J., Topology of the Four-Mode Strain Energy of Thermally Buckling Plates. *J. Thermal Stresses*, 2002, **25**, 813-857.
9. McEwan, M.I., Wright, J.R., Cooper, J.E. and Leung, A.Y.T., A Combined Modal/Finite Element Analysis Technique for the Dynamic Response of a Non-Linear Beam to Harmonic Excitation. *J. Sound and Vibration*, 2001, **243**, 601-624.
10. Mei, C., Dhainaut, J.M., Duan, B., Spottswood, S.M. and Wolfe, H.F., Nonlinear Random Response of Composite Panels in an Elevated Thermal Environment. Report AFRL-VA-WP-TR-2000-3049, 2000.
11. Murphy, K.D., Virgin, L.N. and Rizzi, S.A., Characterizing the Dynamic Response of a Thermally Loaded, Acoustically Excited Plate. *J. Sound and Vibration*, 1996, **196**, 635-658.
12. Ng, C.F., Nonlinear and Snap-Through Responses of Curved Panels to Intense Acoustic Excitation. *J. Aircraft,* 1989, **26**, 281-288.

13. Rizzi S.A. and Muravyov, A.A., Equivalent Linearization Analysis of Geometrically Nonlinear Random Vibrations Using Commercial Finite Element Codes. NASA Technical Paper TP-2002-211761, 2002.
14. Spottswood, S.M. and Mignolet, M.P., Experimental Nonlinear Response of Tapered Ceramic Matrix Composite Plates to Base Excitation. *AIAA J.*, 2002, **40**, 1682-1687.
15. Spottswood, S.M. and Wolfe, H.F., Comparing fatigue life estimates using experimental and spectral density based probability distributions. *Proc. 42nd Structures, Structural Dynamics and Materials Conference*, 2001.
16. Sun, J.Q., Bao, W. and Miles, R.N., Fatigue Life Prediction of Nonlinear Plates Under Random Excitations. *J. Vibration and Acoustics*, 1998, **120**, 353-360.
17. Vaicaitis, R., Nonlinear Response and Sonic Fatigue of National Aerospace Space Plane Surface Panels. *J. Aircraft,* 1994, **31**, 10-18.

Appendix E

ELSTEP/FAT User's Manual Version β2.0

ELSTEP/FAT

Version β2.0

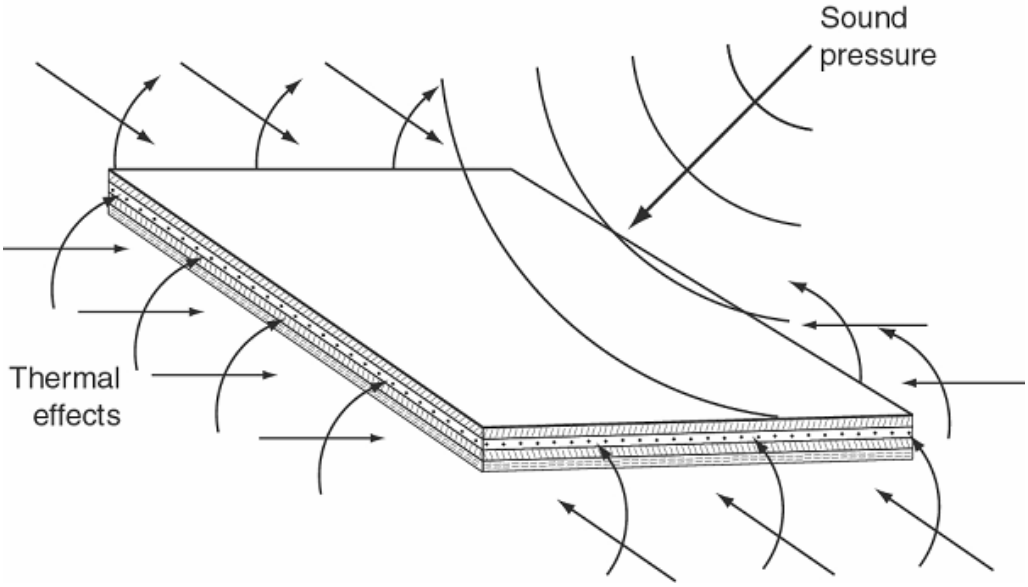

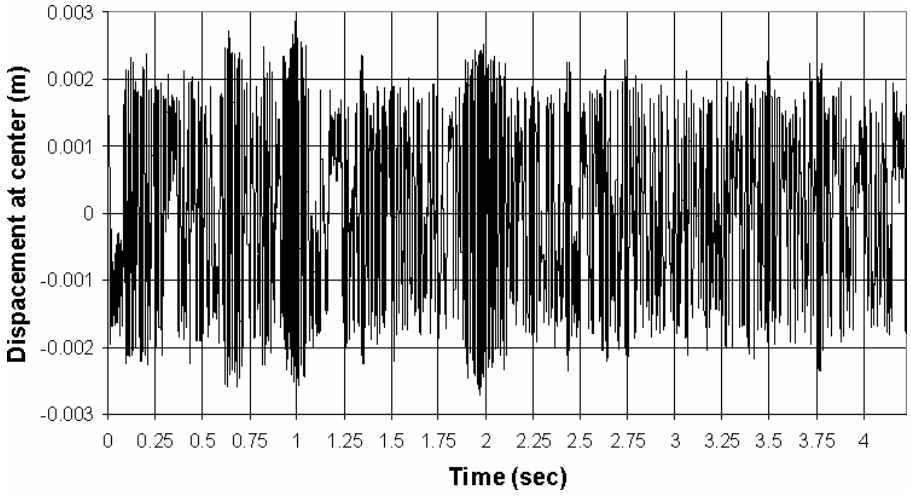

USER'S MANUAL

ZONA TECHNOLOGY
7430 E. Stetson Drive, Ste. 205
Scottsdale, AZ 85251

Arizona State University
Tempe, AZ 85287

Table of Contents

List of Figures

List of Tables

1. INTRODUCTION

The code ELSTEP/FAT has been developed for the estimation of the response, displacements and stresses, and fatigue life of panels subjected to a combined strong random acoustic loading and steady thermal effects. Overall, the code in its current form proceeds from an MSC NASTRAN finite element model. A nonlinear reduced order model in terms of an approximate modal basis is first estimated. Next, these nonlinear equations are marched in time for a given time history of the random acoustic loading to produce a record of displacements and stresses in the panel. The damage accumulated at specified points of the panel is then estimated using a rainflow analysis.

The NASA code ELSTEP (Equivalent Linearization using a STiffness Evaluation Procedure), more specifically its stiffness evaluation procedure, served as the basis for the present code. Four broad modifications had to be performed to the code for its use in the present context. Specifically,

(i) the temperature effects had to be accounted for,

(ii) a second set of modes, referred to as the dual modes, were added to the original set

(iii) the reduced order model of a specified *stress* at a specified location was also produced (constant, linear, and quadratic terms), and

(iv) a simulation and rainflow analysis component was added for the prediction of the fatigue life of the panel.

The overall structure of ELSTEP/FAT is shown in Fig. 1 with future additions (steps 6, 7, and 8) shown in grey. Currently, ELSTEP/FAT involves the five steps 1-5, a brief description of which directly follows. A more complete discussion of the steps currently present, i.e. 1-5, will be presented in the next sections.

1.1. Overall Structure and Steps:

1.1.1. Determination of the dynamic reduced order model:

This first step represents an extended version of the STEP component of ELSTEP. The goal of the reduced order modeling is to produce a set of equations of motion complete enough to represent well the dynamic response (displacement vs. time) of the panel but small enough in number to permit fast predictions. The original STEP component was modified to include:

(a) the effects of temperature

(b) a second set of modes, referred to as the dual modes

(c) the reduced order model excitation

Note that the determination of the response reduced order model requires a sequential set of MSC.NASTRAN runs directed by the ROM part of the code. There is thus a back and forth interaction between MSC.NASTRAN and the ROM part of the code as indicated in Fig. 1 by the two sided arrows.

1.1.2. Determination of the stress reduced order model:

The focus of ELSTEP/FAT includes the prediction of the response of panels but also the estimation of their fatigue life. Since the fatigue life is governed by the stresses, it was necessary to add a representation of the stresses in terms of the reduced order coordinates, i.e. those present in the equations of motion of step 1. Note that the determination of the stress reduced order model (as for the response ROM) requires a sequential set of MSC.NASTRAN runs directed by the ROM part of the code. There is thus a back and forth interaction between MSC.NASTRAN and the ROM part of the code as indicated in Fig. 1 by the two sided arrows.

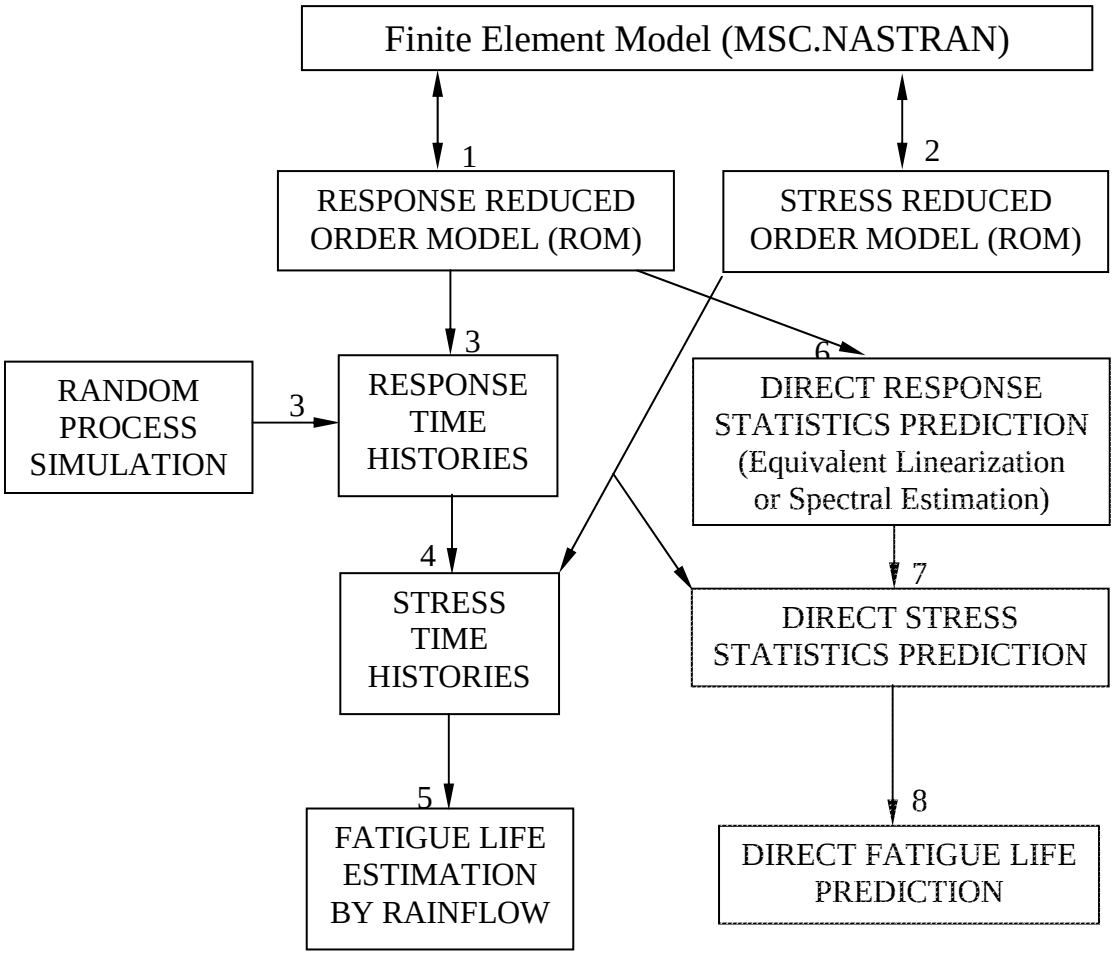

Figure 1. Structure of ELSTEP/FAT

1.1.3. Numerical simulation of time histories of the panel response from the ROM

The estimation of the fatigue life of structures (linear or nonlinear, panels or others) subjected to random excitations is a challenging problem because the damage accumulated over a given time strongly depends on the distribution of peaks which is a difficult function to estimate unless a very good model of it is available. It is thus important to always dispose of a simulation capability, coupled with rainflow analysis, that permits the assessment of any other prediction capability. The present step focuses on the simulation of the response of the panel from the reduced order model. For generality, it is assumed that the random excitation is given as an autoregressive process

of a specified order with pre-determined parameters. This representation is particularly convenient and converges for any non-predictable process. Separate routines for the estimation of the autoregressive parameters from a specified spectrum are available from the investigators.

1.1.4. Numerical simulation of time histories of the stresses

The output of the previous step is processed through the stress reduced order model to obtain time histories of the user specified stresses at user pre-determined locations on the panel.

1.1.5. Estimation of fatigue life from rainflow analysis

This step is actually composed of two computations. The first sub-step is the rainflow analysis that processes the time histories of stresses of step 4 to produce a series of stress ranges with corresponding mean values. The second sub-step is then the prediction of the damage accumulated over the time interval of the record. In addition to Miner's rule, several nonlinear damage accumulation rules are available for the estimation of the fatigue life.

2. DETAILED THEORETICAL DESCRIPTION

The reduced order modeling procedure relies on a finite element (MSC.NASTRAN) model of the panel. In the present situation of "large" deflections, the von Karman strain definition is generally adopted and thus the finite element displacements satisfy the cubic nonlinear equations

$$M\ \underline{\ddot{w}} + C\ \underline{\dot{w}} + \underline{K}_{NL} = \underline{F}_0 + \underline{F}(t) \tag{1a}$$

where $\underline{K}_{NL}$ is the vector of nonlinear restoring forces the elements of which can be expressed as

$$\left(\underline{K}_{NL}\right)_i = \sum_{j=1}^{N} K_{ij}^{(1)}\ w_j + \sum_{j,l=1}^{N} K_{ilj}^{(2)}\ w_l\ w_j + \sum_{j,l,p=1}^{N} K_{iljp}^{(3)}\ w_l\ w_j\ w_p\,. \tag{1b}$$

where N is the total number of degrees-of-freedom in the finite element model. Further, every stress component S at every point of the panel can be written in the form

$$S = S^{(0)} + \sum_{i=1}^{N} S_i^{(1)}\ w_l + \sum_{i,j=1}^{N} S_{ij}^{(2)}\ w_i\ w_j\,. \tag{2}$$

In practical problems, the total number of degrees-of-freedom in the finite element highly time consuming effort. It is thus desirable to obtain a simplified approach. To this end, it has been suggested to proceed with an approximate, assumed mode representation of the displacement field as

$$\underline{w}(x,y,z,t) = \sum_{i=1}^{m} q_i(t)\,\underline{\Psi}_i(x,y,z). \tag{3}$$

This *linear* change of variables does not change the character of Eq. (1) and (2) which simply become

$$\overline{M}\ \underline{\ddot{q}} + \overline{C}\ \underline{\dot{q}} + \underline{\overline{K}}_{NL} = \underline{\overline{F}}_0 + \underline{\overline{F}}(t) \tag{4a}$$

$$\left(\underline{\overline{K}}_{NL}\right)_i = \sum_{j=1}^{N} \overline{K}_{ij}^{(1)}\ q_j + \sum_{j,l=1}^{N} \overline{K}_{ilj}^{(2)}\ q_l\ q_j + \sum_{j,l,p=1}^{N} \overline{K}_{iljp}^{(3)}\ q_l\ q_j\ q_p \tag{4b}$$

where $\underline{q}$ denotes the vector of components q_j and

$$S = \overline{S}^{(0)} + \sum_{i=1}^{N} \overline{S}_i^{(1)}\ q_l + \sum_{i,j=1}^{N} \overline{S}_{ij}^{(2)}\ q_i\ q_j\,. \tag{5}$$

It is then concluded that

(i) the nonlinearity is in stiffness only, and

(ii) the determination of the reduced order models of Eq. (4) and (5) only requires the estimation of the coefficients $\overline{K}_{ij}^{(1)}$, $\overline{K}_{ilj}^{(2)}$, $\overline{K}_{iljp}^{(3)}$, $S^{(0)}$, $\overline{S}_{i}^{(1)}$, $\overline{S}_{ij}^{(2)}$.

These observations were well recognized by Rizzi and Muravyov (2002) and Muravyov and Rizzi (2003) who devised an elegant strategy for the evaluation of the coefficients $\overline{K}_{ij}^{(1)}$, $\overline{K}_{ilj}^{(2)}$, and $\overline{K}_{iljp}^{(3)}$ from a series of static solutions in which the forces required to obtain a specified displacement field are determined (through a DMAP alter in MSC.NASTRAN). Specifically, assume first that a single mode is kept in the expansion of Eq. (3), i.e.

$$\underline{w}(x,y,z,t) = q_j(t)\,\underline{\Psi}_j(x,y,z). \tag{6}$$

Then, the external force that must be exerted on the panel to obtain this static displacement is

$$F_{1i} = \overline{K}_{ij}^{(1)}\, q_j + \overline{K}_{ijj}^{(2)}\, q_j^2 + \overline{K}_{ijjj}^{(3)}\, q_j^3. \tag{7}$$

Further, the displacement field

$$\underline{w}(x,y,z,t) = -\,q_j(t)\,\underline{\Psi}_j(x,y,z) \tag{8}$$

can similarly be accomplished with the forces

$$F_{2i} = -\,\overline{K}_{ij}^{(1)}\, q_j + \overline{K}_{ijj}^{(2)}\, q_j^2 - \overline{K}_{ijjj}^{(3)}\, q_j^3. \tag{9}$$

The knowledge of the forces of Eq. (7) and (9) provides a direct strategy for the evaluation of the coefficient $\overline{K}_{ijj}^{(2)}$. Specifically, it is found that

$$\overline{K}_{ijj}^{(2)} = \frac{F_{1j} + F_{2j}}{2\, q_j^2} \tag{10}$$

To determine the remaining two coefficients, $\overline{K}_{ij}^{(1)}$ and $\overline{K}_{ijjj}^{(3)}$, an additional force equation must be obtained. For example, a *linear* static solution sequence can be performed that yields directly $\overline{K}_{ij}^{(1)}$ so that $\overline{K}_{ijjj}^{(3)}$ can then be computed from

$$\overline{K}_{ijjj}^{(3)} = \frac{F_{1i} - \overline{K}_{ij}^{(1)}\, q_j - \overline{K}_{ijj}^{(2)}\, q_j^2}{q_j^3}. \tag{11}$$

This approach is not appropriate if the panel temperature effects are to be included in the reduced order model as the MSC.NASTRAN linear static solver (SOL 101) does not account for in-plane stresses, e.g. thermal stresses. In this case, one proceeds with the nonlinear force evaluation corresponding to the displacement field

$$\underline{w}(x,y,z,t) = \hat{q}_j(t)\, \underline{\Psi}_j(x,y,z) \tag{12}$$

where $\hat{q}_j \neq q_j$. That is,

$$F_{3i} = \overline{K}_{ij}^{(1)}\, \hat{q}_j + \overline{K}_{ijj}^{(2)}\, \hat{q}_j^2 + \overline{K}_{ijjj}^{(3)}\, \hat{q}_j^3. \tag{13}$$

Combining Eq. (7), (10), and (13) then permits the evaluation of the remaining two coefficients, $\overline{K}_{ij}^{(1)}$ and $\overline{K}_{ijjj}^{(3)}$.

During these static solution sequences, both the forces and the entire stress field are evaluated. While the forces lead to the coefficients $\overline{K}_{ij}^{(1)}$, $\overline{K}_{ijj}^{(2)}$, and $\overline{K}_{ijjj}^{(3)}$, the stress fields

$$S = \overline{S}^{(0)} + \overline{S}_j^{(1)}\, q_j + \overline{S}_{jj}^{(2)}\, q_j^2, \tag{14}$$

$$S = \overline{S}^{(0)} - \overline{S}_j^{(1)}\, q_j + \overline{S}_{jj}^{(2)}\, q_j^2 \tag{15}$$

and

$$S = \overline{S}^{(0)} + \overline{S}_j^{(1)}\, \hat{q}_j + \overline{S}_{jj}^{(2)}\, \hat{q}_j^2. \tag{16}$$

can similarly be used for the determination of the coefficients $S^{(0)}$, $\overline{S}_j^{(1)}$, and $\overline{S}_{jj}^{(2)}$ for any stress *S* at any grid point of the finite element model.

The evaluation of the coefficients $\overline{K}_{ilj}^{(2)}$, $\overline{K}_{illj}^{(3)}$, and $\overline{S}_{lj}^{(2)}$ for $l \neq j$ proceeds as above but in connection with the displacement fields

$$\underline{w}(x,y,z,t) = q_j(t)\,\underline{\Psi}_j(x,y,z) + q_l(t)\,\underline{\Psi}_l(x,y,z) \tag{17}$$

and

$$\underline{w}(x,y,z,t) = q_j(t)\,\underline{\Psi}_j(x,y,z) - q_l(t)\,\underline{\Psi}_l(x,y,z). \tag{18}$$

Finally, the coefficients $\overline{K}_{iljp}^{(3)}$ can be evaluated from the single assumed displacements field

$$\underline{w}(x,y,z,t) = q_j(t)\,\underline{\Psi}_j(x,y,z) + q_l(t)\,\underline{\Psi}_l(x,y,z) + q_p(t)\,\underline{\Psi}_p(x,y,z). \tag{19}$$

It should be noted that the above procedure for the evaluation of the coefficients is exact, the only approximation in the reduced order modeling is the modal expansion of Eq. (3).

The above procedure has been described for an arbitrary basis $\underline{\Psi}_j(x,y,z)$, j = 1, ..., N, but these functions must be defined to obtain numerical results. Further, the closeness of the ROM results to their finite element counterparts can be expected to be dependent on the choice of the functions $\underline{\Psi}_j(x,y,z)$. Since the present problem focuses mainly on the transverse vibrations of the panel, it is appropriate to include in the set $\underline{\Psi}_j(x,y,z)$ functions such as the mode shapes of the panel under small deflections around one of its typical configuration, e.g. unbuckled or buckled. These functions represent a basis for the transverse deflections but unfortunately do not include any in-plane motions. In large deflections, a coupling of the transverse and in-plane deflections exists with the latter inducing the “membrane” stiffening effect. It is thus necessary to include both in-plane and transverse displacement bases in the set $\underline{\Psi}_j(x,y,z)$.

In this regard, it should be noted that

(i) the in-plane motions are typically induced by their transverse counterparts and exhibit an amplitude that is related in first approximation to the square of the out-of-plane displacements,

and

(ii) the natural frequencies of the in-plane modes (for a flat panel) are generally much higher than their transverse counterparts so that the in-plane problem is, to first order, a static one.

On this basis, it has been proposed (Mignolet et al., 2003) to rely on a dual basis $\underline{\Psi}_i = (\underline{\hat{\Psi}}_i, \underline{\overline{\Psi}}_i)$ in which $\underline{\hat{\Psi}}_i$ would be represent the selected transverse modes of the linear panel and $\underline{\overline{\Psi}}_i$ would be representative of the second order, in-plane displacements induced by $\underline{\hat{\Psi}}_i$. These functions would be obtained from the static nonlinear response of the panel to transverse loads $p\,\underline{\hat{\Psi}}_i$. Specifically, consider two different values of *p*, i.e. *p* and 2*p*, where *p* is referred to as the load factor. Then, the corresponding two displacement fields (each including both in-plane and out-of-plane components) $\underline{w}_1$ and $\underline{w}_2$ can be combined to form $\underline{\overline{\Psi}}_i$ through an elimination of the linear (out-of-plane) terms, e.g. as

$$\underline{\overline{\Psi}}_i = \underline{w}_2 - 2\,\underline{w}_1 . \tag{20}$$

Note that a similar discussion has been conducted by Gordon et al. (2003) to justify the use of in-plane modes (referred to as the dual basis above and as the companion by Gordon et al. (2003)).

The above discussion focused on the representation of the nonlinear terms in the ROM. The coefficients of the linear terms, i.e. $\overline{M}$, $\overline{C}$, $\overline{F}_0$, and $\overline{F}(t)$ must also be determined. In fact, from the formulation of the ROM as a Galerkin approximation, it is found that the components of these matrices and vectors are

$$\overline{M}_{ij} = \underline{\Psi}_i^T \; M \; \underline{\Psi}_j ; \quad \overline{C}_{ij} = \underline{\Psi}_i^T \; C \; \underline{\Psi}_j ; \quad \overline{F}_{0,i} = \underline{\Psi}_i^T \; \underline{F}_0 ; \quad \text{and } \overline{F}_i(t) = \underline{\Psi}_i^T \; \underline{F}(t). \quad (21)$$

To use the first two relations, the global mass and damping matrices (*M* and *C*) of the full finite element model are written during a SOL 103 analysis using a standard DMAP alter and the matrix-vector products are evaluated as shown above.

Similarly, the reduced order model external forces, $\overline{F}_0$ and $\overline{F}(t)$, are obtained by forcing the writing of the nodal forces in one or a series of static (SOL 101) MSC.NASTRAN analyses, the above inner products are then computed. To exemplify the latter process, consider for example the case of an acoustic pressure at normal incidence for which

$$\underline{F}(t) = \underline{v} \; p(t) \quad (22)$$

where $\underline{v}$ is a constant (with respect to time) vector. From Eq. (21), it is then found that

$$\overline{F}_i(t) = \left[\underline{\Psi}_i^T \; \underline{v} \right] p(t) = \mu_{i,0} \; p(t) \quad (23)$$

so that it is only required to evaluate the inner products of each of the modes with the vector $\underline{v}$ which in fact represents the nodal forces of the finite element model to a unit pressure. In the case of an acoustic excitation at non-normal incidence, Eq. (22) and (23) take the form of

$$\underline{F}(t) = \sum_j \underline{v}_j \; p\left(t - \tau_j\right) \quad (24)$$

$$\overline{F}_i(t) = \sum_j \left[\underline{\Psi}_i^T \; \underline{v}_j \right] p\left(t - \tau_j\right) = \sum_j \mu_{i,j} \; p\left(t - \tau_j\right) \quad (25)$$

where the time shifts $\tau_j = j \, \Delta t$ are associated with the propagation of the wave along the panel. The computation of the coefficients $\mu_{i,j}$ is achieved through a linear quasistatic solution (e.g. as a series of SOL 101 in MSC.NASTRAN) in which the degrees-of-freedom of the panel are blocked and with an excitation corresponding to an acoustic pulse of unit magnitude, of duration Δt, and initiated at $t = 0$ in the direction of propagation of the actual excitation. The reactions at time $\tau_j = j \, \Delta t$ at the blocked degrees of freedom (after a sign change) represent the vectors $\underline{v}_j$. Premultiplication of these vectors by $\underline{\Psi}_i^T$ then yields the force ROM coefficients $\mu_{i,j}$.

Steps 3 to 5 proceed from the reduced order modeling and from simulated time histories of the random acoustic excitation. The generation of these time histories is accomplished by modeling the process $p(t)$ as an autoregressive process for which

$$p_n = b_0\ w_n - a_1\ p_{n-1} - a_2\ p_{n-2} \ldots - a_m\ p_{n-m}. \tag{26}$$

In the above equation, $p_n = p(n\,\Delta t)$, n = 1, 2, 3... are the generated sampled values of the excitation process, w_n are independent Gaussian random numbers forming a discrete white noise process, and a_1, a_2, ..., a_m, b_0 are fixed, deterministic coefficients. This representation was selected because

(1) the generation of a new sample of the excitation process from the m prior ones is accomplished extremely efficiently from Eq. (26),

(2) the autoregressive coefficients a_1, a_2, ..., a_m that yield the best match between the generated output of Eq. (26) and a given stationary process are evaluated through the solution of a linear system of algebraic equations,

(3) the autoregressive representation converges to any non-predictable process as $m \to \infty$, and

(4) the representation of Eq. (26) is extendable to multivariate and multidimensional processes.

The input to the simulation step is thus the coefficients of the autoregressive model and the order m of the recursion. The generation of *stationary* samples of the acoustic excitation process $p(t)$ can then be accomplished in two ways:

(a) the recursion of Eq. (26) is marched forward in time from a set of initial conditions, e.g. zero, until the transient associated with these initial conditions has decayed sufficiently, or

(b) by simulating random initial conditions consistent with the autocorrelation function of the autoregressive process.

Note in the latter approach that all samples generated correspond to the stationary behavior. See Mignolet (1987) for a complete description of the autoregressive simulation algorithm.

Once the samples of the excitation have been generated, the simulation of the panel response (step 3) is accomplished by numerical solving the nonlinear equations of motion of the reduced order model, Eq. (4). Currently, this step is accomplished using the subroutine DIVPRK from the IMSL library.

The time histories of the response coordinates q_j can then be inserted in Eq. (5) to yield the corresponding records of the stresses.

Finally, these time histories are transmitted to the rainflow analysis code of Downing and Socie (1982) that yields a series of stress ranges R_j from which the accumulated damage over the simulation time is evaluated according to one of the five damage accumulation rules implemented (Palmgren-Miner, Marko-Starkey, Marin, Schaff-Davidson, Hashin).

3. DETAILED DESCRIPTION OF THE CODE ELSTEP/FAT

In fact, ELSTEP/FAT is not a single code but rather a series of FORTRAN executables and MSC.NASTRAN solutions. Figure 2 provides a global flowchart of ELSTEP/FAT while Table 1 is a detailed description of the different steps involved with each input, output, and a short description. These different steps can be run automatically in succession with the aid of the script and make files described in Table 2.

Through these various steps, a series of temporary files are created but the following denote the true input and output files of the process.

3.1 Input Files

ssplate_eg.bdf: MSC.NASTRAN input file providing the geometry, material description, and specifications of boundary conditions for the problem. The file is used repeatedly for various different solutions and thus does not contain the specification of a particular solution number.

fixed.mod: Input file providing the specifications for the reduced order modeling and for the time history computations, see Table 3.

nlparam.dat: File providing MSC.NASTRAN commands to be used for the construction of a finite element input file, see Table 4. This file is not to be changed by the user unless there is a change of MSC.NASTRAN version.

S_A_B.dat: Input file specifying the autoregressive (AR) model of the acoustic excitation process, see Table 5.

wn_file.dat: Input file providing the time history of the white noise to be used in conjunction with the AR model to produce the acoustic loading, see Table 6.

Damage accumulation input file: An input file is needed to specify the parameters of the damage accumulation rule (for estimation of the accumulated damage/fatigue life). There is a different file for each of the damage rules currently implemented, i.e. Palmgren-Miner (Palmgren_Miner.dat), Marko-Starkey (Marko_Starkey.dat), Marin (Marin.dat), Schaff-Davidson (Schaff_Davidson.dat), and Hashin (Hashin.dat), see Table 7.

In addition to the files above, there is a series of short header files that provide essential parameter values (e.g. flags) for the computations. These header files are:

Param.h: State maximum values of the number of elements, number of nodes, number of degrees of freedom, number of modes shapes to be determined in the SOL 103, and number of transverse modes used in the reduced order model, see Table 8.

Ldamplif.h: Provides the value of the load amplification factor *p*. See Table 9.

Solve.h: Specifies the critical parameters for the numerical integration of the reduced equations of motion. See Table 10.

Center.h: Specifies the node of which the displacement is to be outputted. See Table 11.

Rainflow.h: Provides the basic inputs for the rainflow cycle counting and for the selection of the damage accumulation rule. See Table 12.

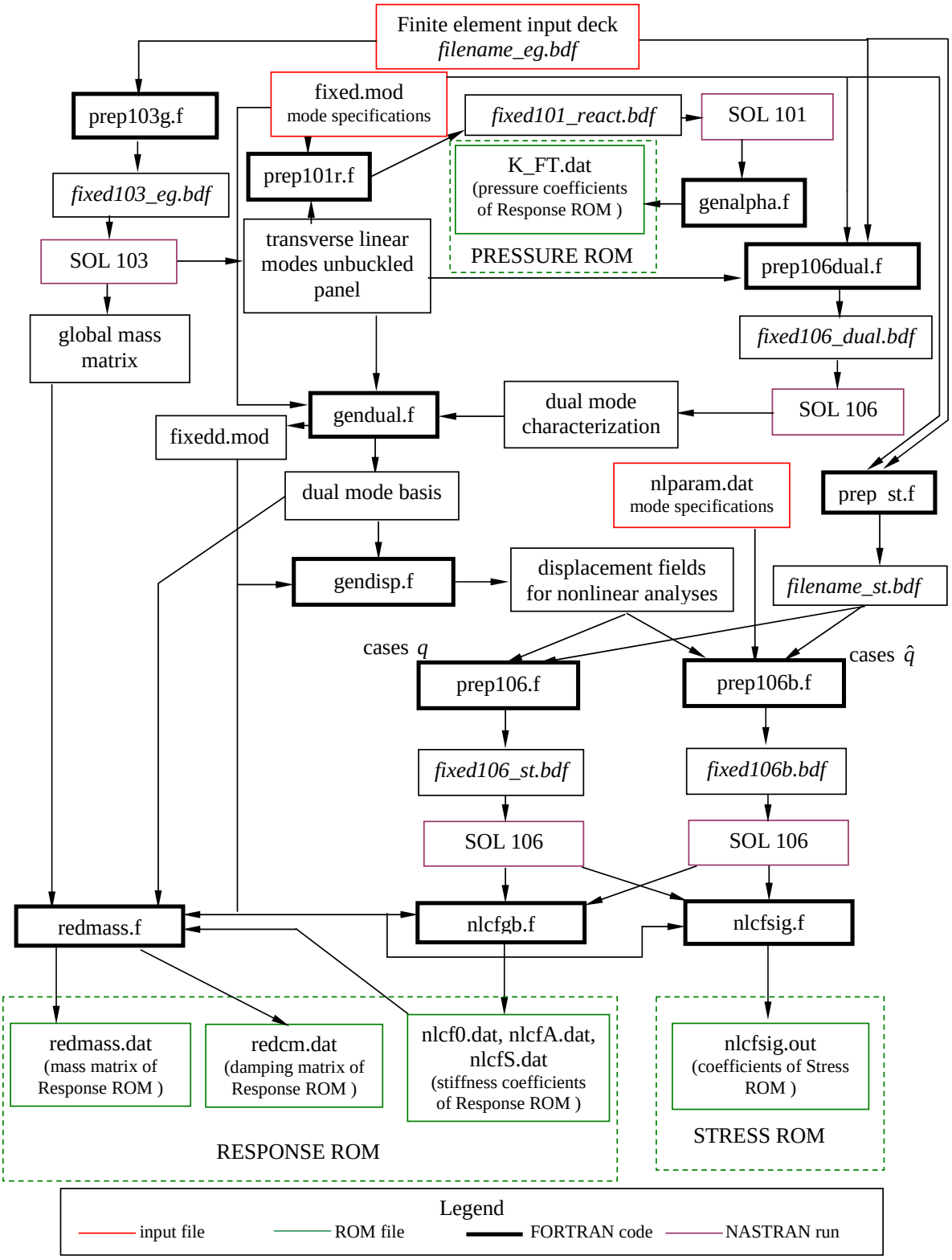

Figure 2a. Global flowchart of the reduced order modeling (ROM) part of ELSTEP/FAT

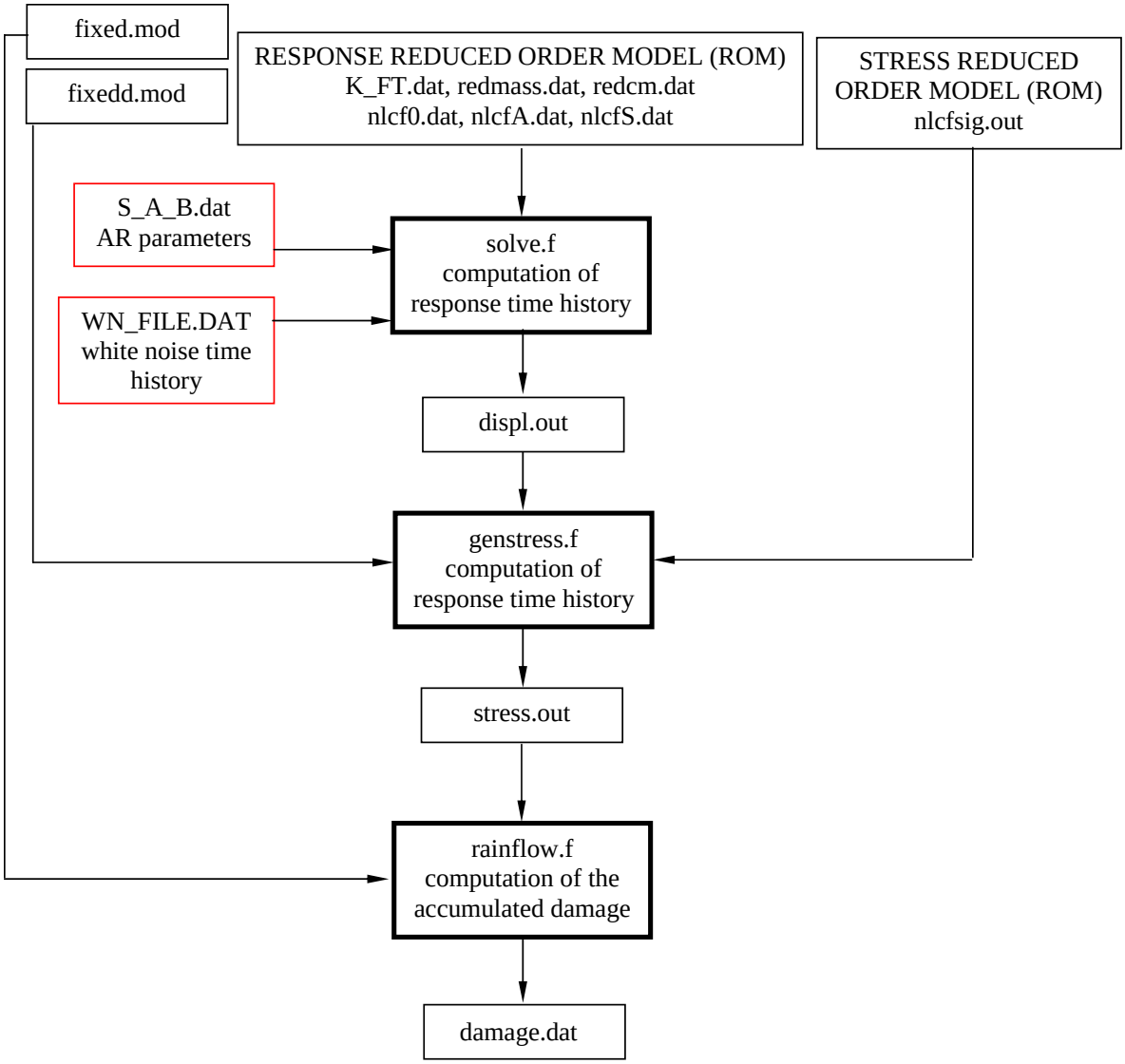

Figure 2b. Global flowchart of ELSTEP/FAT

No.	File name	Input	Output	Purpose
1	prep_st.f => prep_st.exe	ssplate1_eg.bdf	ssplate1_st.bdf	Prepare the MSC.NASTRAN input file for the forces computations
2	prep103g.f	ssplate1_eg.bdf	fixed103_eg.bdf	Create the input file for MSC.NASTRAN eigenvalue analysis
3	fixed103_eg.bdf		egvec.dat egvecH.dat gmass.dat	Obtain the following: - *N* eigenvectors (formatted) - *N* eigenvectors (unformatted) - mass matrix
4	prep106dual.f => prep106dual.exe	ssplate1_eg.bdf fixed.mod egvec.dat	fixed106_dual.bdf	Create the input file for MSC.NASTRAN nonlinear analysis. There are 2*N* subcases corresponding to *N* distributed load profiles. The *N* load profiles duplicate the *N* eigenvectors. The 2*N* loads correspond to two different scale factors.
5	fixed106_dual.bdf		fixed106_dual.pch	Contains the 2*N* displacements/deformations obtained from the MSC.NASTRAN nonlinear analysis
6	gendual.f => gendual.exe	fixed106_dual.pch fixed.mod egvec.dat	fixedd.mod egvecd.dat	Creates the new parameter file (fixedd.mod) and the eigenvectors file in alternating order (linear eigenvectors and their dual). The dual modes contain only the Tx,Ty and Rz dof.
7	combinat.f	param.h	combin.h	Creates the header file fo gendispg.f, nlcfgb.f and nlcfsig.f.
8	gendispg.f => gendispg.exe	fixedd.mod egvecd.dat	displ.pr2 displ.pr3 displ.inn displ.inn egveCa.dat	Multiply the eigenvectors by the scale factors from fixedd.mod and obtain the linear combinations of loads for nonlinear analysis
9	prep106.f => prep106.exe	ssplate1_st.bdf egveCa.dat displ.pr2 displ.pr3	fixed106_st.bdf	Create the input file for MSC.NASTRAN nonlinear analysis (cases q)
10	fixed106_st.bdf		f_N.frc displ.inn fixed106_st.pch	Obtain displacements & forces corresponding to the linear combinations of the eigenvectors (including duals)
11	prep106b.f => prep106.exe	ssplate1_st.bdf egveCa.dat nlparam.dat	fixed106b.bdf fixed106b.pch	Create the input file for MSC.NASTRAN nonlinear analysis (cases $\hat{q}$)

Continued on the next page

12	fixed106b.bdf		f1_L.frc displb.inn	Obtain displacements & forces corresponding to the $\hat{q}$ (including duals)
13	prep101ri.f => prep101ri.exe	fixed.mod egvec.dat wave.dat WN_FILE.DAT (noise)	fixed101_reacti.bdf nint.h	Create the input file for MSC.NASTRAN linear analysis under uniform pressure; all the T3 dof are constrained. Create the header file containing the number of intervals N_{int} resulting from load inclination.
14	fixed101_reacti.bdf		fixed101_reacti.pch	Obtain the nodal reaction forces to the uniform pressure load.
15	genalphai.f => genalphai.exe	egveCa.dat fixed101_reacti.pch	K_FT.DAT	Obtain the $2NxN_{int}$ load coefficients (α) by multiplying the reaction force with the $2N$ eigenvectors
16	nlcfgb.f => nlcfgb.exe	egveCa.dat fixedd.mod displ.pr2 displ.pr3 f1_L.frc f1_N.frc	nlcf0.dat nlcfA.dat nlcfS.dat	Obtain the linear quadratic and cubic stiffness coefficients respectively.
17	nlcfsig.f => nlcfsig.exe	fixedd.mod fixed106b.pch fixed106_st.pch	nlcfsig.out	Obtain the stress coefficients
18	redmass.f => redmass.exe	gmass.dat egveCa.dat fixedd.mod nlcf0.dat	REDMASS.DAT REDCM.DAT egvec_selmds_cols.dat	Obtain the reduced mass and damping matrices. Arrange selected modes in columns.
19	solve.f => solve.exe	nlcf0.dat nlcfA.dat nlcfS.dat S_A_B.DAT REDMASS.DAT REDCM.DAT K_FT.DAT(α) WN_FILE.DAT (noise)	DISPL.OUT	Obtain the displacement/time history.
20	cntrldspl.f => cntrldspl.exe	egveCa.dat egvec_selmds_cols.dat DISPL.OUT	PHSDSP.OUT	Obtain the physical displacement/time hystory in the center of the panel.
21	genstress.f => Genstress.exe	egveCa.dat nlcfsig.out WN_FILE.DAT DISPL.OUT fixedd.mod	STRESS.OUT	Obtain the stress time history
22	rainflow.f => rainflow.exe	STRESS.OUT “damage input file”	damage.dat range.dat	Computes the damage accumulated and the range information

Table 1. Detailed characteristics (input, output, description) of the various FORTRAN executables and MSC.NASTRAN input files

The xdoit.bat file:

```
fl32 prepst.f
prepst.exe
fl32 prep103g.f
prep103g.exe
C:\Msc\bin\nastran.exe fixed103_eg.bdf scr=yes news=no
fl32 prep106dual.f
prep106dual.exe
C:\Msc\bin\nastran.exe fixed106_dual.bdf scr=yes news=no
fl32 gendual.f
gendual.exe
fl32 combinat.f
combinat.exe
fl32 gendispg.f
gendispg.exe
fl32 prep106.f
prep106.exe
C:\Msc\bin\nastran.exe fixed106_st.bdf scr=yes news=no
fl32 prep106b.f
prep106b.exe
C:\Msc\bin\nastran.exe fixed106b.bdf scr=yes news=no
fl32 prep101r.f
prep101r.exe
C:\Msc\bin\nastran.exe fixed101_react.bdf scr=yes news=no
fl32 genalpha.f
genalpha.exe
fl32 nlcfgb.f
nlcfgb.exe
fl32 nlcfsig.f
nlcfsig.exe
fl32 redmass.f /math_library:check smathd.lib
redmass.exe
fl32 solve.f /math_library:check smathd.lib
solve.exe
fl32 cntrdspl.f
cntrdspl.exe
fl32 genstress.f
genstress.exe
fl32 rainflow.f
rainflow.exe
```

Note: xdoit.bat is valid for the following software configuration:

- *PC/Windows 2000;*
- *Compaq Visual Fortran Standard Edition version 6.5.0;*
- *IMSL Fortran 90 MP Library version 3.0 for Microsoft Windows NT(R) and Microsoft Windows95(R) running Digital Visual Fortran;*
- *MSC.Nastran VERSION - 2001.0.7.*

Table 2. Description of the script file

3.2 Output Files

nlcf0.dat: Output file containing the linear stiffness terms $\overline{K}_{ij}^{(1)}$ printed according to the format (($\overline{K}_{ij}^{(1)}$, j = 1, ..., N), i = 1, ..., N), see Table 13.

nlcfA.dat: Output file containing the quadratic stiffness terms ((($\overline{K}_{ilj}^{(2)}$, j = l, ..., N), l = 1, ..., N), i = 1, ..., N), see Table 14.

nlcfS.dat: Output file containing the cubic stiffness terms ((((($\overline{K}_{iljp}^{(3)}$, p = j, ..., N), j = l, ..., N), l = 1, ..., N), i = 1, ..., N), see Table 15.

redmass.dat: Output file containing the mass matrix of the reduced order system written as (($\overline{M}_{ij}$, j = 1, ..., N), i = 1, ..., N) with N written on the very first line, see Table 16.

redcm.dat: Output file containing the damping matrix of the reduced order system written as (($\overline{C}_{ij}$, j = 1, ..., N), i = 1, ..., N), see Table 17.

nlcfsigout.dat: Output file containing the stress reduced order terms $S^{(0)}$, $\overline{S}_i^{(1)}$, $\overline{S}_{ij}^{(2)}$ for each of the stress components at every point. This data is written by blocks formatted as follows (see Table 18):

element number node number within element face number stress number
$S^{(0)}$
($\overline{S}_i^{(1)}$, i = 1, ..., N)
(($\overline{S}_{ij}^{(2)}$, j = i, ..., N), i = 1, ..., N)

where
element number = number of the element which contains the node of interest
node number within element = number ranging from 1 to 4 for CQUAD4 element, denotes which of the nodes of the element is of interest
face number = 1 for the lower face or 2 for the upper face
stress number = 1 for σ_{xx}, 2 for σ_{yy}, or 3 for τ_{xy}

displ.out: Output file containing the time histories of the N modal coordinates q_i at the first time step, the second time step, etc., see Table 19.

stress.out: Output file containing the time histories of the user selected stress written as (see Table 20):

time step number stress value at that time step

range.dat: Output file containing the rainflow ranges and their starting and ending points (peaks or valleys), see Table 21.
rainflow range starting point ending point

damage.dat: Output file containing a single number which represents the accumulated damage for the given excitation and damage accumulation rule, see Table 22.

`3`	= number of transverse modes selected ($N/2$)
`1 5 7`	= number of the $N/2$ modes to be selected
`1.e-4 1.e-4 1.e-4`	= scaling factors q_i of the transverse modes
`2.`	= common ratio of scaling factors $\hat{q}_i / q_i$
`0.01`	= common damping ratio of all modes
`65`	= number of the element which contains the node of interest for stress computation*
`3`	= node number within element of which the stress is to be computed*
`1`	= face number (up/down) of the node*
`1`	= stress type (1-3) *
`0.0 0.0`	= initial and actual temperatures of the panel

* See description of these input in the specifications of the file nlcfsigout.dat

Table 3. Input file fixed.mod

```
NLPARM = 1
NLPARM   1       1               AUTO    1       1       PW      NO
          1.+13   1.+13   1.+13                           0.9         *    B
MATS1    1               PLASTIC 99999.9    1     1     1.E30
```

Table 4. Input file nlparam.dat

```
1    0.   1.
```

= values of the autoregressive order m (1 here), the autoregressive coefficients a_i (here only a_1), and value of b_0.

Table 5. Input file S_A_B.dat

```
32262      1.363277164103491e-002
461.761828       4.27E-02
416.2953629
251.6654559
-31.98876518
551.9573821
319.9525911
277.6953788
-197.1800686
179.6904642
797.1929697
528.3447662
-847.3506325
205.0921062
-875.0819954
-299.5584699
669.3796228
1931.050537
-1651.506464
-1219.581612
-847.6017105
5.167880676
1311.542806
-1521.742181
-1047.130011
394.8680324
-38.50517847
389.2109615
-317.7760543
-1653.794445
-1371.942124
-895.1431199
      .
      .
      .
```

= number of time steps and time step (Δt)

= value of w_n at first time step

= value of w_n at second time step

.
.
.

Table 6. Input file wn_file.dat

```
1.0    1.0
```

= constant *K*; exponent *m*

```
1.0   1.0                          = constant K; exponent m
0.0   10000000000.0   5            = lower limit of lowest range,
                                   = upper limit of highest range,
                                   = number of different range domains
1.0                                = exponent in first range
1.0                                = exponent in second range
1.0                                = ...
1.0                                = ...
1.0                                = exponent in last range
```

(a)

```
1.0    1.0                         = constant K; exponent m
0.0                                = exponent q
```

(b)

```
1.0     1.0                        = constant K; exponent m
1000000000.0                       = static strength at zero fatigue
                                     damage
0.0   10000000000.0   5            = lower limit of lowest range,
                                   = upper limit of highest range,
                                   = number of different range domains
1.0                                = exponent in first range
1.0                                = exponent in second range
1.0                                = ...
1.0                                = ...
1.0                                = exponent in last range
```

(c)

```
1.0    1.0                         = constant K; exponent m
1.0    100000000000.0              = exponent A, static strength at
                                     zero fatigue damage
```

(d)

Table 7. Input files for fatigue damage accumulation Palmgren_Miner.dat (a), Marko_Starkey.dat (b), Marin.dat (c), Schaff_Davidson.dat (d), and Hashin.dat (e)

```
      PARAMETER(MAXEL=141,MAXNOD=166,NSX=MAXNOD*6,NEIGX=30,NSELX=3)
C      MAXEL = MAX NUMBER OF ELEMENTS
C      MAXNOD = MAX NUMBER OF NODES
C      NSX = MAXIMUM NUMBER OF DOF
C      NEIGX = MAX NUMBER OF EIGENVECTORS IN SOL 103
C      NSELX = MAX NUMBER OF SELECTED EIGENVECTORS
```

(a)

Table 8. Header files param.h

```
      PARAMETER(ald1=60.)
C  ALD1 is the load factor
```

Table 9. Header files ldamplif.h

```
      PARAMETER (MXPARM=50,NTP=5000,MODE=6,NFORC=100,NDX=0)
C     MAXPARM = maximum number of parameters DSET subroutine (IMSL)
C     NTP = maximum number of wave passes (for the inclined wave)
C     MODE = number of modes (includes dual modes)
C     NFORC = number of time steps (i.e. size of force vector)
C     NDX = solver method selector
C             if 0 full solution
C             if 1 static condensation
```

Table 10. Header files solve.h

```
      PARAMETER(nodx=107,ndofx=3)
C     - nodx is the node for which displacement is computed.
C     - ndofx is the DOF for which displacemnt is computed; it
C     can have the following values:
C       - 0 for z-rotation;
C       - 1 for y-rotation;
C       - 2 for x-rotation;
C       - 3 for z-displacement;
C       - 4 for y-displacement;
C       - 5 for x-displacement.
```

Table 11. Header files center.h

```
       INTEGER NFORC,OPTION,ICYCLE
       PARAMETER(NFORC=100,OPTION= 1,ICYCLE=1)
C      NFORC = number of time steps (i.e. size of force vector)
C      OPTION 1 stands for Palmgren-Miner linear accumulation rule
C      OPTION 2 stands for Marko-Starkey nonlinear accumulation rule
C      OPTION 3 stands for Marin nonlinear accumulation rule
C      OPTION 4 stands for Schaff_Davidson nonlinear accumulation rule
C      OPTION 5 stands for Hashin nonlinear accumulation rule
C      ICYCLE: Flag to specify the chronological order of the cycles
C           ICYCLE = 1 cycles ordered by their beginning
C           ICYCLE = 2 cycles ordered by their ending
```

Table 12. Header files rainflow.h

```
 5.8020293311736488E+05  -1.8759237548139101E-12   1.3475046588665757E+01
 1.2040322002605539E-12  -5.0756547551017889E+01  -1.2270718849426023E-12

 1.8845122445106013E-03   2.9923760192455537E+00  -1.7235498245119146E-02
 6.9605760645760226E-02  -6.0749780912502792E-02  -1.3195668150940737E-01

 3.3171663851354005E-01   8.8608248125169263E-12   5.9761163946617907E+06
-1.3709827718730106E-12  -1.6546700605207000E+01  -2.3265746678935267E-12

-1.7324277028405734E-04   6.9605760634427055E-02   4.4141362146924552E-02
 9.8700447113337897E-01   9.0590423490036053E-03   4.4316607278758455E-02

-3.7793202079860377E-01   2.5558904193437080E-14  -4.1776973839192486E+00
-1.8676842609452491E-14   1.1711383392185265E+07   1.1629621115699973E-14

-1.8973425066744139E-04  -1.3195668149600231E-01   3.9663562468470887E-03
 4.4316607301433816E-02   8.6557049903377536E-02   5.3570987883497878E-01
```

Table 13. Output file nlcf0.dat (*N* = 6)

```
-1.0057284499546413E-05   3.2246712137787258E+06  -1.9287393414799365E-05
-9.2717216525462398E+04   4.4486252693209558E-05  -7.1626356127908002E+04
-5.2296825961998116E-16  -2.7221554291209215E+06  -6.7757541180097950E-16
 4.5904809029118586E+06  -1.0346867746825816E-16
-7.2995752697588800E-06   7.6859925056394935E+05  -1.2017118860560439E-05
 3.9871623412026337E+05
-1.9052691269225598E-16  -5.0714900084930082E+05   8.7249060112383340E-17
-2.1421897646329606E-05  -1.5905917901461220E+06
-1.1622283696159962E-16

 1.6123758982490064E+06   5.3029263723017784E-06  -2.7220930381418401E+06
 4.6129426390267002E-07   4.5904804400511924E+06  -1.1037765078195388E-07
-4.7312717851138215E-07   5.9617900893815792E-06  -1.1444680574580435E-06
 2.4048471547466472E-06   5.2016138604002936E-06
-1.7838763563694074E+06  -1.2993563891460862E-06  -3.3788678166054090E+05
-2.9096583407809140E-07
 2.5643302058452994E-06  -2.2109397646019599E-07   1.7940738992801374E-07
-4.8625978927895688E+06  -6.7949784403457409E-06
 4.7823270315368404E-07

-1.6954551297087542E-07  -2.7223642537101163E+06  -3.8794763826307815E-05
 7.6889181834117603E+05   2.3886300444719096E-05   3.9878314353883616E+05
-4.8149017878976384E-16  -3.5671591767214597E+06  -5.2235947016684001E-16
-3.3911774826446443E+05   3.3411432914429115E-16
-3.0003694153293738E-05   1.1916683515505107E+07  -2.0397624823670137E-05
 9.5396679285520036E+05
-2.5533672788310394E-17   5.6557613272768824E+04   6.0208370127147288E-17
-3.1199170877591086E-05   2.7225313277769316E+05
-2.8930505487255426E-16

-4.6359008667986018E+04   2.3481237461625160E-07   7.6817009303951426E+05
 6.4796489492709874E-08  -5.0727180231726915E+05   8.1622762419718827E-08
-5.7243789774524537E-07   7.2649386506640204E-06   5.1276018943662309E-06
```

```
 1.6588900392244808E-06   1.7967768735842663E-07
 5.9592584941695686E+06   6.1254021201273335E-06   5.5410395657202149E+04
 2.0721186317066345E-07
 5.5415181833147200E-06   2.4257679198669274E-07  -4.0790516208326197E-06
 6.3213758938870940E+05   1.2071359650227864E-06
-1.1464887634144153E-06

 4.6305623030544968E-08   4.5921395951387631E+06  -3.2616701660767785E-06
-5.0745041383088677E+05  -1.7162998120796696E-07  -1.5919924366951694E+06
-2.1532536708430528E-19  -3.3872752884595876E+05  -1.9422663624743607E-18
-9.7227894163999092E+06  -2.8983903354026818E-18
-7.8918565310103689E-08   5.6285062040773060E+04  -1.1045730652998513E-07
 2.7193663649057306E+05
-1.5647776276172158E-18   1.2638991912205322E+06   1.0661509672322732E-18
 2.0153952124346247E-07   1.2235405868083838E+07
 1.0645951512019171E-19

-3.5819464001635570E+04  -2.0824039717465851E-09   3.9869311920906202E+05
-6.0473362355106833E-09  -1.5910012931940129E+06   2.5406580607224273E-07
 2.6006470032889666E-06   2.8249191180718109E-07   1.7960980144451357E-07
 3.5231470518759518E-06   9.5737800764734671E-07
 4.7705625574327126E+05   5.4202190349601381E-07   2.7140680671319249E+05
 2.3169513738669754E-07
-2.0393053626724085E-06   2.6174895584318842E-07  -2.2927028823660306E-06
 6.1195318922005398E+06   9.0133146661615709E-06
 4.5016740655781134E-06
```

Table 14. Output file nlcfA.dat (*N* = 6)

```
 1.0658427051387697E+13   1.0749073551177545E-06   1.6640989461793127E+13
-3.6997715321713218E-05  -2.1863115418560840E+13  -1.8756942557296653E-03
-4.0587596288332861E+03  -3.5534595768172592E+06   3.9092448527753965E+02
-6.6468710776886027E+06   8.4183908155003303E+02
 6.9883327299441992E+13  -6.6920165048628235E+06  -3.2499648542634129E+13
-2.3229450087981534E+05
-9.7032209396274993E+02  -2.6889789196299011E+05  -1.4108621824076869E+02
 1.1663690114255744E+14  -8.0034151498487797E+06
-7.1151309697370380E+02
-1.0753025845329979E-18   5.2463921599260436E+02  -3.2592040734695770E-18
-1.8557468409573924E+03   3.4901052381495772E-18
 1.0097820031687718E-03   3.0638471012030914E+03  -2.8685160021909084E+06
 1.7537211193998299E+01
 6.2314994357102719E-18  -4.4508245601211638E+02  -8.7509302626471194E-18
-1.4718159013785725E-08  -2.8113688774425973E+03
 2.9576414820653095E-18
 3.1760826871095449E+13  -7.1604715349121357E-06  -5.3033580847748500E+13
 1.1148332046148044E-02
-4.4156503696862922E+02   2.5194149556085826E+06  -3.3548567994146242E+02
 6.1977795206595266E+13  -2.4910105729103875E+06
-1.0795002934921479E+02
 2.0622693879842325E-18   2.6700015056009551E+02   4.9449477631071342E-18
-1.1943775708658020E-04   2.7116251203938282E+02
 4.6510702546415298E-18
```

```
-7.6227447485448750E+13  -1.6377901624012705E-06
 2.3249754674759674E+03
-1.0135602595531256E-17

-1.8845122445106014E+05  -4.0584631404855240E+03   1.8777693387775349E+06
 1.9536868440519703E+02   1.6100940519181420E+06   4.2091444910248578E+02
 5.3029263722894043E-04   1.0544441530440492E+03   4.2649271701084006E-05
-3.7056189671801130E+03   1.0220340199151854E-05
-1.8777693387594237E+06   3.0608723397508238E+03  -5.8932556137884371E+06
 1.7097057886193006E+01
 4.6129773335618780E-05  -4.4548877285436873E+02   1.1770380677067481E-05
-1.6100940519451343E+06  -2.8130007253168892E+03
-1.0561063066772720E-05
-3.3893107428303019E-08  -5.9617916551219831E-04  -8.0153331888377353E-08
-2.4048471555936806E-04   1.1316707120012647E-07
-1.2560860648755390E+04   1.4523835042620779E-03  -9.9691549077739965E+03
 5.4983947082865012E-05
 2.7491897647280434E-07   3.2200999924850084E-04  -6.8825067173206012E-07
-1.8479689015866996E+04   6.9276932281037140E-04
 1.8286760994357107E-07
 1.7235498245119147E+06   9.2380614102882669E+02  -9.2341384123929869E+06
 1.4146361248168134E+03
-1.2993563892718695E-04   1.3904215545419386E+03  -1.8948449580225010E-04
 9.2341384124633651E+06   1.5305279959100353E+03
-2.8562982498138174E-05
-1.6508212276017876E-07   2.2109253396308684E-05   3.5915584742363111E-07
 1.5546982958371345E+03  -1.5534043235759795E-04
 2.3553479045618217E-07
 6.0749780912502790E+06   5.1559316561491059E+03
-6.7949784415081700E-04
-3.2753388112317417E-07

 5.5485144731379756E+12   6.5368305291689229E-06   6.9874648175989938E+13
 5.7162219320564970E-05  -1.6238322930222463E+13   5.8748108780223157E-03
 5.2485852046275556E+02   1.5361361879513422E+07   3.0644929634769760E+03
-3.2294457807046962E+06   1.7399795281117971E+01
 9.5271294624470828E+13  -1.9536597147725165E+07  -1.0609065372623009E+14
-2.9675214384444100E+06
-4.4160357282534954E+02  -7.2282556023412314E+05  -3.3562093714204644E+02
 6.1981623651868828E+13  -3.3109084648296596E+06
-1.0800605450483074E+02
 1.7764213999273242E-18  -1.2564229848521791E+04  -2.2164672185649078E-18
-4.9901387408426062E+03  -1.4766624175959700E-18
-8.2138218659624492E-04   1.8512108467870451E+03   2.2051981571169809E+07
 2.8299368091739734E+03
-1.0207607678070220E-18   1.3924001848932694E+03   3.8177144389224320E-18
-7.6572255845233655E-08   1.5332442786385375E+03
-1.9904538360536567E-20
 2.3352875898035891E+14   4.8280435123563718E-05  -1.4618506389891164E+13
-3.1464209886170949E-02
-8.7315129803755553E+03  -1.6971989489862587E+07  -1.1930488162165532E+03
 2.5426118092015906E+14  -1.6500511675750127E+07
-5.7629159755379078E+02
 9.3724813578739065E-18  -4.6705038027857523E+02  -6.4092739738672581E-19
 7.9138131934609166E-05   7.1567868309274076E+01
-1.8780884887139757E-18
-1.4095933493022818E+13  -3.2649258555762036E-06
```

```
-3.2961876647217245E+01
-8.7916879144881316E-18

 1.7324277028405737E+04   1.9533906164262078E+02   3.0412032796019875E+06
-9.6953682205899725E+02   2.6630775938792125E+05  -7.0635609779345387E+01
 2.3481237461409322E-05   3.0610310190906921E+03   1.0816538636992944E-04
-4.4594818839441103E+02  -1.2693128883037306E-05
-3.0412032796021467E+06  -8.8037959002779110E+02   3.7267528736162395E+06
-3.3483205619862667E+02
 6.4796055808428767E-06   5.3624336107811916E+02  -3.4987149895998595E-06
-2.6630775938894844E+05   2.7181815190444479E+02
 8.5325095993798695E-06
 9.1027700562235109E-08  -7.2649392385048866E-04   1.2153646145041105E-07
-1.6588900390127227E-04   2.5090368151181592E-07
 9.2240593166305507E+02  -2.5409448850544075E-04   1.3896740172484629E+03
-1.9213394980913121E-04
 2.4793426860181262E-07  -4.4966377688027815E-05  -5.7813600911824071E-07
 1.5553315874897601E+03  -1.4631313738702742E-04
-1.1638227274263223E-07
-4.4141362146924557E+06  -8.7307462845465088E+03   8.8656428683050759E+06
-5.9649845442493086E+02
 6.1254021213580758E-04  -9.3266874883825108E+02   1.0560376900205225E-04
-8.8656428683610614E+06   7.3620278519259671E+01
 2.1148622234695973E-05
-1.0826262983986843E-06  -2.4257792034045766E-05   3.6206194292676125E-07
-1.2459861189681453E+03   5.5371636095702379E-05
 4.2060105398533660E-07
-9.0590423490036058E+05  -9.5861481821946086E+02
 1.2071359652366387E-04
-1.5410305915560140E-07

-7.2917611857502207E+12   6.3258937777452590E-06  -1.6242507498206141E+13
-6.6966143266576983E-05   1.1661138086351866E+14  -4.5619591472720296E-03
-1.8551989926508068E+03  -5.6862028017585771E+06  -4.4553531503346426E+02
-4.3089767127639778E+07  -2.8142107472850744E+03
-5.3046555633380297E+13   5.6474762035197495E+06   1.2396235199842931E+14
 2.6216005488877087E+06
 2.6718518491002527E+02   5.3147635026107300E+06   2.7196561031763974E+02
-2.2864480926213803E+14   3.3167429307921994E+07
 2.3269403118141754E+03
-8.7715188193039657E-21  -4.9878742266131203E+03   9.4713598509229241E-21
-1.8471748626325279E+04  -2.3519394851098701E-20
 9.6566139332990221E-04   1.3909610826709259E+03   2.1853773323527999E+07
 1.5331074559221399E+03
-2.1808848585740089E-20   3.1057268643053249E+03   3.7278682108060298E-20
-2.0310529622961200E-11   1.0305755608885385E+04
-8.9505144382507511E-21
-4.8762035990897920E+12  -4.0997644971774919E-06   2.5424824874390378E+14
 2.1628202003635411E-02
-4.6587055074670576E+02  -1.7565621674293648E+07   7.1843228862468408E+01
-4.2271049345184758E+13  -8.7766933620526101E+06
-3.2986877839425318E+01
 7.6252478992795931E-20  -1.2466556654544547E+03  -2.5174400378349095E-20
 2.8416599702083570E-04  -1.9154512529101219E+03
-1.9936413271488153E-20
 4.6158062376628331E+14   3.4364174676117807E-05
-1.0650959075064748E+04
```

```
 3.1720553095891058E-20

 1.8973425066744137E+04   4.2115241483250617E+02   3.9557897832387600E+04
-7.0641674003446568E+01   4.4274644241636135E+06  -7.1143957758833255E+02
-2.0824039714880916E-07   1.6825819800631685E+01  -1.2731368693660870E-05
-2.8124366387611881E+03  -1.5892929333682911E-05
-3.9557897823283631E+04  -3.3532103915865241E+02  -1.5909828402803519E+06
-2.1642666489692095E+02
-6.0472278161206162E-07   2.7152383821418761E+02  -2.4084033378723997E-06
-4.4274644240911920E+06   4.6508594790141406E+03
 2.5647837274485482E-05
-2.9912476547413984E-07  -2.8249166187952214E-05   1.0292455906654728E-07
-3.5231470518759522E-04  -8.7490778510890249E-09
 1.4163624786401631E+03  -1.9655868729526180E-04   1.5308157826175279E+03
-6.5792163383981958E-05
 9.3066613443548705E-08  -1.5019047288532478E-04  -4.0111317045621314E-07
 5.1558373448282000E+03  -1.3664865246287847E-03
 4.0496902706244058E-08
-3.9663562468470895E+05  -5.9685678450549074E+02   7.7914143599530794E+06
-5.7557961354558199E+02
 5.4202190369701875E-05   7.3487337439697683E+01   2.5955019383738783E-05
-7.7914143600256555E+06  -6.3474276086952770E+01
 2.3391211419253408E-05
-1.9031875125379947E-07  -2.6174919809461138E-05   8.0783470191025928E-08
-9.5828663281146646E+02   2.3662538942148531E-04
 1.9761546999480514E-07
-8.6557049903377537E+06  -1.0656428171785734E+04
 9.0133146663651112E-04
-1.3888406170773245E-07
```

Table 15. Output file nlcfS.dat (*N* = 6)

```
   6
 1.000000000E+00  5.768477135E-23 -2.311896335E-11 -2.711757665E-23  2.772249390E-13 -4.488264566E-23
 5.768477135E-23  7.236205255E-11  3.472395315E-22 -7.886050120E-12  5.270014554E-25 -8.458802792E-12
-2.311880325E-11  3.472395315E-22  1.000000000E+00 -5.047741010E-23 -8.853099121E-13 -8.763632749E-23
-2.711757665E-23 -7.886050120E-12 -5.047741010E-23  6.419804915E-12 -7.647959044E-26  1.192653529E-12
 2.772010611E-13  5.270014554E-25 -8.853230242E-13 -7.647959044E-26  1.000000000E+00  2.110394293E-26
-4.488264566E-23 -8.458802792E-12 -8.763632749E-23  1.192653529E-12  2.110394293E-26  3.696911872E-12
```

Table 16. Output file REDMASS.dat (*N* = 6)

```
5.331973717E+00  6.656517013E-11 -1.226346499E-05 -8.058884874E-12  2.349965392E-05 -7.979658485E-12
 6.656517013E-11  1.012058005E-07 -1.000317273E-09 -6.669707065E-09 -2.879309771E-09 -9.502276209E-09
-1.226346499E-05 -1.000317273E-09  1.711226763E+01  8.156907848E-10  3.192062830E-05  1.515619648E-10
-8.058884874E-12 -6.669707065E-09  8.156907848E-10  1.702087731E-08  3.822839856E-10  1.526371284E-09
 2.349965392E-05 -2.879309771E-09  3.192062830E-05  3.822839856E-10  2.395532897E+01  1.607491161E-09
-7.979658485E-12 -9.502276209E-09  1.515619648E-10  1.526371284E-09  1.607491161E-09  9.336008746E-09
```

Table 17. Output file REDCM.dat (*N* = 6)

```
  1      1      1      1
              1.333333E-03
              1.287609E+09   -3.517979E+06   -6.371138E+09   -2.195077E+06    8.189134E+09   -1.846588E+06
             -1.010000E+10   -1.466667E+04    1.150349E+11   -3.800000E+04   -1.387435E+11   -2.000000E+04
             -6.666667E+01   -5.466667E+04   -1.333333E+01   -1.380000E+05   -3.333333E+01
             -3.275500E+11   -1.880000E+05    7.900015E+11    3.000000E+04
              6.666667E+01   -7.133333E+04   -6.666667E+01
             -4.763467E+11   -2.533333E+05
             -1.333333E+01
  1      1      1      2
              1.333333E-03
              1.067009E+09   -3.160254E+06   -5.823949E+09   -2.287069E+06    5.687341E+09   -1.408392E+06
             -2.112600E+10    3.866667E+04    2.405459E+11    2.200000E+04   -2.900808E+11    7.000000E+04
              0.000000E+00   -1.113333E+05   -8.000000E+01    2.200000E+04    1.000000E+02
             -6.848700E+11   -6.800000E+04    1.651824E+12   -2.300000E+05
              6.666667E+01   -1.346667E+05   -6.666667E+01
             -9.960033E+11    2.033333E+05
             -1.333333E+01
.        .                    .               .               .               .               .
  .
.        .                    .               .               .               .               .
  .
.        .                    .               .               .               .               .
  .
```

Table 18. Output file nlcfsig.out (*N* = 6)

```
-2.172196E-05 -4.466398E-04  8.323139E-06 -2.031729E-04 -2.634866E-06  1.133293E-04
-8.141535E-05 -3.828326E-03 -1.621303E-06  5.846920E-04 -3.036293E-06 -2.170996E-05
-1.161589E-04 -8.040228E-03  5.741441E-06  1.584445E-03 -6.951345E-07 -5.058802E-04
 1.114526E-05 -4.167306E-05  1.449594E-06 -1.842968E-05 -5.792243E-07 -3.692825E-05
 2.039739E-05 -1.936618E-04 -2.018316E-07  2.757911E-05 -1.191463E-06 -1.074792E-04
 6.584959E-05 -2.064157E-03  4.257970E-06  3.407142E-05 -2.927137E-07 -5.036310E-04
 2.772608E-06  1.433100E-05  2.165428E-06 -3.561814E-05 -1.692595E-06 -4.618250E-05
-6.276848E-05 -1.747560E-03 -3.758963E-06  1.061624E-05  1.873097E-06 -7.421226E-04
-1.590590E-05 -2.084104E-04  3.564380E-07  5.136831E-05 -3.484931E-06 -7.498427E-06
-5.012125E-05 -1.511082E-03 -1.385438E-06  2.284601E-04 -3.063058E-06  7.051507E-05
-2.411767E-05 -5.900594E-04  1.058723E-05 -3.744153E-04 -3.979972E-06  1.406722E-04
-8.892171E-06 -4.753164E-05 -2.112668E-06 -2.555629E-05 -2.540390E-06 -3.097287E-05
-9.795492E-05 -6.324519E-03  1.455031E-05  7.210527E-04  2.714470E-07 -1.854788E-04
 4.066865E-05  4.710535E-04  2.692888E-05 -5.110259E-03  2.951548E-06 -5.968385E-04
 9.847240E-06 -5.720819E-05  2.598068E-06 -4.038214E-05  3.326697E-06 -6.393621E-05
 7.954694E-05 -3.063959E-03  7.979397E-06 -2.621150E-04  2.195999E-06 -3.839027E-04
-4.139535E-04 -1.191831E-01  3.874771E-05  2.365478E-02 -2.170454E-05  1.252556E-02
-3.946480E-04 -1.048481E-01  5.415519E-06  2.193584E-02 -3.444770E-05  1.131721E-02
-1.940008E-04 -2.395080E-02  5.159949E-05 -5.897312E-03  1.241031E-05 -7.063836E-03
 4.296829E-04 -1.385196E-01 -5.556918E-05  2.393568E-02  3.173832E-05  2.112512E-02
 3.062944E-04 -6.275869E-02 -4.685511E-05  6.876266E-03  6.032132E-07 -4.730322E-04
 2.036727E-04 -2.294935E-02 -2.739766E-05  2.288048E-03 -1.336136E-05 -9.893842E-03
-2.884378E-04 -5.246168E-02  2.791734E-06  1.029318E-02 -1.633524E-05  3.371720E-03
 3.647681E-04 -8.055417E-02 -3.531099E-05  1.390135E-02 -4.998090E-06 -9.401646E-03
 9.676533E-05 -6.613273E-03 -1.474683E-05  8.163593E-04  2.803002E-06  5.336958E-04
-3.643675E-04 -9.206849E-02  3.407541E-05  1.823862E-02 -1.858130E-05  9.414087E-03
 2.988312E-04 -6.507979E-02 -2.508159E-05  1.391448E-02  2.519783E-05  9.221902E-03
 3.930438E-05 -1.194066E-03  2.721148E-06  1.814644E-04  1.032330E-05 -3.201631E-04
 2.568110E-04 -3.807297E-02 -1.001837E-05  7.327659E-03 -2.013611E-07 -3.909207E-03
-2.784079E-05 -6.140788E-04  5.732824E-06  2.525510E-05 -1.939770E-06  1.093321E-04
.             .              .                .              .              .
```

Table 19. Output file displ.out (*N* = 6)

1	2.1884478096111814E+05
2	5.2831875733370371E+06
3	6.4911802976146713E+06
4	-2.6663627553476905E+06
5	-2.1029852955631576E+06
6	-3.7225333006151551E+06
7	4.5747901672517946E+06
8	5.4655668206529180E+06
9	-2.9926618582684314E+06
10	6.4751217939703325E+04
11	-1.2410712954796604E+06
12	-1.5900541799111836E+05
13	4.1075973339720694E+06
14	-4.3986905593915507E+06
15	3.5489243835512633E+06
16	9.3297288417093933E+05
17	2.0716987205355708E+07
18	1.1303366173121907E+07
19	1.2706484832463996E+06
20	1.9382636063034073E+07
21	2.2772729257566463E+06
22	1.1971869941410248E+06
23	-3.0906303119268687E+06
24	-9.8573569422800597E+06
25	1.8180547284970365E+07
26	-7.9110802265779208E+05
27	-6.1596198575313762E+06
28	-4.0797030780867683E+06
29	-6.0018814285831973E+06
30	-4.8979544968135301E+06
.	.
.	.

Table 20. Output file stress.out

0.306923809E+06	1	3
0.288577428E+06	1	15
0.161057672E+06	4	6
0.168612263E+08	6	6
0.767839769E+07	6	14
0.372190786E+05	7	9
0.963381506E+06	9	11
0.943549492E+06	12	14

Table 21. Output file range.dat

0.272403329365595

Table 22. Output file damage.dat

4. VALIDATION

The validation efforts have been carried out on three fully clamped rectangular panels, two of them isotropic and one composite. The analysis of the isotropic panels will be described first. These two panels had dimensions 0.3556m x 0.254m x 0.00102m (Panel 1) and 0.3048m x 0.254mx 0.00102m (Panel 2), both were discretized with 14x10 CQUAD4 elements, and they were subjected to a uniform pressure, static or dynamic. The material properties were assumed to be $E = 7.3\ 10^{10}$ Pa, $\nu = 0.31623$, $\rho = 2763$ kg/m^3, $\alpha = 2.5\ 10^5$ (°K)$^{-1}$. Rayleigh damping was assumed to be present on panel 1 so that its finite element damping matrix was expressed as

$$C = \alpha_C\ M + \beta_C\ K \tag{27}$$

where M and K are the corresponding (finite element) mass and stiffness matrices. The values of the coefficients α_C and β_C were selected to achieve damping ratios of approximately 1% on all modes retained in the reduced order model of panel 1. The values of these coefficients and the modes retained in the reduced order models and their frequencies and damping ratios are given in Table 23 for the two panels. Finally, both nonheated and heated panels have been considered for the validation which is discussed below.

Panel 1				Panel 2		
$\alpha_C = 12.838;\ \beta_C = 2.061\ 10^{-6}$						
Mode Numb.	Mode Type	Frequency (Hz)	Damping Ratio	Mode Numb.	Mode Type	Frequency (Hz)
1	(0,0)	110.2747	0.00998	1	(0,0)	121.2299
4	(2,0)	300.745	0.00534	5	(2,0)	389.0692
8	(0,2)	536.2466	0.00538	7	(0,2)	544.6526
11	(2,2)	712.1201	0.00605	11	(4,0)	788.8278
12	(4,0)	717.5684	0.00607	13	(0,4)	956.5229
18	(4,2)	1114.488	0.00813	21	(2,2)	1480.949
22	(6,0)	1434.047	0.01000			
24	(0,4)	1466.896	0.01019			

Table 23. Modal properties of the validation panels 1 and 2.

4.1 Consistency

Prior to the assessment of the reduced order modeling for the prediction of the displacement and stress fields, it was deemed noteworthy to confirm its general consistency/stability, more specifically to investigate the selection of the scaling factors q and $\hat{q}$, see Eq. (13), (15), and (19). To this end, a series of computations were performed with values of these coefficients ranging from 10^{-6} to 10^{-1}, i.e. from a thousand times smaller to a hundred times larger than the panel thickness, on panel 2 first in the absence of thermal effects. It was found that the resulting reduced order coefficients (stiffnesses and stresses) were very stable, keeping at least 5 significant digits say for the dominant terms, except for very small and very large values of the scaling factors. Accordingly, it seems recommended to select q and $\hat{q}$ to be of the order of the panel thickness. Further, it was noticed that the terms $K_{iii}^{(2)}$ and $S^{(0)}$, although not quite zero, were very small in comparison with the remaining stiffness and stress coefficients.

Similar computations performed at different nonzero temperatures demonstrated that only the first terms, i.e. $\overline{K}_{ij}^{(1)}$ and $S^{(0)}$, were dependent on temperature. In fact, the linear stiffness coefficients $\overline{K}_{ij}^{(1)}$ appeared to vary almost exactly linearly with temperature. All of these results, which are perfectly in agreement with the von Karman strains and with approximate analyses (e.g. Lee, 1993, 1997, 2001, 2002), support the validity of the reduced order modeling scheme.

4.2 Static Validations

The validation of the reduced order modeling strategy was achieved first on a series of static problems and with increasing number of modes. Shown in Fig. 3(a) are the transverse displacements of the center of the panel 2 predicted by the MSC.NASTRAN solution (SOL 106), the corresponding single-mode (with dual) reduced order model obtained by selecting the lowest transverse mode with the load factor p = 60 Pa, and the

approximations derived by Lee (1993) and Lee (2002). The reduced order displacement was obtained, as in all static validations, by marching in time the differential equations for the transverse and dual degrees of freedom from zero initial conditions with a step loading applied at $t = 0$. The tolerance was set at $5\ 10^{-8}$ for this and all ensuing, static or dynamic, validations analyses. Note from Fig. 3 the excellent agreement of the displacements obtained by including only the first transverse mode and its dual.

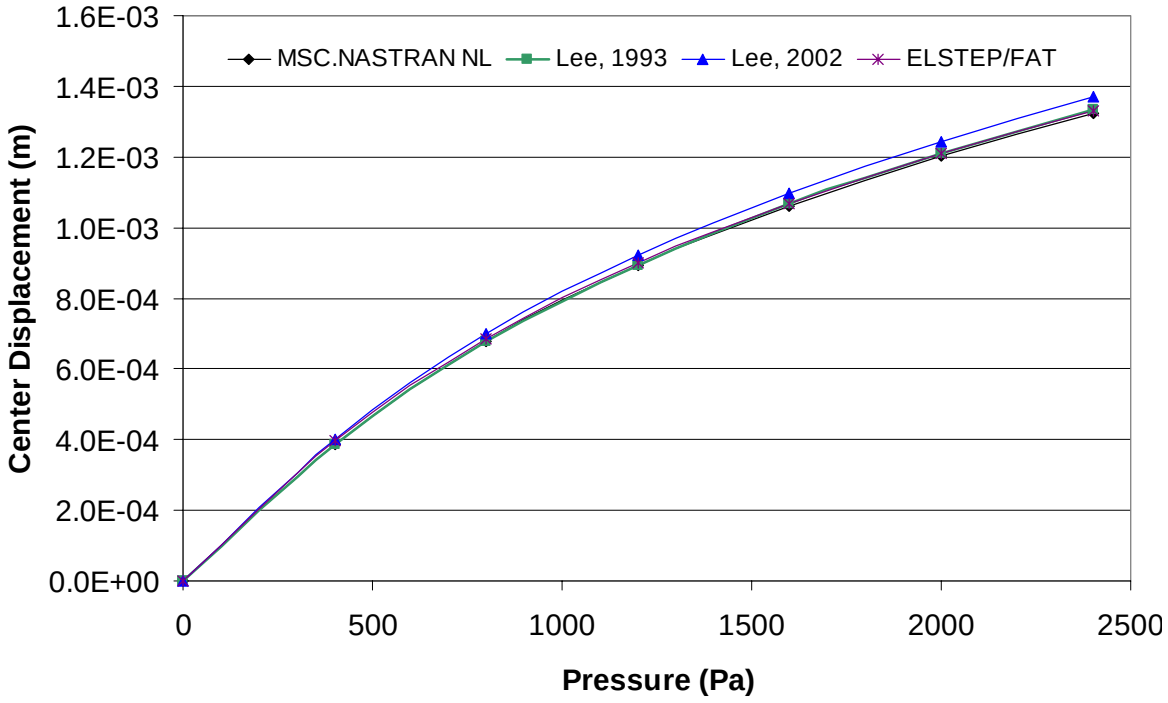

Figure 3. Static response of the panel to a uniform pressure. Center displacement as a function of pressure

Turning now to the stresses, it is first noted that the stresses are not independent of the displacements: they are determined through the memoryless quadratic transformation of Eq. (2) or (5). The stresses predicted by the reduced order modeling thus result from two cascaded approximations: the modeling of the displacement field and the approximation of the quadratic transformation. Having established the reliability of the displacement field obtained from the reduced order models, see Fig. 3, it remains to assess the accuracy of the estimated quadratic transformation. To this end, the stress in the *x*-direction at the center of the bottom of the panel (largest normal stress at that point) was analyzed as a

function of the displacement of that point. Shown in Fig. 4 are the corresponding plots for the MSC.NASTRAN data, the one mode reduced order model, and the two approximations of Lee (1993) and Lee (2002). Surprisingly, it is found that these latter approximations substantially overpredict the stress while the reduced order model provides a much closer fit of the MSC.NASTRAN data over that range. It should be noted that both the reduced order modeling and the approximations of Lee are perfect parabolas but, interestingly, the MSC.NASTRAN data is also very close to a quadratic polynomial (R^2=0.999977), see Table 24. Note that the constant stress coefficient $S^{(0)}$ was found to be very close to zero in all cases as can be expected from the lack of temperature. Further, the linear coefficients $S_i^{(1)}$ were all found to exceed their MSC.NASTRAN counterpart by 7% to 19% but a much larger scatter exists in connection with the quadratic terms: the reduced order model coefficient exceeds the MSC.NASTRAN value by 52% but the approximations of Lee (1993 and 2002) are larger, by a factor of 2.5.

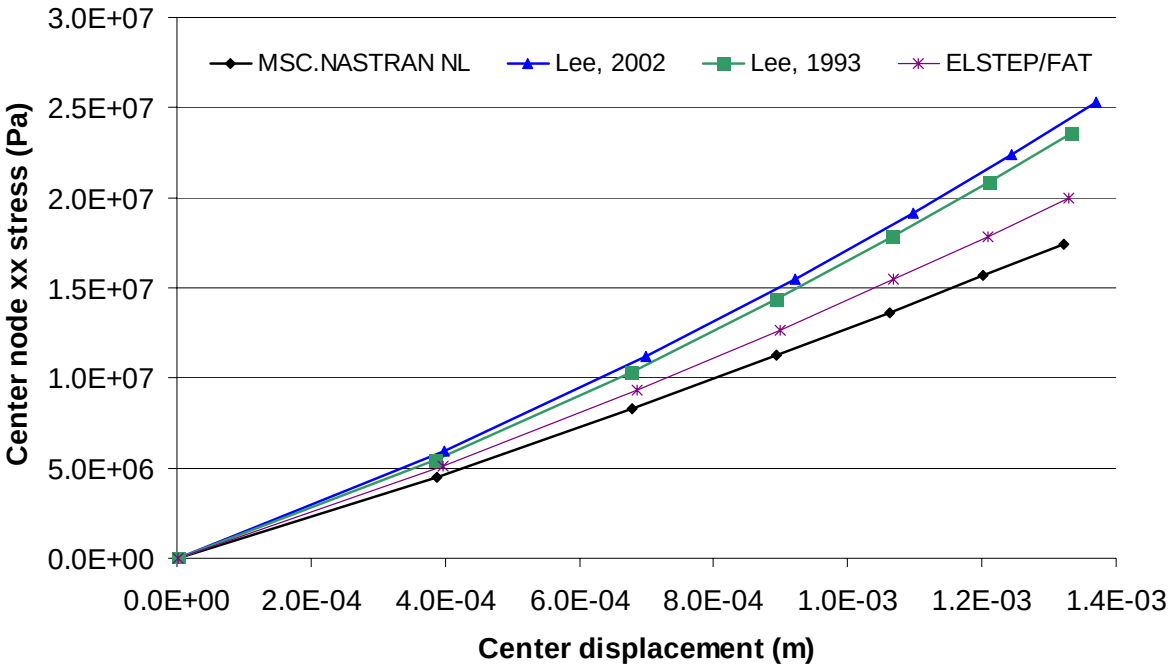

Figure 4. Static response of the panel to a uniform pressure. Stress σ_{xx} at center as a function of its transverse displacement

Solution	$S^{(0)}$	$S_i^{(1)}$	$S_{ij}^{(2)}$
MSC.NASTRAN	$-2.241\ 10^{4}$	$1.123\ 10^{10}$	$1.513\ 10^{12}$
Harmonic approximate modes (Lee, 1993)	$4.112\ 10^{-2}$	$1.275\ 10^{10}$	$3.705\ 10^{12}$
Clamped beam approximate modes (Lee, 2002)	$-7.118\ 10^{-2}$	$1.339\ 10^{10}$	$3.704\ 10^{12}$
Current Reduced Order Modeling ELSTEP/FAT	$5.180\ 10^{1}$	$1.201\ 10^{10}$	$2.299\ 10^{12}$

Table 24. Stress coefficients obtained from MSC.NASTRAN, the approximations of Lee (1993) and Lee (2002), and the present one-mode reduced order model.

In regards to these last results, it should be noted that the stresses are directly related to the curvatures of the transverse displacement field, not the displacements themselves. Thus, a good matching of the deformed shapes, see Fig. 3, does not guarantee an equally good approximation of the stresses. This observation, and the findings of Fig. 4, are in fact neither specific to plates nor to nonlinearity, a similar argument can be developed in connection with linear beams where an overprediction of the stress at the middle by 23.4% and 7% using the bases of Lee (1993) and Lee (2002), respectively, is obtained.

The effect of a higher number of modes was considered next. In the linear case, it can be demonstrated that the convergence of the displacements and stresses is achieved in an oscillatory fashion, i.e. by alternatively overshooting the exact solution. Further, modes 5 (the (2,0) mode) and 7 (the (0,2) mode) will provide contributions that are opposite in sign to both the one of mode 1 (the (0,0) mode) and to those of the next three modes (the modes 11, 13, and 21, i.e. (4,0), (0,4), and (2,2)). Accordingly, it is expected that the modes 1 and 5, 1 and 7, and especially 1, 5, and 7 may/will lead to larger negative errors than obtained for mode 1 alone. This result is clearly seen in Fig. 5 for both displacements and stresses. Note however the overall small errors in both displacement and stress estimates obtained with 6 modes (and 6 duals) strongly suggesting that indeed convergence is taking place for the prediction of both displacement and stress fields.

Having established the excellent behavior of the reduced order modeling based on the transverse modes and their duals, it is of interest to assess the need for the dual modes in the formulation. To this end, the computations of Fig. 5 were redone but keeping only the

transverse mode in the reduced order model. This effort led to the results and comparisons of Fig. 6 which clearly demonstrate the need to incorporate the duals.

The panel 2 was next assumed to be subjected, in addition to the uniform loading, to the effects of a uniform temperature equal to 1.8 times the buckling temperature. The determination of the reduced order model was repeated with load factors p = 60 Pa (as in the nonheated case) and p = 1 Pa and the corresponding displacement and stress at the middle of the panels were evaluated and compared to MSC.NASTRAN results, see Fig. 7 and 8. These results clearly demonstrate that the reduced order model obtained with the load factor p = 1 Pa produces a much closer response than the one with p = 60 Pa. In fact, both center displacement and stress obtained with 6 modes (and their duals) and p = 1 Pa are extremely close to their MSC.NASTRAN counterparts over the entire range of pressure considered. Note further that the p = 1 Pa models match quite accurately the behavior at the lowest external pressure, i.e. see Fig. 7 and 8 for 400 Pa. In searching for an explanation for this p-dependent behavior, it was noted that the center displacement obtained in the computations of the dual modes with p = 1 Pa was of the order of the plate thickness while it was 10 times as large for p = 60 Pa. Noting further that the transverse center displacement corresponding to an external pressure in the range of 0 to 7200 Pa is of the order of 1-2.5 plate thicknesses, it is suggested that the improved results obtained with p = 1 Pa (as compared to p = 60 Pa) arise from the close matching of the transverse deformation obtained during the computation of the dual modes and those actually produced by the external loading. This matching assumption serves as the current recommended selection criteria for the value of p.

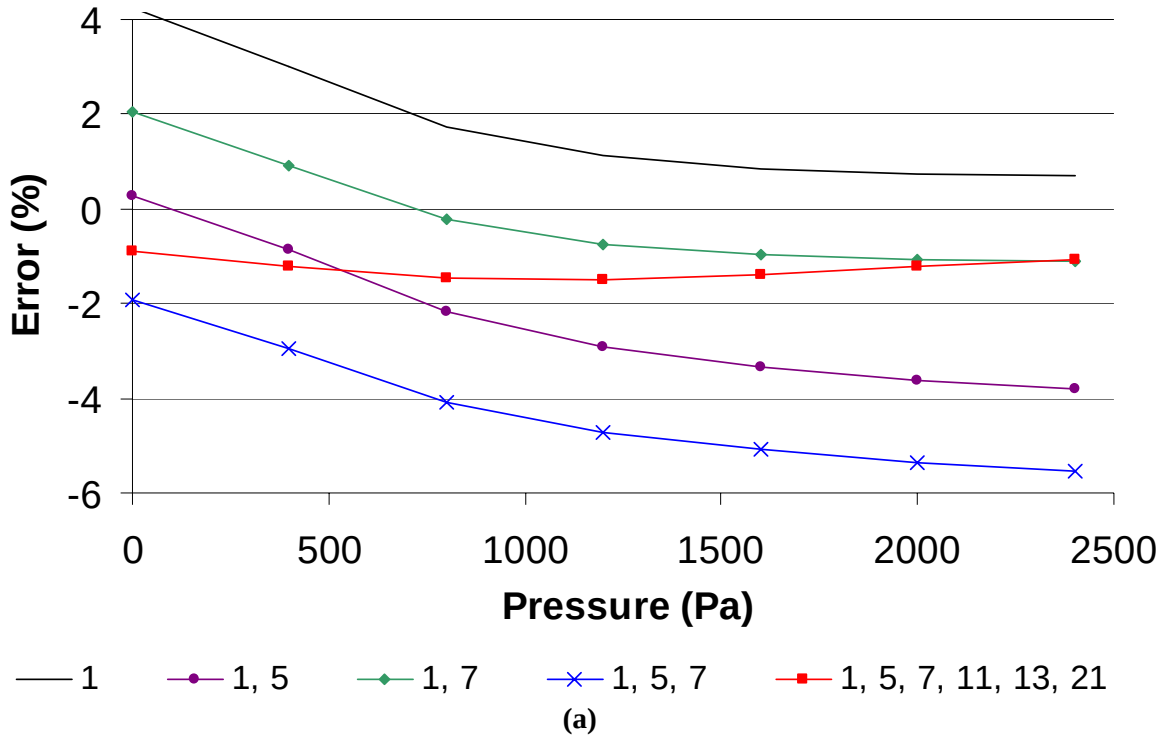

(a)

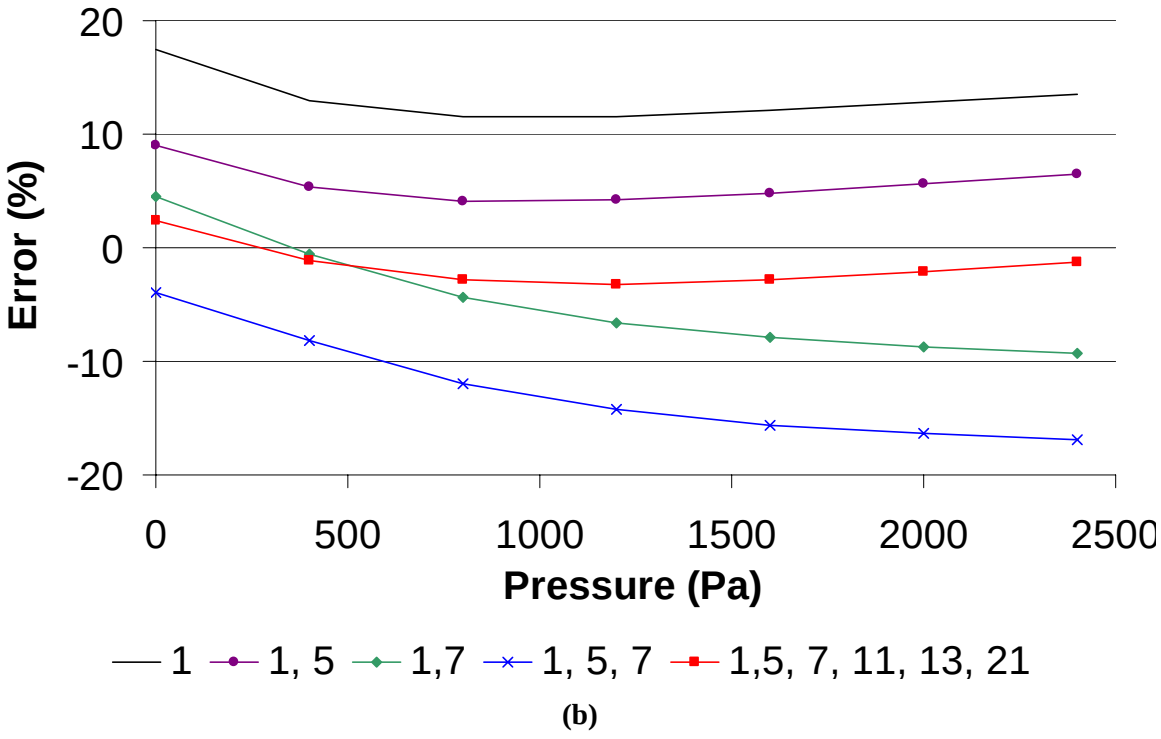

(b)

Figure 5. Reduced order modeling errors in the static response of the panel to a uniform pressure for different combinations of modes. (a) Center displacement as a function of pressure and (b) stress σ_{xx} at center as a function of pressure

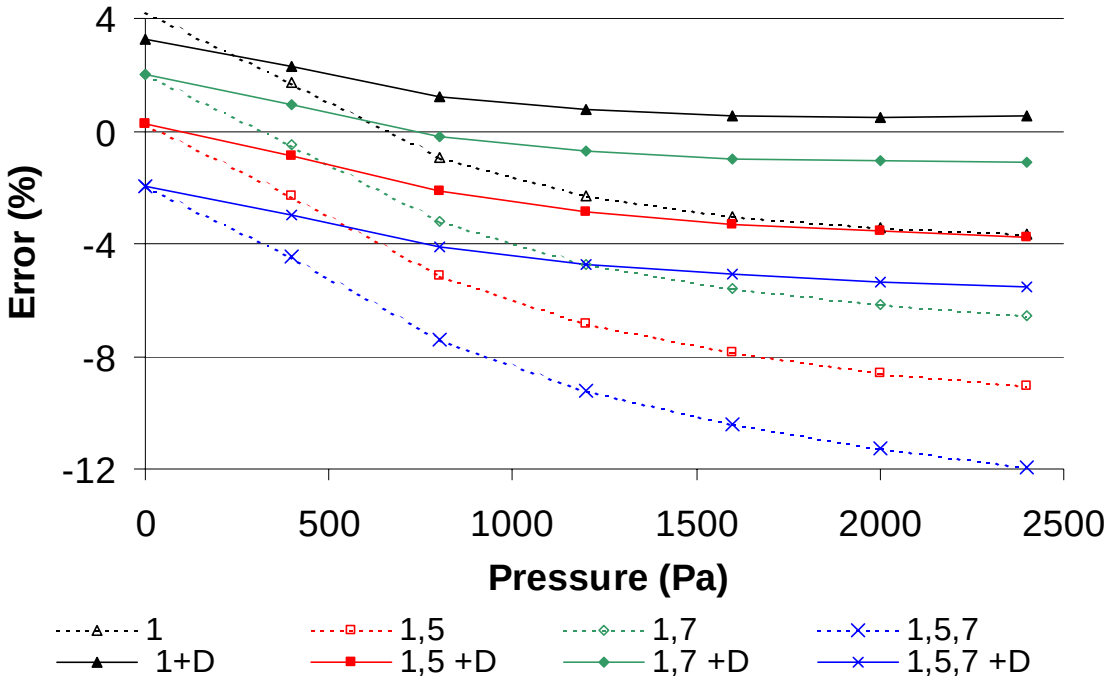

(a)

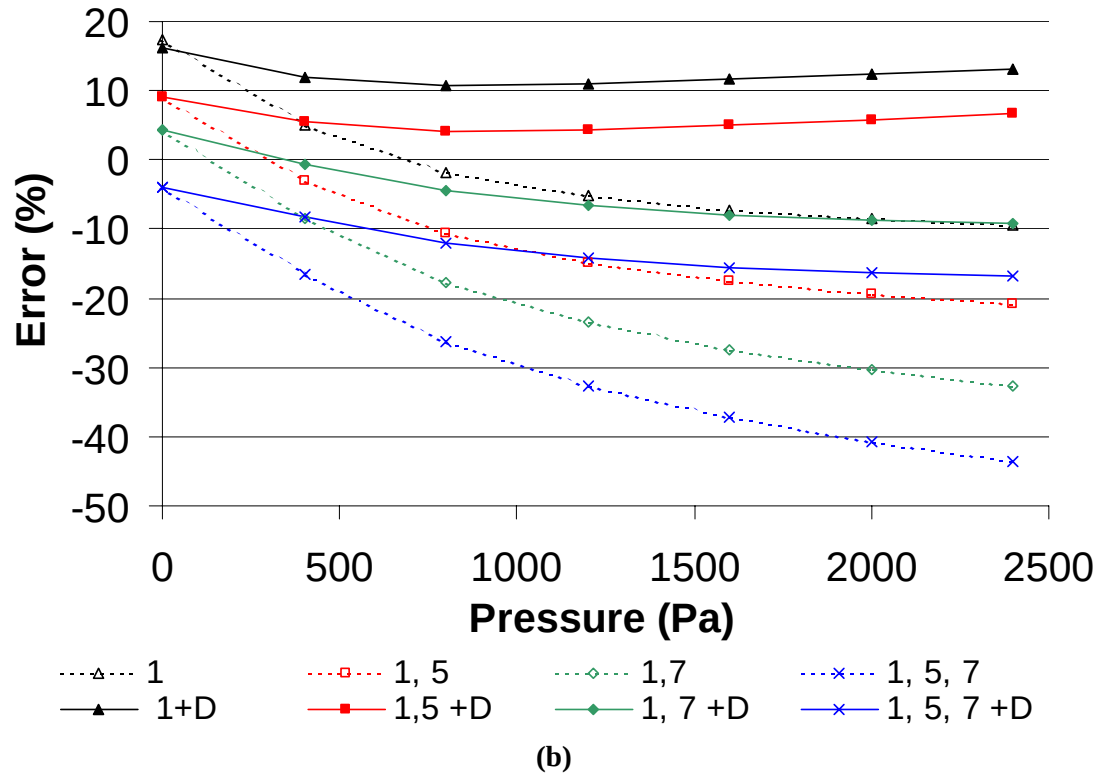

(b)

Figure 6. Reduced order modeling errors in the static response of panel 2 to a uniform pressure for different number of modes with ("+D") and without duals. (a) Center displacement and (b) stress σ_{xx} at center as functions of pressure.

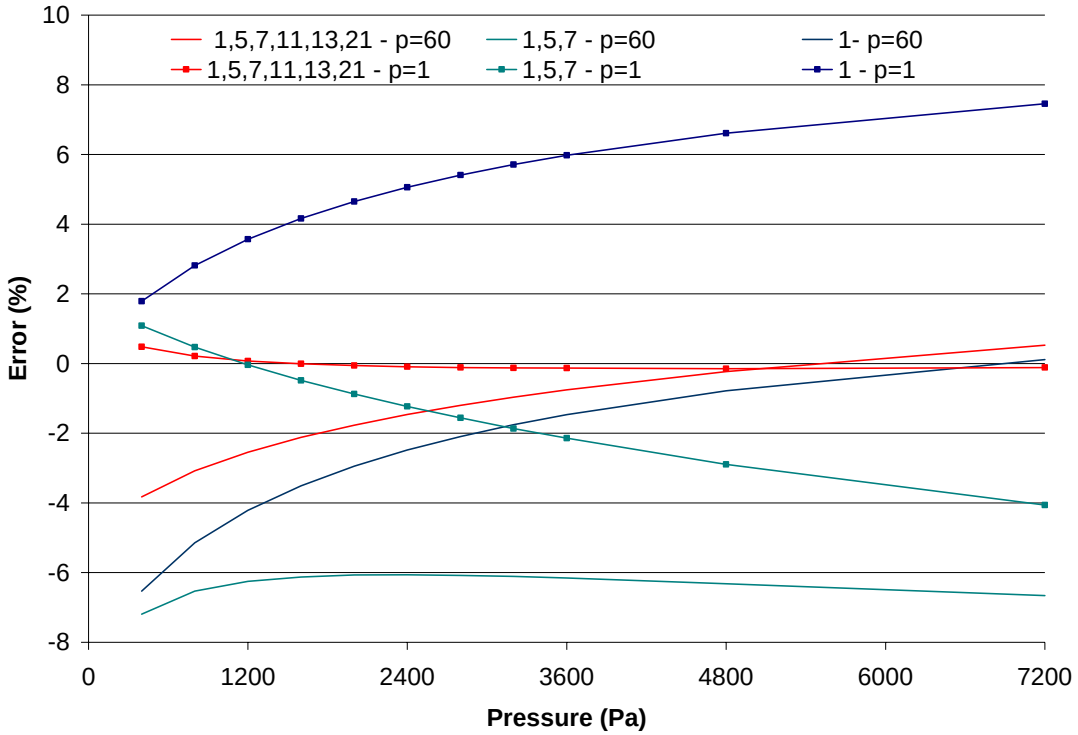

Figure 7. Reduced order modeling errors in the static response (center displacement) of panel 2 to a uniform pressure for different number of modes and different load factors *p* as function of pressure.

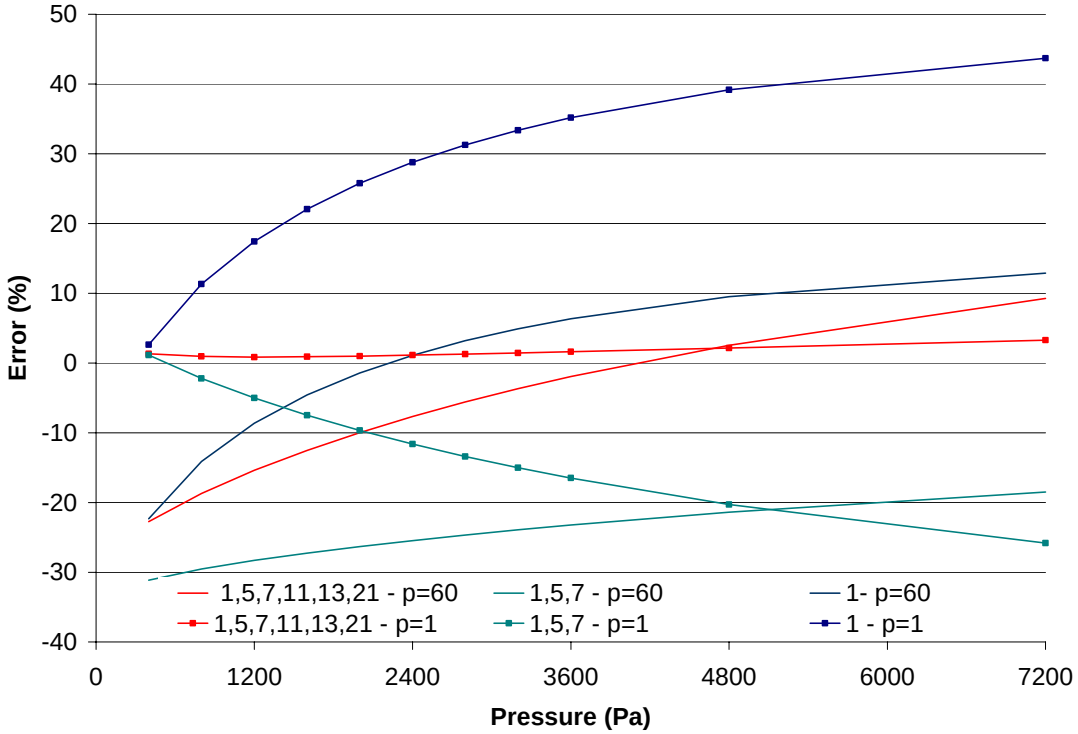

Figure 8. Reduced order modeling errors in the static response (tress σ_{xx} at center) of panel 2 to a uniform pressure for different number of modes and different load factors *p* as function of pressure.

While excellent results had been obtained with p = 60 Pa for the unbuckled panel, see Fig. 5, it was questioned whether further improvements can be obtained by changing, notably reducing, the value of p as noted above in connection with the buckled panel. In fact, a series of tests have shown that the static response of the unbuckled panel is quite insensitive to the selection of p. A slight sensitivity was observed in the dynamic validations to be discussed below where slightly improved results were obtained with p = 1 Pa as compared to p = 60 Pa.

4.3 Dynamic Validations

Having established the reliability of the reduced order modeling in static cases, it was desired next to validate its usefulness in dynamic problems. A straightforward validation approach in which time histories of the panel response to a specific loading would be computed by MSC.NASTRAN and the reduced order model and then compared, proved to be computationally expensive for both MSC.NASTRAN (as expected) but also, more surprisingly, for the reduced order model. In this regard, it was found that the natural frequencies associated with the dual modes are much higher than those corresponding to the transverse mode. Given the in-plane nature of the dual modes, this observation is not unexpected but it implies a substantial increase of the computational effort associated with the numerical integration of the reduced order model equations of motion by requiring an appropriately small time step to track the dual mode dynamics. In many cases, it may be expected that the loading on the panel will not exhibit any energy at such high frequencies and thus it is acceptable to proceed with a static condensation of the dual modes. That is, their mass and damping coefficients are ignored and the values of the dual mode coordinates are evaluated at each time step from their transverse counterparts to satisfy $\underline{\overline{K}}_{NL} = \underline{\overline{F}}_0$. In all examples considered below, it was found that the magnitude of the in-plane displacements is small enough to remain in the linear range. Thus, the nonlinear algebraic equations $\underline{\overline{K}}_{NL} = \underline{\overline{F}}_0$ can be linearized with respect to the dual modes only (all nonlinear terms in the transverse coordinates were left unchanged) to provide an efficient computation of their generalized coordinates.

The dynamic validation process was then achieved in two steps. First, the static condensation procedure described above was evaluated and then, in the second phase, a comparison on the response of the panel to a random loading was performed. For the static condensation validation, the reduced order model of panel 2 was subjected to a white noise excitation of overall sound pressure level (*OASPL*) equal to 153 dB in the range of 0-3667 Hz and a 6 transverse mode model (with associated duals) was considered as before. To better highlight any potential effect of every mode, a damping ratio of 1% was assumed for all modes and the reduced order differential equations were integrated with a time step of $1.363\ 10^{-4}$s. The full solution of the reduced order model equations is compared to its statically condensed counterpart in Fig. 9 (for the displacement at the middle of the panel) and Fig. 10 (for the corresponding stress). Clearly, the spectra of the full and condensed solutions are very close to each other through the entire frequency range of the excitation/response.

On the basis of the excellent matching of Fig. 9 and 10, the static condensation was relied upon for the dynamic validation conducted on Panel 1. The linear response of this panel was first explored to establish a firm ground for the comparison of the nonlinear responses. Shown in Fig. 11 are the power spectral densities of the displacement of the center of the panel estimated from time histories of its linear response when subjected to a 97dB white noise excitation in the range of 0-2083 Hz with the time step of $3\ 10^{-5}$ s for both MSC.NASTRAN and ELSTEP/FAT. Clearly, the agreement between the MSC.NASTRAN and reduced order model results is excellent, as expected.

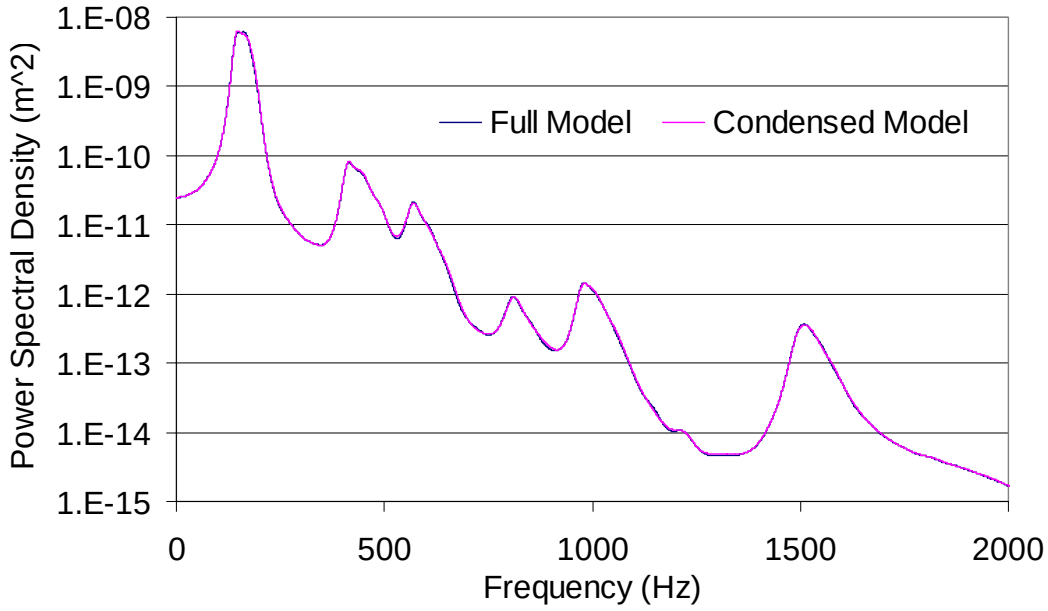

Figure 9. Comparison of power spectra of the displacement at the center of the panel for the full and statically condensed models.

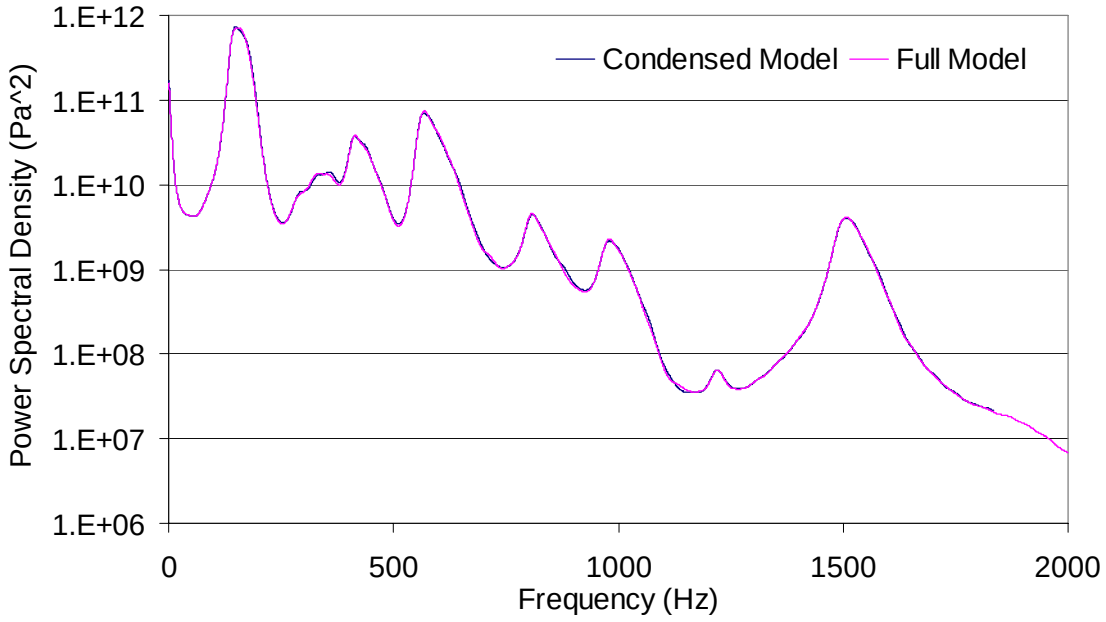

Figure 10. Comparison of power spectra of the stress σ_{xx} at the center of the panel for the full and statically condensed models.

A white noise excitation of sound pressure level 147dB in the same frequency range was generated to assess the dynamic nonlinear prediction capabilities of the proposed reduced

order. A series of MSC.NASTRAN nonlinear solutions were performed with the standard tolerance and maximum time steps DT1 = 2.4 10^{-4} s., DT2 = 4$10^{-5}$ s., and DT3 = 2 10^{-5} s. The corresponding power spectral densities of the displacement at the

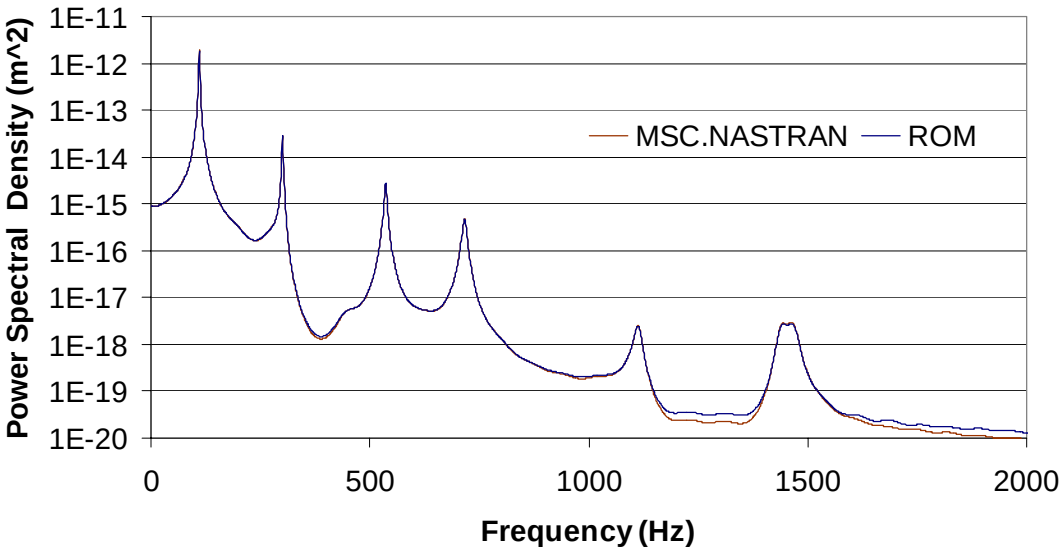

Figure 11. Comparison of power spectra of the displacement at the center of the panel for MSC.NASTRAN and the reduced order model - linear system

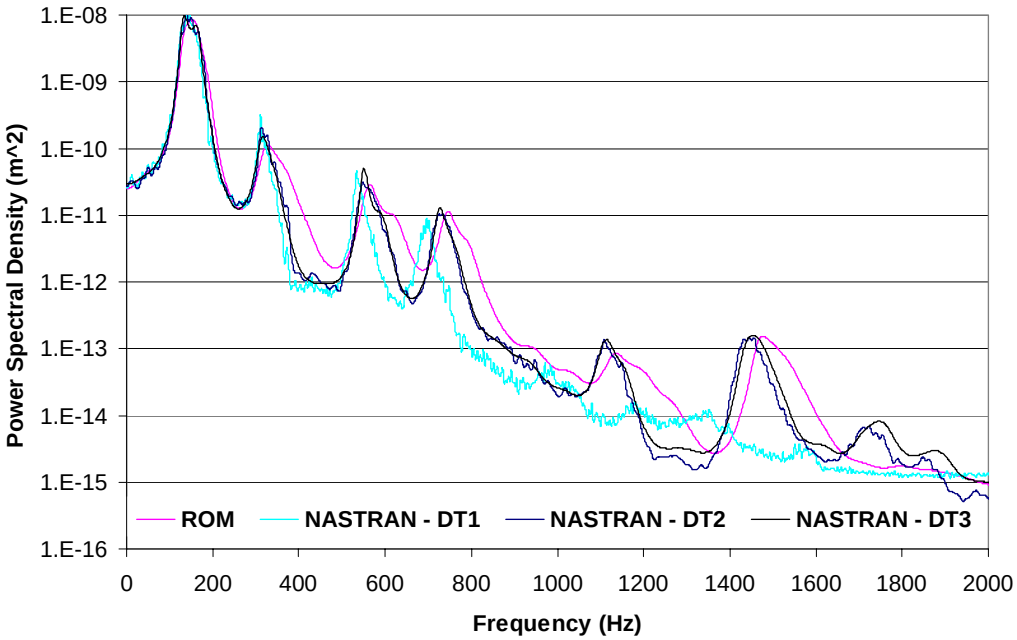

Figure 12. Comparison of power spectra of the displacement at the center of the panel for MSC.NASTRAN and the reduced order model - nonlinear system - 147dB; *p* = 60 Pa.

center of the panel are shown in Fig. 12 together with the 16-mode (8 transverse and 8 duals) reduced order model prediction obtained with the load factor p = 60 Pa and the time step of 2 10^{-5} s. An excellent matching of the dominant component of the response, i.e. the first peak, is achieved. Further, the predicted levels of the next three peaks is also very good although the frequency and width of the peaks do not coincide as well. Overall, a good matching at least is achieved. A similar perspective can be obtained from the power spectral densities of the stress σ_{xx}, see Fig. 13.

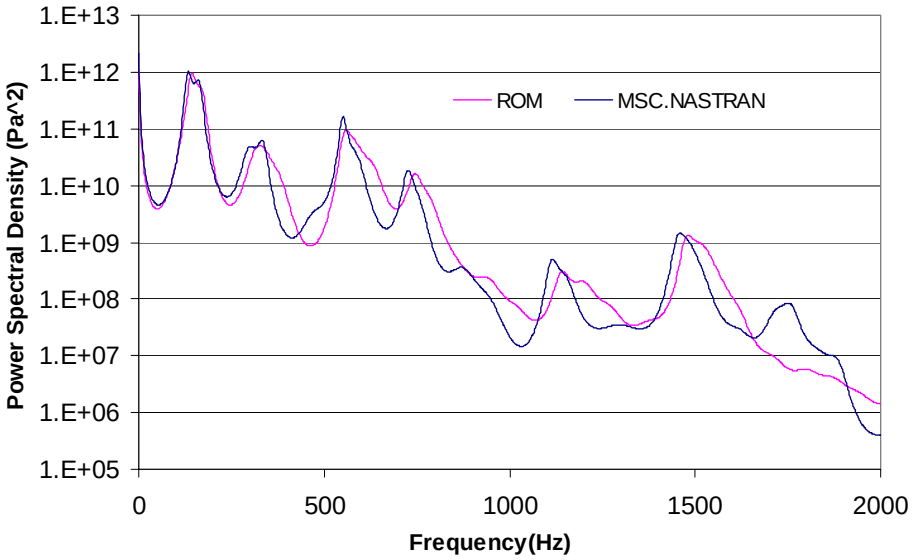

Figure 13. Comparison of power spectra of the stress σ_{xx} at the center of the panel for MSC.NASTRAN and the reduced order model - nonlinear system - 147dB; p = 60 Pa.

4.4 In-Plane Motion Modeling

The prediction of the panel response, even the transverse displacement field but especially the stresses (and thus the damage accumulated and fatigue life), necessitates a good modeling of the in-plane behavior of the panel. The reliability of the reduced order model in predicting the in-plane response was assessed on panel 1 at both 97dB and 147dB in the same conditions as above. By symmetry, the center of the panel does not move and thus a point close to it was selected for analysis, specifically the point of coordinates x = 0.1306m, y = 0.127m for the rectangular plate $x \in$ [0, 0.3048m] and $y \in$

[0, 0.254m]. Given the location of the point considered on an axis of symmetry of the panel, it only experiences an x displacement. Then, shown on Fig. 14 is the power spectral density of this x-displacement for the first 3, 5, and 8 modes (with their duals) with p = 60 Pa for a 97 dB *OASPL* white noise excitation. Clearly, the ELSTEP/FAT result with 8 modes and 8 duals provides a close qualitative model of the in-plane displacements and represents a good quantitative approximation for many modes - the largest difference appears to be on the first peak at 220 Hz where the peak magnitude may be off by as much as a factor of 8.

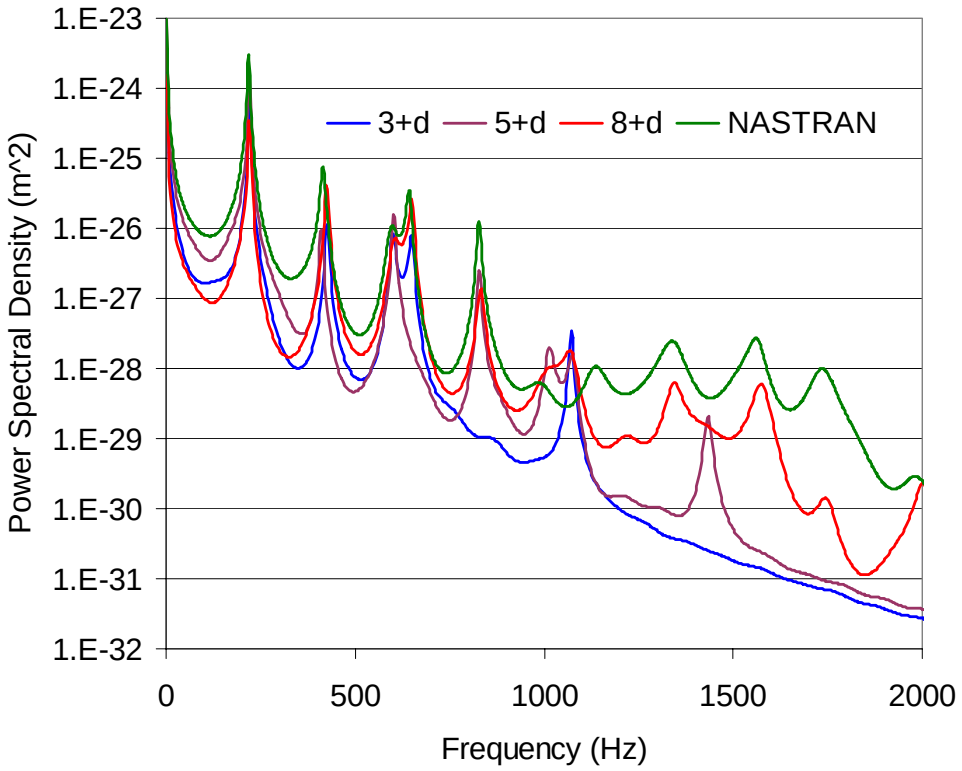

Figure 14. In-plane *x*-displacement spectrum for aluminum panel, *SPL* = 97dB, computed from MSC.NASTRAN and ELSTEP/FAT with 3, 5, and 8 modes and duals, *p* = 60 Pa.

In an effort to improve the quality of this prediction, the modeling process was repeated with the load factor p = 1 Pa and with 8 modes and their duals. Shown in Fig. 15 are the displacement spectra obtained from MSC.NASTRAN and the 8-modes (+ duals) reduced order modes with both p = 60 Pa and p = 1 Pa. It is seen that the latter load amplification factor leads to a very close match of the peak values of the spectrum, especially on the

first and dominant mode, thereby providing an excellent modeling of the in-plane dynamics of the panel. These computations were also repeated at 147dB and shown in Fig. 16 is a comparison of the MSC.NASTRAN and ELSTEP results which demonstrate a very good overall match of the spectral features.

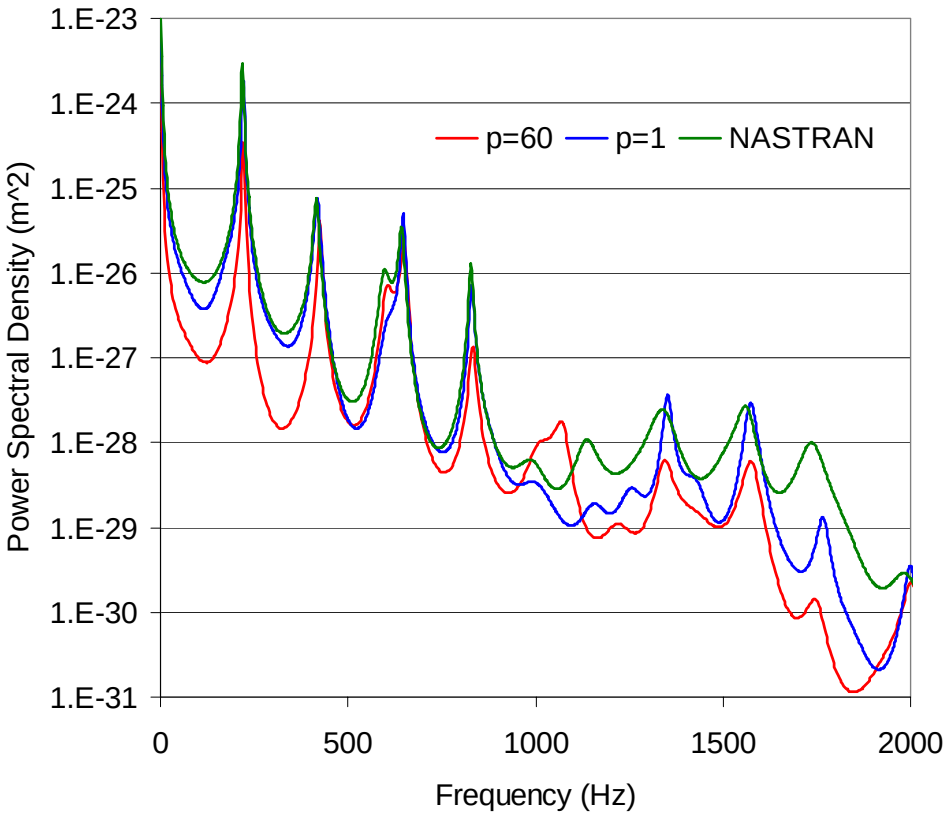

Figure 15. In-plane *x*-displacement spectrum for aluminum panel, *SPL* = 97dB, computed from MSC.NASTRAN and ELSTEP/FAT with 8 modes and duals, *p* = 60Pa and *p* = 1Pa.

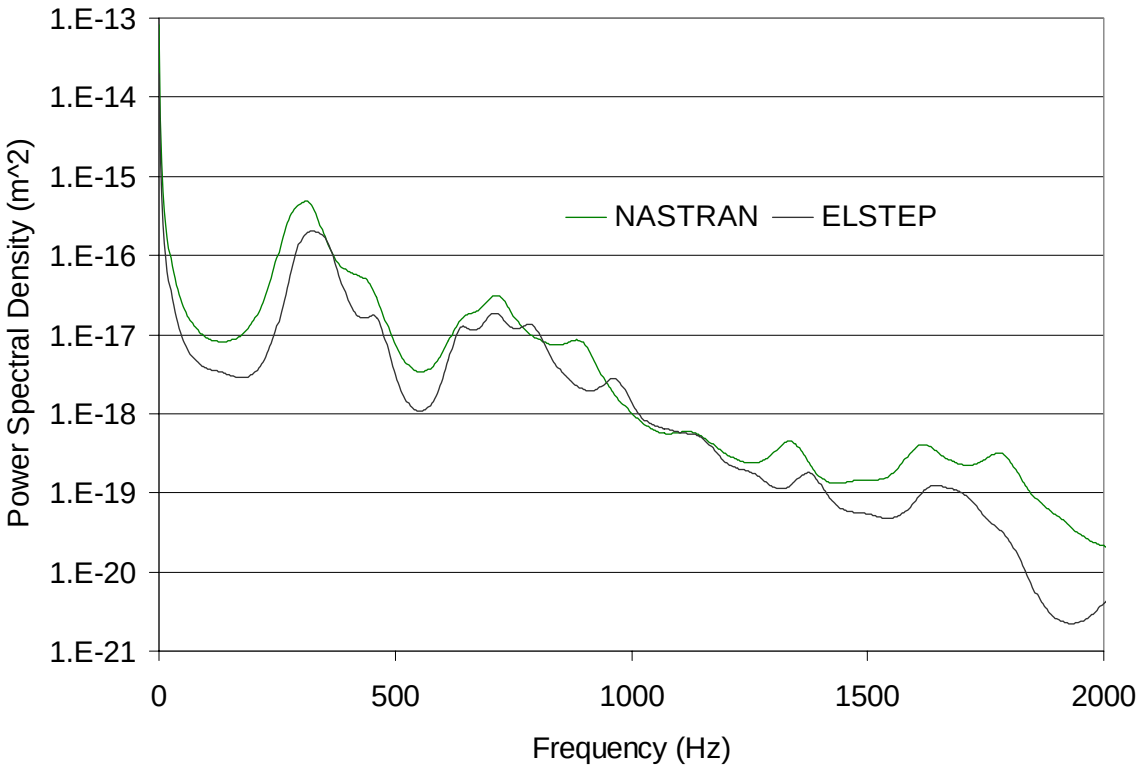

Figure 16. In-plane *x*-displacement spectrum for aluminum panel, *SPL* = 147dB, computed from MSC.NASTRAN and ELSTEP/FAT with 8 modes and duals, *p* = 60 Pa.

4.5 Composite Panel

To complete the validation of ELSTEP/FAT, a fully clamped rectangular composite panel was considered that is formed of 6 plies of AS4/3501-6 and has dimensions 0.3429m x 0.1905m. The 6 plies had orientations (0º,90º,0º) and the common thickness of 0.00013716m. The material properties of AS4/3501-6 were found to be E_1=1.448 10^{11} Pa; $E_2 = E_3$= 9.655 10^9 Pa; $G_{12} = G_{13}$= 5.862 10^9 Pa; G_{23}= 4.414 10^9 Pa; $\upsilon_{12} = \upsilon_{13}$=0.29; υ_{23}=0.55; and ρ=1591 kg/m^3. The panel was modeled with 18x10 CQUAD4 elements and Rayleigh damping was assumed. The modal properties of this panel that are pertinent to the reduced order modeling are presented in Table 25.

α_C = 9.52; β_C = 1.9 10^{-6}			
Mode Numb.	Mode Type	Frequency (Hz)	Damping Ratio
1	(0,0)	141.9646	0.00618
4	(2,0)	365.2717	0.00425
9	(0,2)	731.5963	0.00540
11	(2,2)	848.3268	0.00596
12	(4,0)	877.1326	0.00610
15	(4,2)	1227.861	0.00795

Table 25. Modal properties of the composite validation panel.

This composite panel was subjected to white noise excitation of 135dB and 140dB in the frequency range 0-2083 Hz and the displacement of the center point was determined through a full MSC.NASTRAN solution with maximum time step of 2 10^{-5}s as well as by application of the reduce order modeling strategy with the 6 modes of Table 25, p = 1 Pa, and the time step of 2 10^{-5}s. The comparisons of the power spectral densities of the center point displacement seen in Fig. 17 demonstrate again that the reduced order modeling strategy provides a reliable approximation of the full finite elements in a broad range of panel applications. A comparison of the stress power spectral density is not possible as the current version of MSC.NASTRAN does not allow to output the stress time history for composite materials undergoing large deformations.

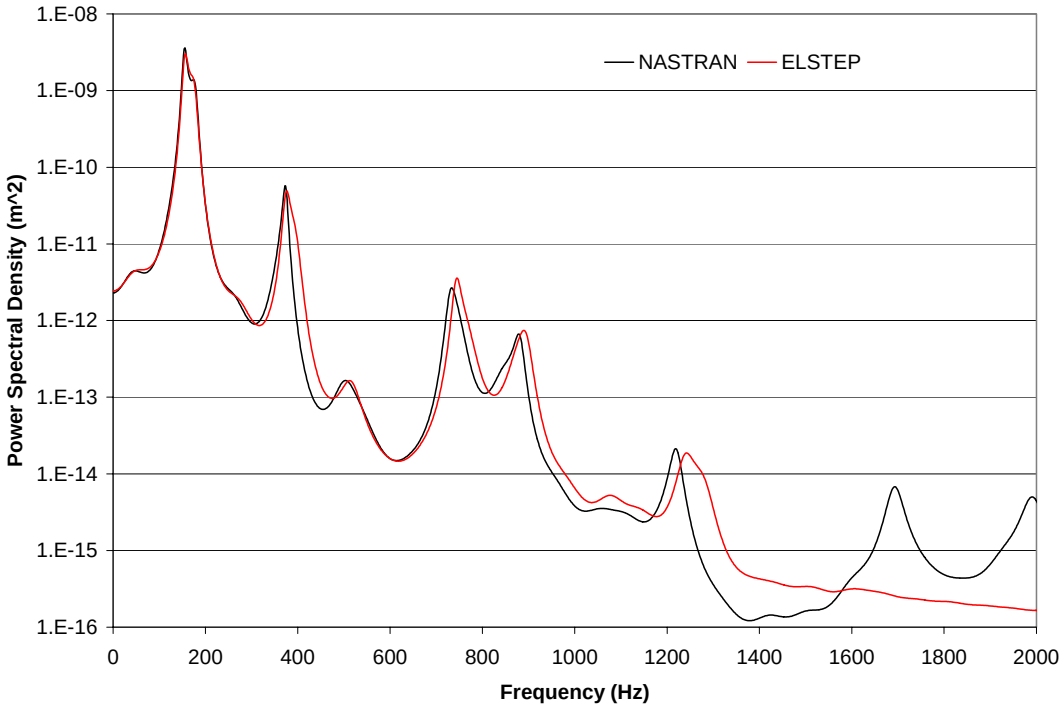

(a)

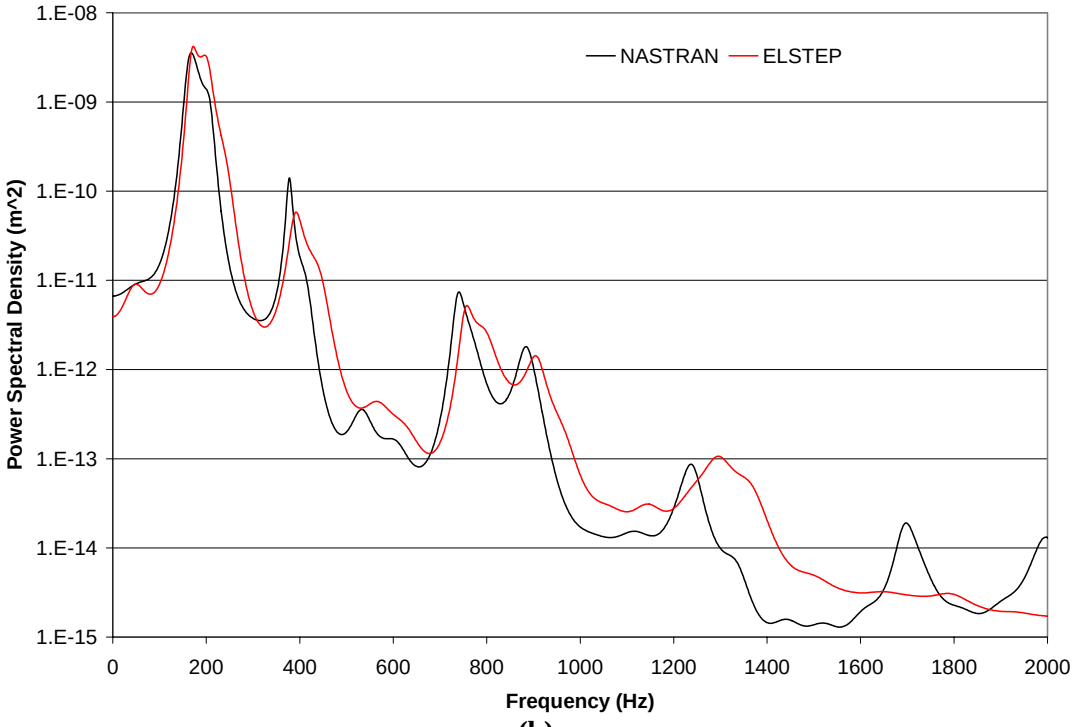

(b)

Figure 17. Comparison of power spectra of the displacement at the center of the panel for MSC.NASTRAN and the reduced order model, p = 1 Pa, (a) 135dB, (b) 140dB.

5. DAMAGE ACCUMULATION RULES

Several damage accumulation rules are available in ELSTEP/FAT to provide an estimate of the fatigue life of the panel under the acoustic excitation. The rule is selected according to the value of option in the header file rainflow.h and its parameters are read from an input file the name of which matches the rule name. The accumulated damage is estimated by performing first a rainflow analysis on the stress selected according to the algorithm of Downing and Socie (1982). The identified ranges are arranged chronologically by either their starting point or their endpoint, depending on the value of ICYCLE in rainflow.h. The accumulated damage is then estimated by application of the accumulation rule to the identified rainflow ranges. In all cases, the *S*-*N* curve is assumed to be of the form

$$N = K\, S^{-m} \tag{28}$$

where N denotes the number of cycles until failure when the stress ranges have an amplitude S.

(1) Palmgren-Miner Rule:

Let D correspond to the damage induced by a stress cycle of magnitude S. Then,

$$D = \frac{1}{N(S)}\,. \tag{29}$$

(2) Marko-Starkey Rule (see Collins, 1993)

Let D correspond to the damage induced by a stress cycle of magnitude S and let n the number of such consecutive cycles. Then,

$$D = \left[\frac{n}{N(S)}\right]^{m(S)} \tag{30}$$

where $m(S)$ is an exponent depending on S. In the present implementation, the function $m(S)$ is assumed to be piecewise constant with values provided in Marko_Starkey.dat.

(3) Marin Rule (see Collins, 1993)

Let D correspond to the damage induced by a stress cycle of magnitude S and let n the number of such consecutive cycles. Then,

$$D = \left[\frac{n}{N(S)}\right]\left(\frac{S}{S_{\max}}\right)^{q} \tag{31}$$

where q is an fixed exponent and $S_{\max}$ is the largest stress range.

(4) Schaff-Davidson Rule (Schaff and Davidson, 1997, Sarkani et al., 2001)

Let D_{k-1} and D_k be the damage accumulated after the k-1$^{\text{th}}$ and k^{th} cycle and S_{k-1} and S_k the ranges of those cycles. Further, let R_0 be the static strength at zero fatigue damage (i.e. of the virgin material). Then,

$$D_k = D_{k-1}\frac{2R_0 - S_{k-1}}{2R_0 - S_k} + \left(\frac{1}{N(S_k)}\right)^{C(s)}. \tag{32}$$

In the present implementation, the function $C(S)$ is assumed to be piecewise constant with values provided in Schaff_Davidson.dat.

(5) Hashin Rule (Hashin, 1985, Sarkani et al., 2001)

Let D_{k-1} and D_k be the damage accumulated after the k-1$^{\text{th}}$ and k^{th} cycle and S_k the ranges of the latter cycle. Further, let R_0 be the static strength at zero fatigue damage (i.e. of the virgin material). Then,

$$D_k = \frac{2R_0 - \left\{\left[2R_0 - D_{k-1}\left(2R_0 - S_k\right)^{A} - \left(2^{A}R_0^{A} - S_k^{A}\right)\left(\frac{1}{N(S_k)}\right)\right]\right\}^{1/A}}{2R_0 - S_k} \tag{33}$$

where A is a material constant (assumed independent of the stress amplitude).

6. CURRENT LIMITATIONS

In its current version, the code has a few limitations/specificities:

(1) the maximum number of nodes, elements, etc. is fixed in param.h and paramd.h files.

(2) only the cartesian stresses can currently be computed. Neither the von Karman nor Tresca stress is available, this issue will be addressed in the next version of ELSTEP/FAT.

(3) the current implementation of the dual modes limits the analysis to planar panels (plates vs. shells), this issue will be addressed in a future version of ELSTEP/FAT.

(4) only CQUAD4 elements have been used so far in the validation process, it is unclear at this point if/what changes must be made to vary the element type.

(5) the loading is only in the form of a planar wave but with arbitrary angle of incidence. The next version of ELSTEP/FAT will also include a spatially fully correlated excitation but non-uniform.

7. REFERENCES

Collins, J.A., 1993, *Failure of Materials in Mechanical Design. Analysis, Prediction, Prevention*, John Wiley.

Downing, S.D., and Socie, D.F., 1982, "Simple Rainflow Counting Algorithms," *International Journal of Fatigue*, pp. 31-40.

Gordon, R., Spottswood, S.M., and Hollkamp, J., "Nonlinear Sonic Fatigue Response Prediction from Finite Element Modal Models: A Comparison with Experiments," *Presented at the 44th Structures, Structural Dynamics, and Materials Conference*, Norfolk, Virginia, Apr. 7-10, 2003. Paper AIAA-2003-1709.

Hashin, Z., 1985, "Cumulative Damage Theory for Composite Materials: Residual Life and Residual Strength Method," *Composite Science and Technology*, Vol. 13, pp. 1-19.

Lee, J., Large-Amplitude Plate Vibration in an Elevated Thermal Environment. *Applied Mechanics Rev.*, 1993, **46**, Part 2, S242-S254.

Lee, J., Random Vibration of Thermally Buckled Plates: II Nonzero Temperature Gradient Across the Plate Thickness. *Applied Mechanics Rev.*, 1997, **50**, Part 2, S105-S116.

Lee, J., Displacement and Strain Statistics of Thermally Buckled Plates. *J. Aircraft*, 2001, **37**.

Lee, J., Topology of the Four-Mode Strain Energy of Thermally Buckling Plates. *J. Thermal Stresses*, 2002, **25**, 813-857.

Mignolet, M.P., 1987, *ARMA Simulation of Multivariate and Multidimensional Random Processes*, Ph.D. Dissertation, Rice University.

Mignolet, M.P., Radu, A.G., and Gao, X., 2003, "Validation of Reduced Order Modeling for the Prediction of the Response and Fatigue Life of Panels Subjected to Thermo-Acoustic Effects," 7th International Conference on Recent Advances in Structural Dynamics, Southampton, United Kingdom, July 14-16, 2003.

Muravyov, A.A., and Rizzi, S.A., 2003, "Determination of nonlinear stiffness with Application to Random Vibration of Geometrically Nonlinear Structures," *Computers and Structures*, Vol. 81, pp. 1513-1523.

Rizzi, S.A., and Muravyov, A.A., 2002, “Equivalent Linearization Analysis of Geometrically Nonlinear Random Vibrations Using Commercial Finite Element Codes,” NASA Technical Paper NASA/TP-2002-211761, Langley Research Center, Hampton, Virginia.

Sarkani, S., Michaelov, G., Kihl, D.P., and Bonanni, D.L., 2001, “Comparative Study of Nonlinear Damage Accumulation Models in Stochastic Fatigue of FRP Laminates,” *Journal of Structural Engineering*, Vol. 127, No. 3, pp. 314-322.

Schaff, J.R., and Davidson, B.D., 1997, “Life Prediction Methodology for Composite Structures; Part I: - Constant Amplitude and Two-Stress Level Fatigue,” *Journal of Composite Materials*, Vol. 31, pp. 128-157.

Schaff, J.R., and Davidson, B.D., 1997, “Life Prediction Methodology for Composite Structures; Part II: - Spectrum Fatigue,” *Journal of Composite Materials*, Vol. 31, pp. 158-181.